XVIII International Feofilov Symposium on Spectroscopy of Crystals Doped with Rare Earth and Transition Metal Ions (IFS-2022)

BOOK OF ABSTRACTS

August 22-27, 2022
Moscow, Russia

IFS-2022

Organizers

Lebedev Physical Institute of the Russian Academy of Sciences (LPI RAS, Moscow)
Institute for Spectroscopy of the Russian Academy of Sciences (ISAN, Troitsk, Moscow)
Moscow State Pedagogical University (MSPU, Moscow)

Russian Academy of Sciences

General sponsors
Avesta Ltd (Moscow)
AZIMUTH PHOTONICS (Moscow)
NT-MDT Spectrum Instruments (Moscow)

Media partner
Journal PHOTONICS RUSSIA

XVIII International Feofilov Symposium on Spectroscopy of Crystals Doped with Rare Earth and Transition Metal Ions (IFS-2022)

BOOK OF ABSTRACTS

August 22-27, 2022
Moscow, Russia

УДК 535.33
ББК 22.344

XVIII International Feofilov Symposium on Spectroscopy of Crystals Doped with Rare Earth and Transition Metal Ions (IFS-2022). Book of abstracts. August 22-27, 2022. Moscow, Russia. – Moscow: Trovant, 2022. – 191 p.: il.

Рецензент: д.ф.-м.н., зав. кафедрой «Математика» Московского политехнического университета Андреев С.Н.

ISBN 978-5-89513-513-6

This book contains materials of the XVIII International Feofilov Symposium on Spectroscopy of Crystals Doped with Rare Earth and Transition Metal Ions (IFS-2022) which took place in Moscow (Lebedev Physical Institute of the Russian Academy of Sciences) from 22 till 27 August, 2022.

The IFS-2022 continues a sequence of symposia organized by Petr P. Feofilov and started in Moscow in 1965. The first nine events were held as national meetings. Already more than 20 years, symposia have been gathering researchers working in the fields of optical spectroscopy, condensed matter physics and solid state chemistry from all over the world. After the Xth (Saint Petersburg, 1995), XIth (Kazan, 2001), XIIth (Ekaterinburg, 2004), XIIIth (Lake Baikal, 2007), XIVth (St. Petersburg, 2010), XVth (Kazan, 2013), XVIth (St. Petersburg, 2015), XVIIth (Ekaterinburg, 2018) Symposia.

IFS-2022 was organized in Moscow by the Lebedev Physical Institute of the Russian Academy of Sciences (LPI RAS, Moscow), Institute for Spectroscopy of the Russian Academy of Sciences (ISAN, Troitsk, Moscow), and Moscow State Pedagogical University (MSPU, Moscow), and managed by the Interinstitutional scientific team working in laser selective spectroscopy and nanoscopy of single molecules, condensed matter and nanostructures (www.single-molecule.ru).

The organization of IFS-2022 was sponsored by hi-tech companies: Avesta Ltd (Moscow, Russia), NT-MDT Spectrum Instruments (Moscow, Russia), and AZIMUTH PHOTONICS (Moscow).

УДК 535.33
ББК 22.344

ISBN 978-5-89513-513-6

Honorary Chairman: Acad. of RAS Alexander A. Kaplyanskii

Chairman: Corr. Member of RAS Andrey V. Naumov

International Advisory Committee

Evgeny B. Aleksandrov (Russia)
Marco Bettinelli (Italy)
Georges Boulon (France)
Miroslav Dramicanin (Serbia)
Philippe Goldner (France)
Vladimir V. Hizhnyakov (Estonia)
Marie-France Joubert (France)
Vladislav Kataev (Germany)
Daniel I. Khomskii (Germany)
Marco Kirm (Estonia)
Paul H.M. van Loosdrecht (Germany)
Oscar Malta (Brasil)
Andries Meijerink (The Netherlands)
Sergey I. Nikitin (Russia)
Michael F. Reid (New Zealand)
Renata Reisfeld (Israel)
Nikolai N. Rosanov (Russia)
Alok M. Srivastava (USA)
Wiesław Stręk (Poland)
Bruno Viana (France)

Program Committee

Co-chair: Boris Z. Malkin (KFU, Kazan)

Co-chair: Andrey V. Naumov (ISAN, LPI, Troitsk)

Co-chair: Marina N. Popova (ISAN, Troitsk)

Mikhail V. Eremin (KFU, Kazan)
Alexey A. Kalachev (Kazan Sci. Center RAS, Kazan)
Vladimir N. Makhov (LPI RAS, Moscow)
Sergey A. Moiseev (Kazan Quantum Center, Kazan)
Alexander S. Moskvin (UrFU, Ekaterinburg)
Roman V. Pisarev (Ioffe PTI RAS, St.Petersburg)
Valerii S. Zapasskii (SPbSU, St.Petersburg)

Local Organizing Committee

Andrey Naumov (Head)
Kamil Karimullin (Sci. secretary)
Artem Arzhanov
Kirill Boldyrev
Maxim Gladush
Alina Golovanova
Sergey Klimin
Natalia Lozing
Konstantin Magaryan
Anastasiya Molchanova
Alexander Savostianov

CONTENTS

INTRODUCTION

Foreword

The XVIII International Feofilov Symposium on Spectroscopy of Crystals Doped with Rare Earth and Transition Metal Ions (IFS-2022) is organized by the Lebedev Physical Institute of the Russian Academy of Sciences (LPI RAS, Moscow), Institute for Spectroscopy of the Russian Academy of Sciences (ISAN, Troitsk, Moscow), and Moscow State Pedagogical University (MSPU, Moscow).

The XVIII International Feofilov Symposium on Spectroscopy of Crystals Doped with Rare-Earth and Transition Metal Ions (IFS-2022) continues a sequence of symposia organized by Petr P. Feofilov and started in Moscow in 1965. The first nine events were held as national meetings. The series of subsequent International Feofilov Symposia [Xth (Saint Petersburg, 1995), XIth (Kazan, 2001), XIIth (Ekaterinburg, 2004), XIIIth (Lake Baikal, 2007), XIVth (St. Petersburg, 2010), XVth (Kazan, 2013), XVIth (St. Petersburg, 2015), XVIIth (Ekaterinburg, 2018)] has been exceptionally successful, bringing together participants from leading research teams in the field of optical spectroscopy, condensed matter physics and solid-state chemistry from all over the world to discuss the latest advances in fundamental science, applications of spectroscopy and related topics.

We look forward to meeting you in Moscow!

Chairman of the IFS 2022, Corr. member of RAS Andrey Naumov,
Co-chairs of the Program Committee Prof. Marina Popova and Prof. Boris Malkin,
Honorary Chairman Acad. RAS Alexander Kaplyanskii.

About Petr P. Feofilov

Petr P. Feofilov, one of the most famous Russian researchers in optical spectroscopy in the XX century, began his research under the supervision of the Academician Sergey I. Vavilov. Feofilov has made a great contribution to the development of physics of crystals doped with transition metal ions. He is one of the first in the world to have begun the systematic investigation of the optical properties of crystals comprising ions with uncompleted shell, e.g. rare earth (RE) ions and uranium. He was the first to state such essential problems as multiple activator sites problem, crystal-chemical conditions of activation, physical structure, and energy of the RE-sites. Feofilov has developed and successfully implemented the method of polarized luminescence for investigation of the RE-sites. The book “Polarized luminescence of molecules, solutions and crystals” now is a classical course book to study luminescence spectroscopy. The studies of luminescence properties of crystals performed by Feofilov have allowed the creation one of the first solid state lasers based on calcium fluoride doped with samarium and uranium ions. The research by Feofilov has a great impact on such areas of solid-state physics as crystallography and optical spectroscopy of defects in crystals. Besides, Feofilov was a friendly, open-minded, and talented person.

INVITED AND PLENARY TALKS

High-resolution luminescence spectroscopy of functional materials

Kirill N. Boldyrev[a], *Nicolay Yu.* Boldyrev, *Marina N.* Popova

Institute of spectroscopy, Russian Academy of Sciences, 108840, Troitsk, Moscow, Russia

Abstract. Luminescent spectroscopy is one of the most informative methods for studying various substances. It combines high sensitivity with a rich and varied data set to reveal the deep nature of materials. Here we describe a unique setup developed and implemented at the Institute of Spectroscopy for broadband high-resolution luminescence spectroscopy and show several examples of solid-state studies performed.

1 Introduction

Luminescence spectroscopy as an optical research method has the advantage of high sensitivity over transmission/absorption/reflection research methods, since only the useful signal is recorded in it. In addition, luminescence provides more information, as it allows studies to be carried out at different excitation wavelengths, which makes it possible to separate different optical centers (so-called site-selective spectroscopy) and allows studying transitions between excited energy levels. All this makes luminescence spectroscopy methods indispensable assistants in studying the properties of materials. So far, high-resolution broadband luminescent methods have not been used in solid-state research. In this work, we fill this gap. A Fourier-spectrometer-based setup for recording high-resolution luminescence spectra in an ultrawide spectral range was created and its capabilities and advantages were demonstrated on several examples of crystal studies.

2 Experimental Setup

Based on a Bruker IFS 125HR high-resolution all-wavelength Fourier spectrometer, a setup was created for recording low-temperature luminescence spectra (see Fig. 1). For this, a high-vacuum luminescent module with a large luminosity was designed, in which it was possible to place several cryostats, as well as magnets for Zeeman luminescence spectroscopy. In addition, a high-aperture luminescence-registration module was developed with the possibility of installing a large set of various highly sensitive detectors. A wide range of tunable diode lasers, a Ti:sapphire laser, or an X-ray tube can be used to excite luminescence. All this makes it possible to record emission spectra in the range 20–20000 cm^{-1} at temperatures from 4 to 350 K with a spectral resolution better than 0.001 cm^{-1}.

[a] Corresponding author: kn.boldyrev@gmail.com

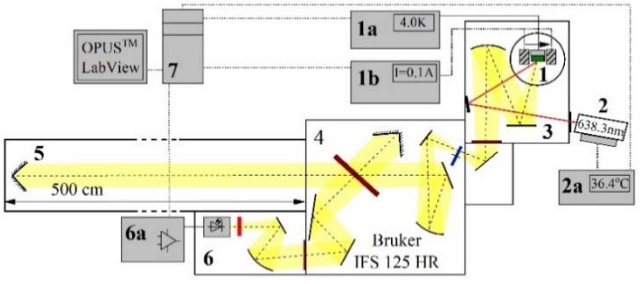

Fig. 1. Setup: 1 - cryostat with magnetic coils (gray hatched); 1a – temperature controller; 1b - current source for magnetic coils; 2 - temperature-stabilized diode laser, 2a – temperature controller and current source for laser; 3 – luminescence module; 4 - Fourier spectrometer; 5 - luminescence-registration module, 5a - preamplifier and an analog to digital converter; 6 - workstation for spectra calculation and automatic control of magnetic field and temperature.

3 High-resolution luminescent studies of crystals

The most interesting results were obtained for $LiYF_4$:Ho single crystals [1,2]. The hyperfine and isotope structure [1,2], anticrossings of hyperfine levels in an external magnetic field [1] and related additional structures [2], and deformation splittings [1] were observed for the first time in the luminescence spectra of crystals. The measured width 0.002 cm^{-1} of the photoluminescence line [1] is, as far as we know, the smallest inhomogeneous linewidth ever observed in the luminescence spectra of crystals. We propose to use the luminescence of $LiYF_4$:Ho for creating remote magnetic field sensors that do not require an additional constant or variable magnetic field and/or microwave field and are capable of operating in a very wide range of measured magnetic fields. Among other results, giant deformation splitting of lines in the spectra of $LaAlO_3$ pseudocubic perovskite crystals [3,4], studies of the crystal-field levels in $YPO_4:Pr^{3+}$ [5] and $ASL:Pr^{3+}$ [6] crystals, and isotopic shifts in diamond with SiV color centers [7] should be mentioned.

Financial support from the Russian Science Foundation under Grant #19-72-10132 is acknowledged. K.N.B. is a member of the Leading Scientific School of the Russian Federation (grant of the President of the Russian Federation NSh-776.2022.1.2).

References

1. K.N. Boldyrev, B.Z. Malkin, M.N. Popova, Light Sci. Appl., accepted (2022)
2. K.N. Boldyrev, M.N. Popova, submitted to J. Lumin (2022)
3. K.N. Boldyrev, N.M. Abishev, I.E. Mumdzi, S.I. Nikitin, B.Z. Malkin, R.V. Yusupov, M.N. Popova, Opt. Mat. X **14**, 100155 (2022)
4. K.N. Boldyrev, N.M. Abishev, I.E. Mumdzi, S.I. Nikitin, P. Deren, B.Z. Malkin, M.N. Popova, Phys. Rev. B **103**, 054103 (2021)
5. S.A. Klimin, E.P. Chukalina, K.N. Boldyrev, T.A. Igolkina, M.S. Radionov, M.C. Chou, M.N. Popova, J. Lumin **235**, 118003 (2021)
6. S. Sattayaporn, P. Loiseau, G. Aka, S. Klimin, K. Boldyrev, B. Mavrin, J.Lumin **219**, 116895 (2020)
7. V.G. Ralchenko, V.S. Sedov, A.K. Martyanov, A.P. Bolshakov, K.N. Boldyrev, V.S. Krivobok, S.N. Nikolaev, S.V. Bolshedvorskii, O.R. Rubinas, A.V. Akimov, A.A. Khomich, E.V. Bushuev, R.A. Khmelnitskiy, V.I. Konov, ACS Photonics **6**(1), 66–72 (2019)

Cr^{2+} – Fe^{2+} energy transfer in ZnSe based solid solutions

Maxim Doroshenko[1,b] and *Helena* Jelinkova[2]

[1]General Physics Institute, 119991 Vavilov Str. 38, Moscow, Russian Federation
[2]Czech Technical University, 115 19 Břehová 7, Prague, Czech Republic

Abstract. Spectroscopic properties of Cr^{2+} and Fe^{2+} ions in a set of solid solutions based on ZnSe crystal will be demonstrated and discussed. Energy transfer process between Cr^{2+} and Fe^{2+} ions in these solid solutions at different temperatures will be characterized. Lasing of Fe^{2+} ions under Cr^{2+} ions optical pumping will be demonstrated.

Introduction

Along low-phonon energy laser materials perspective for development of broadly tunable or utrashort (femtosecond) pulse lasers in mid IR spectral range zinc selenide crystals doped by divalent chromium or iron ions are attracting great attention. Using ZnSe:Cr crystals CW operation with output power up to 140 W in CW as well as femtosecond (41 fs) operation with peak power of 500 kW and ZnSe:Fe lasers with output energy up to 10 J and 10 W CW output power (at 77K) [1] were developed. Fe^{2+} based lasers use less convenient optical pump sources, therefore, several attempts to use ZnSe crystals co-doped by divalent chromium and iron ions for optical pumping of chromium ions and further excitation energy transfer to iron ions were made. Though, in ZnSe crystal negative effect of iron ions lasing threshold increase and oscillation efficiency decrease in co-doped crystals most probably due to iron ions fluorescence quenching by chromium ions was observed [3].

Fe^{2+} ions clustering

Resent investigations have shown that even at small concentrations of Cr^{2+} or Fe^{2+} active ions some process (like fluorescence line maximum shift, lifetime concentration dependence) characteristic for formation of different optical centers including clusters can take place. Thus, ZnSe:Fe^{2+} crystal excitation by 2.94 μm and 4.1 μm radiation results, for example, in sufficiently different Fe^{2+} ions fluorescence spectra and decay kinetics (see Fig. 1). In Fig. 1 decay curve for 2.94 μm excitation wavelength is seen to contain a short time component most likely due to quenching of clustered Fe^{2+} ions which is absent for 4.1 μm excitation. At the same time such strong dependence of Fe^{2+} spectroscopic properties on excitation wavelength in $Zn_{1-x}Mn_xSe$ solid solutions was not observed. Possible formation of some similar Cr^{2+}-Fe^{2+} clusters in ZnSe based co-doped crystals and their spectroscopic properties will be discussed.

Cr^{2+}– Fe^{2+} ions energy transfer

[b] Corresponding author: dorosh@lst.gpi.ru

In ZnSe based solid solutions all necessary conditions for Cr^{2+}-Fe^{2+} ions energy transfer (i.e. nonzero overlap integral between Cr^{2+} ions fluorescence and Fe^{2+} ions absorption in a wide temperature range, Cr^{2+} ions non-exponential decay in co-doped samples, quite intensive Fe^{2+} ions fluorescence under Cr^{2+} ions excitation) are fulfilled and non-radiative Cr^{2+}-Fe^{2+} integral energy transfer efficiency up to ~50% is realized. Both fast ordered stage of energy transfer to nearest acceptor Fe^{2+} ions and slower disordered stage are observed and characterized (see Fig. 2). Dipole-dipole mechanism of non-radiative energy transfer is revealed. Possible influence of Cr^{2+}-Fe^{2+} clustering on energy transfer process is analyzed and will be discussed.

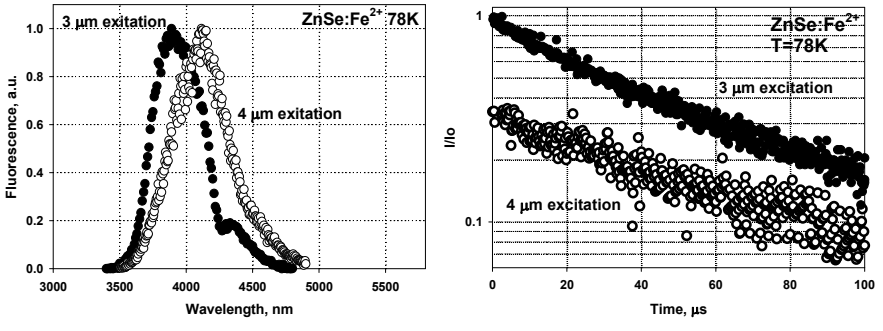

Fig. 1. Low temperature fluorescence spectra and decay curves of Fe^{2+} ions in ZnSe crystal for different excitation wavelengths.

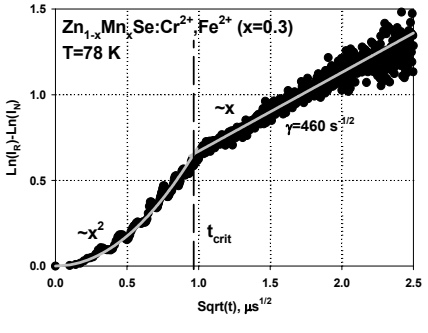

Fig. 2. Cr^{2+}- Fe^{2+} ions energy transfer function plotted in $\sqrt{t}$ axis

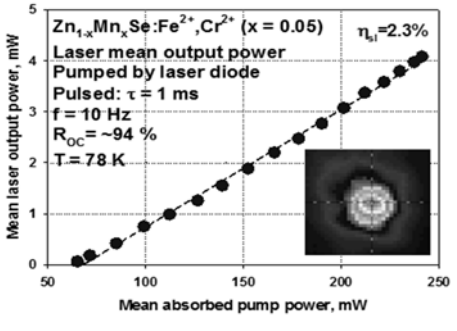

Fig. 3. $Zn_{1-x}Mn_xSe:Cr^{2+},Fe^{2+}$ output power vs the absorbed 1700 nm laser-diode pump.

As a result, lasing of Fe^{2+} ions in a set of ZnSe based solid solutions under Cr^{2+} ions optical pumping by different commercial pump sources operating within 1700 – 2000 nm is realized (see example in Fig. 4) at temperatures up to 220 K and will be presented in details.

References

1. I. Moskalev, S. Mirov, M. Mirov, S. Vasilyev, V. Smolski, A. Zakrevskiy, V. Gapontsev, Laser Technik Journal, **4**, 24 (2016).
2. J.J. Adams, C. Bibeau, R.H. Page, S.A. Payne, OSA TOPS, **26**, 435 (1999).
3. K.N. Firsov, E.M. Gavrishchuk, V.B. Ikonnikov, S.Yu. Kazantsev, et. al., Physics of Wave Phenomena, **27**(3), 211 (2019).

Theory of crystal fields and excitation spectra (optical and terahertz) in $Fe_2Mo_3O_8$

Mikhail Eremin[1,c], *Kirill* Vasin[1], and *Alexey* Nurmukhametov[1]

[1]Institute of Physics, Kazan Federal University, 16a Kremlyovskaya St., Kazan, Russia 420008

Abstract. The energy levels and wave functions of Fe^{2+} (^5D) ions in $Fe_2Mo_3O_8$ have been calculated using crystal field theory. The interaction parameters of copper 3d-electrons with the electrical field are evaluated using experimental data about absorption coefficients. The origin of the magnetoelectic coupling is also discussed.

1 Introduction

The $Fe_2Mo_3O_8$ compound was studied by Mössbauer spectroscopy in [1]. Fe^{2+} ions in $Fe_2Mo_3O_8$ occupy tetrahedral and octahedral positions. The Neel` temperature is $T_N = 60$ K. The interest to this compound has increased due to the discovery of strong magnetoelectric effects [2,3]. The technique of terahertz spectroscopy is actively used to study the energy level scheme [4, 5]. The ground multiplet in the A site is Fe^{2+} (^5E), and in the B site is Fe^{2+} (^5T). The fine structure of these multiplets is quite complicated and has not yet been determined. The purpose of this work is to apply modern methods of crystal field theory to contribute for solving this problem.

2 Energy levels and wave functions

We start with Hamiltonian:

$$H = \sum_{k,q} B_q^{(k)} C_q^{(k)} + \lambda \boldsymbol{LS} + \sum_l J_{il}\, \boldsymbol{S}_i \boldsymbol{S}_l + \mu_B (\boldsymbol{L} + 2\boldsymbol{S})\boldsymbol{B}. \quad (1)$$

The crystal field parameters were calculated using the Hartree–Fock wave functions of free Fe^{2+} ions, taking into account the spatial distribution of 2s and 2p oxygen electrons. The exchange charge on the Fe^{2+}-O^{2-} bonds was chosen to fit the splitting energy of the ^5D terms into ^5E and ^5T multiplets. For the tetrahedral (A) and octahedral (B) positions, it turned out to be approximately the same G(A) = 9 and G(B) = 12. The spin-orbit coupling constants are $\lambda(A) = -70$ cm^{-1}, $\lambda(B) = -85$ cm^{-1}. The exchange (molecular) field parameters in the antiferromagnetic (AFM) and ferrimagnetic (FiM) phases and crystal field parameters are given in Table 1.

Table 1. Crystal molecular field parameters for various magnetic phases (in cm^{-1}).

Site	$B_0^{(2)}$	$B_0^{(4)}$	$B_3^{(4)}$	$\sum J_{il}\langle S_l^z \rangle$		
				AFM, 4.4 K	AFM, 55 K	FiM, 55 K

[c] Corresponding author: meremin@kpfu.ru

Tetra (A)	1200	5490	6040	∓77	∓12.5	∓20
Octa (B)	1020	-10420	-11490	±55	±32	±5

The calculated values of the energies of the three lowest states (terahertz region) are given in Table 2. To control the identification of the excited states nature, the probabilities of magnetic and electric dipole transitions were also calculated.∓20

Table 2. Low lying energy levels (in cm^{-1}).

AFM, 4.5 K		AFM, 55 K		FiM, 55 K	
Tetra (A)	Octa (B)	Tetra (A)	Octa (B)	Tetra (A)	Octa (B)
90	186	41	109	51	43
41	113	20	83	26	17
0	0	0	0	0	0

The obtained wave functions of the ground states of iron ions are used to calculate the average iron ions' magnetic moments and to estimate the electric polarization vector components. The electric polarization jump upon the transition from the antiferromagnetic to the ferrimagnetic phase, discovered in [2, 5] under applied an external magnetic field, is explained by the combined action of the electronic and striction mechanisms.

We are grateful to Dr Joachim Deisenhofer for stimulating discussion of the teraherz spectroscopy data. This work was supported by the RSF (Project No. 19-12-00244).

References

1. F. Varret, H. Czeskleba, F. Hartmann-Boutron, and P. Imbert, J. Phys. **33**, 549 (1972) M. V. Eremin, and A. R. Nurmukhametov, JETP Lett., **114**, 35-39 (2021)
2. T. Kurumaji, S. Ishiwata, and Y. Tokura, Phys. Rev. **5**, 031034 (2015).
3. Yazhong Wang, Gheorghe L. Pascut, Bin Gao, Trevor A. Tyson, Kristjan Haule1, Valery Kiryukhin & Sang-Wook Cheong, Scientific Reports **5**, 12268 (2015)
4. T. Kurumaji, Y. Takahashi, J. Fujioka, R. Masuda, H. Shishikura, S. Ishiwata, and Y. Tokura, Phys. Rev. B **95**, 020405(R) (2017)
5. T.N. Stanislavchuk, G.L. Pascut, A.P. Litvinchuk, Z. Liu, Sungkyun Choi, M.J. Gutmann, B. Gao, K. Haule, V. Kiryukhin, S.-W. Cheong, and A. A. Sirenko, Phys. Rev. B. **102**, 115139 (2020)

Electromagnetically induced transparency in isotopically purified rare-earth doped crystals

Alexey Kalachev[d]

Kazan Scientific Center of Russian Academy of Sciences, 420111 Kazan, Russia

Abstract. The recent progress in experimental and theoretical study of isotopically purified rare-earth-ion doped crystals is discussed in the context of quantum information storage. The focus is on the effect of electromagnetically induced transparency in Y^7LiF_4 crystals doped with Nd-143 ions and Er-167 ions with the use of hyperfine zero-first-order Zeeman transitions.

Rare-earth-ion doped crystals have raised a strong interest in the field of quantum information storage and microwave-to-optics frequency converters. Among them, isotopically purified crystals are of particular interest. They can demonstrate very small inhomogeneous broadening of optical transitions, which proves to be smaller than the hyperfine splitting of the energy levels of impurity ions, and provide high optical densities. As a result, these crystals are promising candidates for implementing quantum storage via off-resonant Raman absorption/emission of single photons without spectral tailoring of optical transitions.

In the present work, the recent progress in experimental and theoretical studying these materials is discussed [1-5]. In particular, we have observed the effect of electromagnetically induced transparency (EIT) in Y^7LiF_4 crystals doped with Nd-143 ions [3] and Er-167 ions [4] with the use of hyperfine zero-first-order Zeeman transitions. In the first case (Nd ions), narrow peaks in the EIT profile have been resolved, which might be caused by the superhyperfine splitting of the neodymium hyperfine levels in the ground electronic state [6]. In the second case (Er ions), we have found that EIT feature can only be observed at mK temperatures. In addition, we compare and discuss coherence properties of Y^7LiF_4 [1] and Y_2SiO_5 [4] crystals doped by Er-ions, where we observed that the deep freezing results in an increase of optical coherence time compared to temperature of 1.5 K and magnetic field of ~0.2 T.

References

1. N. Kukharchyk, D. Sholokhov, O. Morozov, S.L. Korableva, A.A. Kalachev, P.A. Bushev, New J. Phys. **20**, 023044 (2018)
2. N. Kukharchyk, D. Sholokhov, O. Morozov, S. L. Korableva, J. H. Cole, A. A. Kalachev, P. A. Bushev, Opt. Lett. **43**, 935 (2018)
3. R. Akhmedzhanov, L. Gushchin, N. Nizov, V. Nizov, D. Sobgayda, I. Zelensky, A. Kalachev, Phys. Rev. B **97**, 245123 (2018)
4. N. Kukharchyk, D. Sholokhov, A. A. Kalachev, P. A. Bushev, arXiv:1910.03096 (2019)
5. N. Kukharchyk, D. Sholokhov, O. Morozov, S. L. Korableva, A. A. Kalachev, P. A. Bushev, Optics Express, **28**, 29166 (2020)
6. A.D. Berezhnoi, A.A. Kalachev (in preparation)

[d] Corresponding author: a.a.kalachev@mail.ru

Laser-driven ultrafast magnetization switching in rare-earth iron oxides

Alexandra Kalashnikova[e]

Ioffe Institute RAS, 194021 St. Petersburg. Russia

Abstract. We discuss laser-induced switching of magnetization in rare-earth iron oxides – orthoferrites and garnets, which is enabled by specific response of the rare-earth (*R)* magnetic moment to laser excitation and by its interactions with magnetization of iron. Laser-induced change of magnetic moments of rare-earth ions occurring at picosecond timescale appears to be a triggering mechanism for the spin-reorientation transition in orthoferrites RFeO$_3$ and for the switching via compensation point in garnets R_3Fe$_5$O$_{12}$.

1 Introduction

Switching magnetization in solids using femtosecond laser pulses is among paramount goals in modern magnetism, magneto-optics and spintronics [1,2]. Several pathways to steer magnetization between different potential minima has been suggested and demonstrated, exploiting laser-driven highly-nonequilibrium state [3] or large-amplitude precessional motion [4,5]. Of particular interest are laser-driven processes in materials possessing abrupt changes of magnetization orientation under moderate external impacts. Examples of such materials are those having spin-reorientation transitions or magnetization compensation points.

Large family of rare-earth iron oxides include both types of materials. Rare-earth orthoferrites RFeO$_3$ demonstrate spin-reorientation phase transitions order in a wide range of temperatures depending on type of R^{3+}. Rare-earth iron garnets R_3Fe$_5$O$_{12}$, in turn, possess magnetization compensation points, which are also determined by R^{3+}. In this talk we discuss magnetization dynamics induced by femtosecond laser pulses in these materials and show that it is specific and distinct responses of rare-earth and iron magnetic moment to laser excitation which enable ultrafast magnetization switching in these materials.

2 Switching via laser-driven spin reorientation transition in a rare-earth orthoferrite

Rare-earth orthoferrites RFeO$_3$ are weak ferromagnets with Néel temperature of ~650 K. Below this temperature weak magnetic moment is directed along the crystallographic c-axis, and the anisotropy is dictated by the single-ion anisotropy of Fe^{3+} ions. However, as a temperature decreases, another contribution starts to dominate stemming from the exchange coupling of magnetic moments of Fe^{3+} and R^{3+} ions and the strong anisotropy of R^{3+} ions. As a result, spin-reorientation transition occurs [6]. In [7] it has been shown for the first time that such a phase transition can be triggered by ultrafast laser-induced heating.

Here we discuss how such laser-induced spin reorientation transition can be exploited for deterministic switching of magnetization by femtosecond circularly-polarized laser pulses in (Sm,Pr)FeO$_3$ [8]. Ultrafast laser-induced heating induces reduction of magnetic moment of

[e] Corresponding author: kalashnikova@mail.ioffe.ru

rare-earth ions within several picosecond after excitation resulting in spin-reorientation phase transition. During the laser pulse impact, there is also an effective laser-induced magnetic field pulse which determines the direction of the magnetization in the new laser-induced phase. This two-fold effect of laser pulse allows unique deterministic switching of magnetization controlled by laser pulse polarization, fluence, and initial sample temperature.

3 Switching via compensation point in a rare-earth garnet

Rare-earth iron garnets $R_3Fe_5O_{12}$ are ferrimagnets with antiferromagnetically coupled rare-earth and net iron magnetizations. Néel temperature is of ~550 K. Different temperature dependences of magnetization of the two sublattices results in magnetization compensation temperature defined by the type of R^{3+} ion [9]. It has been shown previously that presence of compensation point in metallic ferrimagnets enables their switching by femtosecond laser pulses [10].

Here we discuss the path the magnetizations of rare-earth and iron sublattices take during the laser-induced switching thought compensation point in $Ho_3Fe_5O_{12}$ [11]. Using time-resolved optical pump / soft X-ray probe technique, we reveal that the switching is triggered by fast, within picoseconds, demagnetization of Ho^{3+} sublattice, while magnetization of Fe^{3+} sublattice remains nearly unchanged. This sudden change of ratio between sublattice magnetizations triggers complex magnetization dynamics including transition into canted phase [9] which eventually results in net magnetization reversal after ~100 ps.

Support from RFBR (grant No. 20-02-00938) is acknowledged.

References

1. A. V. Kimel, A. M. Kalashnikova, A. Pogrebna, A. K. Zvezdin, Phys. Rep. **852**, 1 (2020).
2. A. V. Kimel and Mo Li, Nature Rev. **4**, 189 (2019).
3. K. Vahaplar, A. M. Kalashnikova, A. V. Kimel, *et al*., Phys. Rev. Lett. **103**, 117201 (2009).
4. A. Stupakiewicz, K. Szerenos, D. Afanasiev, *et al*., Nature **542**, 71 (2017).
5. C. S. Davies, K. H. Prabhakara, M. D. Davydova, *et al*., Phys. Rev. Lett. **122**, 027202 (2019).
6. K. P. Belov, A. K. Zvezdin, A. M. Kadomtseva and R. Z. Levitin, Sov. Phys. Usp. **19**, 574 (1976).
7. A. V. Kimel, A. Kirilyuk, A. Tsvetkov, *et al*., Nature 429, 850 (2004).
8. J. A. de Jong, I. Razdolski, A. M. Kalashnikova, *et al*., Phys. Rev. Lett. 108, 157601 (2012).
9. A. K. Zvezdin, Field induced phase transitions in ferrimagnets, Handbook of Magnetic Materials 9, 405 (1995).
10. I. Radu, K. Vahaplar, C. Stamm, *et al*., Nature **472**, 205 (2011)
11. A. M. Kalashnikova, L. A. Shelukhin, R. V. Pisarev et al., *in preparation*.

Upconversion nanocrystals for biophotonics and nanomedicine

Evgeny Khaydukov[1,f], *Roman* Akasov[1], *Alla* Generalova[1,2]

[1] Federal Scientific Research Centre «Crystallography and Photonics» Russian Academy of Sciences
[2] Shemyakin - Ovchinnikov Institute of Bioorganic Chemistry Russian Academy of Sciences

Abstract. Today, nanoengineering has enabled the creation of special photoluminescent nanomaterials in a programmable way. Among the broad class of newly developed inorganic nanomaterials, nanocrystals doped with lanthanide ions attract attention due to their unique optical properties. The "inverted" luminescence (anti-Stokes), which occurs due to upconversion in such nanocrystals, is not typical for "living" nature, where normally higher energy light is converted into lower energy photons. The physical phenomenon of upconversion, where near-infrared photons are converted into visible and even ultraviolet light quanta, has therefore opened unique opportunities for researchers in the field of biotechnology and medicine. The aim of this lecture is to present an interdisciplinary approach to the use of the upconversion phenomenon with applications in biomedicine and biophotonics. We will consider the results of studies of photophysical processes in upconverting nanomaterials, the peculiarities of their growth, the creation of biocompatible shells on the nanoparticle surface, the development of theranostic nanoconstructions, bioimaging methods, photodynamic and photothermal therapy of tumour tissues, and the nanocrystal application for regenerative medicine.

State of the art

In the last decade, a wide class of newly developed inorganic nanomaterials, nanocrystals doped with lanthanide ions attract much attention due to their unique optical properties. Anti-Stokes nanoparticles based on $NaYF_4$ nanocrystals co-doped with $Yb^{3+}Tm^{3+}$ or $Yb^{3+}Er^{3+}$ can convert near-infrared photons into visible and ultraviolet (UV) photons through an upconversion mechanism. The luminescence excitation light (980 nm) falls into the so-called "transparency window" of biological tissue (from 650 to 1500 nm), where the penetration of light into the tissue occurs with minimal absorption and scattering [1]. NIR light can penetrate deeper into biological tissues than UV/VIS light, providing an optical imaging from greater depths. The upconversion phenomenon leads to unique optical properties of nanoparticles, including minimal photo-impact on living organisms and high signal-to-noise ratio of photoluminescence compared to conventional fluorescent labels. In addition, this class of nanoparticles are characterized by high chemical and photostability, low cytotoxicity [2]. The luminescence of upconversion nanoparticles (UCNPs) is very stable, lacks the photobleaching, which allows continuous monitoring for a long period. The use of upconversion nanoparticles capable of penetrating the tumours and even blood-brain barrier (BBB) has been demonstrated earlier. The inorganic platform of UCNPs makes it possible to include the modalities that ensure their integration into medical practice, namely: magnetic resonance imaging (MRI), X-ray computed tomography (CT), positron emission tomography (PET), and single photon

[f] Corresponding author: khaydukov@mail.ru

emission computed tomography (SPECT) [3], [4]. The surface of UCNPs after synthesis usually requires polymer coating to increase their biocompatibility and prolong their circulation time in the circulatory system. Polyethylene glycol (PEG), polyacrylic acid (PAA), polyvinylpyrrolidone (PVP), polyethyleneimine (PEI), etc. are often used as the polymer coating [5]. An increase in the time of UCNPs circulation in the bloodstream is assumed to provide a higher efficiency of delivery to the tumour due to the effect of enhanced permeability and retention (EPR), which allows nanoparticles to accumulate in tumour tissues.

The aim of this lecture is to present an interdisciplinary approach to the use of the upconversion phenomenon with applications in the field of biomedicine and biophotonics. The presentation will consider the results of studies of photophysical processes in upconverting nanomaterials, the peculiarities of their growth, the creation of biocompatible coatings on the surface of nanoparticles, the development of theranostic nanoconstructions, the development of bioimaging methods, photodynamic and photothermal therapy of tumour tissues, and the UCNP application for regenerative medicine (Fig. 1). New approaches to increase the complexity of the hierarchy of manufactured nanoparticles, to expand the arsenal of nanoengineering techniques in biotechnology and antimicrobial photodynamic therapy, and to address the problem of antibiotic resistance of microorganisms will also be considered.

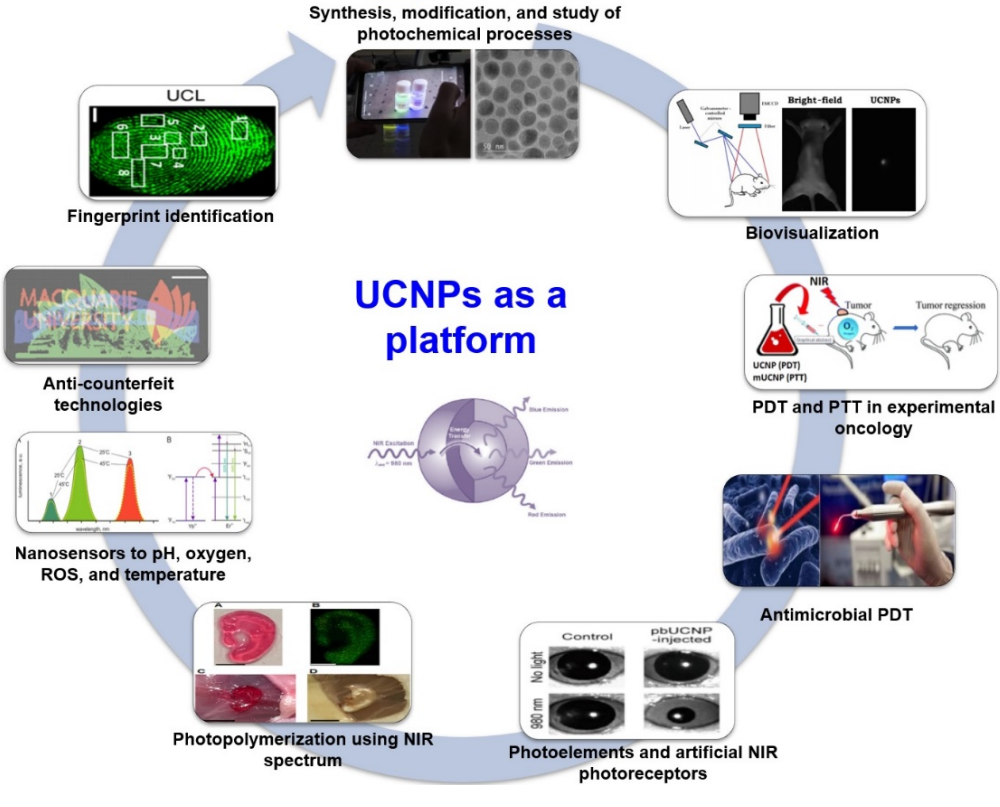

Fig. 1 The scheme of UCNPs applications

This work was financially supported by the Russian Science Foundation, grant 18-79-10198.

References

1. J. Zhou, Q. Liu, W. Feng, Y. Sun, and F. Li, “Upconversion luminescent materials: Advances and applications,” Chemical Reviews, vol. 115 (1), pp. 395–465 (2015). doi: 10.1021/cr400478f.
2. S. Wen, J. Zhou, K. Zheng, A. Bednarkiewicz, X. Liu, and D. Jin, “Advances in highly doped upconversion nanoparticles,” Nature Communications, vol. 9 (1), p. 2415 (2018). doi: 10.1038/s41467-018-04813-5.
3. J. Yao, C. Huang, C. Liu, and M. Yang, “Upconversion luminescence nanomaterials: A versatile platform for imaging, sensing, and therapy,” Talanta, vol. 208, p. 120157 (2020). doi: 10.1016/j.talanta.2019.120157.
4. A. N. Generalova, B. N. Chichkov, and E. V. Khaydukov, “Multicomponent nanocrystals with anti-Stokes luminescence as contrast agents for modern imaging techniques,” Advances in Colloid and Interface Science, vol. 245, pp. 1–19 (2017). doi: 10.1016/j.cis.2017.05.006.
5. P. A. Demina et al., “A versatile platform for bioimaging based on colominic acid-decorated upconversion nanoparticles,” Biomaterials Science, vol. 8 (16), pp. 4570–4580 (2020). doi: 10.1039/D0BM00876A.

Electric activity of different magnetic textures

Daniel Khomskii[g]

Koeln University, Germany

Abstract. No

Close connection between electricity and magnetism is one of the cornerstones of modern physics. In application to solids this connection takes different forms. There exist materials with linear magnetoelectric effect and multiferroics - the systems which simultaneously have magnetic and ferroelectric ordering [1]. In my talk I will discuss electric properties of different magnetic objects: spin triangles [2,3]; monopoles in spin ice systems; domain walls and cylindrical magnetic domains (CMD); skyrmions; systems with spin fragmentation; ordinary spin waves, and the inverse effect: the appearance of magnetic monopoles on charges in magnetoelectrics. I will pay special attention to the purely electronic mechanisms of such phenomena and will discuss the appearance of spontaneous currents, electric dipoles, and magnetic monopoles in frustrated Mott insulators, in spin-ice systems [4-7].

References

1. D.I. Khomskii, Physics (Trends) 2, 20 (2009)
2. L.N. Bulaevskii, C.D. Batista, M.V. Mostovoy and D.I.Khomskii, Phys. Rev. B 78, 028402 (2008)
3. D.I. Khomskii, JPCM 22, 164209 (2010)
4. D.I. Khomskii, Nature Communications 3, 904 (2012)
5. D.I. Khomskii, Nature Communications 5, 4793 (2014)
6. D.I. Khomskii, Journal of Experimental and Theoretical Physics, 132, (2021)
7. D.I. Khomskii, Nature Communications 12, 3047 (2021)

[g] Corresponding author: khomskii@ph2.uni-koeln.de

Luminescence of manganese and chromium ions in spinel hosts

Nicholas M. Khaidukov[1], *Maria* N. Brekhovskikh[1], *Nataliia* Yu. Kirikova[2], *Valentin* A. Kondratyuk[2], and *Vladimir* N. Makhov[2,h]

[1]N.S. Kurnakov Institute of General and Inorganic Chemistry, Moscow 119991, Russia
[2]P.N. Lebedev Physical Institute, Moscow 119991, Russia

Abstract. Ceramic samples of $MgAl_2O_4$, $ZnAl_2O_4$ and $LiAl_5O_8$ spinels doped with manganese or chromium ions have been synthesized by a solid-state reaction method. It has been shown that luminescence properties of synthesized phosphors, in particular, the appearance of intense Mn^{4+} luminescence, depend strongly on the ability of the spinel hosts to exhibit the high degree of cation inversion.

1 Introduction

Currently, one of the actively developing areas in the luminescent technology is extensive research and development of phosphors emitting in the red and far-red spectral region. Such phosphors are needed for obtaining "warm" white LEDs, as well as LED light sources used to stimulate plant growth in greenhouses. Compounds doped with $3d^3$ ions such as Mn^{4+} and Cr^{3+}, which replace matrix cations in sites with octahedral coordination, are considered to be the most promising materials for such phosphors. Spinel group compounds provide wide opportunities for the "chemical design" of crystal matrices, whose structures have octahedral sites for Mn^{4+} and Cr^{3+} ions. The spinel-like compounds are characterized by the cubic close-packed oxygen sublattice in which cations of two different types usually occupy octahedral and tetrahedral sites, e.g., Al^{3+} and Mg^{2+} in the mineral spinel $MgAl_2O_4$. In the present work, luminescence properties of three spinel-type compounds doped with manganese and chromium ions have been studied and generalized.

2 Methods and materials

Manganese or chromium ions doped ceramic samples of $MgAl_2O_4$, $ZnAl_2O_4$ and $LiAl_5O_8$ spinels were prepared by high-temperature solid-state reactions. The structures and the phase purities of the samples were confirmed with powder X-ray diffraction analysis.
Photoluminescence (PL) and PL excitation (PLE) spectra as well as luminescence decay kinetics were studied using standard optical equipment including blue (455 nm) or UV (400 nm) LEDs (Mightex) as excitation sources, grating monochromator MDR-12 and CM2203 spectrofluorometer (Solar).

3.1 $MgAl_2O_4$

Manganese ions doped partially inverted $MgAl_2O_4$ spinel shows intense Mn^{4+} red luminescence peaking at 651 nm with a rather large inhomogeneous broadening [1,2]. Besides, a green luminescence coming from Mn^{2+} ions substituting for Mg^{2+} ions in tetrahedral sites is

[h] Corresponding author: makhovvn@lebedev.ru

observed. The ratio of intensities for the red and green bands depends on the synthesis conditions. By applying a special multi-step annealing procedure, the $MgAl_2O_4:Mn^{4+}$ phosphor containing only tetravalent manganese ions, Mn^{4+}, can be synthesized. Manganese ions doped $MgAl_2O_4$ spinel with an optimal intensity ratio of green Mn^{2+} and red Mn^{4+} luminescence can be a promising single-phase bicolor phosphor suitable for the development of warm white LEDs by using the conventional RGB scheme. Cr^{3+} doped $MgAl_2O_4$ ceramics has a characteristic Cr^{3+} luminescence band with a peak at 687.5 nm and large inhomogeneous broadening which shows relatively weak changes with temperature.

3.2 $ZnAl_2O_4$

Manganese ions doped $ZnAl_2O_4$ shows a bright green emission at 510 nm from Mn^{2+} ions substituting for Zn^{2+} ions in the tetrahedral sites. In contrast to partially inverse $MgAl_2O_4$ spinel, normal $ZnAl_2O_4$ spinel cannot be doped with Mn^{4+} ions into the octahedral sites, i.e. does not demonstrate any Mn^{4+} luminescence since the charge compensation of Mn^{4+} ions substituting for Al^{3+} ions in the octahedral sites cannot be provided in cases of small degree of inversion in the $ZnAl_2O_4$ structure [2]. On the other hand, chromium ions doped $ZnAl_2O_4$ shows efficient Cr^{3+} luminescence with a zero-phonon line at 688 nm and vibronics due to the perfect normal spinel structure of synthesized $ZnAl_2O_4$ ceramics.

3.3 $LiAl_5O_8$

Manganese ions doped partially inverted $LiAl_5O_8$ shows intense Mn^{4+} red luminescence (662 nm). On the other hand, prolonged annealing at high temperature (1300 °C) leads to complete ordering of Li^+ and Al^{3+} in ratio 1:3 in different octahedral sites in the $LiAl_5O_8$ structure ($P4_132$ space group) in which Mn^{4+} luminescence is not observed due to the lack of a charge compensation mechanism [3,4]. In contrast, Cr^{3+} doping of $LiAl_5O_8$ does not need charge compensation and intense far-red Cr^{3+} luminescence at 714 nm is observed with well-pronounced zero-phonon lines and vibronic structure. The temperature dependencies of the intensity, spectral shift and width of R-lines of Cr^{3+} luminescence have been analyzed in the range of 80 - 295 K within the known models for optical centers in crystals. The observed dependencies have been considered for the possible use in luminescence thermometry

This work was supported by the Russian Science Foundation (RSF), project No. 18-13-00407.

References

1. N.M. Khaidukov, M.N. Brekhovskikh, N.Yu. Kirikova, V.A. Kondratyuk, V.N. Makhov, Russ. J. Inorg. Chem. **65**, 1135 (2020)
2. N.M. Khaidukov, M.N. Brekhovskikh, N.Yu. Kirikova, V.A. Kondratyuk, V.N. Makhov, Ceram. Int. **46**, 21351 (2020)
3. N.M. Khaidukov, M.N. Brekhovskikh, N.Yu. Kirikova, V.A. Kondratyuk, V.N. Makhov, Russ. J. Inorg. Chem. **67**, 547 (2022)
4. N.M. Khaidukov, M.N. Brekhovskikh, N.Yu. Kirikova, V.A. Kondratyuk, V.N. Makhov, J. Lumin. **248**, 118942 (2022)

Effects of spherical metallic nanoparticles plasmon on 4f–4f luminescence: a theoretical approach

Albano N. Carneiro Neto[1], *Marcos A.* Couto dos Santos[2], *Sarah M.* Bezerra[3], *Victoria* Levchenko[4], *Ricardo L.* Longo[5], *Oscar L.* Malta[5,i], *Renata* Reisfeld[4]

[1] Physics Department and CICECO, University of Aveiro, Aveiro, Portugal
[2] Departamento de Física, Universidade Federal de Sergipe/CCET, São Cristóvão/SE, Brazil
[3] Wigner Research Centre for Physics, Budapest University of Technology and Economics, Hungary
[4] The Hebrew University of Jerusalem, Chemistry Institute, Jerusalem, Israel
[5] Departamento de Química Fundamental, Universidade Federal de Pernambuco, Recife/PE, Brazil

Abstract. The main theoretical point of this presentation is centred on the influence of spherical metallic nanoparticles (NPs) on the 4f–4f luminescence of rare earth ions in bulk materials. Two aspects are emphasized: i) the balance between local field enhancement due to surface plasmons, nonradiative energy transfer from the rare earth ions to the NPs and nonradiative decays between 4f levels, which may result in luminescence enhancement or luminescence quenching; ii) the role that may eventually be played by the width of the bulk material sample, once the NPs absorption coefficient is very high [1,2]. Experimental cases are treated under the viewpoint of these theoretical aspects, namely, spherical silver and copper NPs. In the latter case, since copper NPs are easily oxidized, CuO NPs may play a significant role, through interband transitions, on the 4f–4f photophysical behavior [3].

Since the discovery of the Surface Enhanced Raman Scattering phenomenon (SERS), in 1974 [1], great advances raised on the influence of metallic nanoparticles (NPs) on the optical properties of composite materials [2-5]. Potential applications have readily appeared as luminescent functionalized NPs for bioassays, cell temperature sensors, photo and thermal therapy, and efficiency gain in photovoltaic cells. The cases of surface and bulk materials present quite different dependences on the shape, size, filling factor, and distribution (including possible agglomeration) of NPs. The latter case (bulk materials) has been theoretically approached for the first time in 1985 [2]. With excitation at 314 nm, the observed Eu^{3+} luminescence enhancement, by a factor of 7, apparently could be rationalized by the local field enhancement produced by the surface plasmons in silver NPs with a very small average radius of 1.8 nm.

Theoretical quantitative models describing the interaction of the effective field with the emitting ions, leading to emission enhancement (or quenching in certain conditions), have been developed in detail and quantified by the enhancement factor c_R [2-5], which is the ratio between the lanthanide emission intensities in the presence and absence of the NPs, being guaranteed that the number of emitters is the same in both cases. To summarize this effect, it is important to notice that it depends on the average distance between metallic NPs (R_0), the concentration, and the type of NPs used (*e.g.*, Ag, Cu). As illustrative examples, Fig. 1 shows the emission enhancement factor of Eu-based complexes in the presence of Ag-NPs (left panel)

[i] Corresponding author: oscar.malta@ufpe.br

and Cu-NPs/CuO-NPs (right panel). Further information on the Eu^{3+} complexes used as well as the c_R measurements can be found in references [3] and [5].

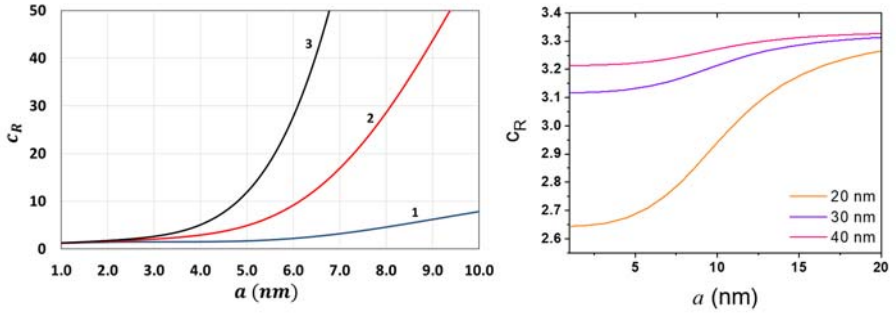

Fig. 1. **Left panel**: enhancement factor c_R as a function of spherical Ag-NPs of radius a and an average distance $R_0 = 30\ nm$. Curves **1**, **2**, and **3** stand for different nonradiative multiphonon rates from upper levels above the emitting one ($W = 10^3$, 10^4, and $10^5 s^{-1}$, respectively) [3]. **Right panel**: c_R as a function of the Cu-NPs/CuO-NPs of radius a and different average distances of R_0 (20, 30, and 40 nm) [5].

The great difference between the graphs above is the fact that the right one has the effect of the copper oxide NPs, and the fact that the Cu-NPs have plasmon band lying at much lower energy than the Ag-NPs plasmon band.

References

1. A.J. Fleischmann, M. Hendra, P.J. McQuillan, Raman spectra of pyridine adsorbed a silver electrode, Chem. Phys. Lett. 26 (1974) 163–166. https://doi.org/10.1016/0009-2614(74)85388-1
2. O.L. Malta, P.A. Santa-Cruz, G.F. De Sá, F. Auzel, Fluorescence enhancement induced by the presence of small silver particles in Eu^{3+} doped materials, J. Lumin. 33 (1985) 261–272. https://doi.org/10.1016/0022-2313(85)90003-1
3. A.N. Carneiro Neto, M.A. Couto dos Santos, O.L. Malta, R. Reisfeld, Effects of Spherical Metallic Nanoparticle Plasmon on 4f-4f Luminescence: A Theoretical Approach, in: L.R.P. Kassab, C.B. de Araujo (Eds.), Metal Nanostructures for Photonics, 1st ed., Elsevier, 2019: pp. 19–36. https://doi.org/10.1016/B978-0-08-102378-5.00002-7
4. X. Qin, A.N. Carneiro Neto, R.L. Longo, Y. Wu, O.L. Malta, X. Liu, Surface Plasmon–Photon Coupling in Lanthanide-Doped Nanoparticles, The Journal of Physical Chemistry Letters. 12 (2021) 1520–1541. https://doi.org/10.1021/acs.jpclett.0c03613
5. S.M. Bezerra, *et al*., submitted (2022).

Microspectroscopy of the single color centres in alkali halide crystals

Evgueni Martynovich[1,j], *Vladimir* Dresvyanskiy[1], *and Sergey* Zilov[1]

[1]Irkutsk Branch of Institute of Laser Physics, Siberian Branch, Russian Academy of Sciences, 664033, 130a, Lermontov Street, Irkutsk, Russia

Abstract. We present the results of study of the trajectories of luminescence intensity and the decay time constants of single color centers in lithium fluoride crystals irradiated with a small dose of X-ray radiation. The luminescence intensity trajectories exhibit blinking. The blink parameters are different for different centers of the same type, while their decay time constants are the same. These properties of single color centers in monocrystals are discussed in the paper.

The study of single quantum systems (atoms, molecules, defects in crystals, quantum dots, and others) by methods of luminescent microscopy is a relevant direction of modern research of substances and materials in physics, chemistry, and life sciences [1-2]. General interest in the study of luminescence of single centers is determined by the needs of development of theoretical concepts, as well as by the development of various applications. Coor centers in various crystals are widely used as working centers of gamma radiation detectors, track detectors of charged particles and mixed fields of nuclear radiation, optical media for storing visual and digital information, laser media and passive laser gates, thin-film storage luminescent screens for visualization and digitization of X-ray microimages. The development of new principles of spectroscopic differentiation of radiation defects, complementing the traditional spectral-kinetic methods, the application of new spectroscopic characteristics, is relevant. This is particularly emphasized by the practical significance of radiation defects, including color centers, that can be artificially created in condensed media by the action of hard radiation or laser radiation, and are used as model quantum systems in various fundamental studies.

Single color centers in alkali-halide crystals were studied for the first time by the authors of the publications [3-4]. They found that the time trajectories of luminescence intensity of the single color centers carry information about the electronic and structural dynamics of these centers. The parameters of such trajectories can serve as additional spectroscopic features that allow differentiating between centers of different types [3]. The aim of the presented studies is to investigate the possibilities of spectroscopic differentiation of individual types of luminescent defects induced by radiation in condensed media, based on comparison of generalized numerical characteristics of quantum trajectories of photoluminescence intensity, that are measured by confocal scanning luminescence microscopy on single defects in the mode of spatially selective time-correlated counting of single photons.

The registered trajectories and corresponding kinetic curves of two different single centers of the same type are shown in Fig. 1. The decay time constants for these centers are the same and equal to 26.5±1 ns. This confirms the identity of the nature of these two centers – they are centers of the same type. The presented trajectories of these two centers of the same type differ markedly in their form. The reasons for such differences may be different. The type of

[j]Corresponding author: femto@bk.ru

trajectories may depend on the intensity of the exciting radiation. However, in this experiment, the intensities were the same. Differences in the trajectory parameters may be caused by differences in the orientation of centers of the same type and corresponding differences in the efficiency of excitation of centers. In addition, inhomogeneous local intracrystalline fields can affect the trajectory parameters. To answer this question, a separate study is required.

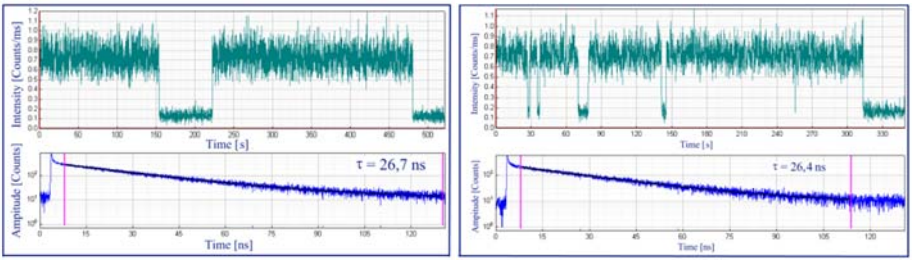

Fig. 1. Luminescence intensity trajectories and kinetic curves of two different single centers of the same type

In addition to the centers described above, we registered other defects in the crystals – well known F_2 centers. They were identified by the value of the luminescence decay time constant, equal to 17±2 ns. Thus, the problem of the difference in parameters of the luminescence intensity trajectories of different centers of the same type is a common problem and it needs to be studied specifically.

In our study we experimentally confirmed the feasibility and effectiveness of the method of laser confocal scanning luminescent spectroscopy of single radiation defects based on the characteristics of their photoluminescent trajectories. Dynamic models of F_2 and F_3^+ centers in lithium fluoride crystals were created. Using the mathematical apparatus for fluorescence of single molecules, in particular the equations for *on*– and *off*–intervals for a molecule with a triplet level, as the basis we introduced an additional equation describing the reorientation of the color center.

The work was carried out within the framework of the RAS Basic Research Plan for the period up to 2025, project No. 0243-2021-0004.

References

1. William E. Moerner. Nobel Lecture, December 8 (2014).
2. I.Yu. Eremchev, M. Yu. Eremchev, and A. V. Naumov, Phys. Usp. **62**, 3 (2019).
3. E.F. Martynovich, V.P. Dresvyansky, A.L. Rakevich, S.A. Zilov, S.V. Boychenko, and S. N. Bagayev, Differentiation of types of single radiation defects in crystals through the properties of their fluorescence intensity trajectories, in *Advanced Photonics, OSA (2015)*, paper SeW2B.5.
4. V.P. Dresvyansky, S.A. Zilov, E.F. Martynovich, Opt. and Spectr. **130**, 1 (2022).

Bringing luminescence thermometry to a higher level

Andries Meijerink[k]

Condensed Metter and Interfaces, Debye Institute, Utrecht University, The Netherlands

Abstract. Luminescence thermometry has rapidly developed in the past decades to a powerful method for remote temperature sensing. Here we first discuss basic principles and limitations to the sensitivity and accuracy of lanthanide based thermometers and the role of Boltzmann equilibrium, host lattice, photonic effects and brightness of the probes. Next, we demonstrate the unique capabilities of luminescence intensity ratio thermometry by discussing applications in catalysis, microfluidics and high resolution temperature mapping. We will end with an outlook on the future of luminescence nanothermometry.

Luminescence thermometry has rapidly developed in the past decades to a powerful method for remote temperature sensing. More recently, nanothermometry relying on the temperature dependent luminescence of lanthanide ions doped into nanocrystals has emerged, especially in biological applications for accurate sensing and mapping of temperature profiles in the range 270-330 K [1-3]. In our work, we have extended the temperature range to beyond 900 K by creating range temperature stable silica coated (upconversion) nanocrystals [4-6]. In the present study we first discuss fundamental aspects of luminescence thermometry, especially the role of Boltzmann equilibrium and a new theoretical approach to understand and predict the optimum single ion (nano)thermometer [7, 8]. Maximizing thermal sensitivity will be demonstrated with real-case examples based on these predictions. Models for the failure of the Boltzmann distribution as well as possible approximations frequently encountered in the applied field of *in vivo* imaging are presented. These considerations have resulted in a fully predictive model and clear guidelines for designing the most suitable ratiometric lanthanide-based luminescent thermometer dependent on the desirable application. Temperature accuracy is important and reports relying solely on the relative sensitivity S_r tend to ignore the fact that artefacts, spectral noise and photonic effects affect the overall accuracy. We will show here that the optimum accuracy that can be realized is above 0.1 K and that noise reduction by designing highly efficient luminescent (nano)probes is crucial to realize high accuracy.

In the second part of the talk examples of the unique capabilities of luminescence nanothermometry will be given. Temperature mapping with μm resolution is demonstrated to probe temperature variation in microheaters used in synchrotron and TEM experiments (Figure 1). Temperature sensing in catalytic reactors under realistic operating conditions is demonstrated and shown to be capable of measuring spatial and temporal temperature variations inside catalytically active particles. In the field of microfluidics measuring temperature inside the microchannels is notoriously difficult. For three different types of microfluidic reactors, it will be shown how including nanoparticles in the flow medium allows for temperature sensing inside microchannels (Figure 2). To conclude, an outlook will be given towards the future of lanthanide doped nanoparticles temperature sensing.

[k]Corresponding author: a.meijerink@uu.nl

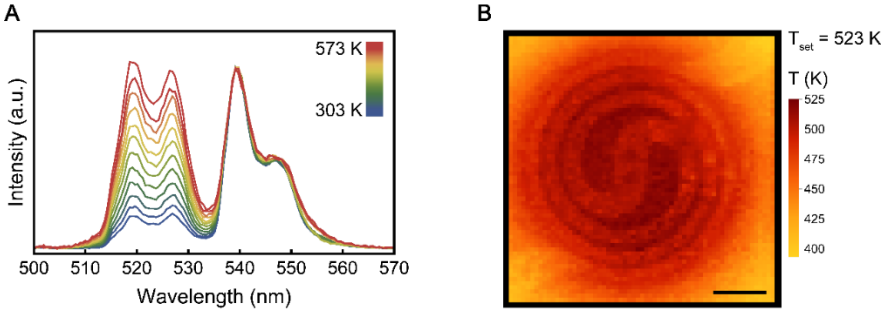

Fig. 1. (A) Luminescence spectra of NaYF4:Er3+(2%), Yb3+(18%) NCs upon excitation with 980 nm light at varying temperatures. At higher temperatures the 2H11/2 emission (510 – 530 nm) is increased with respect to the 4S3/2 emission (537 – 560 nm) (B) Temperature map of a spiral-shaped microheater at 523 K. The scale bar corresponds to a length of 50 µm.

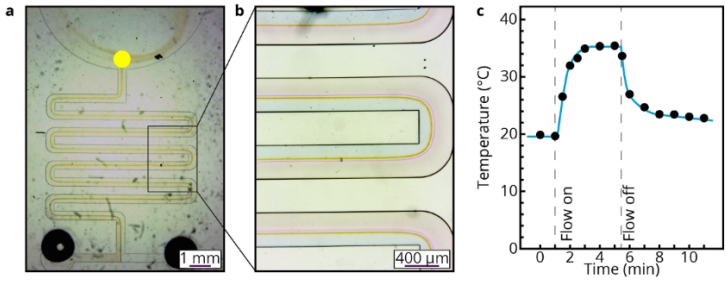

Fig. 2. (a) PDMS microfluidic device. Optical microscopy image of a simple microfluidic device (a) with two inlets in which concentrated ammonia (5M) and hydrochloric acid (4M) are introduced in combination with a pH indicator thymol blue. The limited mixing is visualized with the indicator having the red colour at low pH, yellow colour at intermediate pH and blue colour at high pH (b). Temperature measurements which show the rise in temperature due to the exothermic reaction between ammonia and hydrochloric acid (c). The yellow circle in a indicates the spot used for temperature sensing using luminescence thermometry with $NaYF_4$ NPs added to both solutions.

References

1. D. Jaque, F. Vetrone, Nanoscale **4**, 4301-4326 (2012)
2. C. D. S. Brites *et al.*, *Nanoscale 4*, 4799-4829 (2012)
3. C. D. S. Brites, A. Millán, L. D. Carlos, Lanthanides in Luminescent Thermometry, in: Handbook on the Physics and Chemistry of Rare Earths (eds.: J.-C. Bünzli, V.K. Pecharsky), Vol. **49**, Ch. 281, pp. 339-427, Elsevier, Amsterdam (2016).
4. R. G. Geitenbeek et al., ACS Catal. **8**, 2397-2401
5. R. G. Geitenbeek et al., Chem. Eng. Sci. **198**, 235-240 (2019)
6. R. G. Geitenbeek, Lab Chip **19**, 1236-1246 (2019)
7. R. G. Geitenbeek, H. W. de Wijn, A. Meijerink, Phys. Rev. Appl. **2018**, 10, 064006 (2018)
8. M. Suta, A. Meijerink, Adv. Theory Sim. **3,** 2000176 (2020)

Pulse area theorem and ROSE protocol of optical memory in a crystal waveguide

Sergei A. Moiseev[1,l], *Aleksandr V.* Pavlov[1], *Mansur M.* Minnegaliev[1], *Konstantin I.* Gerasimov[1], *Evgeniy S.* Moiseev[1], *Timur* Rupasov[1], *Aleksandr* Kalinkin[2] and *Sergei* Kulik[2]

[1]Kazan Quantum Center, Kazan National Research Technical University, Kazan, Russia
[2]Quantum Technologies Center and Faculty of Physics, M.V. Lomonosov Moscow State University, Moscow, Russia

Abstract. In this work, we implemented an optical quantum memory protocol in the revival of silenced photon echo for light pulses in a Tm^{3+}:$Y_3Al_5O_{12}$ crystal with laser-written single-mode waveguide. The structure of optical waveguide mode, absorption coefficient, coherence time and inhomogeneous broadening of the optical transition of the thulium ions in the waveguide were experimentally determined. We also derived pulse area theorem for the light pulse propagation in an optical waveguide with two-level medium and found its analytical solution for Gaussian spatial mode of the light beams. The theory was applied for the description of experimental data obtained in realized quantum memory protocol. Possible ways to improve the basic parameters of the quantum memory protocol were discussed.

Optical quantum memory (QM) provides storage of quantum light with its subsequent retrieval on demand at arbitrary time [1]. Recent progress in the integrated photonics pushes the creation of on-chip QMs, which will become the key tools in many quantum technologies [2]. The laser-written waveguides in crystals doped with rare-earth ions (REI) seem as a convenient platform for investigation of on-chip QMs. Solids with REI provide long coherence time (phase relaxation time T_M) of optical and spin quantum transitions. Recently, several experiments demonstrated optical storage in such REI-doped waveguides [3-5]. Using photon echo AFC-protocol, the quantum storage was demonstrated for heralded photons [3], frequency-multiplexed fields [4], on demand qubit storage [5].

In this work, we used Tm^{3+}:$Y_3Al_5O_{12}$ crystal with doping concentration of 0.01 % and dimensions 2x9x19.5 mm and fabricated type-III laser-written waveguides. The advantage of these waveguides is the possibility of light propagation with arbitrary polarization. The created waveguide supports the transverse Gaussian fundamental light mode (membrane mode function $f(r_\perp)$ with half width $a \approx 5.5$ μm on half maximum for both axis) with the parameters of the waveguide: diameter - 18 μm, vertical polarization losses (parallel to 2 mm edge) - 0.66 dB/cm, horizontal losses (parallel to 19.5 mm edge) - 1.13 dB/cm. We defined optical transition absorption for bulk crystal - αL=0.266 and for the waveguide - αL= 0.12±0.04, respectively (L=19.5 mm). We also investigated the absorption line of Tm ions transitions in the waveguide compared it to bulk crystal. Central absorption line is ν_0=378.130 THz (793.377 nm) for bulk crystal and ν_0=378.140 THz (793.356 nm) for the waveguide. From the two-pulse photon echo experiment, we defined the coherence time in the bulk crystal T_M=72.2μs (x=1.55) and in the waveguide T_M =63 μs (x=1.82).

Next, for the first time, we implemented the revival of silenced echo (ROSE) protocol in the fabricated single-mode waveguide. The storage of coherent optical pulses attenuated to the

[l] Corresponding author: s.a.moiseev@kazanqc.org

level of one photon field in the silent echo with an equal signal-to-noise ratio has been achieved. It was observed that the retrieval efficiency of the input signal decreased despite the use of rephasing pulses with amplitude and frequency modulation. We correlate this effect with the instantaneous spectral diffusion of atomic frequencies. The experimentally achieved efficiency of restoring input pulses was 0.5% with a storage time of 30 μs, with the maximum achievable efficiency $\eta_{max} = 0.76\%$.

To explain the observed experimental data, we develop theory of light pulse propagation and photon echo irradiation in an optical waveguide. Considering the transverse structure of the waveguide light mode and its interaction with atoms, we derive the equations for the pulse areas of exciting pulses (n=1,2,3) and echo signal (e). The equations for the pulse areas of exciting pulses are:

$$\frac{\partial \vartheta_n(z)}{\partial z} = \sum_{m=1}^{M} \frac{\beta_m}{2S} \iint_S dr_\perp \Omega_m(r_\perp) w_{1,2,3}(r_\perp, z) sin\big(\Omega_m(r_\perp)\vartheta_{1,2}(z)\big), \qquad (1)$$

where $\vartheta_n(z) = \int dt \alpha_n(t,z)$, (n=1,2,3,e), $\beta_m = \frac{4\pi G(0) N_m}{v_g L}$, S - cross-section, v_g is a group velocity of light mode, N_m - number of atoms with dipole moment $\vec{d}_m$, G(Δ) – inhomogeneous broadening of atomic transition, L - length of the waveguide, $w_{1,2}(r_\perp) = -1/2$, $w_3(r_\perp, z) = -\frac{1}{2} cos(\Omega_m(r_\perp)\vartheta_1(z))$, $\Omega_m(r_\perp) = \Omega_m f(r_\perp)$, $\Omega_m = E_0(\vec{d}_m \vec{e})/\hbar$, and $E_0 \alpha_n(t), \vec{e}$ - amplitude, polarization of the fields.

Considering the membrane function $f(r_\perp)$ of Gaussian spatial shape in (1), we obtain the following equation for $\vartheta_1(z)$ of first exciting pulse:

$$\frac{\partial \vartheta_1(z)}{\partial z} = -\sum_{m=1}^{M} \frac{\varkappa_m}{\Omega_m} \frac{sin^2\left(\frac{\Omega_m \vartheta_1(z)}{2}\right)}{\frac{\Omega_m \vartheta_1(z)}{2}}, \qquad (2)$$

where $\varkappa_m = \frac{\pi \Omega_m^2 \beta_m}{a^2 S}$ – absorption coefficient due to the interaction with m-atomic group.
In the case of single atomic group (M=1), we find the solution of (2) for $\Theta_1(z) = \Omega_1 \vartheta_1(z)$:

$$\mathrm{T}(\Theta_1(z)) = \mathrm{T}(\Theta_1(0)) - z/2 \qquad (3)$$

where $\mathrm{T}(\Theta) = \ln(\sin(\Theta/2)) - \frac{1}{2}\Theta\,\mathrm{ctg}(\Theta/2)$, which shows formation of $n2\pi$ – pulses, but in the absence of branching points of solutions: $\pi, 3\pi, \ldots$, which hold for the McCall and Hahn area theorem. Developing the pulse area theorem (1), (2) and using photon echo pulse area theorem [6], we obtained the equation for the echo pulse area in the single mode waveguide:

$$\frac{\partial \vartheta_e}{\partial z} = \sum_{m=1}^{M} \frac{\beta_m}{2S} \iint_S dr_\perp \Omega_m(r_\perp)\big\{2P_{m,e}(r_\perp, z) cos^2(\Omega_m(r_\perp)\vartheta_e) + w_m(r_\perp, z) sin(\Omega_m(r_\perp)\vartheta_e)\big\}, \qquad (4)$$

where $P_{m,e}(r_\perp, z) = e^{-4\tau/T_2} \Omega_m(r_\perp)\vartheta_1(z) \prod_{p=2}^{3} sin^2\big(\Omega_m(r_\perp)\vartheta_p(z)\big)$ is a phasing coherence of m-th atomic group, $w_m(r_\perp, z) = -\prod_{p=2}^{3} cos\big(\Omega_m(r_\perp)\vartheta_p(z)\big)$ – the component of an atomic inversion slowly varying on the frequency, τ – time delay between first two pulses .

The experimental data obtained in the implemented waveguide ROSE-protocol are analyzed using the solution of (4) and we discuss possible ways to improve the basic parameters of the QM protocol.

The study was conducted with the financial support of the Ministry of Education and Science of Russia № NIOKTR 121020400113-1.

References

1. A. I. Lvovsky, B. C. Sanders, and W. Tittel, Nat. photonics 3, 706464 (2009).
2. J.-H. Kim, et.al, Optica 7, 291 (2020).
3. M. F. Askarani, et.al, Phys. Rev. Appl. 11, 054056 (2019).
4. A. Seri, et.al, Phys. Rev. Lett. 123, 080502 (2019).
5. C. Liu, et.al, Phys. Rev. Lett. 125, 260504 (2020).
6. S. A. Moiseev, M. Sabooni, and R. V. Urmancheev, Phys. Rev. Res. 2, 012026(R) (2020).

Charge transfer excitons in HTSC cuprates and nickelates

Alexander Moskvin[m]

Department of Theoretical Physics, Ural Federal University, 620083 Ekaterinburg, Russia

Abstract. We argue that the charge transfer (CT) transitions and CT excitons not only determine the optical response of strongly correlated 3d compounds over a wide energy range, but also, in many cases, are a precursor to the formation of unusual phase states. The paper discusses the role of CT excitons in the formation of exotic normal and HTSC (high-T_c supeconducting) states of "old" cuprates and "novel" nickelates.

It is now believed that the most intensive low-energy electron-hole excitations in insulating 3d oxides correspond to the charge transfer (CT) transitions while different phonon-assisted crystal field transitions are generally much weaker. Namely the CT transitions are considered as a likely source of the optical response of the parent quasi-2D cuprates (La_2CuO_4, …) and nickelates such as $NdNiO_2$ in a wide spectral range 1-10 eV, in particular, the fundamental absorption edge. Low-energy inter-cluster transfer $[CuO_4]^{6-}$-$[CuO_4]^{6-} \rightarrow [CuO_4]^{7-}$-$[CuO_4]^{5-}$ ($[NiO_4]^{7-}$-$[NiO_4]^{7-} \rightarrow [NiO_4]^{8-}$-$[NiO_4]^{6-}$), symbolically 11 → 02, 20, under photoexcitation in parent cuprates (nickelates), or Franck-Condon CT-transition, does create a bounded electron-hole (EH) pair, or CT exciton, and defines an optical CT gap U_{opt}, or effective local correlation parameter U, with a magnitude near 2.0 eV (1.5 eV), typical for all the undoped cuprates with the T-type (T′-type) structure (see Fig. 1) characterized by the presence (absence) of apical oxygen above/below the CuO_2 planes [1,2]. Such an exciton is a fairly stable entity with a "length" of the order of 8 Å , which is especially clearly visible in linear and nonlinear optical response for 1D cuprates [3]. However, after photoexcitation, the strong electron-lattice polarization effects lead to a relaxation of these CT excitons with the formation of localized low-energy metastable polaronic-like EH dimers, or, more precisely, coupled electron and hole centers (02, 20) with the true thermal, or adiabatic CT gap U_{th} as small as 0.4-0.5 eV in parent insulating T-type cuprates [4], while for parent apexless T′-cuprates this value can be close to zero, or even negative. The Fig.1 describes the dramatic effect of a relatively small decrease in U_{opt} from ∼2 eV to ∼1.5 eV (either due to screening as a result of doping, or due to a change in the "out-of-plane stuff"), at which U_{th} turns into zero or even changes the sign and the system becomes unstable with respect to disproportionation 11 → 20 (02) and formation of the system both of coupled and individual electron and hole centers.

In other words, all the three charge centers (charge triplet) $[CuO_4]^{5-,6-,7-}$ ($[NiO_4]^{6-,7-,8-}$) must be considered on equal footing [4]. The EH dimers can be the progenitors of several new phases, however, the ground state of the CuO_2/NiO_2 planes will be the result of the competition between charge and spin fluctuations. At some critically low energy U_{th}, it is the system of charge triplets, rather than a simple antiferromagnetic insulator, that can form the ground state of the parent cuprates/nickelates.

[m] Corresponding author: alexander.moskvin@urfu.ru

In accordance with experimental data for apexless cuprates and nickelates [5,6] we argue that not only antiferromagnetic insulating (AFMI), but charge ordered (CO), bosonic superconducting (BS), and Fermi-liquid (FL) phases are possible phase states of a model parent cuprate/nickelate, while typical phase state of a doped system, in particular, mysterious pseudogap phase in cuprates, is the result of a phase separation [7].

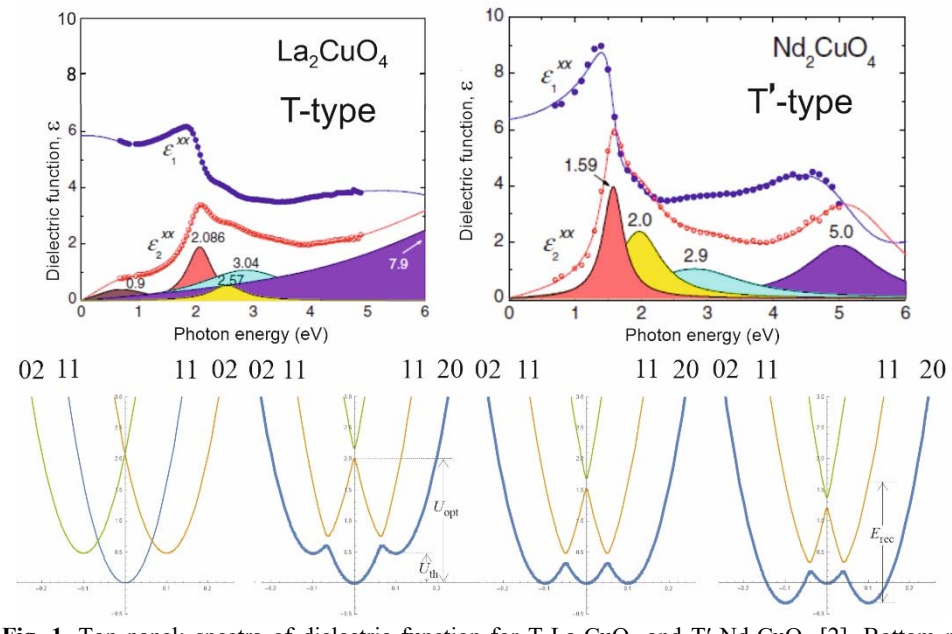

Fig. 1. Top panel: spectra of dielectric function for T-La_2CuO_4 and T′-Nd_2CuO_4 [2]. Bottom panel: simplified potential energy curves (adiabatic potentials) for the "11-02-20 problem".

Support from the Ministry of Science and Higher Education of the Russian Federation (project # FEUZ-2020-0054) is acknowledged.

References

1. A.S. Moskvin, R. Neudert, M. Knupfer et al., Phys. Rev. B **65**, 180512(R) (2002)
2. R.V. Pisarev, V.V. Pavlov, A.M. Kalashnikova, A.S. Moskvin, Phys. Rev. B **82**, 224502 (2010)
3. A.S. Moskvin, J. Malek, M. Knupfer et al., Phys. Rev. Lett. **91**, 037001 (2003)
4. A.S. Moskvin, Phys. Rev. B **84**, 075116 (2011)
5. M. Naito, Y. Krockenberger, A. Ikeda et al., Physica C **523**, 28 (2016)
6. D. Li, K. Lee, B.Y. Wang et al., Nature (London) **572**, 624 (2019)
7. A.S. Moskvin, Yu.D. Panov, JMMM, **550**, 169004 (2022)

Terahertz optical activity and gyrotropic birefringence in rare-earth magnetoelectrics

A.A. Mukhin[1,n], *A.M.* Kuzmenko[1], *V.Yu.* Ivanov[1], *A.* Shuvaev[2], *A.* Pimenov[2]

[1]Prokhorov General Physics Institute of the Russian Academy of Sciences, Moscow, Russia
[2]Institute of Solid-State Physics, Vienna University of Technology, Vienna, Austria

Abstract. Terahertz spectroscopic investigations of the polarization plane rotation determined by natural optical activity and gyrotropic birefringence near crystal field electron transitions were performed in rare earth magnetoelectric alumoborates $TmAl_3(BO_3)_4$, $YAl_3(BO_3)_4$:Tm (5%) and $YbAl_3(BO_3)_4$) and Nd langasite. The data were analyzed in terms of allowed magnetoelectric coupling.

It is now well established that magnetoelectric coupling manifests itself not only in static properties, but also in a various spectroscopic (dynamic) phenomena. Among the latter, one can note a directional dichroism and strong optical activity (i.e. polarization plane rotation), which are caused by the cross-coupling of electric and magnetic components, especially near the frequencies of intrinsic excitations (electromagnons) and are described by dynamic magnetoelectric susceptibility. Here we present results of terahertz spectroscopic investigations of the optical activity (both natural and magnetic field induced) near crystal field (CF) electron transitions in rare earth magnetoelectric alumoborates $TmAl_3(BO_3)_4$, $YAl_3(BO_3)_4$:Tm (5%) and $YbAl_3(BO_3)_4$) and Nd langasite. The polarization measurements of the transmission spectra T(ω) and polarization plane rotation were carried out by a

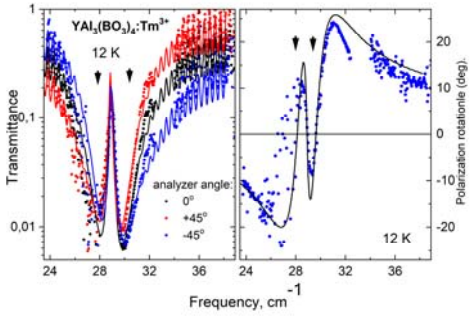

Fig. 1. Transmission spectra for ac magnetic field **h**⊥*c*-axis (left) and polarization rotation (right) of $YAl_3(BO_3)_4$:Tm^{3+} c-cut plate near $A_1 \rightarrow E$ CF transition in Tm^{3+} split due to random local distortions Points – experiment, solid lines – theory.

quasioptical backward - wave-oscillator spectrometer in the frequency range 10 – 40 cm^{-1} (300 – 1000 GHz) at temperatures 4 - 300 K in magnetic fields up to 7 T.

Strong natural optical activity was revealed in Tm^{3+} (for both pure and diluted alumoborites) near the CF transitions from the lowest singlet A_1 to the next excited doublet E split by the crystal field of D_3 symmetry (Fig.1). Fine structure of the transitions was also observed at low temperatures which were assigned to random distortions of the local CF [1].

[n] Corresponding author: mukhin@ran.gpi.ru

The transmission and natural optical activity spectra are explained and quantitatively described by contributions of both magnetic and electric dipolar CF transitions to dynamic magnetic, magnetoelectric and dielectric susceptibilities taking into account also distortions of the local CF. It is shown that these transitions also determine static field induced magnetoelectricity in $TmAl_3(BO_3)_4$.

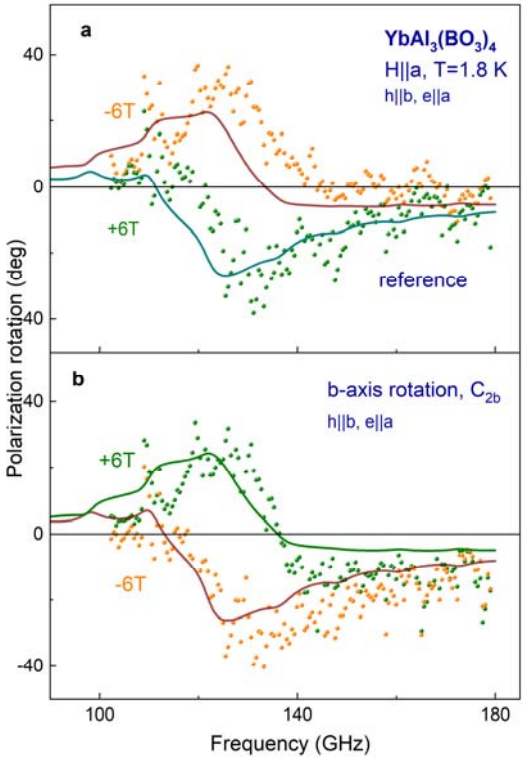

Fig. 2. Evolution of the spectra of polarization rotation in $YbAl_3(BO_3$ near electromagnon excitation determined by ground Yb^{3+} doublet split in the field H||a for different experimental geometries simulating changing of the natural optical activity and gyrotropic birefringence contributions. Points - experiment, lines - theory.

In magnetoelectric $YbAl_3(BO_3)_4$ in transverse magnetic field H||a inducing the electric polarization P||a we observed the electron transitions in the ground Kramers Yb^{3+} doublet which are excited either by magnetic (h||b, e||a) or electric (h||a, e||b) *ac* fields (electromagnon) and revealed significant polarization plan rotation exhibiting change sign under both time and space inversion inherent to the gyrotropic birefringence [2]. In these experiments the time inversion was realized by a changing of the applied field sign (H→-H), while the space inversion was simulated by the sample rotation around the b^* axis (C_{2b}). In all geometries the rotation angle near the resonance is inverted if the external magnetic field changes sign or after the sample rotates around the *b* axis while it remains the same under both simultaneous operations (Fig.2). This proves that the polarization rotation in $YbAl_3(BO_3)_4$ must be classified as gyrotropic birefringence [3]. In addition, a nonperfect asymmetry is observed after the field reversal and the sample rotation, indicating on an additional contribution identified with the natural optical activity. We have developed theory which considers magnetoelectric contribution to the spin Hamiltonian of the ground Yb^{3+} doublet and have calculated dynamic magnetic, magnetoelectric and dielectric susceptibilities and simulated the observed transmission and

polarization rotation spectra which made it possible to describe the last ones. It was shown that the $\chi^{me}_{yy} \equiv \chi^{me}_{bb}$ component in the magnetoelectric susceptibility tensor is mainly responsible for the observed phenomena. It includes magnetoelectric contributions determining both the gyrotropic birefringence and natural optical activity and their connection to observed static magnetoelectric $YbAl_3(BO_3)_4$ properties was found.
Our spectroscopic study of $Nd_3Ga_5SiO_{14}$ langasite, where Nd ions occupy lower symmetry (C_2) sites, also showed existence of resonance magnetoelectric excitations.

This work was supported by the Russian Science Foundation (No. 22-42-05004).

References

1. A.M. Kuzmenko, A.A. Mukhin, V.Yu. Ivanov et al., Phys. Rev. B **94**, 174419 (2016).
2. R. M. Hornreich and S. Shtrikman, Phys. Rev. **171**, 1065 (1968).
3. A.M. Kuzmenko, V. Dziom, A. Shuvaev, et al., Phys. Rev. B **99**, 224417 (2019).

Site-selective laser spectroscopy and EPR of SrY_2O_4 crystals doped with Ho^{3+}, Yb^{3+} and Nd^{3+} ions

Sergey Nikitin[1,o], *Boris* Malkin[1], *Roman* Yusupov[1], *Gilman* Shakurov[2], *Bulat* Gabbasov[1], *Ruslan* Batulin[1], *Airat* Kiiamov[1], *Ekaterina* Kutasheva[1], *Ivan* Mumdzhi[1]

[1]Institute of Physics, Kazan Federal University, Kazan, Russia
[2]Zavoisky Physical-Technical Institute, FRC Kazan Scientific Center of RAS, Kazan, Russia

Abstract. No

One of the modern research areas in condensed matter physics is the search for new phases in various materials, in particular, in frustrated magnets (magnetic ion system with competing exchange interactions). It has been found recently that in SrR_2O_4 and BaR_2O_4 compounds, where R is a rare earth ion, due to a quasi-1D crystal structure, geometric frustration and particular rare earth ion Stark multiplet pattern unusual ground states are realized. These states are stabilized at the temperatures much lower than it is expected from the values of the magnetic ion-ion interactions. Among the peculiar properties of the up-to-date studied compounds one can mention a coexistence of a long-range antiferromagnetic and a short-range incommensurate magnetic order in $SrEr_2O_4$ [1] and $SrHo_2O_4$ [2], noncollinear magnetic structure in $SrYb_2O_4$ [3] and the absence of long-range magnetic correlations in $SrDy_2O_4$ [4] down to the lowest temperatures achieved in the experiment. Unusual and coexisting magnetic structures with different propagation vectors in external magnetic fields in the crystals of $SrNd_2O_4$ [5] and $SrHo_2O_4$ [6] were discovered.

To clarify the origin and simulate unusual magnetic properties of these compounds representing geometrically frustrated multisublattice magnets with quasi-1D crystal structure, it is necessary to determine energy spectrum of the magnetic subsystem formed by rare-earth ions. One of the possible ways to find energy spectrum structure of rare earth ions at two nonequivalent crystallographic sites of SrR_2O_4 is an investigation of the energy spectrum of isostructural SrY_2O_4 crystals doped with low concentration of rare earth ions by site selective laser spectroscopy and EPR. Results of our successful implementation of the approach for study of SrY_2O_4:Er^{3+} crystal have been published in 2015 [7].

In our talk, we will discuss the results of the site-selective laser spectroscopy and EPR study of SrY_2O_4 crystals doped with Ho^{3+}, Yb^{3+} and Nd^{3+} ions. Site-selective laser spectroscopy indicates that in all investigated crystals more than two types of rare earth ion centers are formed, not only at Y(1) and Y(2) sites. For example, impurity centers of Nd^{3+} ions at the Sr^{2+} cites were observed. Site-selective spectroscopy has allowed us to elucidate the Stark structure of rare earth ion centers at intrinsic Y(1) and Y(2) sites. Calculations of the crystal field splittings for the ground and excited multiplets of RE ions agree well with optical and EPR spectroscopy results.

References

[o] Corresponding author: sinikitin1@gmail.com

1. O. A. Petrenko, G. Balakrishnan, N. R. Wilson, S. de Brion, E. Suard, and L. C. Chapon, Phys. Rev. B **78**, 184410 (2008).
2. J.-J. Wen, W. Tian, V. O. Garlea, S. M. Koohpayeh, T. M. McQueen, H.-F. Li, J.-Q. Yan, J. A. Rodriguez-Rivera, D. Vaknin, and C. L. Broholm, Phys. Rev. B **91**, 054424 (2015)
3. D. L. Quintero-Castro, B. Lake, M. Reehuis, A. Niazi, H. Ryll, A. T. M. N. Islam, T. Fennell, S. A. J. Kimber, B. Klemke, J. Ollivier, V. Garcia Sakai, P. P. Deen, H. Mutka, Phys. Rev. B **86**, 064203 (2012).
4. T. H. Cheffings, M. R. Lees, G. Balakrishnan, and O. A. Petrenko, J. Phys.: Condens. Matter **25**, 256001 (2013)
5. N. Qureshi, A. R. Wildes, C. Ritter, B. Fåk, S. X. M. Riberolles, O. A. Petrenko, Phys. Rev. B **103**, 134433 (2021)
6. Olga Young, Dmitry D. Khalyavin, Oleg A. Petrenko, Crystals **9**, 488 (2019)
7. B.Z. Malkin, S.I. Nikitin, I.E. Mumdzhi, D.G. Zverev, R.V. Yusupov, I.F. Gilmutdinov, R. Batulin, B.F. Gabbasov, A.G. Kiiamov, D.T. Adroja, O. Young, and O.A. Petrenko, Phys. Rev. B. **92**, 094415 (2015)

Linear and nonlinear optical spectroscopy of 3d exciton states in copper metaborate CuB_2O_4

Roman Pisarev[p]

Ioffe Physical Technical Institute, Russian Academy of Sciences, 194021 St Petersburg, Russia

Abstract. Copper metaborate CuB_2O_4 is a unique 3*d* oxide in which its crystallographic, magnetic, optical and magneto-optical properties are defined by the Cu^{2+} ($3d^9$) ions. In this talk, we will discuss our results on both linear and nonlinear spectroscopic study of this material during several years. CuB_2O_4 is characterized by very strong photoluminescence which is unusual for magnetically ordered Cu^{2+} oxides. In addition, we will discuss results on reciprocal and non-reciprocal second harmonic generation and propagation of light by solving the Maxwell equations.

1 Introduction

During the last decade, copper metaborate CuB_2O_4 became a subject of active and sometimes controversial research. This material has a complex non-centrosymmetric crystal structure *-42m* in which magnetic Cu^{2+} ions ($3d^9$, S=1/2) occupy the 4*b* and 8*d* distinctly different crystallographic positions [1]. The 4*b* subsystem is ordered antiferromagnetically below T_{N1}=21 K, whereas the 8*d* subsystem becomes only partly ordered below T_{N2}~9 K. Magnetic interactions between 4*b* and *8d* ions result in complex magnetic phase diagram with commensurate and incommensurate spin structures [2].

2 Electronic (exciton) structure and absorption spectra

Electronic structure of the $3d^9$ states of Cu^{2+} ions at the 4*b* (planar square of O^{2-} ligands (local symmetry -4) and 8*d* (distorted octahedron, symmetry 2) positions is shown in Fig. 1. Though the environment and the local symmetry at both positions are different, in overall the energy positions of electronic states differ by only ~10% (Fig. 1). The absorption α spectrum is shown in Fig. 2 [3]. It is characterized by narrow lines attributed to zero-phonon (ZP) lines (Frenkel excitons) each being followed by rich and well resolved sequence of phonon sidebands. ZP lines are reliably attributed to exciton transition at both Cu^{2+} subsystems according to the scheme shown in Fig. 1. The absorption spectra are strongly polarized. For example, the absorption of the 4*b* subsystem is strongly suppressed in the π spectrum, whereas that due to the 8*d* subsystem is well pronounced in the α, σ, and π spectra. Another interesting difference between exciton absorption in the Cu^{2+} subsystems should be marked – while sharp 4*b* exciton lines rapidly broaden and disappear above T_N=21 K, by contrast the 8*d* lines survive up to about 150 K. Zeeman and Davydov splitting of Frenkel excitons, and the theoretical model were reported in [4].

[p] Corresponding author: pisarev@mail.ioffe.ru

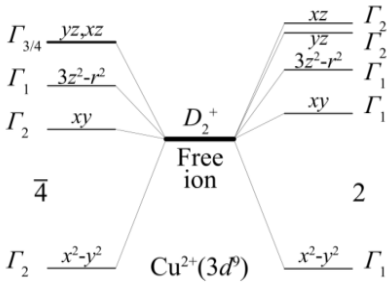

Fig 1. Electronic (exciton) structure of 4*b* (left) and 8*d* (right) Cu^{2+} ions.

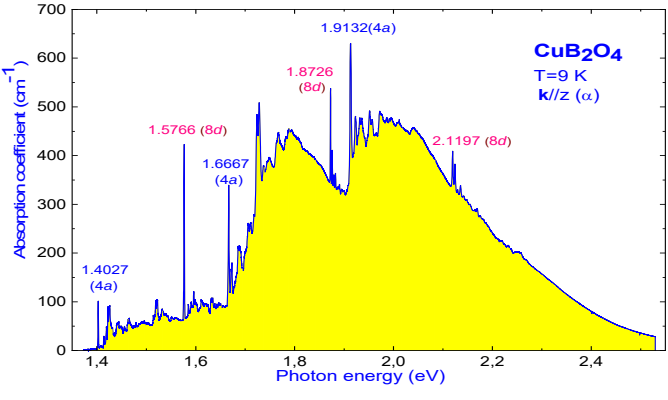

Fig 2. Absorption α-spectrum of CuB_2O_4 at T=9 K for the propagation of light along the optical z axis

Summarizing the main results on the absorption spectra, we can say that they differ radically from the spectra of other 3d magnetic oxides. Such differences are the presence of unusually narrow lines in both subsystems and an unusual structure of phonon sidebands.

3 Exciton and exciton-magnon photoluminescence

CuB_2O_4 is characterised by an unusually strong photoluminescence originating from the (*xy*) exciton (Γ_2) at ~1.404 eV [5]. We identify multiple emission lines, and among them we distinguish three sets of lines, each composed of an exciton line and a satellite attributed to magnon-assisted exciton recombination. The emission intensity of the three sets changes strongly in the temperature range 1.7–40 K, showing pronounced correlations with the magnetic phase transitions between the commensurate and incommensurate phases.

4 Optical second harmonic generation (SHG) on excitons

Noncentrosymmetric crystal structure of CuB_2O_4 open up interesting possibilities to detect SHG on exciton lines as it was realized in [6,7]. We demonstrated mechanisms of SHG reciprocity breaking due to the toroidal dipole moment which characterizes nontrivial spatial distributions of spins. We showed that 100% SHG nonreciprocity is observed for opposite magnetic fields. The experimental results are corroborated by theoretical analysis.

5 Reciprocal and non-reciprocal propagation of light

A description of the magnetic and antiferromagnetic nonreciprocal propagation of light in CuB_2O_4 based on space and time symmetry considerations was reported in [8]. We employed the expansion of the dielectric permittivity tensor as a function of the wave vector of propagating light, an applied magnetic field, and the antiferromagnetic and ferromagnetic order parameters. All these contributions to the dielectric permittivity serve as a basis for solving the relevant Maxwell's equations.

References

1. M. Martinez-Ripoll, S. Martinez-Carrera, and S. Garcia-Blanco, Acta Cryst. B **27**, 677 (1971)
2. A.E. Petrova and A. I. Pankrats, J. Exp. Theor. Phys. **126**, 506 (2018)
3. R.V. Pisarev, A.M. Kalashnikova, O. Schops, *et al*, Phys. Rev. B **84**, 075160 (2011)
4. N.E. Kopteva, D. Kudlacik, D.R. Yakovlev, M.V. Eremin, *et al*, Rev. B **105**, 024421 (2022)
5. D. Kudlacik, V.Y. Ivanov, D. R. Yakovlev, V.F. Sapega, *et al*, Phys. Rev. B **102**, 035128 (2020)
6. R.V. Pisarev, I. Sänger, G.A. Petrakovskii, *et al*, Phys. Rev. Lett. **93**, 037201 (2004)
7. J. Mund, D. R. Yakovlev, A.N. Poddubny, *et al*, Phys. Rev. B **103**, L180410 (2021)
8. A.I. Nikitchenko and R.V. Pisarev, Phys. Rev. B **104**, 184108 (2021)

Quantum information processing using Stark effect

Konstantin Pukhov[1, q] and *Sergey* Sekatskii [2]

[1]Prokhorov General Physics Institute of the Russian Academy of Science, Moscow, Russia
[2]Laboratory of Biological Electron Microscopy (LBEM), IPHYS, Ecole Polytechnique Fédérale de Lausanne (EPFL), and Department of Fundamental Biology, Faculty of Biology and Medicine, University of Lausanne, Lausanne, Switzerland

Abstract. Here we consider the quantum computer hardware based on rare-earth and transition metal ions implanted in inorganic crystals. In a two-level approximation, ions are considered as qubits occupying the state |0> if unexcited and |1> if excited. A distinctive feature of the device is the use of the Stark effect to control qubits.

1 The principle of operation

The luminescent properties of rare earth ions in crystals make them attractive as hardware for quantum computers and their use in various quantum information processing devices [1,2,3]. The principle of operation of the proposed device is illustrated in Fig. 1 below.

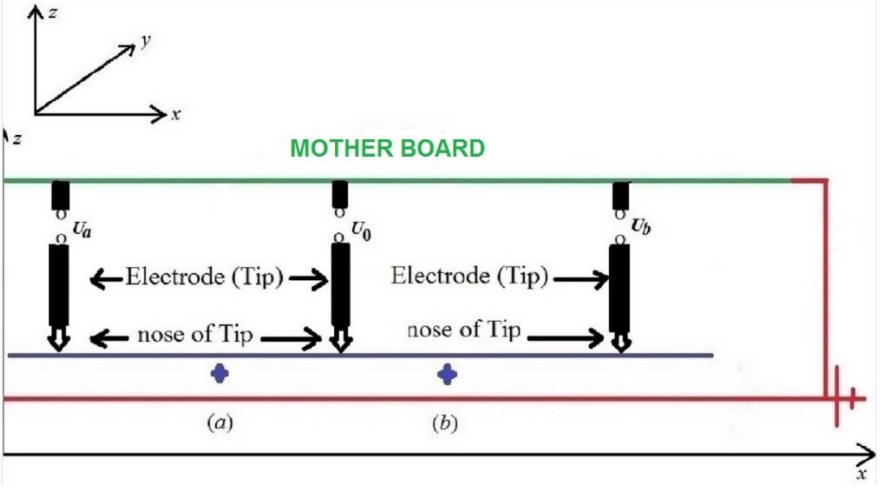

Fig. 1. Planar technology – based fundamental building block of a quantum logic network.

Lower red horizontal line represents the cross-section of rigid and mechanically stable conducting layer (plate) lying in the plane (*x, y*) and used as a common electric ground of the network. This plate supports deposited onto it thin dielectric crystal layer (its upper border is shown by a blue line) containing implanted rare-earth ions *a* and *b* (shown by blue crosses; ideally we have single rare-earth ion in a single crystal cell). Upper horizontal green line represents the cross-section of a thin dielectric layer lying in the plane (*x, y*) and bearing a network of (partially) interconnected conducting lines thus forming a quantum logic network.

[q] Corresponding author: k_pukhov@mail.ru

The tips (nanoelectrodes) are shown above the upper border of the crystal in three different positions nearby the rare earth ions. Voltage pulses U_a, U_0 and U_b are governed by a special software running by a PC. In our case, the dielectric layer containing rare-earth ions is large enough so we consider it as a "bulk" element avoiding the local electromagnetic field correction factor. We also consider the dielectric constants ε of both dielectric layers used as having the same values thus avoiding the effect of the refraction of static electric fields lines.

To calculate the electric field strengths E, tips were modelled as a round thin cylinder of radius R and length ℓ ($\ell/R>>1$). We have obtained an expression for the capacitance of a thin cylinder $C = \ell/\ln(2\ell/R)$ (in fact, this is a rewriting of Eq. (4.18) in the book [7], convenient for further calculations of the characteristics of the proposed device). The electrostatic electric field E is always perpendicular to the surface of a conductor. Close to the surface, we have $\partial E/\partial n = -E[(1/R_1)+ (1/R_2)]$ where the derivative is along the external normal to the surface, R_1 and R_2 are the main radii of the curvature of this surface. It's obvious that for a thin cylinder $\partial E/\partial n = -E/R$.

Using the ratio $q = CU$, the above expressions for the capacitance of a thin cylinder, as well as the expression for $\partial E/\partial$n, we can conclude that, at moderate values of U (~ 10 V), it is possible to control the energy gap between the ground (|0>) and excited (|1>) states in within 5-10 cm^{-1}.

The results of works [1,2,3,4,5,7] were used to estimate the degree of impact of the Stark effect and the control laser beam on qubits.

References

1. S. Sekatskii, M. Chergui, G. Dietler, Europhys. Lett., **63**, 21 (2003)
2. P. Goldner, A. Ferrier, O. Guillot-Noël in "Handbook on the Physics and Chemistry of Rare Earths", Vol. 46 edt by J.-C. G. Bünzli and V. K. Pecharsky, Elsevier (2015)
3. V. Hizhnyakov, V. Boltrushko, H. Kaasik, Yu. Orlovskii, Opt. Comm. **485**, 126693 (2021) see also Refs therein
4. A. Meixner, C. Jefferson, R. Macfarlane, Phys. Rev. B **46**, 5912 (1992)
5. R. Macfarlane, J. Lumin. **125**, 156 (2007)
6. A. Kaplyanskii, J. Lumin. **100**, 21 (2002)
7. L.D. Landau and E.M. Lifshitz. Electrodynamics of continuous media. Second Ed. revised and enlarged by Lifshitz and Pitaevskii. Pergamon Press (1984)

Spectroscopy and modelling of rare-earth ions in Y_2SiO_5

M. F. Reid[1,r], *Y.* Alizadeh[1], *N. L.* Jobbitt[1], *J. L. B.* Martin[1], *S.* Mothkuri[1], *L. F.* Williams[1], and *J.-P.R. W*ells[1]

[1]School of Physical and Chemical Sciences, University of Canterbury, Christchurch, New Zealand

Abstract. Rare-earth doped yttrium silicate (YSO) is a candidate material for quantum information storage. To identify and characterize the six- and seven-fold coordinated C_1 symmetry sites we have carried out site-selective laser fluorescence. Data from absorption measurements in the infra-red and visible regions, including the application of magnetic fields of up to 4T, has been combined with other data, from EPR and other techniques to allow us to determine crystal-field parameters. We have focussed on the Kramers ions Er^{3+}, Sm^{3+}, and Nd^{3+} that have many absorption transitions whose magnetic splittings may be characterized, and also on Ho^{3+}, where hyperfine splittings may be measured by absorption spectroscopy. Some preliminary calculations for Eu^{3+} will also be presented. YSO crystals are difficult and expensive to prepare, so we have also developed techniques to grow microcrystals, which enables us to rapidly prepare samples with a variety of dopant concentrations, and materials doped with more than one rare-earth species to study interactions between rare-earth ions in this host.

Rare-earth doped Y_2SiO_5 (YSO) in the X_2 phase is an attractive material for the development of quantum storage and communications device. Yttrium has a low nuclear spin, and silicon and oxygen isotopes with non-zero spin have low natural abundance. Hyperfine coherence times of up to 6 hours have been obtained in Eu^{3+} YSO [1] and there have been recent demonstrations of control of multiple Er^{3+} ions at the single-photon level [2]. Long coherence times are achieved by working at zero-first-order Zeeman (ZEFOZ) points, at which the effects of magnetic fluctuations are minimized. Our research programme seeks to provide accurate crystal-field models to enable predictions of such points, and other properties, particularly in situations, such as high magnetic fields, where conventional spin-Hamiltonian calculations are inaccurate.

Crystal-field calculations at low-symmetry (C_1) sites are difficult as there are 27 crystal-field parameters (counting real and imaginary parts). Fitting only to electronic energy levels is not sufficient to determine the parameters, Magnetic splittings along multiple axes, via Zeeman spectroscopy or EPR measurements are required to provide orientational information. Software developed by Horvath [3] was used to obtain he first such fits for Er^{3+} in YSO [4]. Independent work on Yb^{3+} in YSO was published by Zhou et al. [5]. Our recent work includes comparisons of measured hyperfine structure of Ho^{3+} in YSO with calculations [6], refinement of fits to Er^{3+} sites by the addition of extensive Zeeman measurements [7], and fits for Sm^{3+} in YSO [8].

Here we will report on the use of calculations for Er^{3+} to predict optical polarization effects and high-field magnetic-hyperfine splittings. Fits for Ho^{3+} in YSO, and calculations for Eu^{3+} in YSO will also be reported. The latter calculations must consider the effect of not only

[r] Corresponding author: mike.reid@canterbury.ac.nz

the coupling of electronic states to the nuclear spin, but also the direct interactions of the nuclear spin with the lattice and external magnetic fields [9].

Growth of YSO crystals is difficult and time-consuming, involving high temperatures and expensive equipment. However, it is possible to grow microcrystals relatively quickly. Samples with a variety of dopant concentrations and materials doped with more than one rare-earth species enable the study of interactions between rare-earth ions in YSO.

References

1. M. Zhong, M. P. Hedges, R. L. Ahlefeldt, J. G. Bartholomew, S. E. Beavan, S. M. Wittig, J. J. Longdell, and M. J. Sellars, Optically addressable nuclear spins in a solid with a six-hour coherence time, Nature **517**, 177 (2015)
2. S. Chen, M. Raha, C. M. Phenicie, S. Ourari, and J. D. Thompson, Parallel single-shot measurement and coherent control of solid-state spins below the diffraction limit, Science **370**, 592 (2020)
3. S. Horvath, The pycf crystal-field theory package, https://bitbucket.org/sebastianhorvath/pycf
4. S. P. Horvath, J. V. Rakonjac, Y.-H. Chen, J. J. Longdell, P. Goldner, J.-P. R. Wells, and M. F. Reid, Extending phenomenological crystal-field methods to C_1 point-group symmetry: Characterization of the optically excited hyperfine structure of $^{167}Er^{3+}$:Y_2SiO_5 , Phys. Rev. Lett. **123**, 057401 (2019)
5. X. Zhou, H. Liu, Z. He, B. Chen, and J. Wu, Investigation of the electronic structure and optical, EPR, and ODMR spectroscopic properties for $^{171}Yb^{3+}$-doped Y_2SiO_5 crystal: A combined theoretical approach, Inorg. Chem. **59**, 13144 (2020)
6. S. Mothkuri, M. F. Reid, J.-P. R. Wells, E. Lafitte-Houssat, P. Goldner, and A. Ferrier, Electron-Nuclear Interactions as a Test of Crystal-Field Parameters for Low Symmetry Systems: Zeeman-Hyperfine Spectroscopy of Ho^{3+} Doped Y_2SiO_5, Phys. Rev. B **103**, 104109 (2021)
7. N. L. Jobbitt, J.-P. R. Wells, M. F. Reid, S. P. Horvath, P. Goldner, and A. Ferrier, Prediction of optical polarization and high-field hyperfine structure via a parametrized crystal-field model for low-symmetry centers in Er^{3+}-doped Y_2SiO_5, Phys. Rev. B **104**, 155121 (2021)
8. N. L. Jobbitt, J.-P. R. Wells, and M. F. Reid, Zeeman and laser site selective spectroscopy of C 1 point group symmetry Sm^{3+} centers in Y_2SiO_5: a parametrized crystal-field analysis for the $4f^5$ configuration, J. Phys.: Condens. Matter **34** 325502 (2022).
9. K. M. Smith, M. F. Reid, M. J. Sellars, R. L. Ahlefeldt, Complete crystal field calculation of Zeeman-hyperfine splittings in europium, Phys. Rev. B **105**, 125141 (2022)

Structure of ytterbium impurity centers in forsterite single crystal according to EPR spectroscopy data

Valerii Tarasov[1,s], *Andrey* Sukhanov[1], *Kev* Salikhov[1], *Evgenii* Zharikov[2], *Kirill* Subbotin[2], *Denis* Lis[2], and *Valentina* Dudnikova[3]

[1]Zavoisky Physical-Technical Institute, Federal Research Center "Kazan Scientific Center of RAS", 420029, Kazan, Russia
[2]Prokhorov General Physics Institute, Russian Academy of Sciences, 119991, Moscow, Russia.
[3]Moscow State University, 119991, Moscow, Russia.

Abstract. Continuous wave and pulse X-band electron paramagnetic resonance spectroscopy are used to determine structure, magnetic and relaxation properties of paramagnetic centers formed by impurity ytterbium ions in forsterite (Mg_2SiO_4) single crystals. It is found that Yb^{3+} ions substitute Mg^{2+} ions both as single ions and as dimeric associates with nearby magnesium vacancy. For all the centers magnetic properties are characterized by the strong easy plane anisotropy.

Rare earth impurity ions in crystals are widely studied as possible material basis for practical implementation of information technologies based on the laws of quantum mechanics. Among them, they are quantum calculations, quantum telecommunications and quantum memory.

We used continuous wave and pulse electron paramagnetic resonance (EPR) spectroscopy to determine structure, magnetic and relaxation properties of impurity ytterbium ions in forsterite (Mg_2SiO_4) single crystals. Measurements were carried out on ELEXSYS E680 spectrometer with a cylindrical dielectric resonator ER4118MD5-W1 of the Flexline series. Mg_2SiO_4:Yb^{3+} single crystal was grown by the Czochralski technique in nitrogen atmosphere from the melt containing 0.15 at. % of ytterbium in respect to Mg^{2+}.

Crystal structure of forsterite was described in Ref. [1]. A unit cell of forsterite crystalline structure has an orthorhombic symmetry with a space group *Pbnm* (the lattice constants equal a = 0.4753, b= 1.019, c= 0.5988 nm) and contains 4 formula units. Ytterbium ions can substitute magnesium ions located in two sites inside two structurally nonequivalent oxygen octahedra denoted M1 and M2. The M1 octahedra form a quasi-one-dimensional chain oriented along the crystal c-axis. The M2 octahedra are adjacent to this chain from the sides. Projection of oxygen M1 and M2 octahedra onto the (bc) plane is presented in Fig. 1. The principal magnetic axes of paramagnetic centers in the M1 sites deviate from the crystallographic planes, and at arbitrary orientation of an external magnetic field there are 4 magnetically nonequivalent M1 sites in the unit cell. The crystal field in the M2 site with the C_s point symmetry has a mirror symmetry plane perpendicular to the c axis. Therefore, there are only 2 magnetically nonequivalent centers for the paramagnetic centers in the M2 sites. This difference makes it possible to unambiguously distinguish centers located in M1 and M2 sites based on orientation dependences of EPR spectra.

[s] Corresponding author: tarasov@kfti.knc.ru

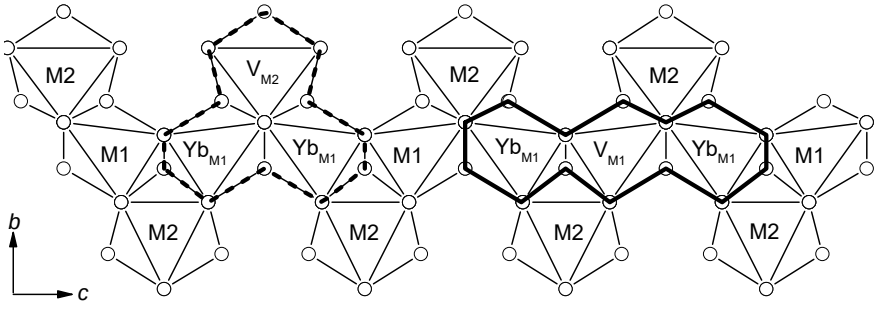

Fig. 1. Projection of oxygen octahedra of the Mg_2SiO_4 structure onto the (*bc*) plane and possible structures of dimeric associates of ytterbium ions localized in the M1 sites (Yb_{M1}). V_{M1} and V_{M2} – magnesium vacancies in the M1 and M2 sites

Three structurally different paramagnetic centers of the ytterbium ions in forsterite were observed and studied. They are single Yb^{3+} ion substituting Mg^{2+} ion in the M1 site and two dimer associates of Yb^{3+} ions substituting Mg^{2+} ions in two M1 sites. At that concentrations of dimer associates were several orders of magnitude higher than the concentration of associates formed randomly at the statistical distribution of impurity ions over the crystal. The first dimer consists of two ytterbium ions and magnesium vacancy between them substituting three magnesium ions in the M1 sites forming a chain parallel to the c crystallographic axis [2]. The second dimer is formed by Yb^{3+} ions in two nearby M1 sites with magnesium vacancy in adjacent M2 site [3]. Structures of these associates are highlighted by solid and dashed lines in the right and left sides of Fig. 1, respectively. For the first associate the spin–spin interaction between Yb^{3+} ions have a predominantly dipole–dipole character. In this case the magnitude and sign of the spin–spin interaction can be controlled by orientation of the external magnetic field. This fact makes this dimer associate promising basis for the practical implementation of elementary quantum computing algorithms based on electron coupled spins. Ytterbium ions of the second dimer associate are located much closer to each other and have common oxygen ions in the octahedral environment. Because of this, there is a strong isotropic exchange interaction between these ions. The ions lose their independence and become a single paramagnetic center. The structure of this center is characterized by mirror symmetry with mirror plane perpendicular to the *c*-axis. The orientation dependence of EPR spectra in this case should be like that of single paramagnetic center located in the M2 site. Very high probability of the formation of such dimeric associates is confirmed by calculations performed in Ref. [4].

References

1. J.D. Birle, G.V. Gibbs, P.B. Moore, J.V. Smith. Amer. Mineral., **53**, 807 (1968)
2. V.F. Tarasov, A.A. Sukhanov, V.B. Dudnikova, E.V. Zharikov, D.A. Lis, K.A. Subbotin. JETP Letters, **106**, 92 (2017)
3. V.F. Tarasov, A.A. Sukhanov, E.V. Zharikov, K.A. Subbotin, D.A. Lis. Appl. Magn. Reson., Publ. online 29.11.2021. DOI: https://doi.org/10.1007/s00723-021-01453-9
4. V.B. Dudnikova, E.V. Zharikov, D.A. Lis, N.N. Eremin, Phys. Solid State **61**, 614 (2019)

Spin noise spectroscopy of RE ions in crystals

Valerii Zapasskii[t]

Spin Optics Laboratory, St. Petersburg State University, 198504 St. Petersburg, Russia

Abstract. A considerable progress in the spin noise spectroscopy, achieved for the last few years, has been related to its successful application to dielectric crystals with RE impurities. This achievement provided magnetic-resonance and optical spectroscopy of RE-activated crystals with a new powerful experimental technique. At the same time, the new field of research has raised several questions specific for application of optical polarization methods to anisotropic materials. In this talk, we consider new possibilities of the spin noise spectroscopy as applied to anisotropic systems.

The method of spin noise spectroscopy (SNS), primarily proposed in 1981 [1], has gained a wide application only in the last two decades. This method implies observation of spontaneous spin precession by detecting Faraday rotation noise of the system at Larmor frequency. Thus, the SNS technique may be considered as a version of the EPR spectroscopy with no AC field driving the spin precession. Initially, the main advantage of the SNS, as compared with the conventional method of EPR, was its nonperturbative character: the system was just probed by laser light the region of its transparency with no disturbance. In the last years, however, it became clear that highly important advantages of the SNS are related to the presence of optical channel of signal detection. Specifically, we have found that the spin-noise signal can be dramatically enhanced for inhomogeneously broadened optical transitions resonantly probed by a spectrally narrow laser light [2]. This fact allowed us to significantly expand the range of objects of the SNS and to successfully apply the SNS to RE ions in crystals [3]. Curiously, the most convenient for the SNS were found to be trivalent RE ions with parity-forbidden f-f transitions in the visible spectral range, rather than divalent ions with allowed optical transitions and strong magneto-optical effects.

Application of SNS to the new class of objects has made us to solve several model problems related to anisotropic impurity centers and anisotropic centers. The most interesting question was whether the SNS that implies detection of the Faraday-rotation noise can be applied to optically anisotropic crystals, which are known to be hardly accessible for measurements of regular Faraday effect. We have shown, however, both theoretically and experimentally, that optically anisotropic crystals that may dramatically distort polarization of the probe light remain suitable for the SNS. Moreover, the spin-noise signal, in such samples, proves to be independent of polarization of the probe light and remains practically unsuppressed as compared with that in optically isotropic materials.

Our recent experiments have shown that *hidden anisotropy* of crystals with anisotropic impurity centers, generally, strongly violates conventional geometries of the SNS experiment, and it becomes possible to observe the spin-noise resonances in the Faraday geometry. We believe that these findings may open new ways of studying crystalline and vitreous systems with paramagnetic impurities.

A specific feature of the SNS, which, under certain conditions, can be considered as its merit, is that the whole spectrum of the SN resonances can be obtained in a single measurement

[t] Corresponding author: vzap@rambler.ru

(in a fixed magnetic field). Such panoramic magnetic-resonance spectra provide additional possibilities for studying paramagnets with impurity centers. We have shown that symmetry of the crystal can be revealed as invariance of certain combination of the spin-resonance frequencies. Such invariants can be helpful in deciphering magnetic-resonance spectra of impurity paramagnets.

One more interesting feature of SNS of crystals with RE impurities is that it implies the use of spectrally narrow laser sources with extremely high spectral brightness. As a result, the SNS measurements are often accompanied by effects of nonlinear optics. Our magneto-optical studies of RE-activated crystals allowed us to establish direct relationship between the nonlinear Faraday effect and spin-noise power [4]. Results of this research can be used not only to predict applicability of the SNS to any optical transition, but also for measuring homogeneous width of the transition.

References

1. E. B. Aleksandrov and V. S. Zapasskii, J. Exp. Theor. Phys**. 54**, 64 (1981)
2. V. S. Zapasskii, A. Greilich, S. A. Crooker, Yan Li, G. G. Kozlov, D. R. Yakovlev, D. Reuter, A. D. Wieck, and M. Bayer, Phys. Rev. Lett., **110**, 176601 (2013)
3. A.N.Kamenskii, A.Greilich, I.I.Ryzhov, G.G.Kozlov, M.Bayer, and V.S.Zapasskii, Phys. Rev. Res. **2,** 023317 (2020)
4. A. N. Kamenskii, E. I. Baibekov, B. Z. Malkin, G. G. Kozlov, M. Bayer, A. Greilich, and V. S. Zapasskii, Phys. Rev. B **104,** 174430 (2021)

ORAL TALKS

Highly luminescent borogermanate glass with $CsPbHal_3$ perovskite nanocrystals

Anastasiia Babkina[1,u], *Ksenia* Zyryanova[1], *Rufina* Kharisova[1], *Aleksandra* Pavliuk[1], *Yevgeniy* Sgibnev[1] and *Nikolay* Nikonorov[1]

[1]Research Centre for Optical Materials Science, ITMO University, 199034 St. Petersburg, Russia

Abstract. The article presents the results of the luminescent properties studies of borogermanate glasses with perovskite $CsPbHal_3$ (Hal=Cl, Br, I) nanocrystals. The crystals are nucleated in a glass matrix by bulk thermal crystallization. The maximum quantum yield of pure iodide and mixed iodine-bromine perovskites was 35%.

In the last 5 years, optical materials with perovskite nanocrystals have gained quite a lot of attention due to the incredibly high external luminescence quantum yield (up to 100% in solution [1]). However, the main problem with oxygen-free crystals is that their luminescent properties degrade over time, making such a material difficult to use in practice, except for use in temperature sensors [2,3]. Therefore, one of the tasks of optical materials science is the development of a mechanically, chemically, and thermally stable transparent medium for growing and stabilizing the properties of perovskite nanocrystals. The glass matrix has all the indicated properties. Perovskite nanocrystals have already been obtained and studied in borosilicate [4] and phosphate [5] glass. Thus, the results of the synthesis of perovskite nanocrystals of the $CsPbHal_3$ type with various halogens in a borogermanate glass matrix are shown in this work.

Borogermanate glasses of the GeO_2-B_2O_3-ZnO-Na_2O system were synthesized by melt-quenching technique at 1000°C in air atmosphere using closed quartz crucibles. Additives Cs_2O-PbO-KI/KBr/KCl were introduced into the glass for subsequent nucleation of the corresponding nanocrystals. The glass samples were heat-treated (HT) at temperatures above Tg=470°C to promote the nucleation of the perovskite nanocrystals in glass matrix. The absorption and luminescence spectra were recorded on a Lambda 650 UV-Vis spectrophotometer and a LS-55 (PerkinElmer) spectrofluorimeter.

Figure 1a,b shows the absorption spectra (recorded at the liquid nitrogen boiling point) of glass samples in which $CsPbBr_3$ and $CsPbI_3$ nanocrystals, respectively, were nucleated during HT at different temperatures. The corresponding luminescence spectra obtained with excitation at 460 nm are shown in Fig. 1b,d. It can be seen from the spectra that, with an increase in the heat treatment temperature, the maximum of exciton absorption and luminescence bands shifts to the longer wavelength's region, which is associated with the size effect. The luminescence decay curve of nanocrystals is described by a two-exponential decay: the short component has

[u] Corresponding author: babkina.anastasya@bk.ru

a duration of 1.5 ns, the long exponent is of the order of 10 ns. The maximum obtained quantum yield for glasses with $CsPbBr_3$ and $CsPbI_3$ nanocrystals was 25 and 35%, respectively.

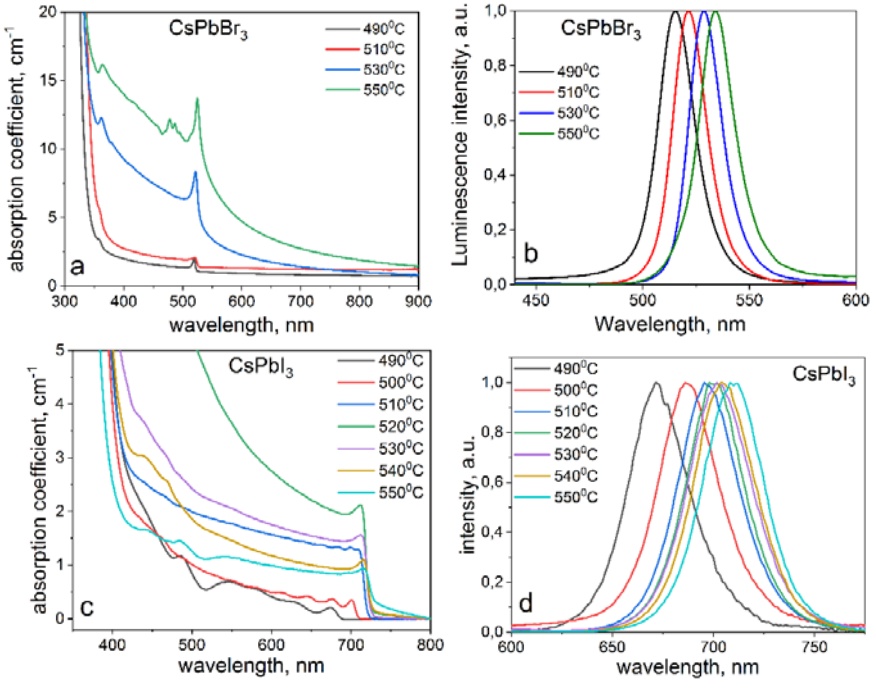

Fig. 1. Absorption (a, c) and luminescence (b, d) spectra of glass with $CsPbBr_3$ (a, b) and $CsPbI_3$ (c, d) nanocrystals.

With the simultaneous introduction of two halogens, for example, iodine and bromine, into the glass composition, so-called "mixed" $CsPb(Br_{1-x}I_x)_3$ crystals are nucleated in the matrix during HT. The luminescence of such crystals covers the whole region between 500 and 700 nm with no less quantum yield. Their absorption spectra are a superposition of the exciton absorption of $CsPbBr_3$ and $CsPbI_3$ crystals.

Investigation of spectral properties was supported by the grant of the President of the Russian Federation for young PhD scientists No. MK-4235.2021.1.3.

References

1. F. Liu, Y. Zhang, C. Ding, S. Kobayashi, T. Izuishi, N. Nakazawa, T. Toyoda, T. Ohta, S. Hayase, T. Minemoto, K. Yoshino, S. Dai, Q. Shen, ACS Nano **11**(10), 10373 (2017)
2. J. Jin, J. Lin, Y. Huang, L. Zhang, Y. Jiang, D. Tian, F. Lin, Y. Wang, X. Chen, Chin. Chem. Lett. **2**, 2 (2022)
3. G. Yao, S. Li, D. Valiev, M. Chen, S. Stepanov, Y. Lu, C. Li, Y. Zhou, Z. Su, F. Zeng, J. Non. Cryst. Solids **582**, 121462 (2022)
4. J. Fridrichová, P. Bačík, A. Ertl, M. Wildner, J. Dekan, M. Miglierini, J. Mol. Struct. **1152**, 79 (2018)
5. B. Ai, C. Liu, J. Wang, J. Xie, J. Han, X. Zhao, J. Heo, J. Am. Ceram. Soc. **99**(9), 2875 (2016)

Effect of the Zr/Hf Ratio on the Structure and Luminescent Properties of Cubic Ceramics $(Zr_{0.82-x}Hf_xY_{0.17}Eu_{0.01})O_{1.91}$

Ekaterina V. Dementeva[1,v], *Azaliya A.* Shakirova[1], *Tatiana B.* Popova[1], *Maria A.* Yagovkina[1], *Aleksey I.* Lihachev[1], *Boris E.* Burakov[1] and *Maria V.* Zamoryanskaya[1]

[1] Ioffe Institute RAS, Politekhnicheskaya st. 26, Saint Petersburg, 194021 Russia

Abstract. Cubic ceramics $(Zr_{0.82-x}Hf_xY_{0.17}Eu_{0.01})O_{1.91}$ with different contents of hafnium (x = 0; 0.2; 0.41; 0.62; 0.82) were synthesized. The synthesis regimes were chosen to get rid of the minor tetragonal phase. The grain size was 2-5 microns. It was shown that, upon excitation by electrons, the sample with the composition $(Zr_{0.62}Hf_{0.2}Y_{0.17}Eu_{0.1})O_{1.91}$ has the highest cathodoluminescent intensity.

1 Introduction

Recently, the tasks associated with the disposal and immobilization of nuclear waste, the analysis of the consequences of large-scale radiation accidents and environmental disasters have become important problems of dosimetry. Thermoluminescent dosimeters are widely used for these applications. One of the important problems at present is the development of radiation-resistant thermoluminescent dosimeters capable of measuring high doses of ionizing radiation. One of the possible materials for creating radiation and chemically resistant dosimeters is $(Zr_{0.82-x}Hf_xY_{0.17}Eu_{0.01})O_{1.91}$ ceramics. $(Zr_{0.82}Y_{0.17}Eu_{0.01})O_{1.91}$ is widely studied as a material for thermoluminescence dosimetry, but this material is transparent to neutrons. In turn, hafnium absorbs neutrons well and its addition makes it possible to expand the applicability of this material in dosimetry.

2 Synthesis of ceramics and research methods

Samples of single-phase ceramics based on cubic yttrium-stabilized zirconium-hafnium oxides with different Zr/Hf ratios were synthesized. The yttrium content was fixed and amounted to 17% at, since such a concentration is guaranteed to stabilize zirconium and hafnium oxides in the cubic phase [1]. The europium concentration was 1% at, since this concentration does not lead to destabilization of the cubic phase in zirconium oxide and to concentration quenching of luminescence. For the synthesis of the initial charge, the method of co-precipitation from a common solution was chosen as the most promising, economically feasible and acceptable for industrial implementation. The charge was ground and pressed into tablets 8 mm in diameter under a pressure of 10 MPa. The resulting tablets were sintered in air at a temperature of 1500°C for 3 hours.

The synthesized samples were studied by the X-ray diffraction (XRD) method, electron backscatter diffraction (EBSD), electron probe microanalysis (EPMA) and cathodoluminescence (CL).

[v] Corresponding author: ivanova@mail.ioffe.ru

3 Result and discussion

It was shown by the XRD method that the cubic phase prevails in ceramics, and the appearance of a minor tetragonal phase is observed in samples with atomic fraction of hafnium x≥0.4. Additional annealing for 3 hours at 1500ºC leads to the disappearance of the minor phase. For each sample, the lattice constant was determined; Fig. 1(a) shows the dependence of the lattice constant on the content of hafnium. One can see that the lattice constant changes linearly with a change in the ceramic composition. The EBSD method showed that ceramics consist of grains with an average size of 2-5 microns.

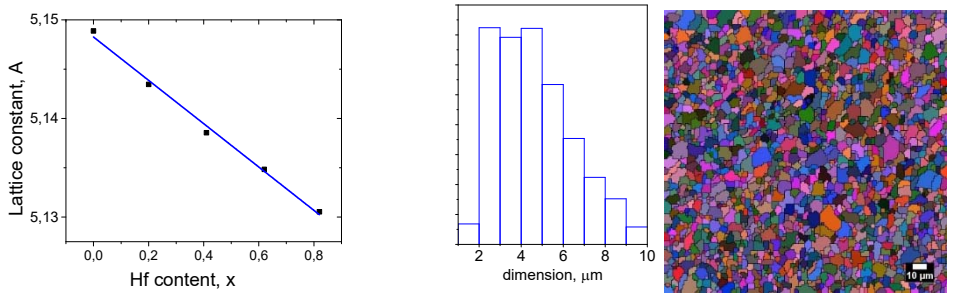

Fig. 1. (a) Lattice constant versus Hf content; (b) histogram of the grains' diameter distribution; (c) map of the distribution of Euler angles in the Zr sample.

The CL spectra and decay times were obtained for the most intense $^5D_0$-$^7F_0$ transition. The CL spectra contain bands associated with Eu3+ transitions, including high transitions ($^5D_0$-$^7F_0$, $^5D_1$-$^7F_1$ and $^5D_3$-$^7F_3$). It is shown that the decay times are well approximated by the sum of two exponentials, which is typical for ceramics [2]. Decay times are independent of the atomic fraction of hafnium. It is shown that, upon excitation by electrons, the sample with the composition $(Zr_{0.62}Hf_{0.2}Y_{0.17}Eu_{0.1})O_{1.91}$ has the highest cathodoluminescent intensity.

The XRD and EBSD characterizations were performed using equipment owned by the Joint Research Center "Material science and characterization in advanced technology" (Ioffe Institute, St.-Petersburg, Russia).

References

1. J. Yuan, X. Zhou, S. Dong, J. Jiang, L. Deng, W. Song, D. B. Dingwell, X. Cao, J. Alloy. Compd., **867**, 159113 (2021).
2. K. Orekhova, R. Tomala, M. Zamoryanskaya, J. Alloy. Compd., **858**, 157731 (2021).

Non-standard quasiadditive integrals of motion and pressure dependence of phonon populations

Fridrikh Dzheparov[w]

NRC "Kurchatov Institute" – KCTEP, Moscow, Russia

Abstract. No

The existing equilibrium statistical physics is based on application of standard quasiadditive integrals of motion, which include energy, momentum, rotation momentum, and number of particles. It is shown [1] that this list is far from complete and that any quasiadditive dynamic variable can be mapped to corresponding quasiadditive integral of motion. As a result, an ensemble with a given external pressure is constructed. It provides the first example of the distribution in which phonon populations depend on pressure differently than in the canonical Gibbs ensemble.

References

1. F.S. Dzheparov. Non-standard quasiadditive integrals of motion and pressure dependence of phonon populations. ArXiv:2112.01895

[w] Corresponding author: dzheparov@itep.ru

Narrow-line transition and photon echo of Er^{3+} in a YPO_4:Er single crystal

Konstantin Gerasimov[1,x], *Timur* Sabirov[1], *Sergey* Moiseev[1], *Eduard* Baibekov[2], *Marco* Bettinelli[3], *Ming-Chi* Chou[4], *Yu-Chun* Yan[4], and *Marina* Popova[5]

[1]Kazan Quantum Center of Kazan National Research Technical University named after A.N. Tupolev-KAI, 10 K. Marx Str., Kazan 420111, Russian Federation
[2]Kazan (Volga Region) Federal University, 18 Kremlyovskaya Street, Kazan 420008, Russian Federation
[3]Dipartimento di Biotecnologie, University of Verona and INSTM, Strada Le Grazie 15, Verona 37134, Italy
[4]Department of Materials and Optoelectronic Science, Center of Crystal Research, National Sun Yat-Sen University, 70, Lien-Hai Rd., Kaohsiung 80424, Taiwan
[5]Institute of Spectroscopy, Russian Academy of Sciences, 5, Fizicheskaya Str., Troitsk, Moscow 108840, Russian Federation

Abstract. We performed high-resolution laser spectroscopy and photon echo investigation of Er^{3+}:YPO_4 at the telecommunication wavelength ($\lambda \sim 1530$ nm) in magnetic fields up to 4 T. A fine spectral structure with a scale of ~ 60 MHz was observed due to even erbium isotopes ^{166}Er, ^{168}Er, and ^{170}Er. The maximum coherence time (T_2) of 113 μs was found in a magnetic field of 4 T for the direction of the magnetic field parallel to the *c* axis of the crystal. Main sources of decoherence were discussed.

Dielectric crystals activated with rare-earth (RE) ions are widely used as laser materials, scintillators, phosphors, optical radiation converters. In the last decade, RE-doped crystals attract a growing interest as one of the most promising materials for quantum information technologies [1], due to long coherence (phase-relaxation) times of RE ions, both at optical and electron-nuclear spin transitions. Among RE ions, Er^{3+} is of particular importance because of the telecom wavelength of its optical transition $^4I_{15/2} \rightarrow {}^4I_{13/2}$ ($\lambda \sim 1.53$ mkm). It is worth noting very long coherence times of Er^{3+} ions in orthosilicate (Y_2SiO_5) crystals for both optical (4.38 ms [2]) and electron-nuclear spin (1 s [3]) transitions.

Recently, we have performed high-resolution spectroscopic measurements of the optical absorption and luminescence of YPO_4: Er^{3+} single crystals and, based on the obtained data, determined reliable crystal-field parameters and decoded the hyperfine structure observed in the spectrum of the $^{167}Er^{3+}$ odd erbium isotope [6]. In the present work, we carried out detailed studies of the $^4I_{15/2}$ ($\Gamma_7{}^1$) $\rightarrow {}^4I_{13/2}$ ($\Gamma_6{}^1$) optical transition of Er^{3+}:YPO_4 in magnetic fields up to 4 T using high-resolution laser spectroscopy and photon echo experiments.

We studied three samples - S1, S2, and S3 of YPO4: Er3+ with a nominal erbium impurity concentration 0.1 (S1), 0.01 (S2), and 0.005 at.% (S3) but grown at different times and in two different growth laboratories. The optical absorption spectrum of the sample S1 at the $^4I_{15/2}(\Gamma_7{}^1)$ $\rightarrow {}^4I_{13/2}(\Gamma_6{}^1)$ transition is a very intense relatively broad line with FWHM of about 600 MHz. For the sample S2, a fine structure is resolved, and the absorption spectrum is well represented by three lines with Lorentzian shapes and linewidths of ~ 70 MHz. The ratio of line intensities (1: 0.81: 0.41) is in a good agreement with the natural percentage of three even erbium isotopes,

[x] Corresponding author: kigerasimov@mail.ru

^{166}Er, ^{168}Er, and ^{170}Er with highest natural abundance. The distances between the isotope lines are close to each other and amount to ~ 60 MHz. We estimated the oscillator strength as $f = 1.1 \cdot 10^{-7}$.

The magnetic-field dependences of the phase relaxation time were measured for samples S1 and S3. We succeeded in detecting the photon echo signal in the sample S1 in magnetic fields starting from 2 T. In the sample S3, the phase relaxation time T_M was ~14(1) μs with x~1.3 in much lower magnetic fields (B ~ 0.5 T) compared to the case of the sample S1. Here, we follow the approach of Mims [7], which describes the nonexponential dependence of the two-pulse spin echo intensity in the presence of spectral diffusion as $I = I_0\exp[-2(2\tau/T_M)^x]$, where τ is the time delay between the first and second exciting pulses. The dependence of the effective homogeneous line width on the magnetic field B is shown in Fig. 1.

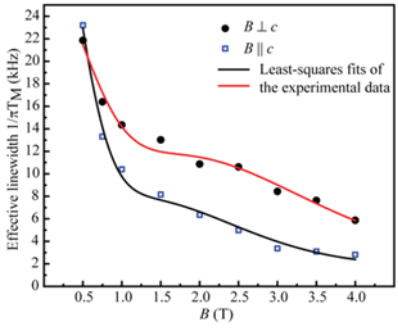

Fig. 1. Magnetic-field dependences of the effective homogeneous linewidth measured in $YPO_4:Er^{3+}$. Blue and black symbols refer to the two orientations of S3 sample in the magnetic field, respectively. The curves approximate the experimental data based on the approach developed in Ref. 3.

The relatively large value of the effective homogeneous linewidth can be associated with the presence of instantaneous spectral diffusion; moreover, we do not rule out the presence of additional magnetic impurities in the crystal, which are related to the crystal-growth method and the presence of Pb ions in the high-temperature flux that affect the linewidth. Both of these circumstances are the subject of further research.

This work was performed within the framework of the state assignment - agreement №. 02.03.2020 №. 00075-02-2020-051 / 1 register №. 78 *KBK* 01104730290059611. E.B. acknowledges the support of the BASIS foundation. M.P. was supported by the Ministry of Science and Higher Education of Russia under Grant 0039-2019-000.

References

1. P. Goldner, A. Ferrier, and O. Guillot-Noël, *Rare earth-doped crystals for quantum information processing, Handbook on the Physics and Chemistry of Rare Earths* (Elsevier, Amsterdam, 2015)
2. T. Böttger, C.W. Thiel, R.L. Cone, Y. Sun, Phys. Rev. B **79**, 115104 (2009)
3. M. Rančić et al., Nat. Phys. **14,** 50 – 54 (2018)
4. M.N. Popova, S.A. Klimin, S.A. Moiseev, K.I. Gerasimov, M.M. Minnegaliev, E.I. Baibekov, G.S. Shakurov, M. Bettinelli, M.C. Chou, Phys. Rev. B **99**, 235151 (2019)
5. W.B. Mims, Phys. Rev. **168**, 370 (1968)

Quantum-kinetic theory of the local fields for guest light emitters

Maxim Gladush[1,2,3,y]

[1] Lebedev Physical Institute of the Russian Academy of Sciences, Russia
[2] Institute of Spectroscopy of the Russian Academy of Sciences, Russia
[3] Moscow State Pedagogical University, Russia

Abstract. No

This study shows how a fully quantum-kinetic theory based on the density matrix formalism can describe the effects of the local fields on the single quantum emitters distributed in continuous dielectric hosts. The key feature of the method is the possibility to calculate the effective values of the radiative lifetimes of the guest particles. The difference of the effective lifetime compared to the natural lifetime occurs due to the generalized Purcell effect (as the change in the field mode density) and the local field configuration inside a medium. The effective lifetimes follow from the radiative relaxation rates in the kinetic equation for the density matrix of a single quantum emitter. This kinetic equation is a constituent of a system of equations of the kinetic Bogolyubov hierarchy for a system with many species of particles. The types of the particles or the subsystems include the quantum emitters, the particles that build the host medium and the field modes. Exclusion of the host and the field bonds from the equation for the emitter's density matrix provides the corrections for the standard parameters including the relaxation rates. The rates and the corresponding lifetimes as functions of the host's refractive index are shown to be in good agreement with the experimental data, both original and collected from the literature. A few examples are shown for the rare earth lifetimes in different hosts.

The author is a member of the Leading Scientific School of the Russian Federation (grant of the President of the Russian Federation NSh-776.2022.1.2).

[y] Corresponding author: gladush@isan.troitsk.ru

Theoretical investigation of magnetic resonance spectra of frustrated pseudoperovskite manganites

Liudmila Gonchar[1,2,z]

[1] Ural State University of Railway Transport, Yekaterinburg, Russia
[2] Ural Federal University, Yekaterinburg, Russia

Abstract. The magnetic resonance spectra of frustrated manganite compounds $La_{1/3}Ca_{2/3}MnO_3$ and $BiMnO_3$ are calculated within the framework of orbitally dependent magnetic interactions model. The specific features of field and angle dependences are proposed.

The pseudoperovskite manganites $R_{1-x}A_xMnO_3$ (where R^{3+} are rare earth or bismuth ions, A^{2+} are alkaline earth ions, and x is a doping level) are known as Jahn-Teller compounds with interesting properties due to interrelation between crystal structure and magnetic subsystem via orbital and charge orderings [1]. Because of cooperative Jahn-Teller effect the symmetry of these crystals is lower than a cubic one, which characterizes perovskite structure.

That effect in conjunction with charge ordering leads to different kinds of orbital structures, which in their turn form unusual magnetic structures, including low-dimensional and frustrated ones. The theoretical description of these structures applied to magnetic resonance spectra is the aim of current work. The compounds under consideration are $La_{1/3}Ca_{2/3}MnO_3$ and $BiMnO_3$.

1 Model of superexchange interaction

The superexchange interaction is dependent upon orbital state of each interacting ion in exchange pair. The Mn^{3+} orbital state is described by an angle Θ of ground state multielectronic wave functions mixing [2].

$$J_{ij}(\Theta_i, \Theta_j) = \frac{J_{0,k}\cos^2\varphi_{ij}}{r_{ij}^{10}} F_{ij}(\Theta_i, \Theta_j), \quad (1)$$

The orbital-mixing angle dependences of superexchange interactions which cause the unusual magnetic structures are of three types:
1. Mn^{3+}–Mn^{3+} interacting pair (k=1)

$$F_{z,ij}(\Theta_i, \Theta_j) = 1 - \alpha(\cos\Theta_i + \cos\Theta_j) + \beta\cos\Theta_i\cos\Theta_j,$$
$$F_{x(y),ij}(\Theta_i, \Theta_j) = 1 + \frac{\alpha}{2}(\cos\Theta_i \pm \sqrt{3}\sin\Theta_i + \cos\Theta_j \pm \sqrt{3}\sin\Theta_j) +$$
$$+ \frac{\beta}{4}(\cos\Theta_i \pm \sqrt{3}\sin\Theta_i)(\cos\Theta_j \pm \sqrt{3}\sin\Theta_j)$$

2. Mn^{3+}–Mn^{4+} interacting pair (k=2)

[z] Corresponding author: l.e.gonchar@urfu.ru

$$F_{z,ij}(\Theta_i) = 1 - \alpha' \cos\Theta_i,\ F_{x(y),ij}(\Theta_i) = 1 + \frac{\alpha'}{2}\left(\cos\Theta_i \pm \sqrt{3}\sin\Theta_i\right)$$

3. Mn^{4+}–Mn^{4+} interaction (k=3) does not depend upon orbital state, so $F \equiv 1$.
Parameters $J_{0,1}=1.24\times10^3$ мэВ·Å^{10}, $J_{0,2}=-2.2\times10^3$ мэВ Å^{10}, $J_{0,3}=0.97\times10^3$ мэВ·Å^{10}, α=1.0, β=4.5, α'=2.8 are semi-empirical [2].

2 Magnetic structure and resonance spectra

The model of magnetic subsystem [2] is following:

$$\widehat{H}_{mag} = \sum_{i>j} J_{ij}(\Theta_i, \Theta_j)(\mathbf{S}_i \cdot \mathbf{S}_j) + \sum_{i,\alpha,\beta} D_i^{\alpha,\beta}(\Theta_i)\, S_i^{\alpha} S_i^{\beta} + g\mu_B \sum_i (\mathbf{H} \cdot \mathbf{S}_i). \qquad (2)$$

The first term is the superexchange interaction, the second one is orbitally-dependent single-ion anisotropy, and the third one is a Zeeman interaction. The dependence of g-tensor upon direction and orbital state of Mn^{3+} ions is neglected.
An especial attention is paid to $BiMnO_3$. This compound being a pure manganite crystal has a crystal structure of monoclinic syngony and an orbital ordering which is strongly different compared with $RMnO_3$ [3]. The orbital ordering calculated in linear vibronic model, contradicts with ferromagnetic structure [4]. The competition of superexchange parameters leads to C-type structure without additional vibronic terms.
The magnetic resonance method in frustrated systems helps to clarify the small components of magnetic structure because of magnetic interactions competition. The angle dependence of magnetic resonance frequencies shows the symmetry of magnetic subsystem. The feature of frustrated manganite compound is improper easy-axis behavior of magnetic field dependences. The angle dependency of magnetic resonance spectra is of uniaxial type for $BiMnO_3$ and of biaxial type for $La_{1/3}Ca_{1/3}MnO_3$. The stability of magnetic easy-axis dependance upon orbital ordering is discussed.

References

1. N.G. Bebenin, R.I. Zainullina, V.V. Ustinov, Phys. Usp. 61, 719 (2018)
2. L.E. Gonchar JMMM, **513** (2020) 167248
3. D. P. Kozlenko, A. A. Belik, S. E. Kichanov et al., Phys. Rev. B, **82**, 014401 (2010)
4. L.E. Goncthar, A.E. Nikiforov. Phys. Rev. B, **88**, 094401(2013)

Impurity, defect-related luminescence, and energy transfer in complex phosphates doped with Pr^{3+} ions

Sviatoslav Kiselev[1], *Elena* Trofimova[1,2,aa], *Vladimir* Pustovarov[1] and *Maria* Petrova[3]

[1]Ural Federal University, 620075 Ekaterinburg, Russia
[2]Scobeltsyn Nuclear Physics Research Institute, 119991 Moscow, Russia
[3]Joint Institute for Nuclear Research, 141980 Dubna, Russia

Abstract. Defect-related luminescence was observed in a series of complex phosphates $LiSrPO_4$, $Sr_9Lu(PO_4)_7$, $Sr_9Sc(PO_4)_7$, $KLuP_2O_7$ and $K_3Lu(PO_4)_2$ all doped with 1 mol.% Pr^{3+} ions. All the objects show intensive fast emission associated with *5d→4f* transitions of Pr^{3+} ions as well as prominent wide band emission associated with defects in the spectral region of 300-820 nm. For deeper understanding of defect creation and their role in energy transfer, some phosphates were irradiated both with reactor neutrons and fast electrons. It was shown that defect-related emission bands are formed by radical groups of phosphorus and oxygen.

In this work luminescence properties of a series of complex phosphates $LiSrPO_4$, $Sr_9Lu(PO_4)_7$, $Sr_9Sc(PO_4)_7$, $KLuP_2O_7$ and $K_3Lu(PO_4)_2$ doped with 1 mol.% of Pr^{3+} ions were investigated using a variety of spectroscopic techniques.

It was shown in earlier works, that the objects demonstrate fast intensive emission, associated with *5d—4f* interconfigurational transitions of Pr^{3+} ions [1-3]. Nevertheless, the luminescence spectra of the objects also demonstrate emission, which cannot be ascribed to Pr^{3+} radiative transitions, in the spectral region of 300-500 nm. The intensity and the positions of these bands slightly differ between the objects, but the nature of the emission is thought to arise from the same type of defects. In this work the defects of crystal lattices of $LiSrPO_4$, $Sr_9Lu(PO_4)_7$, $Sr_9Sc(PO_4)_7$, $KLuP_2O_7$ and $K_3Lu(PO_4)_2$ microcrystalline powders were studied in more detail. Energy transfer processes between defects and activator ions were found, i.e. the defect luminescence can be excited by intracenter Pr^{3+} excitation and *4f—4f* emission of Pr^{3+} ions can be excited via defect excitation.

For example, in Fig.1 (left panel) the photoluminescence spectra of $K_3Lu(PO_4)_2$:Pr^{3+} are shown. The spectrum under excitation λ_{exc} = 235 nm (intracenter Pr^{3+} excitation) shows intensive *5d—4f* emission of Pr^{3+} ions, while defect-related spectral bands appear in 440-550 nm and 810 nm region. The defects are thought to be formed of radical groups of phosphorus and oxygen. The excitation spectra of defect-related emission are shown in Fig. 1 (right panel). Upon excitation with λ_{exc} = 270 nm, the emission spectrum is comprised of three wide bands, associated with defect emission, while lines belonging to Pr^{3+} *4f→4f* radiative transitions are not visible.

To observe the behavior of defect-related luminescence, microcrystalline powders were irradiated with electrons and neutrons. Fast electrons (E = 10 MeV) were obtained from linear electron accelerator in UrFU, Yekaterinburg. Fast neutrons (E > 1 MeV) flux was produced by neutron reactor IBR-2 (FLNP JINR, Dubna). Both irradiation types cause defect formation

[aa] Corresponding author: trofimova.e.s@yandex.ru

inside lattice. Creation of point defects is realized by impact mechanism – elastic collisions of particles with nucleus of lattice atoms.

Luminescence decay kinetics both for d—f transitions and for defect-related emission were studied upon excitation with pulse electron beam (Fig. 2). The resulting curves can be well approximated with two-exponential function. Thus, 445 nm emission band is characterized with $\tau_1 = 40$ ns and $\tau_2 = 0.53$ μs; 530 nm band is characterized with $\tau_1 = 61$ ns and $\tau_2 = 0.60$ μs. In contrary, fast *d—f* transitions decay kinetics is well fitted with monoexponential function with lifetime $\tau = 40$ ns.

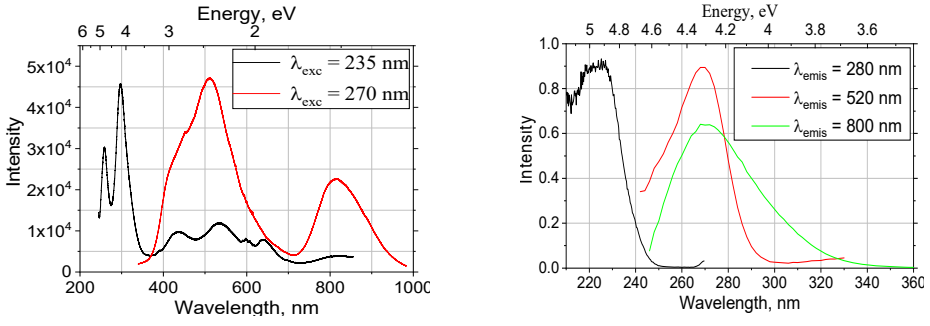

Fig. 1. Left: Photoluminescence spectra of $K_3Lu(PO_4)_2:Pr^{3+}$ (1 %) under excitation wavelength λ_{exc}, T = 295 K. Right: PL excitation spectra of $K_3Lu(PO_4)_2:Pr^{3+}$ (1 %) of emission bands (λ_{emis}), T = 295 K

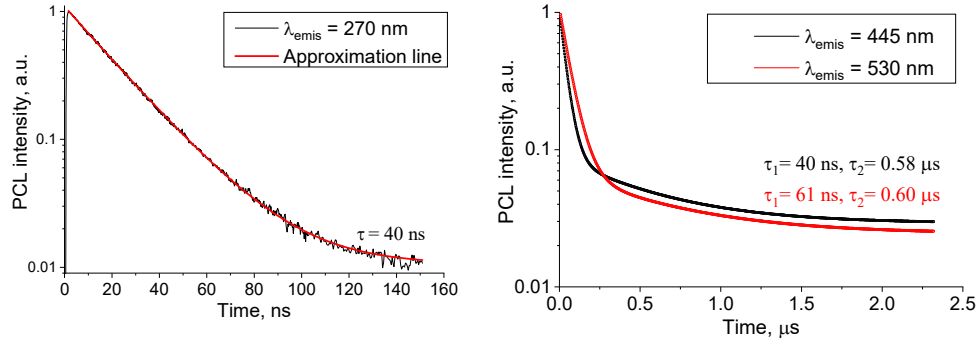

Fig. 2. Left: PCL decay kinetics measured for *d—f* transition. Right: PCL decay kinetics of $K_3Lu(PO_4)_2:Pr^{3+}$ (1 %) measured for defect-related emission

The work was partially supported by the Ministry of Science and Higher Education of the Russian Federation through the basic part of the government mandate, project No. FEUZ-2020-0060.

References

1. E. Trofimova, S. Omelkov, I. Romet, M. Kirm, V. Pustovarov, F. Piccinelli, J. of Lumin. **240** (2021)
2. V.A. Pustovarov, K.V. Ivanovskikh, S.A. Kiselev, E.S. Trofimova, S. Omelkov, M. Bettinelli, Opt. Mater. **108** (2020)
3. K V. Ivanovskikh, V. A. Pustovarov, S. Omelkov, M. Kirm, F. Piccinelli, M. Bettinelli, J. Lumin. **230** (2021)

Modeling of the crystal field, magnetoelastic interactions and random lattice deformations in $Pr_2Zr_2O_7$

Vera Klekovkina[1,bb], *Nurbulat* Abishev[1]

[1]Kazan Federal University, Institute of Physics, 420008 Kazan, Russia

Abstract. We present the results of simulations of the spectral and thermodynamic properties of $Pr_2Zr_2O_7$ crystals based on the distribution function of random strains induced by point defects in an elastically anisotropic continuum.

1 Introduction

Rare earth oxides with the pyrochlore structure and the general formula unit $RE_2M_2O_7$ (where RE is a rare earth ion, M is a 4-valent metal ion) attract attention of the scientific community due to their exotic magnetic ground states. The magnetic properties of these compounds are determined by magnetic exchange and dipolar interactions between RE ions, and by the interaction of RE ions with a crystal field (CF). In the trigonal crystal field of a perfect crystal, the ground electronic state of the Pr^{3+} ion in $Pr_2Zr_2O_7$ is a non-Kramers doublet [1]. The first excited state has the energy of ~110 K [1]. Simulations of the magnetic properties of praseodymium zirconate at low temperatures are usually performed using the spin-Hamiltonian operating in the space of states of the ground doublet. The experimentally observed Schottky anomaly in the temperature dependence of the heat capacity around 2 K [1-4] points on the splitting of the ground doublet of the Pr^{3+} ions. The nature of interactions leading to this splitting remains unclear up to now. The splitting was assumed to be constant [5] or random with the half-Lorentz distribution function [6,7] which has no physical meaning. The dependence of the heat capacity and magnetic susceptibility [8, 9] on the sample indicates the presence of defects in $Pr_2Zr_2O_7$ crystals. Simulations of the spectral properties of $Pr_2Zr_2O_7$ based on the distribution function of random strains derived in [10] were performed in [9].

2 Results and discussion

In the present work, we model the spectral and thermodynamic properties of $Pr_2Zr_2O_7$ assuming the presence of point lattice defects which induce random strains. Parameters of the distribution function of random strains represented by the generalized Lorentz distribution for all six deformation tensor components were simulated with taking into account the elastic anisotropy of the crystal lattice following the theory developed in [11]. The width of the distribution proportional to the concentration of defects is considered as a fitting parameter. We calculated the CF parameters within the framework of the exchange charge model. The resulting set of parameters was corrected by analyzing the inelastic neutron scattering and optical Raman scattering spectra available in the literature. After that, the obtained parameters

[bb]Corresponding author: vera.klekovkina@kpfu.ru

of the exchange charge model were used in the calculations of the parameters of the electron-deformation interaction. The magnetic interactions between the Pr^{3+} ions are considered in the mean-field approximation. The quantum mechanical and quantum statistical observables calculated for fixed values of strains, temperatures and external magnetic fields are averaged with the distribution function of random deformations. This approach allowed us to reproduce successfully low energy profiles of the low temperature inelastic neutron scattering spectra and the specific features of the low temperature heat capacity of $Pr_2Zr_2O_7$.

N. Abishev acknowledges the support by the Russian Foundation for Basic Research (project No. 19-32-90044).

References

1. K. Kimura, S. Nakatsuji, J.-J. Wen, C. Broholm, M.B. Stone, E. Nishibori, H. Sawa, Nat. Commun. **4**, 1934 (2013)
2. K. Matsuhira, C. Sekine, C. Paulsen, M. Wakeshima, Y. Hinatsu, T. Kitazawa, Y. Kiuchi, Z. Hiroi, S. Takagi, J. Phys.: Conf. Ser. **145**, 012031 (2009)
3. K. Kimura, S. Nakatsuji, JPS Conf. Proc. **3**, 014027 (2014)
4. S. Petit, E. Lhotel, S. Guitteny, O. Florea, J. Robert, P. Bonville, I. Mirebeau, J. Ollivier, H. Mutka, E. Ressouche, C. Decorse, M. Ciomaga Hatnean, G. Balakrishnan, Phys. Rev. B **94**, 165153 (2016)
5. P. Bonville, S. Guitteny, A. Gukasov, I. Mirebeau, S. Petit, C. Decorse, M. CiomagaHatnean, G. Balakrishnan, Phys. Rev. B **94**, 134428 (2016)
6. S.M. Koohpayeh, J.-J. Wen, B.A. Trump, C.L. Broholma, T.M. McQueen, J. Cryst. Growth **402**, 291 (2014)
7. O. Benton, Phys. Rev. Lett. **121**, 037203 (2018)
8. M. Ciomaga Hatnean, C.Decorse, M. R. Lees, O. A. Petrenko, D. S.Keeble, G. Balakrishnan, Mater. Res. Express **1**, 026109 (2014)
9. N. Martin, P. Bonville, E. Lhotel, S. Guitteny, A. Wildes, C. Decorse, M. Ciomaga Hatnean, G. Balakrishnan, I. Mirebeau, S. Petit, Phys. Rev. X **7**, 041028 (2017)
10. B.Z. Malkin, D.S. Pytalev, M.N. Popova, E.I. Baibekov, M.L. Falin, K.I. Gerasimov, N.M. Khaidukov, Phys. Rev. B **86**, 134110 (2012)
11. B.Z. Malkin, N.M. Abishev, E.I. Baibekov, D.S. Pytalev, K.N. Boldyrev, M.N. Popova, M. Bettinelli, Phys. Rev. B **96**, 014116 (2017)

Dual-center $Gd_2O_3:Tb^{3+}/Eu^{3+}$ nanophosphors for high-sensitive ratiometric thermometry

Ilya Kolesnikov[1,cc] and *Daria* Mamonova[1]

[1]St.Petersburg State University, 199034 St.Petersburg, Russia

Abstract. Development of novel luminescence thermometers with good thermometric performances is of crucial importance, because the accurate contactless thermal sensing is required in various applications. Here, two types of dual-center $Gd_2O_3:Tb^{3+}/Eu^{3+}$ nanophosphors, namely co-doping and physical mixture, were suggested as ratiometric luminescence thermometers. Luminescence intensity ratio between Tb^{3+} and Eu^{3+} lines was used as a temperature-dependent parameter. Absolute and relative thermal sensitivities and temperature resolution of suggested samples were calculated and compared with earlier reported dual-center ratiometric thermometers. Mixed $Gd_2O_3:Tb^{3+}$ 0.01 at.% + $Gd_2O_3:Eu^{3+}$ 0.2 at.% sample displayed unprecedented high relative thermal sensitivity of 5.6 % K^{-1}@473K.

Nanothermometry is a promising and rapidly developing area in contemporary science. The contactless temperature reading with the good spatial and temporal resolution achieved by monitoring the steady-state and kinetics photoluminescence properties of materials has received immense attention owing to their potential applications in biology, medicine, physical and chemical sciences. Among phosphors of different nature possessing temperature-dependent luminescence properties, crystalline oxides doped with rare earth ions are of special interest as they are photo- and temperature stable, chemically inert, and have immunity to blinking and photobleaching.

Ratiometric technique is the most used for luminescence thermal sensing because of the independence of temperature measurement on external factors such as excitation power, phosphor quantity or spatial distribution of the sample. Ratiometric thermometry is usually based on the analysis of the luminescence intensities ratio (LIR) between thermally coupled levels (TCLs). Temperature dependence of LIR is caused by the redistribution of electrons between the levels. The sensitivity of this technique is determined by the energy difference between the TCLs (ΔE), which defines the relative occupancy of the energy levels. When the energy gap is small (~200 cm^{-1}), the system can provide temperature measurements in a wide range of temperatures but with low relative sensitivity. Increase of the gap leads to the relative thermal sensitivity enhancement, but when the ΔE exceeds 2000 cm^{-1}, the coupling between the levels decreases, and the population of the upper level in the desired temperature range becomes too small to provide accurate sensing. To overcome the intrinsic limitation of relative thermal sensitivity, LIR should be calculated using luminescence bands from two different active centers [1,2].

Dual-center $Gd_2O_3:Tb^{3+}/Eu^{3+}$ thermal sensors were constructed by co-doping ($Gd_2O_3:Tb^{3+},Eu^{3+}$) and physical mixture of single-doped samples ($Gd_2O_3:Tb^{3+}$+ $Gd_2O_3:Eu^{3+}$). Emission spectra of co-doped $Gd_2O_3:Tb^{3+}$ 0.01 at.%, Eu^{3+} 0.2 at.% sample measured at different temperatures upon 311 nm excitation is shown in Fig.1a. Temperature was varied within wide range of 123–773 K. Due to the different thermal behavior of Tb^{3+} and Eu^{3+}

[cc] Corresponding author: ie.kolesnikov@gmail.com

emission intensities, it is possible to utilize LIR between $^5D_4$–$^7F_5$ and $^5D_0$–$^7F_2$ transition as temperature-dependent parameter. LIR temperature evolution for co-doped Gd_2O_3:Tb^{3+},Eu^{3+} sample is presented in Fig.1b. One can see that the suggested LIR can be used as sensing parameters in 123–473 K temperature range. Thermometric parameters including absolute and relative thermal sensitivities and temperature resolution were calculated for co-doped and mixed Gd_2O_3:Tb^{3+}/Eu^{3+} thermometers. It was found that studied thermal sensors could provide superior relative sensitivity at moderately high temperatures and sub-degree sensing at room temperature.

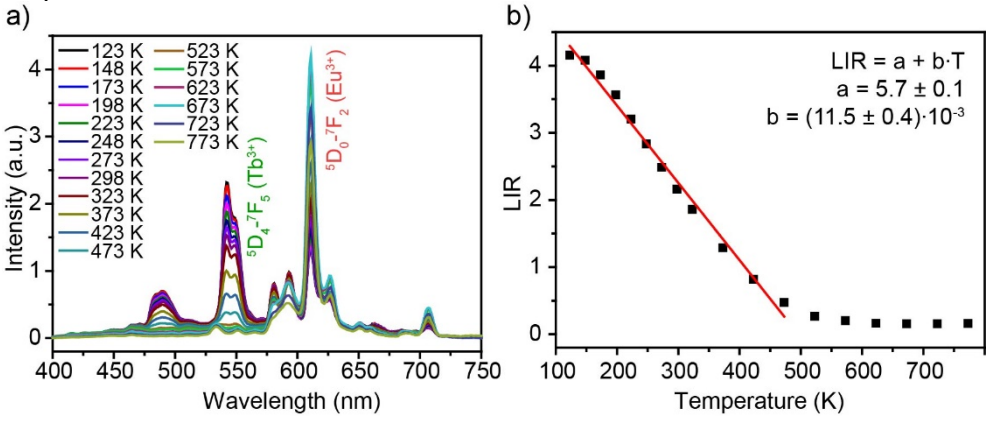

Fig. 1. a) Emission spectra of co-doped Gd_2O_3:Tb^{3+} 0.01 at.%, Eu^{3+} 0.2 at.% phosphors. b) Temperature evolution of LIR.

This research was funded by the Russian Science Foundation (№ 21-79-10018). Experimental measurements were carried out in «Center for Optical and Laser materials research», «Research Centre for X-ray Diffraction Studies», «Interdisciplinary Resource Center for Nanotechnology», Resource Center «Innovative technologies of composite nanomaterials» (St. Petersburg State University).

References

1. I. Kolesnikov, D. Mamonova, M. Kurochkin, E. Kolesnikov, E. Lähderanta, A. Manshina, ACS Appl. Nano Mater. **4**, 12481−12489 (2021)
2. Q. Wang, M. Liao, Q. Lin, M. Xiong, Z. Mu, F. Wu, J. Alloys Compd. **850**, 156744 (2021)

Raman spectroscopy of $SrLnCuS_3$ (Ln=La, Nd, Tm): experiment and ab initio calculation

Svetlana Krylova[1,dd], *Vladimir* Chernyshev[2], *Anna* Ruseikina[3], *Maxim* Grigoriev[3], *Aleksandr* Aleksandrovsky[1] and *Alexander* Krylov[1]

[1]Kirensky Institute of Physics, FRC KSC SB RAS, Krasnoyarsk, 660036, Russia
[2]Institute of Natural Sciences and Mathematics, Ural Federal University, Ekaterinburg, 620002, Russia
[3]Institute of Chemistry, University of Tyumen, Tyumen, 625003, Russia

Abstract. The Raman spectra of $SrLaCuS_3$, $SrNdCuS_3$, $SrTmCuS_3$ compounds have been investigated. Ab initio calculations of the crystal structure and phonon spectrum of the compounds have been carried out. The types and wave numbers of the fundamental modes have been determined. The experimental Raman spectra have been interpreted.

1 Introduction

The investigated sulphides belong to the family $ABCX_3$, where A –alkaline-earth metal, B – d- or f-element, C – d-element, X – chalcogenide. The chalcogenide compounds containing transition and rare earth elements are of interest because the wide freedom in the combination of cations makes it possible to change the type of structure and a sharp change in the band gap, electrical and optical characteristics. The magnetic, semiconductor, optical and thermodynamic properties have been studied for some compounds from this family [1-4]. Complex sulphides have interesting physical properties, which makes it possible to use them in optical and electronic technologies. The compounds $ABCX_3$ can crystallize in seven structural types [5]. $SrLaCuS_3$, $SrNdCuS_3$, $SrTmCuS_3$ was synthesized in different structural types. $SrLaCuS_3$ and $SrNdCuS_3$ was crystallized in *Pnma* space group, Ba_2MnS_3 and $BaLaCuS_3$ structural types, respectively. The crystals of $SrTmCuS_3$ are rhombic, space group *Cmcm*, $KZrCuS_3$ structural type.

1 Experiment and ab initio calculation

Raman spectra of $SrLaCuS_3$, $SrNdCuS_3$, $SrTmCuS_3$ compounds were collected in backscattering geometry, using a triple-monochromator Jobin Yvon T64000 Raman spectrometer. Single-mode krypton 647.09 nm of Lexel Kr+ laser was used as excitation light source for $SrTmCuS_3$, the power at the sample being limited to 5 mW in order to avoid laser-induced effects within the sample during the measurement. DPSS laser Excelsior-532-300-CDRH 532 nm and power 5 mW on a sample was used as an excitation light source for $SrLaCuS_3$ and $SrNdCuS_3$.

Ab initio calculations of the phonon spectra of these compounds were carried out for the first time. Frequencies and types of the phonon modes were determined from the ab initio calculation. The degree of participation of each ion in a particular mode is estimated from the analysis of displacement vectors obtained from this ab initio calculations. The calculations were carried out in the framework of density functional theory (DFT) using the B3LYP

[dd] Corresponding author: slanky@iph.krasn.ru

exchange-correlation functional [6, 7], which takes into account both local and nonlocal Hartree-Fock exchanges. The calculations were performed in the CRYSTAL17 program designed to simulate periodic structures [8]. The accuracy of calculating the self-consistent field was set at 10^{-9} a.u. The accuracy of the calculation of the two-electron integrals was set at least 10^{-8}.

The Raman spectra of $SrLaCuS_3$, $SrNdCuS_3$, $SrTmCuS_3$ compounds have been investigated. The experimental spectra have been interpreted. There is good agreement between the experimental and calculated data. The similarities and differences depending on the ion in B position have been established. Strontium and copper ions are appreciably involved in low-frequency modes. Sulfur is involved in all vibrational modes. Sulfur is strongly involved in the modes with frequencies above 180 cm^{-1}. Thulium ions do not participate in Raman scattering modes, in contrast to lanthanum and neodymium.

The work of Krylova S. was financially supported by the Russian Foundation for Basic Research and DFG project number No 21-52-12018. The research of Ruseikina A. was supported by the Tyumen region within the framework of the grant agreement in the form of a grant to non-profit organizations no. 89-don dated 07.12.2020. Chernyshev V. thanks the Ministry of Science and Higher Education of the Russian Federation (project no. FEUZ-2020-0054) for financial support.

References

1. M.F. Mansuetto, P.M. Keane, J.A. Ibers, J. Solid State Chem. **101,** 257-264 (1992).
2. Kwasi Mitchell, Fu Qiang Huang, Adam D. McFarland, Christy L. Haynes, Rebecca C. Somers, Richard P. Van Duyne, and James A. Ibers, Inorg. Chem. **42**, 4109-4116 (2003).
3. F. Furuuchi, M. Wakeshima, Y. Hinatsu, J. Solid State Chem. **177** (11), 3853-3858 (2004).
4. M. Wakeshima, F. Furuuchi, Y. Hinatsu, J. Phys.: Condens. Matter **16** (30), 5503 (2004).
5. Lukasz A. Koscielski, James A. Ibers, Z. Anorg. Allg. Chem. **638** (15), 2585-2593 (2012).
6. A.D. BeckeJ. Chem. Phys. **98**, 5648-5652 (1993).
7. P.L. Stephens, F.J. Devlin, C.F. Chabalowski, M.J. Frisch, J. Phys. Chem. **98**, 11623-11627 (1994).
8. R. Dovesi, V. R. Saunders, C. Roetti, R. Orlando, C. M. Zicovich-Wilson, F. Pascale, B. Civalleri, K. Doll, N. M. Harrison, I. J. Bush, Ph. D'Arco, M. Llunel, M. Causa, Y. Noel, L. Maschio, A. Erba, M. Rerat, S. Casassa, CRYSTAL17 User's Manual (2018).

Light transport in a random ensemble of resonant atoms in a waveguide: Anderson localization of light v.s. diffuse radiation transfer

Aleksei Kuraptsev[ee]

Peter the Great St. Petersburg Polytechnic University, 195251, St. Petersburg, Russia

Abstract. Light transport in a disordered ensemble of resonant atoms placed in a waveguide is found to be very sensitive to the sizes of cross section of a waveguide. Based on self-consistent quantum microscopic model treating atoms as coherent radiating dipoles, we have shown that the nature of radiation transfer changes from Anderson localization regime in a single-mode waveguide to a traditional diffuse transfer in a multi-mode one. Moreover, the transmittance magnitude undergoes complicated step-like nonmonotonic dependence on the transverse sizes of a waveguide.

1 Motivation and problem statement

Light interaction with atoms in waveguide systems has attracted a considerable attention in recent years. It is caused by both nontrivial physical phenomena occurring in such systems and a wide range of opportunities to control over the optical properties of atomic ensembles. Now it is well known that cavity or waveguide changes the spatial structure of the modes of the electromagnetic field. It leads to an alteration in the character of interaction of an atom with electromagnetic field, including vacuum reservoir. In particular, it causes enhancement or inhibition of the spontaneous decay rate [1, 2].

Actually, modification of the modes of the electromagnetic field alters the character of any electromagnetic interaction between different particles in structured reservoirs. In particular, it leads to the modification of interatomic dipole-dipole interaction [3-6] and associated many-body cooperative effects [7-9]. This effect involves the changes in both far-field induced by long propagating waves in a waveguide and near-field induced by evanescent modes.

Increasing in the number of atoms leads not only to quantitative changes, but also can induce qualitatively new behavior of the considered quantum system. In particular, it causes Anderson localization of light. Therefore, the study of polyatomic cooperative effects in a waveguide deserves a special attention. However, many-body phenomena, such as multiple and recurrent scattering, single-photon superradiance and subradiance have not been studied in detail yet. In this work, we focus on many-body effects, which occur in polyatomic ensembles placed in a waveguide.

2 Highlights of the approach and results

General theory employed here considers coupled dipole model together with quantum description for the electromagnetic field. It represents fully quantum microscopic approach based on non-steady-state Schrodinger equation for the joint system which consists of all the atoms and the electromagnetic field including vacuum reservoir. This approach was developed

[ee] Corresponding author: aleksej-kurapcev@yandex.ru

previously for the description of cooperative effects induced by the dipole-dipole interaction in dense atomic ensembles [10] and further approved for atomic clusters in a Fabry-Perot cavity [7] and near a conducting surface [9], as well as for the atomic systems in a waveguide [6].

In this work we report the results of fully three-dimensional calculation of light intensity transmitted through a random ensemble of point scatterers in a waveguide. We show that the nature of light transport dramatically depends on the transverse sizes of a waveguide. Thus, when a waveguide is single-mode with respect to resonant transition wavelength, the regime of Anderson localization is realized even for an arbitrarily low atomic density. An increase in the transverse size turns a single-mode waveguide to a multimode one, that, in turn, instantly cancels Anderson localization and restores classical diffuse radiation transfer [11].

This work was supported by the Russian Science Foundation (Grant No. 21-72-10004).

References

1. D. Kleppner, Phys. Rev. Lett. **47**, 233 (1981)
2. P. Lambropoulos, G. M. Nikolopoulos, T. R. Nielsen, and S. Bay, Rep. Prog. Phys. **63**, 455 (2000)
3. T. Kobayashi, Q. Zheng, and T. Sekiguchi, Phys. Rev. A **52**, 2835 (1995)
4. G. S. Agarwal and S. D. Gupta, Phys. Rev. A **57**, 667 (1998)
5. G. Fiscelli, L. Rizzuto, and R. Passante, Phys. Rev. A **98**, 013849 (2018)
6. A. S. Kuraptsev and I. M. Sokolov, Phys. Rev. A **101**, 053852 (2020)
7. A. S. Kuraptsev and I. M. Sokolov, Phys. Rev. A **94**, 022511 (2016)
8. M. D. Lee, S. D. Jenkins, Y. Bronstein, and J. Ruostekoski, Phys. Rev. A **96**, 023855 (2017)
9. A. S. Kuraptsev and I. M. Sokolov, Phys. Rev. A **100**, 063836 (2019)
10. I. M. Sokolov, D. V. Kupriyanov, and M. D. Havey, J. Exp. Theor. Phys. **112**, 246 (2011)
11. A. S. Kuraptsev and I. M. Sokolov, arXiv:2105.01578

X-ray luminescence diamond-nanoparticle composites

Sergei Kuznetsov[1,ff], *Vadim* Sedov[1], *Arina* Drobysheva[1], *Artem* Martyanov[1], *Sergei* Batygov[1], *Yulia* Ermakova[1], *Alexander* Alexandrov[1], *Anna* Rezaeva[1], *Valerii* Voronov[1], *Ivan* Tiazhelov[1], *Marina* Nikova[2], *Vitaly* Tarala[2], *Dmitry* Vakalov[2], and *Kirill* Boldyrev[3]

[1]Prokhorov General Physics Institute of the Russian Academy of Sciences, 119991 Moscow, Russia
[2]Scientific and Laboratory Complex Clean Room, North Caucasus Federal University, 355009 Stavropol, Russia
[3]Institute of Spectroscopy of the Russian Academy of Sciences, Troitsk, Moscow, 108840, Russia

Abstract. The X-ray luminescence diamond composites were sufficiently synthesized. Composites consist of diamond film with embedding SrF_2: Eu and $Y_3Al_5O_{12}$: Ce nanoparticles, which prepared by co-precipitation from aqueous solutions. The compositions with highest X-ray luminescence intensity were determined. Designed composites demonstrated bright X-ray luminescence, which promising as X-ray visualization screen.

An increase in the output power of synchrotrons and X-ray free-electron lasers dictates the need to develop efficient X-ray luminescent screens and scintillators that would have long-term stability when exposed to high-energy beams. The currently used bulk crystalline materials, although they exhibit rather intense X-ray luminescence, have low thermal conductivity and, therefore, have a high tendency to degradation under the influence of powerful X-ray radiation. Early, we proposed new approach to preparing composite X-ray visualizer based on the diamond film with embedding nanoparticles [1].

The nanoparticles were synthesized by co-precipitation from aqueous solution technique with followed thermal treatment at 1100 ºC and 600 ºC, respectively. Diamond films were synthesized by chemical vapor deposition in hydrogen-methane gas mixtures in a microwave plasma reactor ARDIS-100. X-ray luminescence spectra were recorded on FSD-10 and Ocean Insight spectrometer model HDX-UV-VIS at W-anode and Ag-anode as X-ray sources, respectively.

We developed composites based on polycrystalline diamond with embedded nanoparticles of $Y_3Al_5O_{12}$: Ce and SrF_2: Eu exhibiting intense X-ray luminescence and, at the same time, resistant to the conditions of diamond synthesis by plasma-chemical vapor deposition.

This work was supported by Russian Science Foundation, grant №22-13-00401.

References

1. V.S. Sedov, S.V. Kuznetsov, V.G. Ralchenko et al. Diamond-EuF_3 nanocomposites with bright orange photoluminescence. Diamond and Related Materials. **72**, 47 (2017). v.72. p.47-52.

[ff] Corresponding author: kouznetzovsv@gmail.com

Current mode of photomultiplier tube operation for recording the kinetics of weak optical signals

Vladimir I. Solomonov[1,2], *Alfiya V.* Spirina[1], *Anna S.* Makarova[1,gg], *Aleksandr I.* Lipchak[1], *Aleksey V.* Spirin[1], and *Vasiliy V.* Lisenkov[1]

[1]Institute of Electrophysics UB RAS, 106 Amundsen St., 620016 Ekaterinburg, Russia
[2]Ural Federal University, 19 Mira St., 620002 Ekaterinburg, Russia

Abstract. A technique for measuring the kinetics of weak optical signals in the current mode of operation of a photomultiplier tube with its load on the high-resistance input of a digital oscilloscope has been developed. The applicability of this technique for determining the kinetic characteristics was evaluated in the study of lines/bands of pulsed cathodoluminescence of ceramic and single-crystal samples of yttrium-aluminum garnet, pure and doped with Nd^{3+} and Cr^{3+} ions.

1 Introduction

In the current mode of photomultiplier tube (PMT) operation, apart from preamplifiers, a high load resistance (about 1 MΩ) can be used to amplify the signal. It seems to lead to an increase in the influence of dark currents and electrical parameters of the circuit on the measured kinetic curves and, consequently, to a decrease in the temporal resolution. Nevertheless, the PMT current mode can be used to measure the kinetics of weak luminescence of condensed matter.

2 Experimental

To carry out kinetic studies of intrinsic and impurity luminescence centers, pulsed cathodoluminescence was excited by irradiating the samples with an electron beam with a duration of 2 ns, a current density of 130 A/cm^2 and an average electron energy of 170 keV. To determine the kinetic instrumental function of the measuring circuit, a signal from the scattered radiation of the LS-2134 neodymium laser second harmonic with a half-amplitude duration of 15 ns and a signal from a DSL65005 LED rectangular pulse with a duration of 1 ms were recorded from FEU-100 and FEU-62 photomultiplier tubes, respectively.

In both cases, the optical signal was transmitted to the entrance slit of an MDR-41 monochromator by means of a multicore fiber. The FEU-100 and the FEU-62 were used as radiation detectors in the spectral ranges of 200–700 nm and 700–1200 nm, respectively. Then the signal from the PMT (R = 1 MΩ) was transmitted to the oscilloscope high-resistance input through a 1.5-meter-long coaxial cable with a wave impedance of 50 Ω. Depending on the intensity of the measured light pulses, the PMT power supply voltage was set from 1200 to 1600 V. All measurements were carried out at room temperature of the samples in air.

3 Results

Figure 1 shows the schematic diagram of the PMT measuring circuit. Due to Kirchhoff's first law, an expression for the photocurrent I_p depending on the voltage across the resistance U_R becomes:

[gg] Corresponding author: anniebubnova@mail.ru

$$I_p = \frac{LC}{R}\frac{d^2U_R}{dt^2} + C\frac{dU_R}{dt} + \frac{U_R}{R}. \quad (1)$$

where L is the circuit inductance, C - capacitance, R - measuring load resistance, t is time.

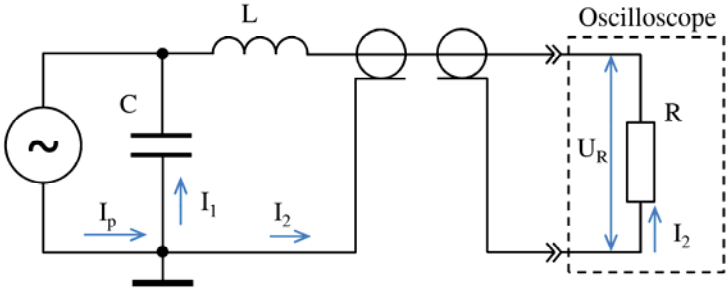

Fig. 1. Schematic diagram of the PMT measuring circuit.

As a result of evaluating each of the equation terms, it was found that the first term with the second-order derivative can be neglected. Then the solution of this equation with respect to the measured signal becomes

$$U_R = R\frac{exp\left(-t/\tau_a\right)}{\tau_a}\int_0^t I_p(t')exp\left(t'/\tau_a\right)dt'. \quad (2)$$

Essentially, expression (2) is a convolution of two signals – the photocurrent pulse I_p and the kinetic instrumental function of the measuring circuit

$$f(t,t') = exp\left[-\frac{t-t'}{\tau_a}\right], \quad (3)$$

where $t - t'$ is the interval between the measurement time of U_R and the current time of the photocurrent, and $\tau_a = RC$ is the characteristic time of the capacitive discharge, or the instrumental time of the measuring circuit. When recording signals from a pulse with a duration of 15 ns and a rectangular pulse with a duration of 1 ms, the curves of the kinetic instrumental function were found to be described by a single-exponential law. The values of τ_a were 169 μs and 172 μs for the FEU-100 and the FEU-62, respectively.

Neglecting the term with the second-order derivative, equation (1) can be used to determine the kinetic parameters. Mathematically, it represents the deconvolution equation of expression (2), which is conveniently written as follows

$$I_p = \frac{\tau_a}{R}\left(\frac{dU_R}{dt} + \frac{U_R}{\tau a}\right) \quad (4)$$

To verify the operability of this technique for determining the kinetic characteristics of luminescence, we studied the lines/bands of pulsed cathodoluminescence of ceramic and single-crystal samples of yttrium aluminum garnet, pure and doped with Nd^{3+} and Cr^{3+} ions. The characteristic kinetic times obtained by fitting the deconvoluted curves were consistent with the literature data.

In cases where the kinetic laws of the luminescence decay are known in advance, the characteristic times can be obtained by fitting the curve of the measured signal U_R directly, considering the kinetic instrumental function of the measuring circuit.

This work was supported in part by the Russian Foundation for Basic Research, grant № 20-08-00018.

Implementation of revival of silenced echo memory protocol in $^{167}Er^{3+}:Y_2SiO_5$ crystal

Mansur Minnegaliev[1,hh], *Konstantin* Gerasimov[1], *Timur* Sabirov[1], *Ravil* Urmancheev[1], and *Sergey* Moiseev[1]

[1]Kazan Quantum Center, Kazan National Research Technical University, Kazan, Russia

Abstract. The development of an efficient multi-qubit quantum memory (QM) is one of the key tasks in optical quantum technologies. In this work a quantum memory protocol based on the revival of silenced echo (ROSE) signal in a $^{167}Er^{3+}:Y_2SiO_5$ crystal at a telecommunications wavelength for input light fields with a small number of photons has been experimentally implemented. A storage efficiency of 44% with a storage time of 40 μs was achieved. The input pulse contained on average ~340 photons, and the reconstructed echo signal ~150 photons, at a signal-to-noise ratio = 4. The main source of noise is the spontaneous emission of atoms remaining in the excited state due to the imperfection of two rephasing pulses. Methods for increasing of signal to noise ratio are proposed and discussed in order to implement efficient quantum memory for single-photon light fields.

Active development of optical quantum technologies including optical quantum computing and long-range quantum communications stimulates the creation of quantum memory (QM). The creation of highly-efficient QM will not only significantly expand the capabilities of these technologies, but also leads to fundamental impact on the creation of new directions in their development [1]. In last decade, there was proposed and experimentally realized a number of protocols of QM. The schemes based on photon echo in solid state systems [2,3] demonstrated very promising results for achieving high quantum efficiencies and information capacity. Herein, the *revival of silenced echo* (ROSE) memory protocol seems especially attractive due to the possible use of natural inhomogeneously broadened line [4] that could significantly simplify practical implementation of QM. Another important task is the implementation of optical quantum memory for telecom wavelengths. In this work we used $^{167}Er^{3+}:Y_2SiO_5$ crystal. The $^4I_{15/2} - {}^4I_{13/2}$ optical transition of erbium ions in the Y_2SiO_5 crystal is interesting because its wavelength λ = 1536 nm lies in the optical transparency window of standard telecom fiber. Moreover, it possesses quietly long coherence time of optical transition 1.4 ms in external magnetic field and a typical inhomogeneous broadening of 500 MHz [5]. The presence of hyperfine sublevels for $^{167}Er^{3+}$ makes it possible to implement a long-lived spin-wave quantum memory, since the coherence time between them can reach 1 second, as was shown in the work [4].

A tunable single-frequency diode laser (Toptica CTL-1500) was tuned to a wavelength λ=1536.46 nm, corresponding to the $^4I_{15/2} - {}^4I_{13/2}$ transition (site 1). The $^{167}Er:Y_2SiO_5$ crystal with concentration of erbium ions c = 0.005 at. % was cooled down to 1.3K. An external magnetic field with amplitude of 2kG and with angle of 135° with respect to D1 axis was applied. Input signal and control laser pulses propagated in opposite directions along the b axis of the crystal. In such condition the absorption for signal pulse was $\alpha L = 2.4$ and the coherence time of optical transition was $T_M = 280$ μs (x = 1.35). We used a 2.4 μs Gaussian pulse (FWHM)

[hh] Corresponding author: mansur@kazanqc.org

as the input signal. The control pulses were with amplitude and frequency modulation. In the first experiments we implemented optical quantum memory ROSE protocol in this crystal for bright input pulses with recovery efficiency up to 58% and storage time of 40 μs. The analysis of the obtained experimental dependence of the photon echo signal recovery efficiency on the rephasing pulse intensity was carried out by us based on the area theorem approach for the photon echo [6]. Finally, the storage of the signal light pulse with n_{signal} ~ 340 photons on average was implemented (black curve at t = 0 in Fig. 1). In this case the ROSE echo signal contained n_{echo} ~ 150 photons on average (blue curve at t = 40 μs in Fig. 1). The optical noise level was ~40 photons within the echo temporal mode.

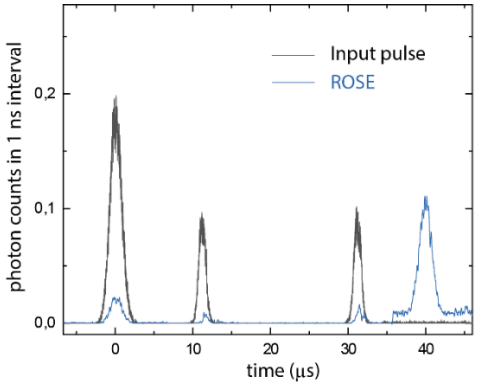

Fig. 1. Storage of weak coherent input pulse (black curve at t = 0) with ~340 photons. Revival of silenced echo signal (blue curve at t=40 μs) contained ~150 photons in average. Retrieval efficiency of input pulse was 40%. Optical noise level from spontaneous emission within the echo temporal mode was ~40 photons.

This research has been supported by Russian Science Foundation (project № 21-72-00115)

References

1. K. Heshami, D. G. England, P. C. Humphreys, P. J. Bustard, V. M. Acosta, J. Nunn, and B. J. Sussman, J. Mod. Opt. **63**, 2005 (2016)
2. S. A. Moiseev and S. Kröll, Phys. Rev. Lett. **87**, 173601 (2001)
3. W. Tittel, M. Afzelius, T. Chaneliére, R. L. Cone, S. Kröll, S. A. Moiseev, and M. Sellars, Laser Photon. Rev. **4**, 244 (2009).
4. M. M. Minnegaliev, K. I. Gerasimov, R. V Urmancheev, A. M. Zheltikov, and S. A. Moiseev, Phys. Rev. B **103**, 174110 (2021).
5. J. Dajczgewand, J.-L. Le Gouët, A. Louchet-Chauvet, and T. Chanelière, Opt. Lett. **39**, 2711 (2014)
6. M. M. Minnegaliev, K. I. Gerasimov, T.N. Sabirov, R. V Urmancheev, and S. A. Moiseev, JETP Letters **115**, 12 (2022).

Investigation of luminescent Mn centers in yttrium-aluminum borate single crystals

Anastasiia Molchanova[1, ii], *Kirill* Boldyrev[1], *Aleksey* Veligzhanin[2], *Kirill* Khaydukov[3], *Evgeniy* Khaydukov[3], and *Marina* Popova[1]

[1]Institute of Spectroscopy of the Russian Academy of Sciences, 108840 Troitsk, Moscow, Russia
[2]National Research Centre "Kurchatov Institute", 123182 Moscow, Russia
[3]Scientific Research Centre "Crystallography and Photonics", Russian Academy of Sciences, 119333 Moscow, Russia

Abstract. An extensive study of the luminescence characteristics of Mn impurity ions in a $YAl_3(BO_3)_4$ single crystal has been carried out. The spin-allowed and spin-forbidden transitions in Mn ions were determined from the absorption, photoluminescence, and luminescence excitation spectra. A broadband temperature-dependent luminescence was registered in the spectral range 8500 – 19000 cm^{-1}. The first decay studies of the $^2E \rightarrow {}^4A_2$ *R*-lines red luminescence in Mn^{4+} have been carried out. In addition, the study of the crystal by the EXAFS method in combination with the methods of optical spectroscopy made it possible to draw a conclusion about the valence states of Mn in $YAl_3(BO_3)_4$.

1 Introduction

Crystals of yttrium aluminum borate $YAl_3(BO_3)_4$ (YAB) doped with various rare-earth and transition-metal ions are well-known phosphors promising for use as materials for display panels, laser media, scintillators, and effective eye-safe microchips [1–3]. Phosphors with Mn ions as luminescence centers are of interest because of the characteristic emission of Mn^{4+} in the red range (*R*-line $^2E \rightarrow {}^4A_2$) [4] and broadband, extremely temperature-sensitive Mn^{3+} luminescence in the near IR and visible spectral ranges (due to which compounds with Mn^{3+} are also topical materials for thermoluminescent sensors).

2 Results

Using the EXAFS method, we found that Mn is contained in YAB mainly in the divalent state substituting for Y^{3+}. This is consistent with EPR results [5]. However, Mn^{4+} *R*-lines have already been registered in [6]. Thus, Mn^{4+} is contained, apparently, in a trace amount. We managed to observe weak lines at 684.4 and 681.8 nm in the YAB:Mn absorption spectra at room temperature in the region characteristic of the $R_1 - R_2$ lines. As the temperature decreases, the peaks shift to longer wavelengths, their intensity increases, and the lines split into two components. These are tentatively assigned to Mn^{4+} in different positions. Absorption and luminescence spectra at 5 K are shown in Figure 1. Besides the zero-phonon lines, vibronic bands are observed both in the absorption and emission spectra.

[ii] Corresponding author: nastyamolchanova@list.ru

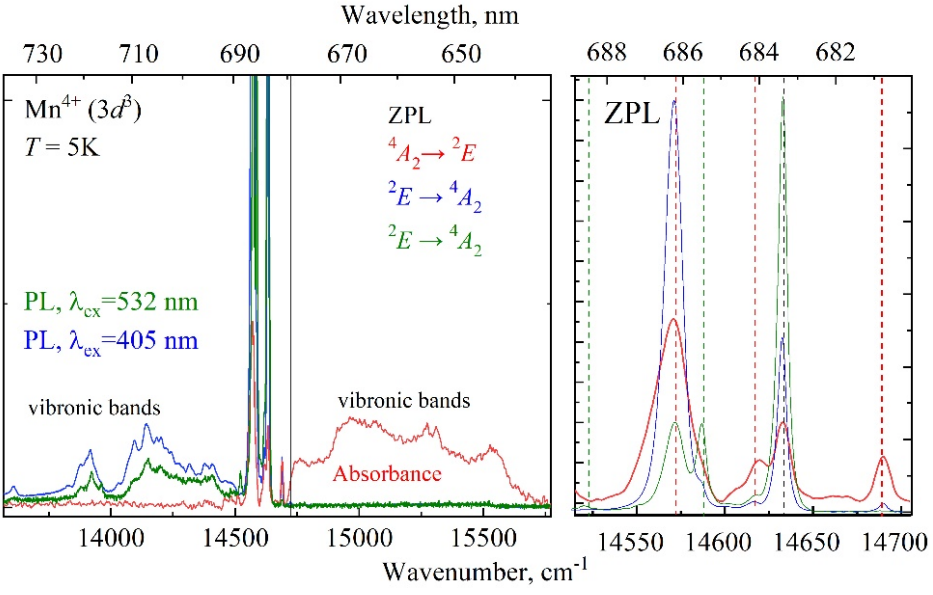

Fig. 1. Absorption and luminescence spectra of YAB:Mn in the region of $^2E \rightarrow {}^4A_2$ transitions of Mn^{4+} at $T = 5$ K.

In addition, broadband Mn^{3+} luminescence (8500 – 19000 cm^{-1}) was observed over the entire temperature range under study. At low temperatures, the spin-forbidden $^1T_2 \rightarrow {}^3T_1$ and $^1T_2 \rightarrow {}^5E'$, $^5E''$ transitions make the main contribution to the spectrum; at room temperature, the population of the $^5T_2$ level increases and broad bands of the corresponding spin-allowed transition $^5T_2 \rightarrow {}^5E'$, $^5E''$ appear in the spectrum, covering the forbidden transitions in Mn^{3+} and *R* lines of Mn^{4+}. The spin-allowed $^4A_2 \rightarrow {}^4T_2$ and $^4A_2 \rightarrow {}^4T_1$ transitions in Mn^{4+} were determined from the excitation spectra. Also, the first studies of the decay of the red luminescence of *R* lines were carried out: the lifetime of the excited state ^2E of the Mn^{4+} ion was measured. It is 1 ms at room temperature.

Financial support of the Russian Science Foundation (grant No 21-72-00134) is acknowledged. A.M. and K.B. are members of the Leading Scientific School of the Russian Federation (grant of the President of the Russian Federation NSh-776.2022.1.2).

References

1. G.V.L. Reddy, L.R Moorthy, T. Chengaiah,, B.C. Jamalaiah, Ceramics International **40**, 3399 (2014)
2. N.S. Bajaj, K.A. Koparkar, P.A. Nagpure, S.K. Omanwar, J. Opt. **46**, 91 (2017)
3. B.C. Jamalaiah, M. Jayasimhadri; G.V.L. Reddy, Phys. Chem. Glasses B **57**, 68 (2016)
4. A.A. Setlur, E.V. Radkov, C.S. Henderson et al., Chem. Mater. **22**, 4076 (2010)
5. A.M. Vorotynov, G.A. Petrakovski, Y.G. Shiyan et al. Phys. Solid State **49**, 463 (2007)
6. A.S. Aleksandrovsky, I.A. Gudim, A.S. Krylov, V.L. Temerov, Phys. Solid State **49**, 1695 (2007)

Excitation capture efficiency and decay kinetics in single crystals and ceramics based on YAG:Re^{3+}

Kseniia Orekhova[1,jj], *Aleksandr* Trofimov[1], *Tatiana* Popova[1], *Maria* Zamoryanskaya[1]

[1]Ioffe Institute RAS, 194021, Politekhnicheskaya st., Saint Petersburg, Russia

Abstract. The work is dedicated to the study of excitation and emission mechanisms in RE^{3+} ions (namely, Nd and Eu) in YAG single crystals and ceramics. Cathodoluminescence technique allowed us studying the dependence of CL rise rate on electron beam current and the dependence of decay times on electron beam energy (determining the electron beam penetration depth). It was demonstrated that the excitation capture efficiency does not significantly differ in single crystals and ceramics. The decay kinetics showed double exponential decay near the surface in single crystals samples and throughout the whole electron beam penetration depth in ceramics. The second decay component was attributed to the type of luminescence ions, which are located near the defects – non-radiative recombination centers. In ceramics they may be connected with grain boundaries and in single crystals – with disturbed crystalline structure due to their polished surface.

1 Introduction

Yttrium aluminium garnet doped with rare earth ions (YAG:RE^{3+}) is a well-known material for scintillation and luminescence applications. Whereas YAG:Eu^{3+} is mainly associated with LED and phosphor applications, YAG:Nd^{3+} is a well-known laser medium material and has a prospective of use as a scintillator. Ceramics form was proposed as an alternative to single crystals (SC), as its optical, mechanical, and thermal properties were found to be like the SC, and its fabrication had numerous advantages over SC growth. However, since there are many grain boundaries in ceramics, it is necessary to take into account and study their influence on the luminescent properties, in particular, on the excitation capture and its relaxation in the material.

Luminescent materials are usually estimated based on their optical and luminescent spectra and kinetics of luminescent bands. Luminescent kinetics is highly important in estimating the presence of trap levels in the material, and other material characteristics, that include interaction of luminescence centres with point defects. The aim of the work was to study the kinetics in YAG:Eu and YAG:Nd materials and to estimate how the matrix perfection, including point defects and interfaces affect it.

2 Samples and methods

The following samples were studied: SC of YAG:Nd and YAG:Eu, microceramics (MICRO) of YAG:Nd, and nanoceramics (NANO) of YAG:Nd and YAG:Eu.

[jj] Corresponding author: orekhova.kseniia@gmail.com

The main technique used for the study of the luminescent properties of the samples was cathodoluminescence (CL) technique. It is based on the E- beam interaction with solid state. Excitation capture efficiency was estimated according to the original method, described in detail in [1]. It is based on the CL rise rate dependence on the excitation density. The study of the excitation capture efficiency allows evaluating the presence of additional excitation channels (transfer from other luminescent centers and defects) and, in particular, to investigate traps that serve as centers of excitation transfer. The decay kinetics of CL bands allows interpreting luminescent bands and estimating the relative content of point defects that affect the nonradiative loss probabilities in the material.

3 Results

Excitation cpature efficiency was quite close for SC and ceramics samples, whereas the decay kinetics differed. The nonradiative loss probabilities were higher in ceramics samples, than in SC samples. Two types of luminescent centers – rare earth ions with different decay times were observed and studied in YAG:Nd and YAG:Eu SC and polycrystalline samples. It was shown that the relation between the content of ions with shorter and longer decay times varied with E-beam penetration depth in single crystals samples and remained constant in polycrystalline samples (Fig. 1).

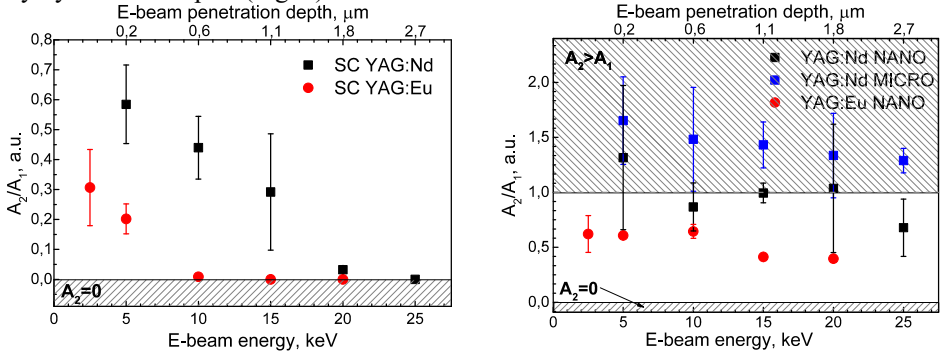

Fig. 1. The dependence of decay times amplitude ratio (A_2/A_1) on electron beam energy in a) SC samples; b) ceramics samples.

It may be explained by the assumption, that the shorter times of luminescent decay centers are associated with defects located nearby those luminescent centers and cause the higher probability of non-radiative energy dissipation from this luminescent center. It was shown that the energy of level affects the relation between the content of ions with shorter and longer decay times.

References

1. M.V. Zamoryanskaya, K.N. Orekhova, E.V. Dementeva, V.A. Kravets, G.A. Gusev Excitation capture efficiency of rare-earth ions emission levels upon electron-beam irradiation. J. Lumin. **239** 118350 (2021)

Influence of the ligand field in tris polyphenylcyclopentadienyl Ln^{3+} complexes on the energy of $4f^n$-$4f^{n-1}d$ band

Lada Puntus[1,kk], *Konstantin* Lyssenko[2], and *Dmitrii* Roitershtein[3]

[1]Kotel'nikov Institute of Radioengineering & Electronics of Russian Academy of Sciences, 125009, 11-7 Mokhovaya, Moscow, Russia
[2]M.V. Lomonosov Moscow State University, Chemistry Department, 1 Leninskie Gory Str., Building 3, 119991, Moscow, Russia
[3]A.V. Topchiev Institute of Petrochemical Synthesis, Russian Academy of Sciences, 29 Leninsky Prospect, 119991, Moscow, Russia

Abstract. The series of Ln complexes containing one, two or three polyphenylsubstituted cyclopentadienyl ligands were studied by means of optical spectroscopy, Xray analysis and quantum chemical calculations. The ligand field in the case of tris cyclopentadienyl Ln^{3+} complexes leads to decrease of the energy of $5dz^2$ orbital and as a result bands assigned to interconfigurational $4f^n$-$4f^{n-1}d$ transitions were observed in the luminescence excitation spectra. Moreover, the contribution of these transitions into the quantum yield of photoluminescence was found as well.

Molecular lanthanide complexes exhibiting bright photoluminescence are very attractive for the development of new materials for various domains from biology to catalyst, optics and material science. Most of Ln^{3+} complexes are luminescent with characteristic narrow-line emission caused by parity-forbidden 4f−4f, while the field of luminescent complexes that have other emitting configurations was almost undeveloped. Contrary to the large understanding of the 4f transitions, the knowledge on the $4f^n$-$4f^{n-1}d$ transitions is insufficient. Cyclopentadienyl (Cp) ligands is the most popular in the organolanthanide chemistry but a few reports on photophysical characteristics of the lanthanide complexes with Cp derivatives are known. One of the reasons is dominance of traditional approach – usage of various σ-bonded antenna ligands for design of luminescent Ln complexes. The energies of 5d states are extremely sensitive to ligand environment. Therefore, rather strong field of Cp ligand can be efficient instrument to enhance of luminescence sensitisation of Ln ion owing to f-d transitions.

The tris complexes of di- and triphenyl cyclopentadienyl ligands with Ln=La, Ce, Pr, Tb, Gd, Dy, Sm, Nd have been synthesized and mononuclear structures confirmed by X-ray diffraction were obtained (Fig. 1). All complexes are luminescent at ambient temperature. The excitation spectrum for the $(Cp^{Ph3})_3Ce$ (Fig. 2) contains two broad bands at 480 nm (*4f–5d*) of Ce^{3+} ion and 370 nm (*p-p** of Cp ligand). Complex $(Cp^{Ph3})_3Ce$ exhibit a broad band photoluminescence peaking at 540 and 620 nm. Energy of *4f–5d* band of Pr^{3+} ion is higher (400 nm). In the luminescence spectrum f-f transitions of the Pr^{3+} ion are also observed ($^1D_2$–$^3H_4$, $^3P_0$–$^3H_6$, $^3P_0$–$^3F_2$). Q_{Ln}^{Lig} of photoluminescence for $(Cp^{Ph3})_3Ce$ complex is 20%, while the one of $(Cp^{Ph3})_3Pr$ is 1% only. Analysis of energy transfer process has been

[kk] Corresponding author: lada_puntus@mail.ru

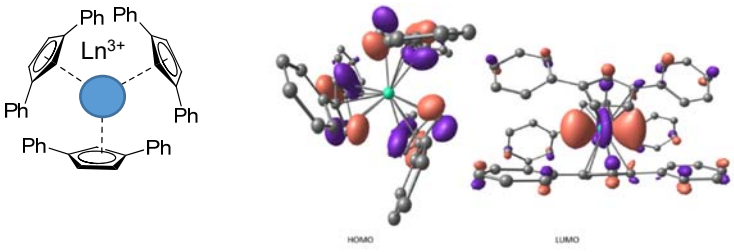

Fig. 1. Tris(cyclopentadienyl) complex (left) and HOMO and LUMO in $(Cp^{Ph2})_3Tb$ (right).

performed and supported by quantum chemical calculations. According to TD-DFT calculation of $(Cp^{Ph2})_3Tb$ for experimental geometry with the C_3 symmetry, the HOMO is almost totally localized on the equivalent Cp rings, while the LUMO is localized by 90% on Tb and corresponds to $5dz^2$ orbital. The significant lowering of the 5d orbital energy and possible contribution of the allowed f-d transitions into the luminescence spectra lead to unusual optical features. For example $(Cp^{Ph2})_2Tb$ complex is highly luminescent with very short lifetime (Q_{Tb}^{Lig} is 50% and $\tau_{obs} = 0.35$ ms). Therefore, the fact that a lanthanide complex is highly luminescent yet possesses a short lifetime does not represent a contradiction but could be the reflection of the participation of allowed f-d transitions in the energy transfer process.

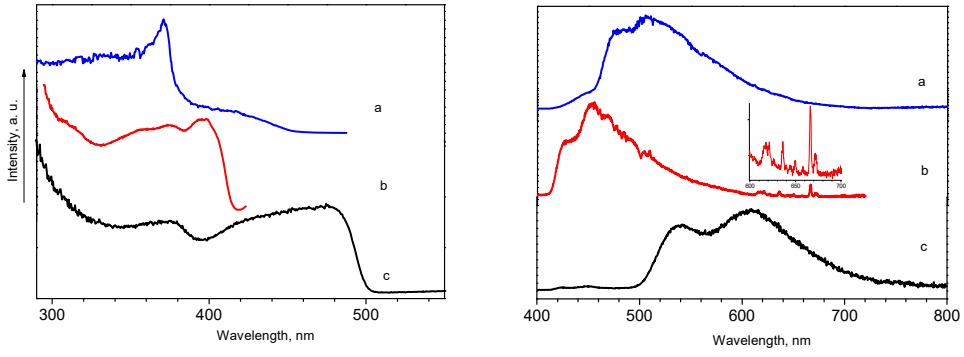

Fig. 2. Excitation (left) and luminescence (right) spectra of solid complexes $(Cp^{Ph3})_3Ln$ (Ln=La, Pr, Ce)

The main outcome of this research is a new strategy proposed for design of highly luminescent Ln(III) complexes based on the usage of π-cyclopentadienyl ligands as the main light harvesting antenna where lowered energy interconfigurational f-d transitions is involved in energy transfer process.

This research was supported by Russian Science Foundation (grant No. 22-13-00312).

References

1. D.M. Roitershtein, L.N.Puntus, A.A.Vinogradov, K.A. Lyssenko, M.E. Minyaev, M.D. Dobrokhodov, I.E. Nifant'ev, Inorganic Chemistry **57,** 16, 10119 (2018)
2. D.A. Bardonov, P.D. Komarov, V.I. Ovchinnikova, L.N. Puntus, M.E. Minyaev, K.A. Lyssenko, I.V. Taidakov, D.M. Roitershtein, Organometallics, **40**, 9, 1235 (2021)

Spectroscopy of f^{13} lanthanides in fluoride crystals

Evgeny Radzhabov[1,ll], *Roman* Shendrik[1], *Vladimir* Pankratov[2]

[1]Institute of Geochemistry SB RAS, Favorskii St. 1a, Irkutsk, 664033, Russian Federation
[2]Institute of Solid-State Physics, University of Latvia, 8 Kengaraga iela, LV-1063, Riga, Latvia

Abstract. The luminescence spectra of 4f-4f and 5d-4f transitions and absorption spectra of 4f-4f transitions of Tm^{2+}, Yb^{3+} ions were studied in crystals of fluorides CdF_2, CaF_2, SrF_2, BaF_2. The splitting of the atomic $^2F_{7/2}$, $^2F_{5/2}$ levels of Tm^{2+}, Yb^{3+} by the cubic field decreases linearly with increasing lattice distance. The positions of the Tm^{2+} or Yb^{3+} bands in fluoride crystals are well described by CASSCF+NEVPT calculations.

The f-f emission spectra of Tm^{2+} and Yb^{3+} at low temperatures consist of two sharp lines and a vibronic wing towards the long-wavelength side. The short-wavelength emission line is due to the Γ_7'-Γ_7 transitions, while the long-wavelength line arising from the Γ_7'-Γ_8 transitions [1, 2] (Fig.1).

The MeF_2-Tm emission was excited by laser radiation at 405 nm or 447 nm. The MeF_2-Yb emission was excited by laser radiation at 940 nm as well as by vacuum ultraviolet 6-9 eV on the photoluminescence endstation FINESTLUMI of MAXIV synchrotron facility (Lund, Sweden).

The distance between the lines decreases in the series CdF_2, CaF_2, SrF_2, BaF_2 (see Fig.1). Both lines will merge into one with an energy equal to the energy difference $F_{7/2}$-$F_{5/2}$ Tm^{2+} [3] or Yb^{3+} levels (8774.02 cm^{-1} or 10214 cm^{-1} respectively [4]).

The scheme of f-levels of Tm^{2+} and Yb^{3+} ions in fluoride crystals was calculated using the ORCA 5.0.3 software package [5]. Relativistic effects were considered with the ZORA method. The ZORA-def2-TZVP basis functions for ligands and SARC2-ZORA-QZVP for the f^{13} ion were used for the calculation. The TmF_8 (or TmF_8Me_{12}) cluster was surrounded by point charges (near 1000 charges) to simulate the crystal field.

Since the magnitude of the crystal splitting of the f^{13} ion levels largely depends on the first sphere of ligands, the geometry of the central (Tm or Yb) F_8 cluster surrounded by a sphere of alkaline earth ions and point charges was optimized. The geometry was optimized using the Gaussian09 package with the SDD (Tm, Yb, F) and LANL2MB (Cd, Ca, Sr, Ba) basis sets.

The results shown in Table 1 reflect the ratio of the crystal radii for coordination 8 of the Tm^{2+}(1.3A), Yb^{3+} (0.98A), Ca^{2+} (1.26A), Sr^{2+} (1.4 A), Ba^{2+} (1.56 A).

Table 1. Calculated and lattice distances in fluorides in angstroms.

	d(Tm^{2+}-F), A	d(Yb^{3+}-F), A	Lattice (Me-F), A
CdF_2	not exist	2.309	2.333
CaF_2	2.437	2.264	2.365
SrF_2	2.512	2.302	2.511
BaF_2	2.595	2.340	2.685

[ll] Corresponding author: eradzh@igc.irk.ru

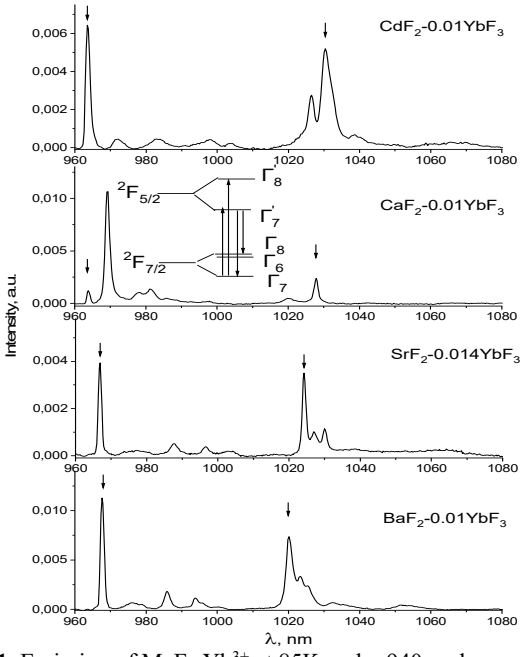

Fig. 1. Emission of MeF_2-Yb^{3+} at 85K under 940nm laser excitation.

The relative splitting of the Tm^{2+} and Yb^{3+} atomic states in fluorides were estimated quite accurately using CAS-SCF-NEVPT2 ab-initio calculation. The calculated energy $F_{7/2}$-$F_{5/2}$ is around two percent lower than the expe-rimental value. For comparison of the calculated and experimental levels we normalised its positions to energy of free spin-orbital splitting (see Fig. 2).

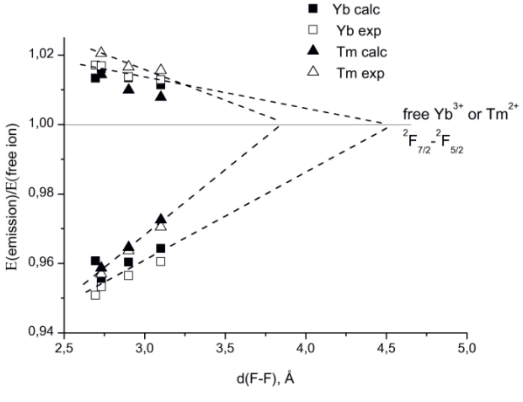

Fig. 2. Experimental and calculated relative position of Yb^{3+} emission lines.

The linear decrease in the splitting of the Tm^{2+} or Yb^{3+} (see Fig.2) levels by the crystal field with an increasing lattice constant is due to the relaxation of the nearest shell of fluorines.

References

1. Z. J. Kiss, Phys. Rev. **127** (3) 718 (1962)
2. I. Ignat'ev, V. Ovsyankin, J. Luminescence **72** 679-680 (1997)
3. E. Radzhabov, R. Shendrik, V. Pankratov (to be published)
4. W. Martin, R. Zalubas, L. Hagan, Tech. rep., No. PB-282067; NSRDS-NBS-60. Manchester Coll. of Science and Technology (UK). Dept. of Chemistry (1978)
5. F. Neese, F. Wennmohs, U. Becker, C. Riplinger, J. Chem. Phys. **152** 224108 (2020)

Light and spins in rare-earth doped garnets

Nikolai Romanov[1,mm], *Yulia* Uspenskaya[1], *Elena* Edinach[1], *Aleksandr* Gurin[1], *Hike* Asatryan[1], *Roman* Babunts[1], and *Pavel* Baranov[1]

[1]Ioffe Institute, 194021 Saint Petersburg, Russian Federation

Abstract. Spin-dependent optical properties of garnet crystals and garnet based ceramics, doped with cerium and also, along with cerium, co-doped with gadolinium or terbium, were studied by magnetic resonance detected via photoluminescence (PL). It was shown that the intensity of PL excited by circularly polarized light depends on the spin state of Ce^{3+}. In garnets co-doped with cerium and gadolinium direct evidence of the cross-relaxation between these two spin systems was obtained. The influence of the magnetic resonance of Tb^{3+} on the Ce^{3+} luminescence was demonstrated. In irradiated crystals and ceramics of cerium-doped gadolinium-gallium garnet, stimulation of the tunnelling afterglow by magnetic field was found. The report is based on an article prepared for a special issue of Journal of Luminescence VSI: Sergey Feofilov Memorial.

The spin-dependent effects that influence the Ce^{3+} emission in garnet crystals and ceramics doped with cerium and also, along with cerium, co-doped with gadolinium or terbium were studied using optically detected magnetic resonance (ODMR) at 35 and 94 GHz via photoluminescence (PL) of cerium. It was shown that the intensity of PL excited by circularly polarized light into the Ce^{3+} absorption bands can be used for selective monitoring the populations of the Ce^{3+} ground-state spin sublevels. Direct evidence of the cross-relaxation effects in garnet crystals containing two electron spin systems, i.e., the simplest one of Ce^{3+} ions with the effective spin $S = 1/2$ and the system of Gd^{3+} ions with the maximum spin $S = 7/2$, has been demonstrated [1]. EPR spectra of Gd^{3+} were detected optically by monitoring the Ce^{3+} luminescence intensity in a wide range of Gd concentrations (from 0.1 % to 100 % relative to Y).

High-frequency (94 and 130 GHz) EPR allowed to find a family of non-Kramers Tb^{3+} centres in yttrium aluminium garnet (YAG) crystals [2]. In YAG:Ce,Tb, EPR of Tb^{3+} ions was found to influence the PL intensity of Ce^{3+}. This suggests a coupling between the Tb^{3+} and Ce^{3+} systems Taking into account that cerium has no nuclear spin and that terbium has 100% of ^{159}Tb with a nuclear spin I = 3/2 and a large nuclear magnetic moment, the $Tb^{3+} - Ce^{3+}$ system in garnet crystals can be promising for coherent information processing.

A giant magnetic field effect on spin-dependent recombination of the radiation-induced defects has been found in cerium doped gadolinium based garnet crystals and ceramics [3], which are promising materials for scintillators. It is illustrated in Fig. 1 (a), which shows a decay of the afterglow measured at 1.8 K in $Gd_3Ga_3Al_2O_{12}$:Ce crystal after switching off UV excitation and its huge increase in magnetic field. The afterglow spectrum shown in the inset coincides with the Ce^{3+} emission. In (b), the magnetic field was increased from 0 to a certain value $B_{max}(n)$, then quickly decreased to a lower value and increased again up to a higher field $B_{max}(n+1)$ and so on. A sharp increase in the intensity of the afterglow in the scan n starts at a magnetic field close to B_{max} in the previous scan of field n-1, i. e. the system remembers the

[mm] Corresponding author: nikolai.romanov@mail.ioffe.ru

maximum field in the previous sweep. A similar afterglow behavior was observed in UV-irradiated $(Lu,Gd)_3(Ga,Al)_5O_{12}$:Ce ceramics. These effects have been attributed to huge Gd-induced internal magnetic fields that suppress recombination for parallel spins of recombining centers, and cross-relaxation with Gd^{3+} ions leading to spin reorientation and enabling recombination.

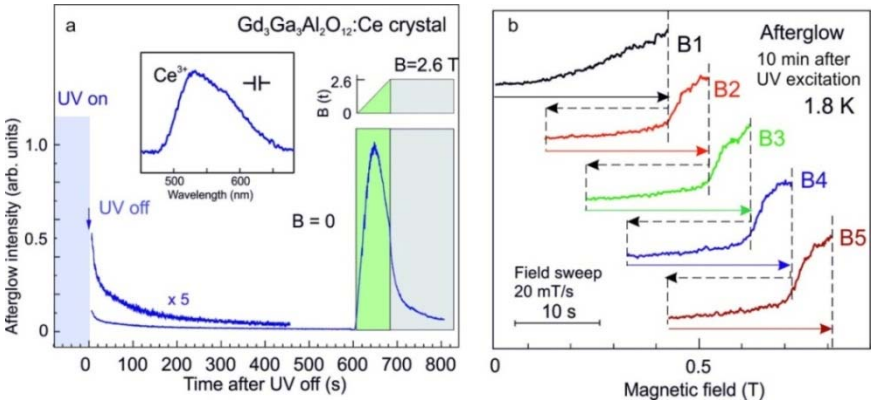

Fig. 1. (a) Time decay of the afterglow intensity in the $Gd_3Ga_3Al_2O_{12}$ single crystal doped with 0.1% of cerium after switching off of UV irradiation and a giant effect of a magnetic field on the afterglow intensity. Inset shows the afterglow spectrum measured at 1.8 K 10 min after UV irradiation switched off. It corresponds to Ce^{3+} emission. (b) A series of dependences of the afterglow intensity on the magnetic field, measured at 520 nm and 1.8 K with increasing field over several scans, in which the magnetic field changed from zero to a certain value at a rate 20 mT/s, then rapidly decreased to a lower value and increased again to a higher value.

In conclusion, the spin dependence of the luminescence intensity in garnets doped with Ce, Gd and Tb ions made it possible to detect magnetic resonance of these ions and to study optically induced spin-dependent processes. It was shown that in magnetic host materials, the energy stored during irradiation can be released in an external magnetic field.

This work was supported by the Russian Science Foundation under Grant № 20-12-00216. H.R.A. is grateful for the support of RFBR grant No.25-52-05002 Arm_a.

References

1. D.O. Tolmachev, A.S. Gurin, Yu.A. Uspenskaya, G.R. Asatryan, A.G. Badalyan, N.G. Romanov, A.G. Petrosyan, P.G. Baranov, H. Wieczorek, and C. Ronda, Phys. Rev. **B 95**, 224 (2017)
2. E.V. Edinach, Yu.A. Uspenskaya, A.S. Gurin, R.A. Babunts, H.R. Asatryan, N.G. Romanov, A.G. Badalyan, P.G. Baranov, Phys. Rev. **B 100** (2019) 104435
3. N.G. Romanov, D.O. Tolmachev, A.S. Gurin, Yu.A. Uspenskaya, H.R. Asatryan, A.G. Badalyan, P.G. Baranov, H. Wieczorek, C. Ronda, Appl. Phys. Lett. **106**, 262404 (2015)

Spectral-luminescent characteristics of zirconium dioxide solid solutions excited by synchrotron radiation

Polina Ryabochkina [1,nn], *Vladimir* Pankratov[2], *Sergey* Artemov[1] , *Elena* Lomonova[3], and *Natalia* Sidorova[1]

[1]National Research Ogarev Mordovia State University, Bolshevistskaya 68, 430005 Saransk, Russia
[2]University of Latvia, Institute of Solid State Physics, 8 Kengaraga iela, LV-1063 Riga, Latvia
[3]Prokhorov General Physics Institute of the Russian Academy of Sciences, Scientific Center for Laser Materials and Technologies, Vavilova 38, 119991 Moscow, Russia

Abstract. The report presents the results of a study of the spectral and luminescent characteristics of ZrO_2-Y_2O_3 and ZrO_2-Y_2O_3- Er_2O_3, ZrO_2-Y_2O_3-Ho_2O_3 crystals upon excitation by synchrotron radiation in the UV region. From the analysis of the luminescence and excitation spectra of these crystals, the energy levels of V^{1+} and V^{2+} defects associated with oxygen vacancies were determined. The influence of these defects on the radiation resistance of ZrO_2-Y_2O_3-Ho_2O_3 crystals is discussed.

1 Introduction

During the formation of the ZrO_2-Y_2O_3-R_2O_3 solid solution, heterovalent substitution of Zr^{4+} ions by trivalent Y^{3+} and R^{3+} ions occur with the formation of oxygen vacancies. These defects can capture electrons from the valence band. Anion vacancies, depending on the number of trapped electrons, can be characterized by energy levels in the band gap, including those near the bottom of the conduction band. The interaction of the nearest oxygen vacancies leads to an overlap of defect levels, and the so-called polyvacancies are formed. An increase in the size of the oxygen polyvacancies leads to the appearance of a wide band of defect energies in the band gap filled with electrons. Several theoretical and experimental works have been devoted to the study of this phenomenon in zirconium dioxide crystals [1 – 4].

In this work, we studied the spectral and luminescent characteristics of ZrO_2-Y_2O_3 and ZrO_2-Y_2O_3- Er_2O_3, ZrO_2-Y_2O_3-Ho_2O_3 crystals upon their excitation by synchrotron radiation in order to reveal luminescence bands in them due to defects associated with oxygen vacancies.

2 Results

Fig. 1 shows the luminescence spectrum of ZrO_2-Y_2O_3-Ho_2O_3 crystals when these crystals were excited by synchrotron radiation with an energy of 5.4 eV and the excitation spectrum obtained at a luminescence detection wavelength of 478 nm.

[nn] Corresponding author: ryabochkina@freemail.mrsu.ru

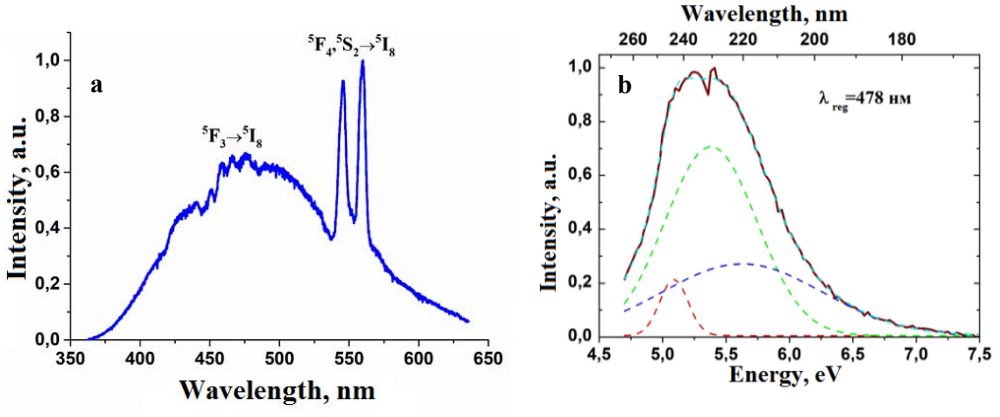

Fig. 1. a) Emission spectra of ZrO_2 –Y_2O_3-Ho_2O_3 crystals under excitation synchrotron radiation with energy of 5.4 eV b) excitation spectra observed under emission 478 nm.

Fig. 1b shows that the spectrum contour has an asymmetric shape. This is due to the superposition of the bands corresponding to the transitions of electrons from the valence band to the energy levels of defects associated with oxygen vacancies and the valence band - conduction band transition.

Considering the simulation results, the complex contour of the excitation spectrum was presented as a superposition of three Gaussian components. The best agreement between the experimental and approximating contours was obtained for the case of Gaussian contours with maxima corresponding to the values of 5.1 eV, 5.4 eV, and 5.6 eV. We attributed the band with a maximum of 5.6 to the band–band transition, while the bands with maxima at 5.1 eV and 5.4 eV, in accordance with the results of calculations performed in [1 – 4], were attributed to electron transitions from the valence band to the energy levels of defects associated with oxygen vacancies V^{1+} and V^{2+}, respectively.

An analysis of the spectral and luminescent characteristics of ZrO_2-Y_2O_3- Er_2O_3 crystals upon excitation by synchrotron radiation showed that the excitation bands of ZrO_2-Y_2O_3- Er_2O_3 have a smaller width, and the maximum of the band for the transition – the conduction band of these crystals is shifted to the region of high energies compared to the similar value for ZrO_2-Y_2O_3-Ho_2O_3 crystals.

Based on the results of this work and simulation data [1 – 4], a scheme was proposed for the positions of the energy levels of defects V^{1+} and V^{2+}, in ZrO_2-Y_2O_3-Ho_2O_3 and ZrO_2-Y_2O_3-Er_2O_3 when excited by synchrotron radiation with an energy of E_{exc} = 5.4 eV.

References

1. D.R. Islamov, V.A. Gritsenko, T.V. Perevalov, A.P. Yelisseyev, V.A. Pustovarov, I.V. Korolkov, E.E. Lomonova, Materialia **15**, 100979 (2021).
2. T.V. Perevalov, Islamov D.R. ECS Trans. **80**, 357 (2017).
3. A.S. Foster, V.B. Sulimov, F.L. Gejo, A.L. Shluger, R.M. Nieminen, Phys. Rev. B. **64**, 224108 (2001).
4. J.-H. Hur, Park S., U.I. Chung, J. Appl. Phys. **112**, 113719 (2012).

Tunable EPR spectroscopy of non-Kramers ions in α-Al_2O_3

Gilman Shakurov[1,oo], *Hike* Asatryan[2], *Ashot* Petrosyan[3]

[1]Zavoisky Physical Technical Institute FRC Kazan Scientific Center of RAS, 420029 Kazan, Russia
[2]Ioffe Institute, 194021 St-Petersburg, Russia
[3]Institute for Physical Research of the National Academy of Sciences of the Republic of Armenia, 0203 Ashtarak-2, Armenia

Abstract. The crystal α-Al_2O_3:Fe was investigated by tunable wide-band (37-850 GHZ) EPR spectroscopy method. The spectra due to resonant transitions from the ground to excited levels of Fe^{2+} ion were observed. In addition, a previously unknown centre of the non-Kramers ion was studied, whose the ground and excited states are singlets. Based on the measured angular and frequency-field dependences, its spectroscopic parameters were determined. The model of the centre and its possible nature are discussed.

A corundum crystal with impurities of transition group ions has numerous applications. Sapphire with titanium and ruby are used in laser physics, while $Al_2O_3:Fe^{3+}$ crystals are used as paramagnetic amplifiers. At the same time, corundum is a convenient model system on which the Jahn-Teller effect was previously studied ($Al_2O_3:Cr^{2+}$, $Al_2O_3:Mn^{3+}$) [1]. To date, there is an extensive literature on the spectroscopic properties of corundum with impurities of transition ions. Many works were carried out using the EPR spectroscopy technique. However, traditional EPR method has limitations associated with the value of a fixed quantum. This leads to difficulties in the study of non-Kramers ions, where there is no degeneracy of electronic states in a zero magnetic field. We used the method of wide-band tunable (37-850 GHz) EPR spectroscopy [2]. Previously, we studied V^{3+}, Cr^{4+}, and Cr^{2+} ions in corundum. This report presents the results of a study of the Al_2O_3:Fe crystal.

A sample of Al_2O_3:Fe (0.3%) was grown in Armenia at the Institute for Physical Research. The measurements were carried out at liquid helium temperature, in magnetic fields up to 1 T. In addition to EPR spectra of Fe^{3+}, the signals from the Fe^{2+} ion were observed. Previously, this ion was studied by the thermally detected EPR method [3]. It was found that the ground state of the ion is a singlet, and the excited doublet is removed by an energy interval of about 3.75 cm^{-1} . We observed resonant transitions between the singlet and the doublet and refined the value of zero-field splitting. Spectra of uncontrolled V^{3+} and Mo^{3+} impurities were also observed. In these cases, we confirmed the previously obtained data.

Previously unknown resonant signals were registered in the frequency range 232-250 GHz. Figure 1 shows the examples of EPR spectra in an Al_2O_3:Fe crystal. An analysis of the frequency dependence of the field allows us to conclude that there are resonant singlet-singlet transitions with splitting in a zero field around 232 GHz. In this case, the intensity of resonant signals was maximum for collinear polarization. ($B_0||B_1$). We observed six magnetically non-equivalent sites of low symmetry. The z-axes of the centres lay near the plane perpendicular to the trigonal axis of the crystal. The angular dependences of the EPR spectra during rotation in the (001), (110) and (100) planes were measured. Based on the results obtained, the possible nature of the observed signals is discussed.

[oo] Corresponding author: shakurov@kfti.knc.ru

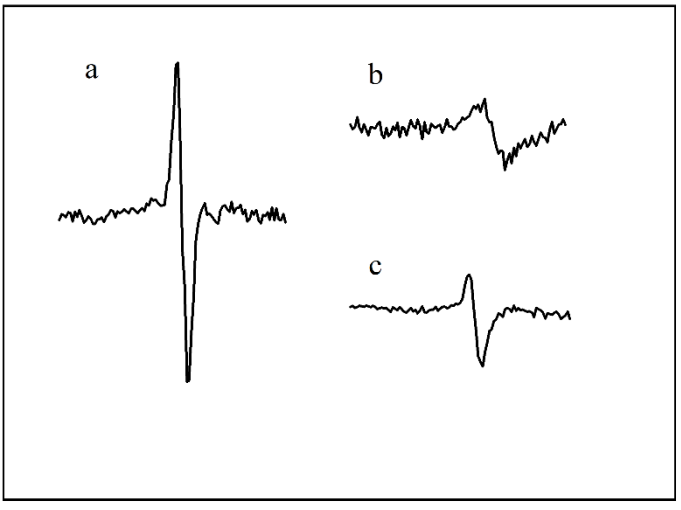

Fig. 1. EPR spectra in Al_2O_3 :Fe crystal. a-Mo^{3+}, frequency 158 GHz ;b-Fe^{2+}, frequency 122.4 GHz ; c-unknown line, frequency 234 GHz.

This work was supported from the governement assignment for FRC Kazan Scientific Center of RAS and Russian Science Foundation under Grant (RFBR) No 20-12-00216. H.R.A. and AGP are grateful for the support of the RFBR grant No.25-52-05002 Arm_a and the State Committee for Science of the Republic of Armenia (grant 20RF-024).

References

1. R.S. Anderson, C.A. Bates and P.C. Jaussaud, J. Phys. C.: Solid State Physics **3**, 3397 (1972)
2. Tarasov V.F., Shakurov G.S. Appl. Magn. Reson. **2**, 571 (1991)
3. W.S. Moore, C.A. Bates and Al-Sharabati, J. Phys. C.: Solid State Physics. **6** L209 (1973)

Spectroscopy of divalent Yb ions in BaBrI single crystals

Roman Shendrik[1,pp], *Vladimir* Kozlovkii[1], *Vladimir* Pankratov[2]

[1]Institute of Geochemistry SB RAS, Favorskii St. 1a, Irkutsk, 664033, Russian Federation
[2]Institute of Solid State Physics, University of Latvia, 8 Kengaraga iela, LV-1063, Riga, Latvia

Abstract. The luminescence spectra of 5d-4f transitions and absorption spectra of 4f-5d transitions of Yb^{2+} were investigated in BaBrI single crystal. It is observed luminescence from the excited *high spin* and low *spin* $4f^{13}5d^{1}$ states. The Yb^{2+} doped BaBrI crystals demonstrate high light output up to 60 000 photons/MeV. The energy transfer mechanisms to Yb^{2+} are clarified.

The scintillator detectors are widely used for dosimetry and homeland security application to identify radioactive materials. The latest progress was achieved in alkali-earth halide system such as BaBrI, Cs_4SrI_6 single crystals [1, 2]. Yb^{2+}-doped halide scintillators are reported much less frequently than those doped with Ce^{3+} and Eu^{2+}. However, the Yb^{2+} ion has also been shown to be an efficient luminescent activator with an allowed 5d → 4f transition. The best result for Yb^{2+} doped scintillators was found for Cs_4CaI_6:Yb^{2+}. The 3% energy resolution and 43000 photons/MeV light output were measured [3]. For crystalline BaBrI the promising results have been also expected [4].

Single crystals of BaBrI doped with 0.01 mol.% and 0.1 mol.% of Yb^{2+} were grown by Bridgman technique in graphite crucible in vacuum.

The BaBrI-Yb emission was excited by xenon lamp, X-ray tube as well as by vacuum ultraviolet 6-40 eV on the photoluminescence endstation FINESTLUMI of MAXIV synchrotron facility (Lund, Sweden) [5].

At room temperature the wide luminescence band in the 400-550 nm spectral region was found. The decay time constant of the observed luminescence is about 2 μs. At 7 K the long wave part of this band attributed to the spin-allowed transition disappears (Fig. 1 a). In the absorption spectra five bands attributed to 4f-5d transitions is observed (Fig. 1b). In excitation spectra measured at 7 K the structure of this band appears.

The excitation spectrum of BaBrI-0.01 mol.% Yb^{2+} emission shows no bands in exciton region (5.5 eV) and an increase in intensity with increasing energy in the VUV spectral region. Therefore, a consecutive electron-hole capture takes place. The light output of BaBrI-0.01 mol.% Yb^{2+} measured under X-ray excitation is about 20000 photons/MeV. The light output is 10,000 photons/MeV, which indicates a high efficiency of the consecutive electron-hole mechanism. In excitation spectrum of BaBrI-0.1 mol.% Yb^{2+} the strong excitation in the exciton region appears. This is an indicator that energy transfer from self-trapped exciton to Yb^{2+} ions occur. The light output of BaBrI-0.1 mol.% Yb^{2+} increases and it is about 60000 photons/MeV.

pp Corresponding author: r.shendrik@gmail.com

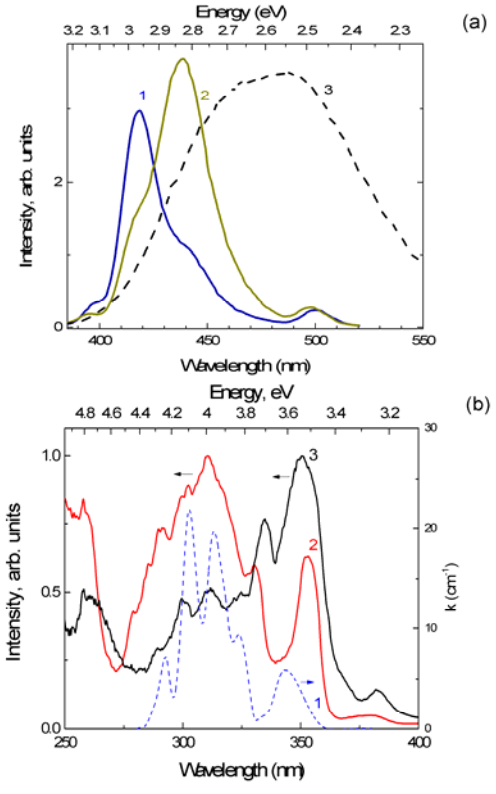

Fig. 1. (a) Emission of BaBrI-Yb^{2+} at 7 K under 300 (curve 1) and 340 nm (curve 2) excitation, curve 1 is emission spectrum under 340 nm excitation measured at room temperature. (b) Excitation spectra of Yb2+ doped BaBrI single crystal monitored at 410 and 450 nm measured at 7 K, dashed curve 3 is absorption spectrum measured at 7 K.

References

1. Shendrik R; Shalaev AA; Myasnikova AS; Bogdanov A; Kaneva E; Rusakov A; Vasilkovskyi. J. Lum. **192** 653 (2017)
2. M. Suta, W. Urland, C. Daul, C. Wickleder. Phys. Chem. Chem. Phys. **18**(19) 13196 (2016)
3. D. Rutstrom, L. Stand, B. Dryzhakov, M. Koschan, C.L. Melcher, M. Zhuravleva. Opt. Mat. **110** 110536 (2020)
4. K. Mizoi, Y. Fujimoto, D. Nakauchi, M. Koshimizu, T.Yanagida, K. Asai. J. Lum, **240** 118399 (2021)
5. Shalaev A, Shendrik R, Rusakov A, Bogdanov A, Pankratov V, Chernenko K, Myasnikova A. NIM B **467** 17 (2020)

EPR of narrow gap semiconductor PbTe doped by manganese and silver

Aleksei Shestakov[1,qq], *Ilshat* Fazlizhanov[1] and *Vladimir* Ulanov[2]

[1]Zavoiskii Kazan Physical Technical Institute, 420029, Sibirski trakt str., 10/7, Kazan, Russia
[2]Kazan State Power Engineering University, 420066, Krasnoselskaja str., 51, Kazan, Russia

Abstract. Here we report the X-band EPR data on deep Mn^{2+} centers in $Pb_{1-x-y}Ag_xMn_yTe$ crystalline samples (x = 0.002; y = 0.001) that were carried out at 4.2 K. Six principal Mn^{2+} hyperfine lines were observed in the spectra. The structure of EPR spectrum formed by six hyperfine lines and its satellites was like the fine-structure of the EPR spectra of the Mn2+ centers distorted trigonally. But, intensities of the satellite lines were significantly lower than it can be found for manganese centers in a wide gap semiconductor (5:8:9:8:5). At manganese concentration of $x \sim 0.001$ the EPR lines were narrowed and superhyperfine structure from the nuclear magnetic moments of isotopes ^{125}Te was observed. The anisotropic behavior of magnetic properties of Mn^{2+} centers was interpreted in terms of local lattice instability induced by Mn^{2+} ions. Moreover, effects of magnetic dependent nonresonant absorption of the microwave power in samples under investigation were observed.

1 Introduction

The PbTe direct narrow band semiconductor belongs to the group of lead chalcogenides PbS, PbSe and PbTe with the cubic rock salt structure. It was the subject of a vast amount of theoretical and experimental work. These works were motivated not only by its technological applications, but also by their unusual physical properties. PbTe is a narrow gap semiconductor with strong ionic character. It has a positive temperature coefficient of the gap width ($dE/dT > 0$), the high static dielectric constant, and the large carrier mobility. These properties make it unique among polar compounds and make it important applications in many fields, such as infrared detectors, light-emitting devices, infrared lasers, thermoelectric materials and solar energy panels. Studies of quantum wires, dots, and wells in the bodies of PbTe semiconductors and possibilities of its applications have caused much attention in the past decades. But, a little of these studies were performed by EPR method. The reason of the latest fact is that most of the paramagnetic impurity centers form resonant levels in the conduction or valence band in the lead chalcogenides and all such centers are not observable by EPR method. But it was found [1] that the Mn^{2+} ions embedded in PbTe are well localized at the Pb sites and form local magnetic moments. Owing to the direct exchange interaction between the *d*-electrons and Bloch electrons of the valence and conducting bands, the latter are magnetically polarized [2]. Through these polarized electrons, the local spins of Mn^{2+} ions interact with each other and with another paramagnetic impurity ions being in resonant states. Consequently, the manganese impurity centers can be used as paramagnetic probes to study some physical properties of PbTe semiconductors codoped by two or more kinds of paramagnetic impurities. The present work was devoted to EPR study of results of double doping of the PbTe semiconductor. Manganese was chosen as magnetic impurity forming in the crystal under

[qq] Corresponding author: aleksey665@gmail.com

investigation deep paramagnetic Mn^{2+} centers. Being embedded in a PbTe crystal manganese plays a role of neutral impurities. Silver was chosen as second acceptor impurity.

2 Result and discussion

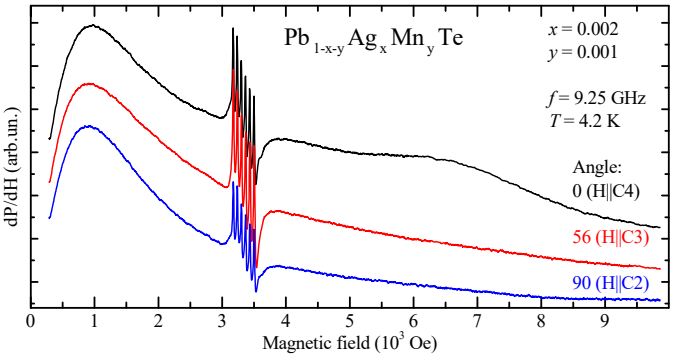

Fig. 1. EPR spectrum of $Pb_{1-x-y}Ag_xMn_yTe$ ($x = 0.002$; $y = 0.001$) at temperature 4.2 K.

We report here the X-band EPR data on deep Mn^{2+} centers in $Pb_{1-x-y}Ag_xMn_yTe$ crystalline samples ($x = 0.002$; $y = 0.001$) grown by vertical Bridgman method in quartz crucibles. The $Pb_{1-x-y}Ag_xMn_yTe$ samples were mounted in a two-circle goniometer and rotated in the (110) crystallographic plane. The measurements were carried out at liquid helium temperature 4.2 K (Fig. 1).

Six principal Mn^{2+} hyperfine lines were observed in the EPR spectra. The field intervals between the lines were found to be isotropic under rotation in the (110) plane within the experimental error of about 0.1 G. All of these hyperfine lines were surrounded by satellites in the orientation $\boldsymbol{H}_0$||<111>. Field positions of the satellites were dependent on magnetic field directions. The structure of EPR spectrum formed by six hyperfine lines and its satellites was like the fine-structure of the EPR spectra of the Mn^{2+} centers distorted trigonally. But, intensities of the satellite lines were significantly lower than it can be found for manganese centers in a wide gap semiconductor (5:8:9:8:5). The mentioned satellite lines were not registered in the $Pb_{1-x}Mn_xTe$ samples at orientations $\boldsymbol{H}_0$||<111>. At manganese concentration of $x \sim 0.001$ the EPR lines were narrowed and superhyperfine structure from the nuclear magnetic moments of isotopes ^{125}Te was observed. The anisotropic behavior of magnetic properties of Mn^{2+} centers was interpreted in terms of local lattice instability induced by Mn^{2+} ions. Moreover, effects of magnetic dependent nonresonant absorption of the microwave power in samples under investigation were observed. All experimental facts observed in this study are discussed.

References

1. Ven-Chung Lee. Phys. Rev. B, **34**, 5430 (1986)
2. J.H. Pifer. Phys. Rev., **157**, 272 (1967)

Photoluminescence spectra and unusual temperature shift of zero-phonon emission line of V^{3+} in $SrTiO_3$

Aleksandr P. Skvortsov[1,rr], *Zdeněk* Potůček[2,3], *Vladimir A.* Trepakov[1], *Zdeněk* Bryknar[3], and *Alexandr* Dejneka[2]

[1]Ioffe Institute RAS, 194021 St. Petersburg, Russia
[2]Institute of Physics of the Czech Academy of Sciences, 182 21 Praha 8, Czech Republic
[3]Czech Technical University in Prague, Faculty of Nuclear Sciences and Physical Engineering, 120 00 Praha 2, Czech Republic

Abstract. This work represents the first observation and study of the V^{3+} impurity photoluminescence spectra in $SrTiO_3$ single crystals. A broad emission band is located in the near IR region and at low temperatures consisted of a pronounced zero-phonon line near 1157 nm (8643 cm^{-1}) accompanied by well-developed vibrational sidebands extending up to 1450 nm. The zero-phonon line is supposed to originate from the $^1T_{2g} \rightarrow {}^3T_{1g}$ transition in V^{3+} $3d^2$ ions substituted for octahedral Ti^{4+}. It is noteworthy that temperature shift of the zero-phonon line is appeared to be unusually large (about -13 cm^{-1} between 4.2 and 77 K) and the line energy decreases with temperature. And it doing so, the temperature shift slope changes abruptly in the vicinity of O_h^1 - D_{4h}^{18} antiferrodistorsive structural phase transition of $SrTiO_3$ crystals (T_{AFD} = 105 K).

1 Motivation

Strontium titanate ($SrTiO_3$, STO) is a very popular and thoroughly studied model system of highly polarizable perovskite-type ABO_3 oxides. At T_{AFD} = 105 K it undergoes a second order O_h^1 - D_{4h}^{18} antiferrodistorsive (AFD) structural phase transition. The dielectric permittivity strongly rises upon cooling due to the softening of the lowest phonon mode TO_1 (incipient ferroelectricity). However, at low temperatures, growing instability and pursuit of ferroelectric ordering is suppressed by quantum mechanical effects (quantum paraelectricity).

Due to a variety of unique properties, STO exhibits interesting impurity related phenomena. Among them a very unusual and large temperature shift of the zero-phonon R-line was found in the emission spectra of photoluminescence of Cr^{3+} and Mn^{4+} ions ($3d^3$ electron configuration) substituted for octahedral coordinated Ti^{4+} ions in STO:Cr and STO:Mn crystals, respectively [1-3]. Besides, the R-line temperature shift occurs for emission of Cr^{3+} and Mn^{4+} ions in the opposite direction.

Surprisingly, quite comparable in magnitude temperature shifts were recently detected also for zero-phonon lines of Er^{3+} ($4f^{11}$ electron configuration) photoluminescence in Er-doped crystals of structurally related incipient ferroelectric $KTaO_3$ [4]. Such behaviour is rather unexpected for three-charged rare earth ions, in which 4f electrons ordinarily interact weakly with the lattice due to the shielding effect of external filled electron shells in contrast to the transition metal ions with an open 3d electron shell. Consequently, the observed peculiarities in temperature behaviour of zero-phonon lines that are very unusual in the spectroscopy of

[rr] Corresponding author: a.skvortsov@mail.ioffe.ru

impurity ions in ionic crystals seems to be inherent to luminescence centres in incipient ferroelectrics with specific properties of energy levels involved in emission transition. To deepen our understanding of these effects we have turned attention to vanadium doped $SrTiO_3$ crystals expecting presence of V^{2+} or V^{3+} ions with suitable spectroscopic properties.

2 Results

Photoluminescence emission spectra of slightly vanadium doped STO single crystal grown by the Verneuil technique [5] were examined within the 350 - 1600 nm spectral range under excitation with the lines of Ar-Kr laser. The spectra revealed only one emission band related to vanadium doping. The band consisted at low temperatures of the pronounced zero-phonon line near 1157 nm accompanied by well-developed vibrational sidebands extending up to 1450 nm. The zero-phonon line was resolved in the spectra at temperatures below 140 K. We suppose that the zero-phonon line originates from the $^1T_{2g} \rightarrow {}^3T_{1g}$ transition in V^{3+} ions ($3d^2$ electron configuration) substituted for Ti^{4+} ions. A detailed analysis of the zero-phonon line temperature behaviour proved also in the case of studied emission centre an unusually large temperature shift (about -13 cm^{-1} between 4.2 and 77 K) to the lower energy side with increasing temperature. The temperature shift slope changes abruptly at the temperature of AFD phase transition An origin of the observed zero-phonon line shift will be discussed taking into consideration the structure of V^{3+} centre energy levels in STO:V crystal and the specificity of impurity-lattice interaction in highly polarisable ABO_3 perovskite-type oxides with soft temperature dependent TO phonon modes.

This work was supported in part by the projects “Centre of Advanced Applied Sciences” (No. CZ.02.1.01/0.0/0.0/16-019/0000778) and “SOLID21” (No. CZ.02.1.01/0.0/0.0/16_019/0000760) of the Operational Program Research, Development and Education co-financed by the European Structural and Investment Funds and the Ministry of Education, Youth and Sports of the Czech Republic.

References

1. S.E. Stokowski, A.L. Schawlow, Phys. Rev. **178**, 464 (1969)
2. V.A. Trepakov, A.V. Babinsky, V.S. Vikhnin, P.P. Syrnikov, Ferroelectrics **83**, 127 (1988)
3. Z. Bryknar, V. Trepakov, Z. Potůček, L. Jastrabík, J. Luminescence **87-89**, 605 (2000)
4. V.A. Trepakov, A.P. Skvortsov, Z. Potůček, L. Jastrabik, A. Dejneka, Physics of the Solid State **62**, 912 (2020)
5. J. Kameník, K. Dragounová, J. Kučera, Z. Bryknar, V.A. Trepakov, V. Strunga, J. Radioanal. Nucl. Chem. **311**, 1333 (2017)

The manifestation of local vibrations in photoluminescence spectrum of ZnO:Fe^{3+}

Victor Sokolov[1,ss], *Nikita* Gruzdev[1], *Vladimir* Menshenin[1], *Arseny* Kiryakov[2], *Anatoly* Zatsepin[2], *Vladimir* Vazhenin[2], and *Gennady* Emelchenko[3]

[1]IMP UB RAS, 620108Yekaterinburg, Russia
[2]UrFU, 620002Yekaterinburg, Russia
[3]ISSP RAS, 142432 Chernogolovka, Russia

Abstract. In this paper photoluminescense (PL) spectra and EPR-signals of ZnO single crystals, doped with manganese and iron, were observed. At the temperature of 4.5 K in PL-spectrum the photoluminescense band in energy interval of 1.55-1.8 eV was observed. This band contains some intensive lines; these lines are caused by Fe^{3+} ions (d^5-configuration). The first and most intensive line at the energy of 1.79 eV corresponds to irradiative recombination $^4T_1$ $(G)\rightarrow{}^6A_1$ (S) of Fe^{3+} ions. The other peaks are vibration repetitions. We have trustworthily shown that part of vibration repetitions are caused by local vibrations of deformedFe^{3+} - $4O^{2-}$ - cluster.

During the investigation of EPR in ZnO:Mn single crystals, which were grown by hydrothermal method, the signals from Fe^{3+}-and Mn^{2+}-ions were discovered, but the signals from Fe^{3+}-ions were weaker by two degrees than that from Mn^{2+}-ions. Earlier Fe^{3+}-ions were observed in PL-spectra in [2,3].

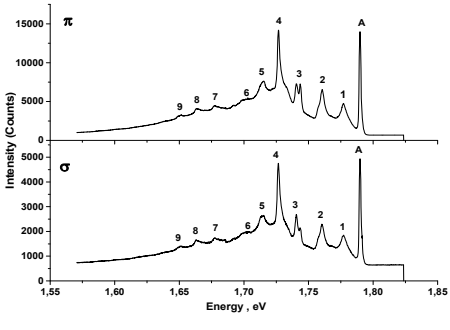

Fig. 1. Photoluminescence spectra of ZnO:Mn single crystal for π- and σ-polarization in spectral region of peaks witch correspond to Fe^{3+} (d^5-configuration) ion. Excitation energy E_{ex}=3eV;T=4.5 K.

The PL spectra of our samples are presented in Figure 1. For both polarizations our spectra are very similar. For both cases on high energy edge of observed PL band we can see an intensive zero phonon line A at the energy of 1.79 eV, which corresponds to intracentral transition $^4T_1$ $(G)\rightarrow{}^6A_1$ (S) of Fe^{3+}ions. Further with the decrease of energy we can see the series of peaks 1-9 against the smooth background, which are the vibrational repetitions of zero phonon line. For both polarizations the energy positions and intensities of these peaks are nearly equal. By their positions the peaks

[ss]Corresponding author: visokolov@imp.uran.ru

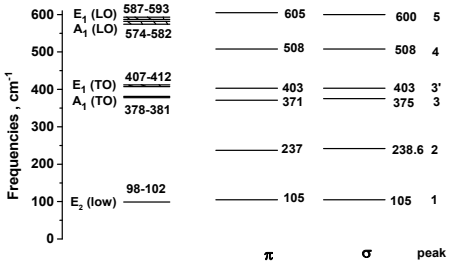

Fig. 2. Frequencies ofA_1- , E_1- и E_2-phonons of the lattice of ZnO [5,6] and vibration repetitions 1-5 of zero phonon line A (Fig.1) for π- and σ-polarization (in cm^{-1}).

observed are in good agreement with the ones described in [2,3]. The authors of [2,3] interpret all vibration repetitions (except of line 4) as phonon repetitions of line A as an interpretation of PL-spectra of II-VI:Mn compounds. But Fe^{3+} ion has two significant differences from Mn^{2+}-ion:Fe^{3+} ion is positively charged relatively to the lattice and the radius of Fe^{3+} ion is less than that of Zn^{2+} ion by 0.11 Å [4]. This fact causes the significant deformation in Fe^{3+} - $4O^{2-}$-cluster and forms the local vibrational modes in this cluster. In Figure 2 the comparison of frequencies of vibration repetitions of peaks 1-5 relatively to line A with the frequencies of optical phonons A_1(TO), E_1(TO), A_1(LO), E_1(LO), E_2(low) [5,6] is presented. It is clearly seen that the energy positions of 3, 3' and 5 peaks correspond similarly to the energies of A_1- and E_1-phonons; near the peak 1 we can see E_2-phonon but near peaks 2 and 4 the optical phonons are not observed. This fact enables us to affirm that the repetitions 2 and 4 of A line are caused by local vibrations of deformed Fe^{3+} - $4O^{2-}$cluster.

The research was carried out within the state task of Russian Ministry of Education and Science (topic "Electron", № 122021000039-4, projects №FEUZ-2020-0059 and № FEUZ -2020-0054), project of RSF № 21-12-00392 and within the state task of ISSP RAS**.**

References

1. V.I. Sokolov, N.B. Gruzdev, V.A. Vazhenin, A.V. Fokin, A.V. Korolev, V.V. Menshenin, JETP,**130**, 5, 681 (2020)
2. R. Heitz, A. Hoffmann, I. Broser, Phys. Rev. B,**45,**16, 8977 (1992)
3. D.V. Azamat, J. Debus, D.R. Yakovlev, V.Yu. Ivanov, M. Godlewsky, M. Fansiulli, M. Bayer, Phys. Stat. Sol. B, **247,** 6, 1517 (2010)
4. A.D. Shannon, ActaCryst. **A32,**751 (1976)
5. C. F. Klingshirn, B. K. Meyer, A. Waag, A. Hoffman, J. Geyrts, *Zinc Oxide* (Springer, Heidelberg, 2010)
6. H. Morkoç, Ü. Özgür, *Zinc Oxide* (WILEY-VCN Verlag, Weinheim, 2009)

Luminescence properties of $Y_{1-x}Sc_xPO_4$ solid solutions

Dmitry Spassky[1,tt], *Andrey* Vasil'ev[1], *Ildar* Kondrat'ev[1], *Dina* Deyneko[2,3], *Ivan* Nikiforov[2], *Boris* Zadneprovski[4]

[1]Skobeltsyn Institute of Nuclear Physics, Moscow State University, Leninskiye Gory 1-2, 11991 Moscow, Russia
[2]Department of Chemistry, Lomonosov Moscow State University, 119991 Moscow, Russia
[3]Laboratory of Arctic Mineralogy and Material Sciences, Kola Science Centre, Russian Academy of Sciences, 14 Fersman str., Apatity 184209, Russia
[4]All-Russian Research Institute for Synthesis of Materials, Institutskaya str. 1, 601600, Alexandrov, Russia

Abstract. An intense emission in the UV-C spectral region has been detected in the $Y_{1-x}Sc_xPO_4$ solid solutions. The origin and characteristics of the luminescence are discussed. Spectral position of the emission band shifts from 5.94 eV to 5.2 eV depending on the Y/Sc ratio. The emission is ascribed to the 2p O – 3d Sc self-trapped excitons and characterized by relatively fast decay ($\tau_{1/e} \sim 10^{-7}$ s). Numerical simulation of substitutional atoms spatial distribution is performed using Monte-Carlo method. It is shown that the ScSc correlation allows formation of Sc clusters even for low concentrations of Sc ($x < 0.1$). Such clusters facilitate the creation of energy wells at the conduction band bottom formed by the 3d Sc states that is preferable for excitations localization at the emission centers, resulting in enhanced thermal stability and quantum yield of the UV-C emission.

Compounds with bright luminescence in the UV spectral region attract attention due to their application in photocatalysis and photochemistry, for disinfection, as persistent phosphors and scintillating detectors [1-4]. Emission in the UV spectral region is an advantageous feature for application in scintillators because it corresponds to the area where solar blind light detectors can be used in open mode without shielding from the daylight radiation [2]. Persistent UV emission can be applied in solar cells, photodynamic therapy, and photo-catalysis [3]. UV phosphors with the emission in the UV-C range (<280 nm) are of particular interest for medical applications. Their excellent bactericide properties are determined by high spectral overlap of the UV-C range and the germicidal effectiveness curve [1]. Moreover, the UV-C irradiation is a useful tool for killing superficial cancer cells without damage to deep tissue [5,6].

An intense emission in the UV-C spectral range is usually observed for wide-bandgap (E_g > 7 eV) phosphors doped with Ce^{3+} or Pr^{3+} rare-earth elements (REE) as well as Bi^{3+} ions [7]. Compounds with intrinsic emission are also in the scope of interest for the UV phosphor applications, however, the luminescence of this type suffers from quenching processes at room temperature in most compounds. Solid solutions allow tailoring of phosphor properties for specific demands. The fluctuations of the energies of the electronic states, forming the conduction band bottom and valence band top, introduced by the electronic states of substitutional atoms, which can form the clusters consisting of one type of such atoms, promotes localization of charge carries, thus increasing the probability of radiative relaxation

[tt]Corresponding author: spas@srd.sinp.msu.ru

and enhancing thermal stability. Here, we present the results of our studies of structural and luminescence properties of undoped $Y_{1-x}Sc_xPO_4$ solid solutions.

The series of phosphates $Y_{1-x}Sc_xPO_4$ (x = 0, 0.01, 0.05, 0.1, 0.2, 0.4, 0.5, 0.6, 0.8, 1) were synthesized by standard solid-state method. According to PXRD data all synthesized samples are single-phased and crystallize in Xenotime-type structure with tetragonal syngony and space group $I4_{1/amd}$ (D^{19}_{4h}, no.141, Z = 4).

All Sc containing phosphates demonstrate an emission band in the UV-C spectral region, while it is absent in pure YPO_4. Additional emission bands related to crystal structure defects were also found in a longer-wavelength region, however, the UV band is dominant in the spectrum of $ScPO_4$ as well as solid solutions, even for the sample $Y_{0.99}Sc_{0.01}PO_4$ with the lowest Sc concentration. The band maximum shifts from 5.94 eV to 5.2 eV with the change of *x* from 1 to 0.6, while its position does not change for lower Sc concentrations. The observed UV-C emission band is characterized by decay $\tau_{1/e}$ = 56-294 ns depending on *x* value and ascribed to the 2p O – 3d Sc self-trapped excitons. The dependence of quantum yield of the UV-C emission on Y/Sc ratio was determined. The quenching of the emission starts at T > 130 K for $ScPO_4$, but thermal stability substantially increases with decrease of Sc content in solid solutions. The effect is related to the creation of deep Sc energy wells on the conduction band bottom. Numerical simulation of substitutional atoms spatial distribution is performed using Monte-Carlo method. The simulation describes the fluctuations of potential at the conduction band bottom in case of the absence or presence of correlations in Sc/Y atoms distributions. It is shown that the ScSc correlation is preferable for excitations localization in $Y_{1-x}Sc_xPO_4$ solid solutions with low Sc content. The results of the studies have shown that $Y_{1-x}Sc_xPO_4$ solid solutions can be considered as bright UV-C phosphors with relatively fast emission decay and excellent thermal stability in ambient conditions.

This work was supported by the Russian Science Foundation under grant 21-12-00219.

References

1. Xianli Wang, Yafei Chen, Feng Liu and Zhengwei Pan, Nature Communications **11**, 2040 (2020)
2. Y. Zhou, D.D. Jia, L.A. Lewis, S.P. Feofilov, R.S. Meltzer, Nucl. Instr. Meth. Phys. Res. A **633**, 31 (2011)
3. Puxian Xiong, Mingying Peng, Opt. Mater. X **2**, 100022 (2019)
4. B. Caillier, J. Caiut, C. Muja, J. Demoucron, R. Mauricot, J. Dexpert-Ghys and Ph. Guillot, Photochemistry and Photobiology, **91**, 526 (2015)
5. Sh. Miwa, Sh. Yano, Yu. Hiroshima, Ya. Tome, F. Uehara, S. Mii, E.V. Efimova, H. Kimura, K. Hayashi, H. Tsuchiya, R.M. Hoffman, J. Cell. Biochem. **114**, 2493 (2013)
6. H. Kimura, C. Lee, K. Hayashi, K. Yamauchi, N. Yamamoto, H. Tsuchiya, K. Tomita, M. Bouvet, R.M. Hoffman, J Cell Biochem **110**, 1439 (2010)
7. J.M.A. Caiut, S. Lechevallier, J. Dexpert-Ghys, B. Caillier, Ph. Guillot, J. Lumin. **131**, 628 (2011)

Influence of the central metal ion on the luminescent and photophysical parameters of metal phthalocyanines

A.S. Starukhin[1,uu], *V.S.* Shershan[1], *A.Yu.* Ilin[1], *T.* Pavich[1], *A.O.* Savostianov[2], *I.Yu.* Eremchev[2,3,4], *A.V.* Naumov[2,3,4]

[1] *B. I. Stepanov Institute of Physics, NASB, Belarus*
[2] *The Institute of Spectroscopy of the RAS, Russia*
[3] *The Lebedev Physical Institute of the RAS, Russia*
[4] *Moscow State Pedagogical University, Russia*

Abstract. Phthalocyanine complexes with Mg(II), Zn(II), Pd(II) and Pt(II) ions and a number of rare earth metal ions have been synthesized and investigated. For these compounds absorption spectra, luminescence spectra, luminescence excitation spectra, life times and quantum luminescence output are measured. It is shown that metallophthalocyanines with ions Mg(II) and Zn(II) are characterized by intensive fluorescence with quantum output greater than 0,3. The inclusion of Pd(II) and Pt(II) into the center of phthalicyanine macrocyanide leads to a near-total absence of fluorescence and the presence of intensive phosphorescence even at room temperature.

Phthalocyanines are widely used in various fields of science, engineering and medicine. These compounds are used to create effective photoconverters and electronic devices, as well as photosensitizers in photodynamic therapy and antimicrobial therapy. Free base and metallocomplexes of phthalocyanines have high photostability in various organic solvents, as well as in solid state. Said compounds exhibit a high molar absorption coefficient at a range of 650-700 nm in the absorption spectrum, which makes it possible to use them as high-efficiency transducers of light radiation into electrical signals. One of the effective methods of phthalocyanine research is selective laser spectroscopy, which makes it possible to study the spectral properties at the level of single molecules [1,2].

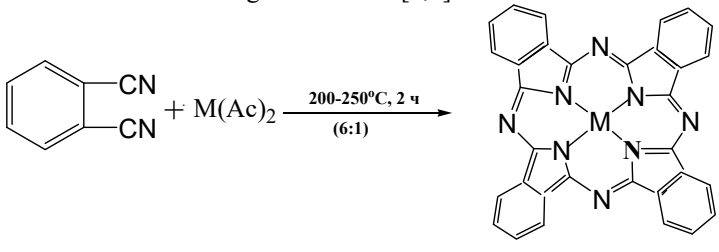

Fig. 1. The synthesis scheme of metallophthalocyanines (M-Rs), where M is H2-, Mg-, Zn-, Pd- and Pt- are rare earth elements.

The aim of this work was to study the influence of metals (Mg(II), Zn(II), Pd(II), Pt(II) ions, and a set of rare earth elements) at the center of the organic phthalocyanine ligand on the spectral parameters of a set of metallophthalcyanine complexes. The most common synthesis of metallocomplexes of phthalocyanins was the template method based on phthalonitrile at

[uu] Corresponding author: starukhin@mail.ru

high temperature. The synthesis of metallophthalocyanines was carried out by fusing the calculated quantities of acetates or dichlorides of corresponding metals with phthalodinitril. The reaction scheme is shown in Figure 1.

Luminescence spectra in the visible and infrared ranges were recorded on the spectrophlorimeter Horiba Jobin Yvon FL3-22 Fluorolog-3.

Figure 2 presents spectra of metallophthalcyanins in the visible and infrared range of spectra. Phthalocyanine compounds with Mg(II) and Zn(II) ions exhibit intense fluorescence (Fig. 2a) with quantum yields ranging from 0,4 (Zn-Rs) to 0,8 (Mg-Rs) and almost no phosphorescence even at low temperatures.

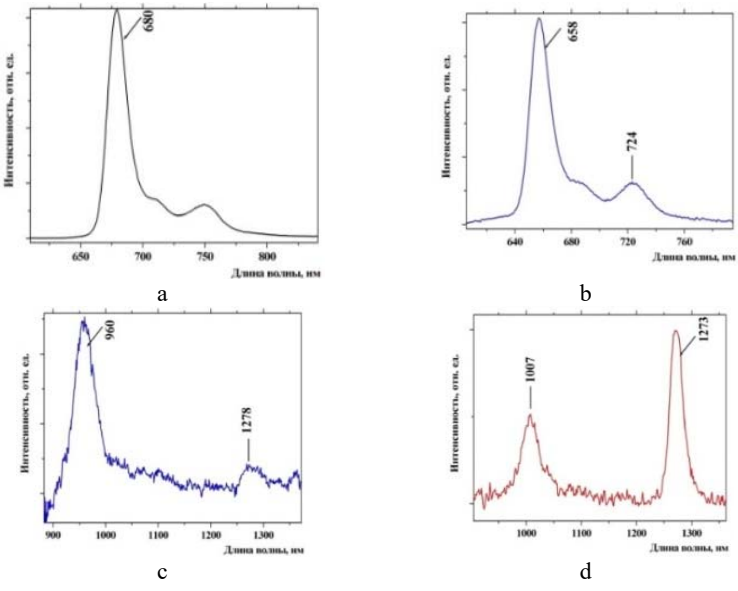

Fig. 2. Spectra of fluorescence of Mg-Pc (a), Pd-Pc (b), phosphorescence spectra of Pd-Pc (c) and Pt-Pc (d) in toluene at 293 K.

Upon increases the mass of the central metal ion at the center of the macrocycle (Pd(II) and Pt(II)) the value of spin-orbital coupling increases significantly that due to the effect of the internal heavy atom. A similar manifestation of the heavy atom effect was previously recorded for porphyrins [3]. Increased spin-orbital coupling for Pd-Ps causes disappear of fluorescence (see fig. 2b) and manifestation of phosphorescence at a maximum of about 1007 nm even in oxygen solutions (fig. 2g). The Pt-Pc complex fluorescence is absent at all and intensive phosphorescence at a maximum of 960 nm take place. Note that the presented results differ significantly from those for similar compounds in [4]. In the spectra of phosphorescence there is also a band of about 1270 nm, which corresponds to the luminescence of singlet oxygen. For H_2-Pc, Mg-Pc, Zn-Pc, Pd-Pc and Pt-Pc, the quantum outputs of singlet oxygen generation were measured.

For single MgTAP molecules in a thin polymer film of polyisobutylene, time dependences of fluorescence excitation spectra at cryogenic temperatures (5K) have been recorded. A spectral diffusion (stochastic jumps of the phoneless spectral line) in a wide spectral range up to 1000 GHz has been identified, apparently caused by conformational changes in the molecule. In addition, a phonon wing is recorded in the spectra, in some cases corresponding to a quasi-localized low-frequency oscillation mode, which determines the parameters of electron-phonon interaction in the impurity system.

Rare earth complexes (Sc, Y, lanthanides from La to Lu) with phthalocyanines ligands also demonstrate the inner effect of the heavy atom. The metals Mg, Zn, Pd and Pt, at the center of the phthalocyanine macrocyanide, do not have their own luminescence, while several rare earth ions demonstrate their own luminescence along with the luminescence of organic ligand. Rare earth element complexes with phthalocyanines are also interesting possibility to obtain structures such as mono-, bis- and triphthalocyanine in which the complexing (metal) ion can conjugated with one or two organic ligands.

Authors (AOS, IYE, AVN) acknowledge RFBR (project 20-03-00923) and Ministry of Education of Russia (state task AAAA-20-120061890084-9). A.O.S., I.Yu.E and A.V.N. are members of the Leading Scientific School of the Russian Federation (grant of the President of the Russian Federation NSh-776.2022.1.2).

References

1. Savostianov A.O., Eremchev I.Y., Gorshelev A.A., Orlov S.V., Naumov A.V., Starukhin A.S. // Optics and Spectroscopy, V. 126, No. 1, P. 44-48 (2019).
2. Savostianov A.O., Eremchev I.Y., Gorshelev A.A., Naumov A.V., Starukhin A.S. // JETP Letters, T. 107, No. 7, P. 406-411 (2018).
3. Gladkova O.L., Starukhin A.S., Kruk M.M. // Optics and Spectroscopy, V. 110, No. 2, P. 234-241 (2011).
4. P.S. Vincett, E.M. Voigt, K.E. Rieckhoff // J. Chem. Phys., V. 55, P. 4131 (1971).

Electromagnetically induced transparency in finite size cells with antirelaxation wall coatings

Gavriil Voloshin[1,vv], *May* Hui[1], and *Igor* Sokolov[1]

[1]Peter the Great St.Petersburg Polytechnic University, 195251, St.Petersburg, Russia

Abstract. The practical interest of the effect of electromagnetically induced transparency is largely due to the narrowness of the transparency line compared to the width of the natural absorption line. One way to reduce collisional broadening is to use gas cells with special anti-relaxation coatings. The purpose of this work is a theoretical study of the influence of various types of coatings on the nature of the effect of electromagnetically induced transparency in a gas cell. The mathematical model for describing the states of an atomic ensemble is based on the single-particle density matrix method in the Wigner representation. The presence of walls is considered by introducing boundary conditions of various types. The use of several approximations makes it possible to obtain analytical expressions for resonant susceptibility contours. As a result, the change in the shape of the resonance of electromagnetically induced transparency is analyzed upon varying the parameters of the medium and laser pumping for different types of coatings. A significant difference between the Stokes and anti-Stokes excitation channels is shown. The authors believe that the effects predicted in this work should be considered in all potential applications of electromagnetically induced transparency using coated gas cells.

1 Introduction

It is known that the interaction of bichromatic laser radiation when interacting with three-level media can lead to the so-called phenomenon of electromagnetically induced transparency (EIT) [1, 2]. As a result of this phenomenon, an opaque medium for one of the fields (probe) becomes transparent in a narrow frequency range. The width of such a resonance turns out to be much smaller than the width of the natural absorption line, which largely determines the practical interest in this phenomenon. The width of such a "dark" resonance is determined by the lifetimes of optically induced quantum coherences. A negative factor for practical applications here are the collisions of atoms with the walls of the atomic cell and among themselves. Collisions reduce the time of coherent interaction of atoms with the field, and the width of the EIT resonance increases. One of the ways to reduct this is the use of special antirelaxation coatings, which make it possible to increase the lifetime of field-induced atomic coherences. The purpose of this work is a theoretical study of the effect of collisions of atoms with walls with different types of coatings on the shape of the EIT resonance. The advantage of the developed theory in comparison with other works on this topic [3, 4] is the possibility of obtaining analytical expressions for the susceptibility of the medium depending on the detuning of the probe field.

[vv] Corresponding author: gavriilvsh@gmail.com

2 Mathematical model

The interaction of the external field with the medium is described semiclassically. The external field is represented by a classical plane two-frequency electromagnetic wave. The states of an atomic ensemble are described in a quantum way using the density matrix method in the Wigner representation in terms of the translational degrees of freedom of atoms. When describing the energy structure of atoms, a three-level model is used. Interaction with the external field occurs through the lambda scheme.

The weak probe field approximation makes it possible to consider only the equations for the optical and low-frequency coherences. Considering a sufficient distance from the walls, at which the optical coherence has time to establish a stationary equilibrium state with the field, these equations can be reduced to a single ordinary differential equation that admits an analytical solution. In this case, the integration constants are determined from the boundary conditions. In this paper, three types of boundary conditions are considered: complete quenching, specular reflection, and diffuse boundary conditions.

3 Results

As a result, we analyzed the change in the EIT resonance contour upon varying various parameters of the medium and laser pumping, such as the Rabi frequency of the binding field, the detuning of the binding field, the cell length, and the nature of the reflection from the cell walls. A significant difference between the resonant circuits for various frequency differences between the coupling and probe fields is found. In the case when the binding field is tuned to resonance with a transition of a lower frequency (Stokes channel), a much smaller resonance amplitude is observed than in the opposite case (anti-Stokes channel). It has been noted that the type of resonances detected by means of the anti-Stokes channel weakly depends on the nature of the reflection from the walls for a cell length of the order of one wavelength of the radio wave transition.

This work was supported by the BASIS Foundation for the Advancement of Theoretical Physics and Mathematics in the studies of the peculiarities of the influence of the ensemble temperature and the associated motion of atoms on the collective effects caused by the finite optical thickness (Grant No. 21 1-1- 36-1); as well as the state task of the Ministry of Education and Science of Russia for the provision of public services (performance of work) in 2022-2024 No. 075-01429-22-00 of December 28, 2021 under the Agreement of January 14, 2022 No. 075-03-2022-010.

References

1. Harris, S.E., Field, J. E. and Imamoglu, A. Phys. Rev. Lett. **64**, 1107 (1990)
2. Boiler, K.J., Imagoglu, A. and Harris, S. E. Phys. Rev. Lett, **66**, 2593 (1991)
3. Kazakov, G., Matisov, B., Litvinov, A., Mazets, I. Journal of Physics B: Atomic, Molecular and Optical Physics, **40**, 3851 (2007)
4. Litvinov, A.N., Sokolov, I.M. Jetp Lett. **113**, 763–768 (2021)

Ultrafast dynamics of orbital and spin ordering in $FeCr_2O_4$ multiferroic spinel

Andrey Petrov[1], *Mikhail* Cherosov[1], *Ruslan* Batulin[1], *Airat* Kiiamov[1], *Almaz* Zinnatullin[1], *Sergey* Nikitin[1], *Mikhail* Eremin[1] and *Roman* Yusupov[1,ww]

[1]Kazan Federal University, Institute of Physics, Kremlyovskaya 18, 420008 Kazan, Russia

Abstract. A single crystal $FeCr_2O_4$ multiferroic spinel was studied with two-color ultrafast optical and magnetooptical spectroscopy in a wide 4 – 300 K temperature range. Specific components emerge with the onsets of the orbital and the magnetic orderings that occur at $T_{OO} = 138$ K and $T_N = 65$ K, respectively. Timescales of the orders' melting, and recovery have been found. A possibility of spectral addressing the iron and chromium magnetic sublattices in a ferrimagnetic state is demonstrated.

Great attention has long been paid to the applied and fundamental studies of crystals with the spinel structure. Modern studies of the compounds with the spinel structure are stimulated by magnetoelectric effects discovered in them [1]. Ferrimagnets $FeCr_2S_4$, $FeCr_2O_4$, and FeV_2O_4 are clearly distinguished among compounds with the spinel structure. Magnetoelectric effects of a still unclear origin were detected in the ferrimagnetic phase of $FeCr_2S_4$ [2, 3]. The temperature dependences of the magnetic-order-induced electric polarization in $FeCr_2O_4$ and FeV_2O_4 are reported in [4, 5] and [6], respectively.

Most of the reported studies have been performed on the polycrystalline powder samples, and it looks that many interesting effects are masked or averaged out in such materials. Our recent study of the high-quality single-crystal of $FeCr_2O_4$ with the spinel structure immediately revealed such intriguing phenomena as the microwave nonreciprocity and magnetic field induced rearrangement of the magnetic structure [7].

The sample was synthesized with a high-temperature solid-state reaction from the stoichiometric mixture of the ferrous oxalate FeC_2O_4 and chromium oxide Cr_2O_3. The known problem of iron oxidation from the Fe^{2+} state to Fe^{3+} state was inhibited by decomposition of FeC_2O_4 compound to FeO, CO_2 and CO, the latter creating the reducing atmosphere in the oven. The polycrystalline ingot then was used for a single crystal growth by the optical floating zone method. A near-absence of the Fe^{3+} ions either in the powder sample or in a single crystal has been verified by the Mössbauer spectroscopy. Specific heat and magnetic susceptibility measurements revealed anomalies at 138 K, 65 K and 38 K inherent for $FeCr_2O_4$ and corresponding to the onsets of the orbital ordering in the Fe^{2+}-ion sublattice, global collinear ferrimagnetic order and a spiral modulation of the magnetic order [8], respectively.

Ultrafast studies were performed with the use of the 1-kHz regenerative amplifier Legend-USP and the optical parametric amplifier (OPA) TOPAS (Coherent, USA) in the conventional pump-probe arrangement. For pump the light at 800 nm (1.55 eV) was used, and the probe wavelength was either the second harmonic, 400 nm (3.10 eV) or the output of the OPA tuned to the wavelengths in the range of 1700 – 2200 nm (0.75 – 0.55 eV). Probing at 3.10 eV corresponds essentially to the Mott-Hubbard-like excitation of the Cr^{3+} ions from the ground $^4A_2$ to excited $^4T_2$ state while with probing in the mid-IR we addressed the Fe^{2+} subsystem via the $^5E \rightarrow {}^5T_2$ single-ion transition. Two kinds of the probing light characteristics were studied:

ww Corresponding author: Roman.Yusupov@kpfu.ru

intensity variation due to the reflectivity modification and the rotation of the polarization plane due to the magnetooptical Kerr effect (TR-MOKE).

Reflectivity transients on probing at 400 nm reveal the signals with characteristic amplitude variation with temperature that allows to associate them with an establishment of the orbital and the magnetic orders. Thus, on cooling below 150 K, the signal with exponential rise and decay appears that indicates that the orbital order melts on the timescale of 1.5 ps and recovers on ~ 180 ps rate. On further cooling, additional components appear below 70 K that are identical to the components of the TR-MOKE transients observed only in the ferrimagnetic state; therefore, these responses originate from partial melting and recovery of the magnetic order that occur at the timescales of ~20 ps and ~800 ps at 10 K, respectively.

Interestingly, the time-resolved MOKE with probing at 2000 nm wavelength shows a behaviour different from that observed at 400 nm. The signals are composed of two rising components. The faster one has a timescale that varies from 25 to 55 ps in the temperature range of 5…35 K, then changes a sign and gets faster, varying from 5 to 15 ps on approaching the Neel temperature. The slow rising component has a time constant of 800 ps at 5 K and gradually becomes faster, approaching a value of 200 ps at 55 K. Magnetic order recovery is much longer though fully develops back within 2 ms, a period between the pump laser pulses.

Thus, we see that the magnetic order probed at different wavelengths reveals rather different characters, which, in our opinion, indicates significantly independent magnetic structures of the simpler Cr^{3+}-ion sublattice and more complicated Fe^{2+} sublattice. The slow (~ 800 ps) component of the Fe^{2+} sublattice dynamics may originate from the magnetic structure rearrangement found by us earlier [7].

The support from Russian Science Foundation, project 19-12-00244, is gratefully acknowledged.

References

1. A. Sundaresan, N.V. Ter-Oganessian, J. Appl. Phys. **129**, 060901 (2021).
2. J. Bertinshaw et al. Sci. Rep. **4**, 6079 (2014).
3. L. Lin et al. Sci. Rep. **4**, 6530 (2014).
4. K. Singh, A. Maignan, C. Simon, C. Martin, Appl. Phys. Lett. **99**, 172903 (2011).
5. A. Maignan, C. Martin, K. Singh, C. Simon, O.I. Lebedev, S.Turner, J. Solid State Chem. **195**, 41 (2012).
6. Q. Zhang, K. Singh, F. Guillou, C. Simon, Y. Breard, V. Caignaert, V. Hardy, Phys. Rev. B **85**, 054405 (2012).
7. R.V. Yusupov, M.A. Cherosov, B.F. Gabbasov, K.V. Vasin, R.G. Batulin, A.G. Kiyamov, M.V. Eremin, JETP Lett. **115**, 167 (2022).
8. G. Shirane, D. E. Cox, and S. J. Pickart, J. Appl. Phys. **35**, 954 (1964).

Excitation capture efficiency of rare-earth ions in wide-gap materials

Maria Zamoryanskaya[1, xx], *Ekaterina* Dementeva[1], *Ksenia* Orekhova[1], *Vlad* Kravets[1], *Grygorii* Gusev[1], *Alexander* Trofimov[1]

[1] Ioffe Institute RAS, 194021, St. Petersburg, Russia

Abstract. Measurement technique for experimental determination of rare-earth ions energy levels exitation capture efficiency in wide-gap materials is proposed. It based on the dependence of the rise time rate of the CL bands on the electron beam current density. This technique allowed us to quantify the excitation capture efficiency for the three different emitting levels of rare-earth ions in yttrium silicate. It was found that the excitation capture efficiency for different levels differs by three orders of magnitude. It was successfully used to determine the excitation energy transfer between Tm^{3+} and Cr^{3+} in YAG, and it was found that $Tm^{3+}$is a sensitizer for Cr^{3+} upon high-energy excitation. Also, this technique was used to study the influence of crystalline matrix perfection (YAG) on the excitation capture efficiency of Eu^{3+}.

1 Introduction

The search for new efficient scintillators with a high optical yield upon excitation by accelerated charged particles – electrons, alpha particles, ions, as well as X-rays and gamma-rays – remains an urgent task. Solution to this problem is of great practical importance in connection with application of the scintillators as sensors of radioactive radiation in medicine, dosimetry, and geology The development of oxide scintillators remains relevant and in demand at the present time, but there is a problem of relatively low light output. To solve this problem, it is required to investigate not only the radiative and nonradiative transitions mechanisms, but also the rate of excitation capture by the emitting levels. It may depend on the synthesis technology, sensitizers, and emission centers with high-energy excitation. In this paper, a quantitative technique that makes it possible to determine the excitation capture efficiency of luminescence centers upon electron beam irradiation (cathodoluminescense, CL) has been proposed. The technique is based on the determination of the CL band intensity rise time dependence on the excitation power density. The CL technique is well suited for such studies. On the one hand, this method allows varying the luminescence excitation density by several orders of magnitude fluently and with a high accuracy by changing the electron beam current density. On the other hand, the CL excitation mechanism is close to the luminescence excitation mechanisms by any charged particles with high energy. Accordingly, the rate of excitation capture at CL is similar to excitation by high-energy electrons, alpha particles, and ions capture rate.

2 The Two-Level Model of Luminescence

The method was used for the experimental determination of the emission levels excitation capture efficiency. The main condition for applicability of this method is the strong localization

[xx] Corresponding author: zam@mail.ioffe.ru

of excited and ground states (energy levels) and absence of interaction between the excited levels (i.e., a relatively low content of luminescence centers). This method can be applied to describe intracenter transitions in wide-gap materials, e.g., for REI in oxide crystals.

According to this model, the luminescence intensity at the beginning of the excitation is described by the following expression:

$$I = A(\lambda)n_1 = A(\lambda)\frac{LJN}{LJ + \tau^{-1}}(1 - exp\{-(LJ + \tau^{-1})t\}), \quad (1)$$

where n_1 stand for the quantity of the excited luminescence centers, N is the total quantity of luminescence centers, J is the current density of the primary electron beam subject to the experiment at one accelerating voltage, [nA/□m^2]; τ^{-1} is the decay rate of the emitting level, [ms^{-1}], and L is the CL excitation capture efficiency of the radiative level coefficient, which represents the number of radiative level excitation acts per 1 ms upon excitation by electron beam with the density of 1 nA/μk^2 [μk^{2}ms^{-1}nA^{-1}]., and

$$(LJ + \tau^{-1}) = \tau^{-1}{}_{rise}, \quad (2)$$

$\tau^{-1}{}_{rise}$ is the CL rise rate. The rise and decay rates are inversed decay and rise times of the CL bands, which are determined by approximating the obtained kinetic curves. The excitation capture efficiency coefficient L is independent from the concentration of the luminescent centers. It can be determined from the dependences of the CL rise rate $\tau^{-1}{}_{rise}$ on the electron beam current density J.

The excitation capture efficiency coefficients L of the REI energy levels were studied for the following oxide crystals used as scintillators and laser crystals: Y_2SiO_5:Tb^{3+},Ce^{3+}, YAG:Tm^{3+},Cr^{3+} and YAG:Eu^{3+} grown by various methods.

3 Results

In Y_2SiO_5:Ce^{3+},Tb^{3+} crystal the excitation capture efficiency of various energy levels differs in orders of magnitude. Ce^{3+} 5d energy level has the highest excitation capture efficiency, although its CL band intensity is noticeably lower than that of the Tb^{3+} energy levels. This is since Ce^{3+} content is one hundred times lower than Tb^{3+} content. However, it is impossible to increase Ce^{3+} content in the material grown by the Czochralski method due to its poor solubility in Y_2SiO_5. With an increase in Ce^{3+} content in the crystal precursor, inclusions of other phases are formed and an inhomogeneous distribution of Ce^{3+} is observed.

The excitation capture efficiency coefficient L was determined for ^{2}E Cr^{3+} energy level in YAG:Cr^{3+} and YAG:Tm^{3+},Cr^{3+}. It was determined that the coefficient L of ^{2}E Cr^{3+} energy level increases by 4 times in the presence of Tm ions. Therefore in YAG:Tm^{3+},Cr^{3+} system Tm^{3+} ions act as sensitizers of Cr^{3+} ions upon high-energy excitation.

On the example of YAG:Eu^{3+} samples it is shown that the presence of grain boundaries increases the excitation capture efficiency of Eu^{3+} high-energy levels.

It was demonstrated that the experimental data is well described using the two-level model of luminescence.

New upconversion bulk- and nano phosphors based on $Sr_2Y_{8-x-y}Yb_yTm_xSi_6O_{26}$

Mikhail Zuev[1,yy], *Andrey* Vasin[1], *Vladislav* Il'ves[2], *Sergey* Sokovnin[2,3], and *Alexander* Berezin[3]

[1]Institute of Solid State Chemistry UB RAS, 91 Pervomayskaya Str., Yekaterinburg, 620990, Russia
[2]Institute of Electrophysics UB RAS, 106 Amundsen Str., Yekaterinburg, 620016, Russia
[3]Yeltsin UrFU, 19 Mira Str., 620002 Yekaterinburg, Russia

Abstract. A bulk phosphors of composition $Sr_2Y_{8-x-y}Yb_yTm_xSi_6O_{26}$ (x=0.005-0.5, y=0.2, 0.3) were synthesized. An nanophosphorus in the an amorphous state with a particle size of ~10.6 nm was obtained by pulsed electron beam evaporation of the $Sr_2Y_{7.695}Yb_{0.3}Tm_{0.005}Si_6O_{26}$ sample. The spectra of upconversion photoluminescence of bulk and nanophosphors were studied. In the range of phosphor pump power of 70.8 mW by laser radiation with λ=980 nm, there is a threshold population of the $^3F_3$ level of the Tm^{3+} ion. At a power above 70.8 mW, there is a sharp increase in the intensity of the glow of bulk and nanophosphorus. There is no threshold pump power for the $^3H_4 \rightarrow {}^3H_6$ transition. This indicates a single photon pumping process during energy transfer $Yb^{3+} \rightarrow Tm^{3+}$.

Nonlinear optical processes are widely discussed by researchers [1]. Upconversion phosphors are used in displays, in bioimaging since the light of the IR range used to excite phosphors does not affect bio tissues [2, 3]. They are also applicable in other areas [4]. Linear logarithmic dependence of intensity (I) of photoluminescence (UCPL) of the samples on pumping power (P) is considered for analysis of upconversion processes in phosphors containing REE ions.

The synthesis of $Sr_2Y_{8-x-y}Yb_yTm_xSi_6O_{26}$ samples (x=0.005-0.5, y=0.2, 0.3) was carried out in air by the sol-gel method. The anneling was fired at 1350–1410 °C for 55 h. According to XRD data, the $Sr_2Y_{8-x-y}Yb_yTm_xSi_6O_{26}$ solid solutions belong to the oxyapatite structural type (sp. gr. P63/m). The Tm atoms are in two crystallographic positions 4f and 6h and form two types of optical centers. The spectra are the total luminescence spectra of these two centers.

Nanoparticles were obtained by electron beam evaporation of targets pressed from bulk samples. During the evaporation of REE silicate targets, they do not decompose. The nanoparticle size of the amorphous sample obtained by evaporation of the $Sr_2Y_{7.695}Yb_{0.3}Tm_{0.005}Si_6O_{26}$ phosphor is ~10.6 nm.

The UCPL spectra were recorded under IR laser excitation (λ=980 nm). On Figure 1 shows the UCPL spectra of the bulk and nano samples at various laser radiation powers (P). Yb^{3+} ions excite Tm^{3+} ions in the $^3H_5$, $^3F_2$, $^1G_4$ states with participation of nonradiative transitions. Compared to the bulk for the nano sample, the transitions intensity decreases.

For a nanosample, as the pump power decreases from 220 to 177 mW, the FWHM of the $^3H_4 \rightarrow {}^3H_6$ transition lines decreases significantly (Fig. 1, b). This is probably due to the difference in the populations of the corresponding levels for the bulk and nano samples.

On Figure 2 shows the dependences of the logarithm of the UCPL intensity on the logarithm of the pump power for some transitions of the Tm^{3+} ion. A characteristic value of the threshold power for the $^3F_3 \rightarrow {}^3H_6$ transition is observed at P~70.8 mW. In the power range of 20–70.8

yy Corresponding author: zuev@ihim.uran.ru

mW, the slope of the dependence line is close to 0.2 (Fig. 2, a), probably due to the small effect of the pump power on the population of the $^3F_3$ level. At a power above 70.8 mW, the UCPL intensity sharply increases. The slope becomes close to 1. This means that the red UCPL is a two-photon process [4]. For the $^3H_4 \rightarrow {}^3H_6$ transition, the slope is close to 0.6 and there is no threshold pump power. This indicates a single photon pumping process during energy transfer Yb→Tm. The same threshold pump power is observed for the nanosample (Fig. 2, b).

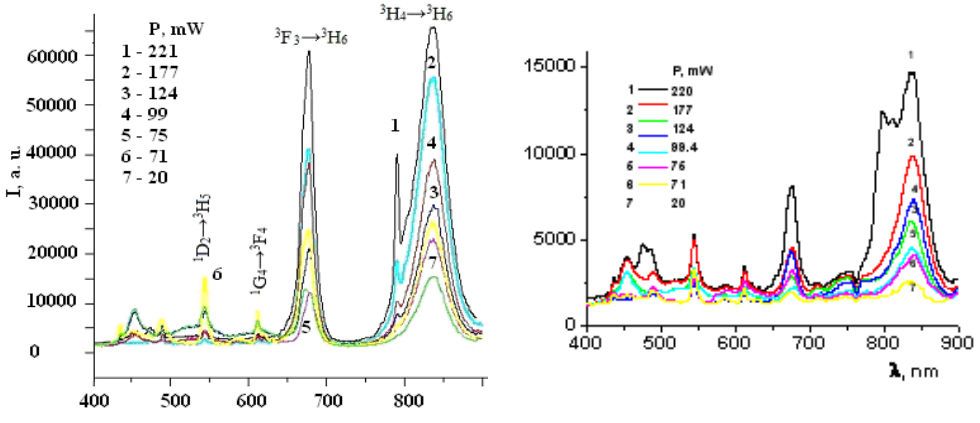

Fig. 1. Spectra UCPL of bulk (a) and nano (b) phosphors.

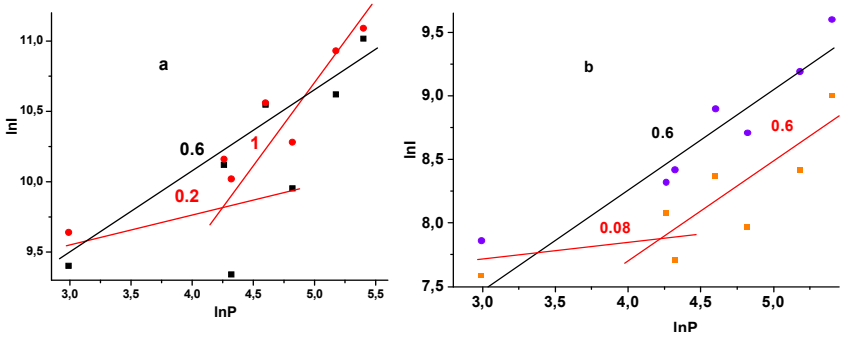

Fig. 2. Dependences of upconversion photoluminescence intensity on pumping power for transitions $^3H_4 \rightarrow {}^3H_6$ and $^3F_3 \rightarrow {}^3H_6$ of bulk (a) and nano (b) phosphors.

References

1. Phosphors, Up Conversion Nano Particles, Quantum Dots and Their Applications. Vol. 2. Editors: Liu, Ru-Shi (Ed.). Springer-Verlag Berlin Heidelberg (2017).
2. Park, Bong Je, Hong, A-Ra, Park, Suntak, Kyung, Ki-Uk, Lee, Kwangyeol, Jang, Ho Seong, Sci. Rep. **7** (2017).
3. Zuev M.G., Ilves V.G., Sokovnin S.Yu., Chimica Techno Acta (to be published) **9** (2022).
4. Feng Wang, Renren Deng, JuanWang, QingxiaoWang, Yu Han, Haomiao Zhu, Xueyuan Chen, Xiaogang Liu, Nature Materials. **10** (2011).
5. Pollnau M., Gamelin D.R., Lüthi S.R., Güdel H.U., and Hehlen M.P., Phys. Rev. B **61** (2000).

POSTER TALKS

Optical spectroscopy of the Er^{3+} ion in $BaY_{1.8}Lu_{0.2}F_8$ crystal

A.V. Astrakhantseva[1, zz], *A.A.* Shavelev[1], *S.V.* Kuznetsov[2], *A.G.* Nikolaev[3], *K.N.* Boldyrev[4], *A.S.* Nizamutdinov[1]

[1]Institute of Physics, Kazan Federal University, 420008 Kazan, Russia
[2]Prokhorov General Physics Institute of the Russian Academy of Sciences, 119991 Moscow, Russia
[3]Institute of Geology and Oil and Gas Technologies, Kazan Federal University, 420008 Kazan, Russia
[4]Institute of Spectroscopy of the Russian Academy of Sciences, 108840, Troitsk, Moscow, Russia

Abstract. Luminescence and absorption spectra for the $BaY_{1.8}Lu_{0.2}F_8$:Er crystals were recorded and analyzed. Luminescence kinetics for $^4I_{11/2}\rightarrow{}^4I_{15/2}$ transition of Er^{3+} ion in $BaY_{1.8}Lu_{0.2}F_8$:Er samples were registered. Absorption cross-section and stimulated emission cross-section spectra were evaluated. The widths of $^4I_{11/2}\rightarrow{}^4I_{15/2}$ and $^4I_{11/2}\rightarrow{}^4I_{13/2}$ transitions lines were estimated.

Er^{3+} is a trivalent rare earth ion with unique features of f-f transitions. Doped into crystalline matrix it results to realization of multiband absorption and emission spectrum, which makes it possible to create up-conversional materials and laser active media [1]. Erbium ions allow to achieve the efficient laser oscillation in the wavelength range around 1,4 and 2,8 μm [2, 3]. This range coincides with the wavelength range of greenhouse gases and water absorption. Thus, erbium doped fluoride crystal lasers are promising candidates for implementation in laser gas analyzers used for differential absorption greenhouse gas detection.

Many applications need large spectral amplification band, which allow wavelength tuning of lasing or generation of ultrashort laser pulses. One of the approaches is to use crystal matrices with significant factor of disorder such as $BaY_{1.8}Lu_{0.2}F_8$:Er crystal.

The spectroscopic characteristics (absorption cross-section spectra, stimulated emission cross-section spectra, lifetimes of excited states) of the $BaY_{1.8}Lu_{0.2}F_8$:Er samples are reported. Absorption cross-section spectrum of $BaY_{1.8}Lu_{0.2}F_8$:Er sample with concentration of Er^{3+} ion 30% presented in Figure 1. Stimulated emission cross-section for $BaY_{1.8}Lu_{0.2}F_8$:Er crystals were calculated and compared with $LiYF_4$:Er crystal for $^4I_{11/2}\rightarrow{}^4I_{15/2}$ and $^4I_{11/2}\rightarrow{}^4I_{13/2}$ transitions (Figure 2, Table 1).

Table 1. Comparison of stimulated emission cross-section.

Transition	Stimulated emission cross-section, × 10^{-20} cm^2		
	$BaY_{1.8}Lu_{0.2}F_8$:Er (30% Er)	$BaY_{1.8}Lu_{0.2}F_8$:Er (20% Er)	$LiYF_4$:Er (15% Er)
$^4I_{11/2}\rightarrow{}^4I_{15/2}$	0.23	0,26	0.57
$^4I_{11/2}\rightarrow{}^4I_{13/2}$	6.4	6.9	16.9

[zz] Corresponding author: anya4324@gmail.com

Also the widths of $^4I_{11/2}\rightarrow{}^4I_{15/2}$ and $^4I_{11/2}\rightarrow{}^4I_{13/2}$ transitions lines were estimated in comparison to the same transitions lines in $LiYF_4$:Er crystal (Table 2).

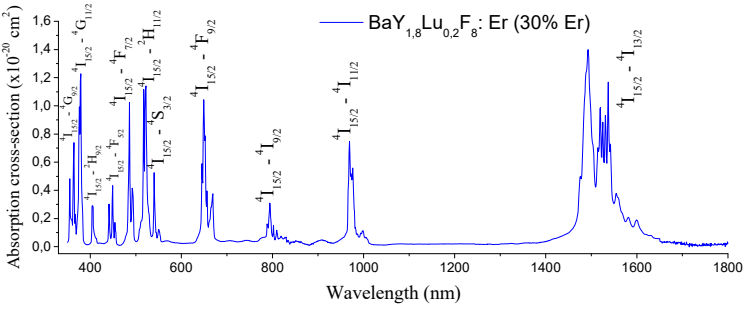

Fig. 1. Absorption cross-section spectrum of $BaY_{1.8}Lu_{0.2}F_8$:Er sample with concentration of Er^{3+} ion 30%.

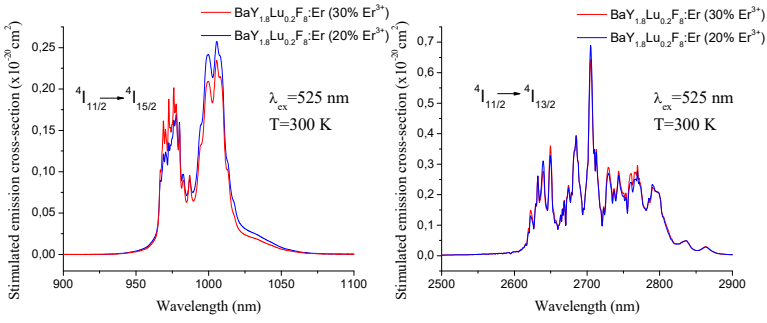

Fig. 2. Stimulated emission cross-section spectra of $BaY_{1.8}Lu_{0.2}F_8$:Er samples with concentration of Er^{3+} ion 30% and 20%.

Table 2. Comparison of $^4I_{11/2}\rightarrow{}^4I_{15/2}$ and $^4I_{11/2}\rightarrow{}^4I_{13/2}$ transitions lines.

Transition	**Line width, nm**		
	$BaY_{1.8}Lu_{0.2}F_8$:Er (30% Er)	$BaY_{1.8}Lu_{0.2}F_8$:Er (20% Er)	$LiYF_4$:Er (15% Er)
$^4I_{11/2}\rightarrow{}^4I_{15/2}$	52	53	46.7
$^4I_{11/2}\rightarrow{}^4I_{13/2}$	183	175	128.6

Thus, the stimulated emission cross-sections of $^4I_{11/2}\rightarrow{}^4I_{15/2}$ and $^4I_{11/2}\rightarrow{}^4I_{13/2}$ transitions were evaluated. The values for $BaY_{1.8}Lu_{0.2}F_8$:Er are similar to $LiYF_4$:Er within the margin of error. The spectral widths of the transition lines were estimated from experimental data. The transition lines of $BaY_{1.8}Lu_{0.2}F_8$:Er showed a broadening in comparison to $LiYF_4$:Er.

Fluoride crystals were synthesized in accordance with the Strategic Academic Leadership Program "Priority 2030" of the Kazan Federal University of the Government of the Russian Federation.

References

1. S. Kuznetsov, Yu. Ermakova, V. Voronov et al. J. Mater. Chem. C. **6**, 598-604 (2018)
2. J. Hong, L. Zhang, M. Xu, Y.Hang, Inf. Ph. & Tech. **80**, 38–43 (2017)
3. T.T. Basiev, Yu.V. Orlovskii, M.V. Polyachenkova et al. Quant. Electron. **36**, 591-594 (2006)

Free-ion, crystal-field and electric dipole parameters of Tm^{3+} ion in $Y_3Al_5O_{12}$ crystal

Eduard Baibekov[1, aaa] and *Alia* Saitova[1]

[1]Kazan Federal University, Physics Department, 420008 Kremlyovskaya 18, Kazan, Russia

Abstract. We calculate the energy levels and the wavefunctions of impurity thulium ion in $Y_3Al_5O_{12}$ crystal. The obtained set of free-ion and crystal-field parameters results in somewhat better agreement with the published experimental data than the existing calculations. We also discuss the possible origins of linear Stark effect observed recently for this crystal which is normally prohibited by the selection rules.

Yttrium-aluminium garnet $Y_3Al_5O_{12}$ (YAG) is widely used as the solid-state host matrix for IR lasing. Among the set of impurity rare earth ions, trivalent thulium ion is known to be suitable for 2 μm laser emission. While the spectra and energy levels of Tm:YAG crystal have been thoroughly analysed during the past decades [1,2], this system has regained interest recently due to its possible applications for quantum information processing. In particular, the presence of weak linear Stark effect in this crystal allowed one to implement silenced echo quantum memory protocol using $^3H_6 \rightarrow {}^3H_4$ optical transition [3]. According to the group theory, for the non-Kramers ion with D_2 site symmetry, there should be no linear (with respect to the external electric field) shift of its energy levels [4]. The existence of such a shift observed in Ref. [3] could result from the presence of crystal lattice defects that lowered the Tm^{3+} site symmetry. For instance, that could be the nearby thulium impurity ions that have the ionic radii slightly differing from that of yttrium ions of the host lattice which they substitute.

To obtain quantitative description of the observed phenomenon, we have revised the published spectroscopic data and performed the computations of the energy levels and corresponding eigenfunctions of the trivalent thulium ion in YAG. In addition to electrostatic, spin-orbit and crystal-field interactions and two-body electrostatic correlation terms, we considered higher-order relativistic terms (spin-spin and spin-other-orbit corrections and electrostatically correlated spin-orbit perturbation) [5], which allowed us to obtain somewhat better agreement with the experimental energy levels than previously published data [2]. Using the value of average linear Stark shift measured for the transition $^3H_6 \rightarrow {}^3H_4$ [3], we estimated the parameter which defined the electric dipole moment operator of thulium ion in the defect-containing Tm:YAG crystal projected onto the subspace of the ground electronic configuration $4f^{12}$. This result, along with found thulium wavefunctions, would allow one to estimate relative values of linear Stark shifts corresponding to different energy levels of the configuration $4f^{12}$ of Tm^{3+} in real Tm:YAG crystal.

E.B. acknowledges the support of the Foundation for the Advancement of Theoretical Physics and Mathematics “BASIS”.

[aaa] Corresponding author: edbaibek@gmail.com

References

1. J.B. Gruber, M.E. Hills, R.M. Macfarlane, C.A. Morrison, G.A. Turner, G.J. Quarles, G.J. Kintz, L. Esterowitz, Phys. Rev. B **40**, 9464 (1989)
2. C. Tiseanu, A. Lupei, V. Lupei, J. Phys.: Condens. Matter **7**, 8477 (1995)
3. M.M. Minnegaliev, K.I. Gerasimov, R.V. Urmancheev, A.M. Zheltikov, S.A. Moiseev, Phys. Rev. B **103**, 174110 (2021)
4. R.M. Macfarlane, J. Lumin. **125**, 156 (2007)
5. W.T. Carnall, G.L. Goodman, K. Rajnak, R.S. Rana, J. Chem. Phys. **90**, 3443 (1989)

Optical pumping of atoms under conditions of breaking the electron-nuclear bond

Konstantin Barantsev[1, bbb] and *Andrey* Litvinov[1]

[1]Peter the Great St. Petersburg Polytechnic University, Institute of Electronics and Telecommunications, 194251 Polytechnicheskaya 29, St. Petersburg, Russia

Abstract. We study the peculiarities of the optical pumping for quantum magnetometers based on magnetic resonance in the gas cell with alkali atoms and buffer gas. The mathematical model based on the density matrix formalism has been developed. This model considers the breaking of the bond between the outer electron and the nucleus of an alkali atom during a collision with the buffer gas. This approach allows us to get the population distribution in the Zeeman sublevels and to calculate the polarization of the magnetic moment. The dependence of polarization on laser detuning and quenching rate has been analysed.

1 Introduction

Recently, miniature quantum magnetometers have been actively developed [1,2]. This is due to the wide range of their applications in such areas as geophysics, medicine, navigation, gyroscopy and astronomy. In our work we consider quantum magnetometers based on the magnetic resonance phenomena in a gas cell with alkali metel atoms. Such magnitometers are miniature which is very useful in encyphalography and cardiography. Today, the sensitivity of quantum magnetometers has proven to be comparable to that of SQUID magnetometers.

One of the main characteristics that determine the sensitivity of optical quantum magnetometers is the degree of atomic polarization that can be achieved by optical pumping. The higher polarization of atoms can be created, the greater sensitivity of the magnetometer can be achieved, if the other parameters are equal. Collisions of atoms between each other, with buffer gas and with the walls of the cell destroy the induced polarization. The spin-exchange processes in the ground state, quenching and spontaneous decay in the excited state lead to an equilibrium population of the Zeeman sublevels. These processes with the laser pumping make the main contribution to the final polarization of the alkali atoms.

For a correct description of the optical pumping process, it is necessary to take into account the breaking of the bond between the outer electron and the nucleus of an alkali atom during a collision. This is due to the fact that the time of the collision is much shorter than the time of the hyperfine interaction. The electron spin is destroyed, and the nuclear spin can be preserved [3] when the alkali atoms collide with atoms of the buffer gas. This fact significantly affects the achievement of the maximum polarization of atoms.

2 Results

We developed a mathematical model of optical pumping of ^{87}Rb atoms in the buffered gas cell. The model is based on the Liouville equation for the atomic density matrix. Atoms are excited by the circularly polarized monochromatic laser radiation.

[bbb] Corresponding author: kostmann@yandex.ru

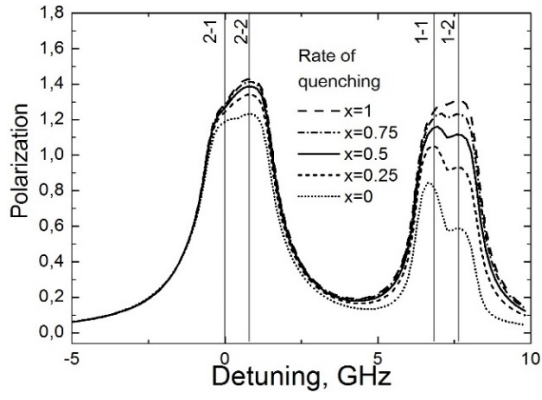

Fig. 1. Mean projection of the atomic angular momentum of the ^{87}Rb atoms depending on the laser detuning. Different curves correspond to variation of the rate of quenching x – fraction of collisions in which the quenching occurs. Vertical lines point the values of detuning that correspond to the transitions in the D_1-line of ^{87}Rb with the change in total angular moment $F_g - F_e$.

It is found the stationary solution of the system of quantum kinetic equations with considering the break of the electron-nuclear bond and nuclear spin preservation during collisions. The nuclear spin is preserved, but the electron state becomes stochastic and uniformly distributed after collision. To describe this, it is necessary to go to electron-nuclear basis.

We calculate the mean projection $\langle M_Z \rangle$ of the full atomic angular momentum, which is proportional to the polarization of the gas cell, depending on the laser detuning (Figure 1). The quantization axis z is co-directed with the wave vector of the radiation. The curves have four resonance peaks corresponding to the transitions in the D_1-line of ^{87}Rb atom. The frequencies of the peaks are pointed by the vertical lines (the numbers on these lines indicate the change in total angular momentum $F_g - F_e$).

We have analysed the effect of the fraction x of inelastic collisions on the mean projection of the full angular momentum. If x is increasing, the collisions leading to transition from the excited state to the ground state become more frequent. This leads to an increase in the rate of polarization transfer from the excited state to the ground state. The polarization of the atom in the ground state lives much longer than in the excited state because the radii of the atom in these states are different. The radius of the excited state is larger, and the atom is more susceptible to depolarizing collisions. Therefore, the polarization increases with the growing of the fraction of inelastic collisions.

The work was supported by Russian Foundation for Basic Research (project 19-29-10004).

References

1. J. Tang, Y. Zhai, L. Cao et al., Opt. Express **29**, 15641 (2021).
2. W. Zheng, S. Su, G. Zhang et al., Biomed. Opt. Express 11, 649 (2020).
3. W. Happer, Y.-Y. Jau, T. G. Walker, *Optically Pumped Atoms* (Wiley, New York, 2010).

Phonon spectrum of $R_2Sn_2O_7$ (R=La-Lu): ab initio calculation

Vladimir Chernyshev[1, ccc]

[1]Ural Federal University, Institute of Natural Sciences and Mathematics, 620002 Mira st. 19, Ekaterinburg, Russia

Abstract. Ab initio study of the phonon spectrum and the elastic properties of rare-earth stannates $R_2Sn_2O_7$ (R = La-Lu) have been performed. The frequencies and types of fundamental modes were determined from ab initio calculations. The degree of participation of ions in phonon modes was determined from an analysis of the displacement vectors obtained from the ab initio calculations. Modes with the absolute or predominant participation of oxygen in the 48*f* position characterized by shift *x* are determined. The elastic constants and hardness H_V are calculated. The effect of hydrostatic pressure on the crystal structure is investigated also. It is shown that the degree of distortion of the oxygen octahedron containing the rare-earth ion changes insignificantly with the pressure. It is shown that the pressure dependence of the unit cell volume is described by the third-order Birch-Murnaghan equation of state.

Rare-earth oxides $R_2B_2O_7$ (where A is a rare-earth ion R^{3+}, B is Ti, Zr, Sn) with a pyrochlore structure have attracted attention because of their various properties and potential application as luminophores [1]. The Raman spectra of some stannates was recently measured [2,3]. However, the phonon modes were not interpreted directly from the experimental data. The Raman spectra in work [3] were measured on a polycrystalline sample, and the types of the modes were defined from calculations at the force constants model. Elastic constants and Vickers hardness were also experimentally determined for some stannates $R_2Sn_2O_7$ [4]. It is actual to calculate the crystal structure, phonon spectrum and elastic properties of the all row of rare-earth stannates $R_2Sn_2O_7$ (R = La–Lu) within the framework of a unified ab initio approach. Rare-earth stannates $R_2Sn_2O_7$ with pyrochlore structure have space group no. 227. Ions are in the positions: Sn 16c (0, 0, 0), R 16d (1/2, 1/2, 1/2), O1 48*f* (*x*, 1/8, 1/8), O2 8b (3/8, 3/8, 3/8).

The density functional theory calculations were carried out using the PBE0 hybrid functional which considers both local and nonlocal Hartree-Fock exchanges. The calculations were carried out in the CRYSTAL17 program [5] designed to simulate periodic crystal structures within the MO LCAO approach. The calculation results are in good agreement with the available experimental data [3,6] (Fig.1-2). From the analysis of the displacement vectors obtained at ab initio calculations, the degree of involvement of ions in each mode was determined. It is shown that the strongest Raman mode with a frequency ~ 300 cm^{-1} is dominated by oxygen ions located in the 48*f* position. It is shown that the intense Raman mode with a frequency ~ 500 cm^{-1} involves only oxygen ions from 48*f* position. It is shown that the pressure dependence of the unit cell volume is well described by the third-order Birch-Murnaghan equation of state. The elastic constants and the Vickers hardness values of the

[ccc] Corresponding author: vladimir.chernyshev@urfu.ru

$R_2Sn_2O_7$ rare-earth stannates are calculated. It is shown that the hardness increases in the series R = La–Lu.

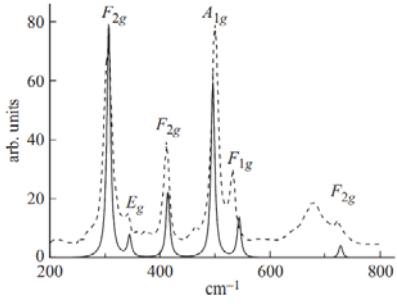

Fig. 1. Raman spectrum of $Nd_2Sn_2O_7$. The dotted line shows the experimental data from [3].

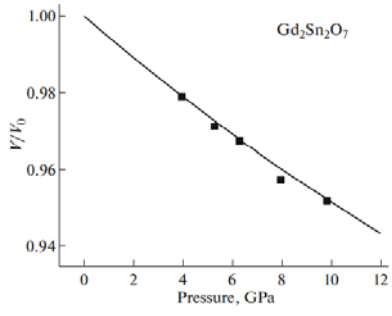

Fig. 2. The dependence of the cell volume of $Gd_2Sn_2O_7$ from pressure described by the third-order Birch-Murnaghan equation of state. Square symbols are the experimental data [6].

This study was supported by the Ministry of Science and Higher Education of the Russian Federation (project no. FEUZ-2020-0054).

References

1. R. Cao, G. Quan, Z. Shi, T. Chen, Z. Luo, G. Zheng, Z. Hu, J. Phys. Chem. Solids **118**, 109 (2018)
2. L. T. Denisova, L. A. Irtyugo, Yu. F. Kargin, V. M. Denisov, V. V. Beletskii, A. A. Shubin, Inorg. Mater. **52**, 811 (2016)
3. Q. Zhixue, W. Chunlei, W. Pan, Acta Mater. **60**, 2939 (2012)
4. J. Feng, B. Xiao, Z. X. Qu, R. Zhou, W. Pan, Appl. Phys. Lett. **99**, 201909 (2011).
5. CRYSTAL17: A Computational Tool for Solid State Chemistry and Physics. http://www.crystal.unito.it/index.php.
6. K. M. Turner, C. L. Tracy, W. L. Mao, R. C. Ewing, J. Phys.: Condens. Matter **29**, 504005 (2017)

Luminescence spectra of Er:YSAG laser ceramics

Vladimir S. Tsvetkov[1], *Vadim* Zhmykhov[1], *Elena* Dobretsova[1, ddd], *Yurii* Pyrkov[1], *Marina* Nikova[2], *Irina* Chikulina[2], *Vitaly* Tarala[2], *Dmitry* Vakalov[2], *Sergei* Kuznetsov[1], and *Vladimir B.* Tsvetkov[1]

[1]Prokhorov General Physics Institute of the Russian Academy of Sciences, 119991 Moscow, Russia
[2]Scientific and Laboratory Complex Clean Room, North Caucasus Federal University, 355009 Stavropol, Russia

Abstract. Luminescence spectra of Er-doped yttrium-scandium-aluminum garnet (Er:YSAG) ceramics are presented in the spectral range of 1450 to 1700 nm at 300 K. The optical properties of the Er:YSAG ceramic solid solutions can be changed by introducing scandium into the dodecahedral and/or octahedral sites. The goal of our work was to characterize optical properties of new Er:YAG ceramics depending on distribution of Sc^{3+} ions in the crystal structure.

We may highlight three groups of solid-state host materials such as single crystals, glasses, and ceramics. Among them Er-doped laser hosts attract special attention due to its application, mainly in medicine [1]. Crystal solid solutions with a garnet structure based on yttrium, aluminum, and scandium oxides are of great interest because of the possibility to control the spectroscopic and laser properties by changing the chemical composition and local symmetry of Er^{3+} ion in the active medium [2].

Here Er-doped YSAG optical ceramics [3] is compared to the Er:YAG (Er-concentration of 30% at.) single crystal. We present the fluorescence spectra being recorded from the ceramic samples and the single crystal in the range of the $^4I_{13/2} \rightarrow {}^4I_{15/2}$ transition in Er^{3+} ion. The spectra were measured at 300K with spectral resolution of 0.1 nm.

The Er^{3+} concentration in the dodecahedral site was constant (1.5 f.u) in all samples. $Y_{1.3}Er_{1.5}Sc_1Al_{4.2}O_{12}$ and $Y_{1.1}Er_{1.5}Sc_1Al_{4.4}O_{12}$ were chosen with the fixed scandium concentration (1 f.u.) and scandium ratio in the dodecahedral $\{Sc^{3+}\}$ and octahedral $[Sc^{3+}]$ sites varying from $\{Sc^{3+}\}/[Sc^{3+}] = 0.8/0.2$ to $\{Sc^{3+}\}/[Sc^{3+}] = 0.2/0.8$. The filling of the tetrahedral site was also constant (3 f.u. Al^{3+}). The distinctive feature of the $Er_{1.5}Sc_{1.7}Al_{4.8}O_{12}$ sample was the total absence of Y^{3+} cations in the oxide composition and the concentration of scandium in the dodecahedral site increased up to 1.5 f.u. Therefore, this composition can be considered scandium-aluminum-garnet doped with erbium (Er:SAG).

We are observing the broadening of lines in different compositions and their shift depending on the position which scandium occupies. $Er_{1.5}Sc_{1.7}Al_{4.8}O_{12}$ is the most suitable for organizing flat spectral gain in the region of 1450–1650 nm at room temperature.

[ddd] Corresponding author: elenadobretsova89@gmail.com

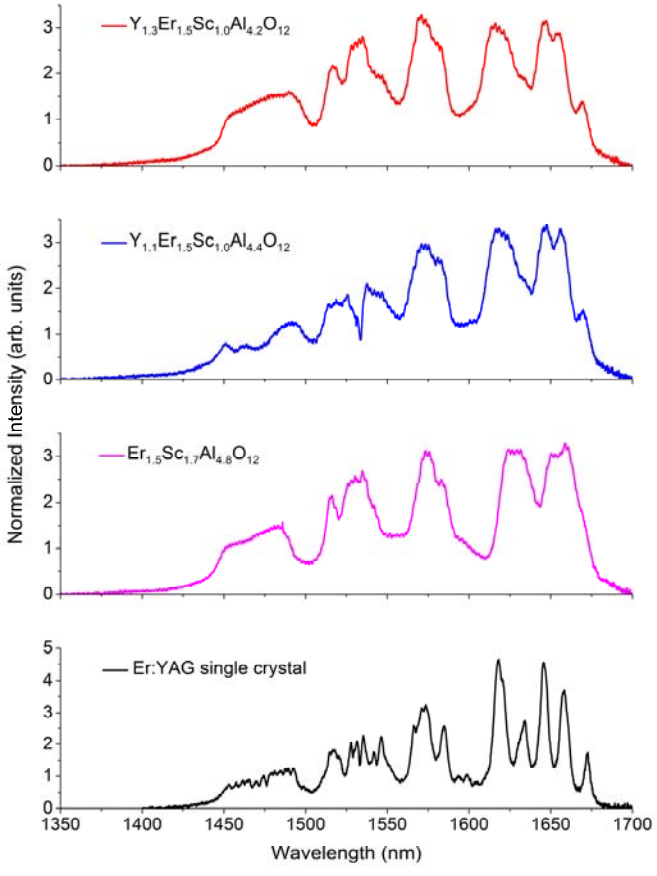

Fig. 1. Room-temperature fluorescence spectra of $Y_{1.3}Er_{1.5}Sc_1Al_{4.2}O_{12}$, $Y_{1.1}Er_{1.5}Sc_1Al_{4.4}O_{12}$ and $Er_{1.5}Sc_{1.7}Al_{4.8}O_{12}$ ceramics and Er:YAG single crystal in the range of the $^4I_{13/2} \rightarrow {}^4I_{15/2}$ transition in Er^{3+} ion.

This work was supported by the Grant of the President of the Russian Federation, grant №MK-72.2022.1.2

References

1. U.B. Ogrinc, S. Senčar, H. Lenasi, Lasers Surg. Med. **47**, 689-697 (2015)
2. Ł. Dobrzycki, E. Bulska, D.A. Pawlak, Z. Frukacz, and K. Woz´niak, Inorg. Chem. **43**, 7656-7664 (2004)
3. V.A. Tarala, M.S. Nikova, S.V. Kuznetsov, I.S. Chikulina, A.A. Kravtsov, D.S. Vakalov, S.O. Krandievsky, F.F. Malyavin, M.G. Ambartsumov, L.V. Kozhitov, L.M. Mitrofanenko, J. Lumin. **241**, 118539 (2022)

Paramagnetic centers of Gd^{3+} in single crystal of Y_2SiO_5 doped with chromium

Andrei Fokin[1,eee], *Vladimir* Vazhenin[1], *Alexander* Potapov[1], *Mikhail* Artyomov[1], *Kirill* Subbotin[2,3], and *Anatolii* Titov[2,3]

[1]Ural Federal University, Institute of Natural Sciences and Mathematics, Mira 19, 620002, Ekaterinburg, Russia
[2]Prokhorov General Physics institute of Russian Academy of Sciences, Vavilova St. 38, 119991, Moscow, Russia
[3]Mendeleev University of Chemical Technology of Russia, Miusskaya Sq. 9, 125047, Moscow, Russia

Abstract. The angular dependencies of previously non-studied EPR signals have been investigated in the Y_2SiO_5 single crystal. These signals have been assigned to two triclinic Gd^{3+} impurity centers localized in two physically nonequivalent yttrium positions. The spin Hamiltonian parameters for two Gd^{3+} centers have been determined.

Y_2SiO_5 (YSO) single crystals doped with chromium are considered as an active medium for solid-state lasers operating in the near-infrared region [1]. The same crystals with Er^{3+}, Yb^{3+}, Nd^{3+}, Tm^{3+} rare-earth ions are studied as possible candidates for quantum information processing, and Ce^{3+}-doped crystals are known as efficient scintillation materials [2].

We studied the YSO single crystal doped with chromium with high content of the odd isotope ^{53}Cr (the nuclear spin is I = 3/2) by the EPR method. The crystal was grown by the Czochralski method in our previous work [3]. The EPR measurements were carried out using Bruker EMX Plus X-band spectrometer at room temperature in the fields up to 1500 mT.

The angular dependencies of the EPR spectrum were measured during rotation of the magnetic field in the crystal ac-plane, as well as in the perpendicular plane containing the b-axis. We found a lot of weak narrow signals in the EPR spectra, which cannot be attributed to either the early studied Cr^{3+} centers described for our previous work [3] or other uncontrolled paramagnetic impurity ions (Fe, Ni, and Cu) revealed in the studied sample by spark mass-spectroscopy [3].

The YSO crystal has a monoclinic structure (space group C2/c) and yttrium ions occupy two non-equivalent sites in the unit cell local point symmetry 1 (C1) and with the coordination numbers 6 and 7. The detailed analysis of the orientation dependencies of the positions of studied signals in several planes showed that all unidentified signals can be assigned to two triclinic paramagnetic centers with the electron spin S = 7/2, which is typical for Gd^{3+} rare-earth ions which EPR spectrum can be observed at room temperature. Also, the hyperfine structure observed in the narrowest signals is typical for odd Gd^{3+} isotopes with the nuclear spin I =3/2. These facts allowed us to conclude that the discussed discovered weak signals belong to low-symmetry paramagnetic centers formed by Gd^{3+} ions which are present in the crystal as an uncontrolled impurity and replace matrix Y^{3+} ions in two sites (Y1 and Y2). We described the properties of two found Gd^{3+} paramagnetic impurity centers in the studied ^{53}Cr:YSO crystal by the triclinic spin Hamiltonian and found fine structure parameters in the laboratory and local coordinate system (in which the second-rank fine structure tensor becomes diagonal).

[eee] Corresponding author: andrej.fokin@urfu.ru

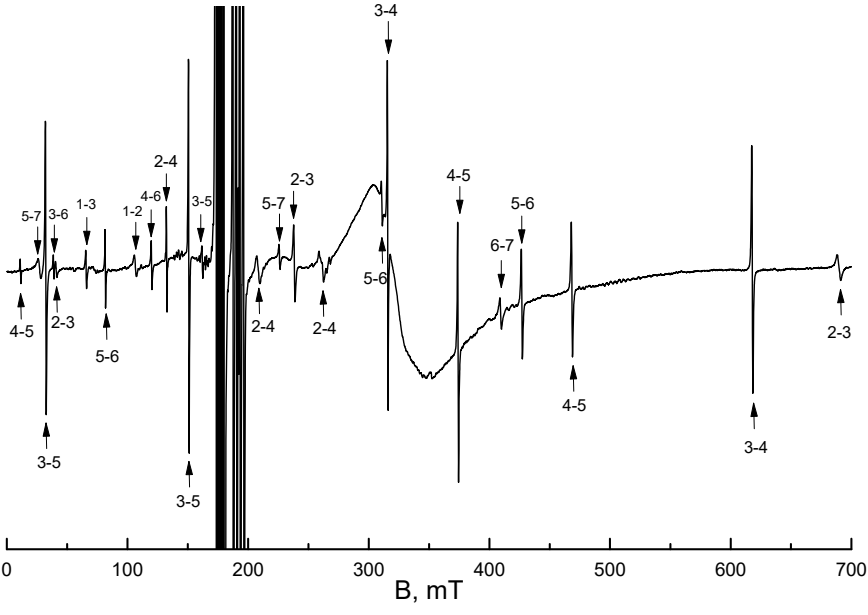

Fig. 1. EPR spectrum of Cr:Y_2SiO_5 at **B**||b at room temperature at frequency 9869 MHz. The signals of the Gd1 and Gd2 centers are indicated by the upper and lower arrows, respectively. Numbers denoted the energy levels.

The work of co-authors from Mendeleev University of Chemical Technology was supported by the Ministry of Science and Higher Education of the Russian Federation, grant No. FSSM-2020-0005. The work of co-authors from Ural Federal university was supported by the Ministry of Science and Higher Education of the Russian Federation, grant No. FEUZ-2020-0054

References

1. J. Koetke, S. Kück, K. Petermann, G. Huber, G. Cerullo, M. Danailov, V. Magni, L.F. Qian and O. Svelto, Opt. Commun. **101**, 195 (1993)
2. M. Buryi, V. Laguta, J. Rosa, M. Nikl, Radiat. Meas. **90**, 23 (2016).
3. V.A. Vazhenin, A.P. Potapov, K.A. Subbotin, D. Lis, M.Yu. Artyomov, V. Sanina, E.V. Chernova, A.V. Fokin, Opt. Mat. **117**, 111107 (2021)

Influence of $Gd_xEu_{1-x}Nb_yTa_{1-y}O_4$ structural properties on Eu^{3+} luminescence features

Grigorii Gusev[1,fff], *Sofia* Masloboeva[2], *Tatiana* Popova[1], *Marya* Yagovkina[1], and *Marya* Zamoryanskaya[1]

[1]Ioffe Institute RAS, 194021 St. Petersburg, Russia
[2]ICT KSC RAS, 184209 Murmansk region, Apatity, Russia

Abstract. In this work, europium-activated ceramic gadolinium tantalum niobates were synthesized for the first time. A detailed interpretation of the obtained photoluminescence and cathodoluminescence spectra has been made. The cathodoluminescence spectra of the samples showed transitions from the $^5D_0$, $^5D_1$, $^5D_2$, and $^5D_3$ Eu^{3+} radiative levels. The main structural phase of the samples corresponded to a monoclinic lattice with space group I2/a. The dependence of the Eu^{3+} Stark splitting luminescence bands on the Nb/Ta ratio in ceramics was studied for various radiative transitions. It is shown that the distance between the splittings of europium luminescence bands increases in the series of solid solutions from $GdNbO_4$ to $GdTaO_4$. This can be explained by the enhancement of the local field action on the Eu^{3+} ions.

Niobates and tantalates of rare earth elements ($LnNbO_4$ and $LnTaO_4$) are promising functional materials due to their physicochemical stability and luminescent properties [1]. These compounds can be used as scintillators for X-ray detection in various devices [2].

A distinctive feature of such materials is the presence of their own luminescence band associated with NbO_4 or TaO_4 complexes [1]. These bands can act as a sensitizer for luminescent ions (Eu^{3+} ions for example) [3]. For applications in high-energy radiation detectors, an important material parameter is its average atomic number. Its increase leads to an increase in the efficiency of absorption of high-energy excitation. Therefore, $GdNbO_4$ deserves special attention. Its average atomic number is higher than that of the commonly used $YNbO_4$. In turn, $GdTaO_4$ is one of the densest known scintillators. However, it has a significantly lower intrinsic luminescence yield compared to $GdNbO_4$ [4].

Partial replacement of niobium with tantalum in $GdNbO_4$ seems promising to increase the average atomic number of the material and preserve the luminescent properties of gadolinium niobate. However, such changes can significantly affect the luminescent properties of activator ions in such a material. Studies of this effect in gadolinium tantalum niobates activated with Eu^{3+} have not been previously performed.

The aim of this work was to study the fine splitting of emission bands from the $^5D_0$, $^5D_1$, $^5D_2$, and $^5D_3$ Eu^{3+} energy levels in the $Gd_{0.94}Eu_{0.06}Nb_yTa_{1-y}O_4$ (where y=0, 0.9, 0.3, 1) ceramics depending on the Nb/Ta ratio in its composition.

Samples of ceramic tantalum-niobates were synthesized by the liquid-phase method, followed by cold pressing. The obtained materials were studied by such methods as x-ray diffraction analysis (XRD), electron probe microanalysis (EPMA), local cathodoluminescence (CL) and photoluminescence (PL).

According to EPMA, the average elemental composition of the obtained ceramics complied with the prescribed composition. XRD showed that in $Gd_{0.94}Eu_{0.06}NbO_4$ and

[fff] Corresponding author: ggusev@mail.ioffe.ru

$Gd_{0.94}Eu_{0.06}Nb_{0.9}Ta_{0.1}O_4$ samples the main structural phase was a monoclinic modification M of $GdNbO_4$; in $Gd_{0.94}Eu_{0.06}Nb_{0.3}Ta_{0.7}O_4$ and $Gd_{0.94}Eu_{0.06}TaO_4$ samples it was a monoclinic modification M of $GdTaO_4$. The obtained CL spectra exhibited bands associated with transitions from the $^5D_0$, $^5D_1$, $^5D_2$, and $^5D_3$ Eu^{3+} energy levels. The behavior of the Stark splitting of CL and PL bands belonging to different energy levels is studied as a function of the Nb/Ta ratio in the material (examples of such dependences for PL are shown in Fig. 1). A higher content of tantalum in the composition of the material can lead to a larger local field acting on rare-earth ions. Consequently, the distance between the splitting bands increased in the series of solid solutions from $GdNbO_4$ to $GdTaO_4$.

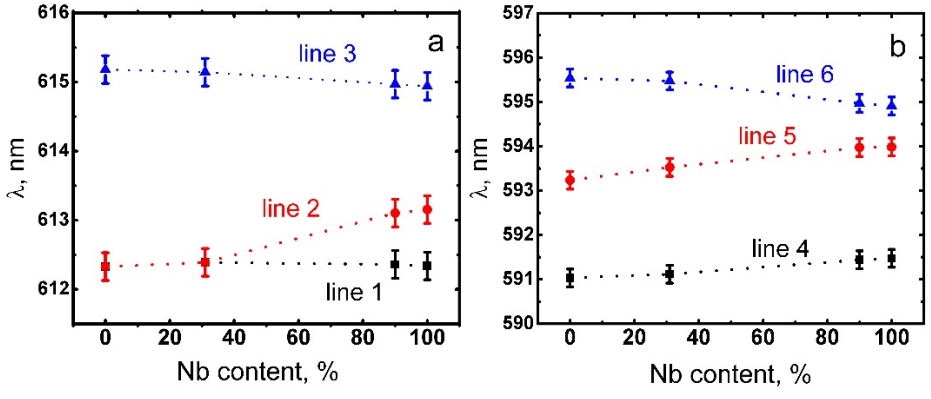

Fig. 1. Dependences of the splitting bands (lines) positions of different $Gd_{0.94}Eu_{0.06}Nb_yTa_{1-y}O_4$ PL spectrum ranges on the Nb content in the composition: (a) Range 1 (605-635 nm), $^5D_0$-$^7F_2$; (b) Range 2 (580-600 nm), $^5D_0$-$^7F_1$.

The results obtained can be useful for a better understanding of the rare earth ions luminescence spectra behavior depending on the structural properties of the material.

References

1. H. Brunckova, H. Kolev, L.A. Rocha, E.J. Nassar, S.B. Moscardini, L. Medvecky, Appl. Surf. Sci. **504**, 144358 (2020)
2. B. Liu, K. Han, X. Liu, M. Gu, S. Huang, C. Ni, Z. Qi, G. Zhang, Solid State Commun. **144**, 484-487 (2007)
3. M.V. Nazarov, D.Y. Jeon, J.H. Kang, E.J. Popovici, L.E. Muresan, M.V. Zamoryanskaya, B.S. Tsukerblat, Solid State Commun. **131**, 307–311 (2004)
4. O. Voloshyna, O. Sidletskiy, D. Spassky, I. Gerasymov, I. Romet, A. Belsky, Opt. Mater **76**, 382–387 (2018)

Enhancement of up-conversion luminescence of SrF_2:Ho phosphors using co-doping Yb^{3+} ions upon excitation of $^5I_7$ level of Ho^{3+} ions

S.V. Gushchin[1,ggg], *S.V.* Kuznetsov[2], *V.Yu.* Proydakova[2], *A.A.* Lyapin[1], *P.A.* Ryabochkina[1], *P.P.* Fedorov[2], and *M.V.* Chernov[1]

[1]Institute of Physics and Chemistry, National Research Ogarev Mordovia State University, 430005, Saransk, Russia
[2]Prokhorov General Physics Institute, Russian Academy of Sciences, 119991, Moscow, Russia

Abstract. Fluorite-type SrF_2:Ho and SrF_2:Ho,Yb phosphors were synthesized using a co-precipitation from the aqueous solution technique. Up-conversion luminescence (UCL) of SrF_2:Ho and SrF_2:Ho,Yb phosphors in the visible and near-infrared spectral region upon excitation of $^5I_7$ level of Ho^{3+} ions were investigated. For quantifying material performance, the concentration of rare-earth (RE) ions dependent on UCL and the UCL energy yields of SrF_2:Ho and SrF_2:Ho,Yb were studied. Chromaticity coordinates and color temperature of SrF_2:Ho and SrF_2:Ho,Yb were calculated.

Over the past few years, up-conversion phosphors doped with RE ions have been many scientific groups' main subject of research. At present, up-conversion phosphors are applied in various fields of science. These include laser physics, biomedicine, solar energy, optogenetics, forensics, etc. [1-7].

In the present paper, the concentration series of fluoride phosphors with the fluorite structure SrF_2:Ho and SrF_2:Ho,Yb were investigated. Fluoride phosphors with a fluorite structure doped RE ions arouse active research interest because of their unique features [6,7]. These materials have low phonon energy (~ 366 cm^{-1} SrF_2) and the tendency to form multiple cluster configurations of dopant ions. The low phonon energy leads to a decrease in the probability of multiphonon relaxation processes. Thereby, the lifetime of intermediate levels of RE ions is increased. The intermediate levels of RE ions play an important role in the up-conversion processes. Besides, the tendency to form multiple cluster configurations of RE ions leads to a decrease in the distance between RE ions. Reducing the distance between RE ions leads to an increased in the probability of up-conversion processes (energy transfer up-conversion, cooperative processes, and cross-relaxation processes) based on interionic interactions.

Figure 1(a) presents the room-temperature diffuse reflection spectrum of Ho^{3+} and Yb^{3+} ions in the range 300–2100 nm of the SrF_2:Ho(3.9%),Yb(2.0%) phosphor. Absorption bands corresponding to the transitions of Ho^{3+} ions from ground level $^5I_8$ to the excitation levels $^3H_6$, $^5G_4$, $^5G_5$, $^5G_6$, $^5F_3$, $^5S_2(^5F_4)$, $^5F_5$, $^5I_4$, $^5I_5$, $^5I_6$, $^5I_7$ and band, which corresponding to $^2F_{7/2}\rightarrow{}^2F_{5/2}$ transition of Yb^{3+} ions are seen clearly on the diffuse reflection spectrum.

Upon excitation of the $^5I_7$ level, the UCL spectrum of Ho^{3+} and Yb^{3+} ions in SrF_2:Ho(3.4%),Yb(1.0%) phosphor at 300 K corresponding to $^5F_3\rightarrow{}^5I_8$, $^5S_2(^5F_4)\rightarrow{}^5I_8$, $^5F_5\rightarrow{}^5I_8$, $^5I_4\rightarrow{}^5I_8$, $^5I_5\rightarrow{}^5I_8$, $^5F_5\rightarrow{}^5I_7$ transitions of Ho^{3+} ions $^2F_{5/2}\rightarrow{}^2F_{7/2}$ transition of Yb^{3+} ions were recorded (Fig. 1(b)). The studied phosphors exhibit intense UCL in the red spectral range.

[ggg] Corresponding author: serg.guschin1703@gmail.com

Maximum UCL energy yields were achieved 0.03% (380-780 nm) and 0.09% (380-1100 nm) for SrF_2:Ho(3.5%) phosphors. Co-doping of Yb^{3+} ions allows to increase UCL energy yields by 0.1% (380-780 nm) and 1.4% (380-1100 nm) for SrF_2:Ho(3.4%),Yb(1.0%) phosphors, respectively. The SrF_2:Ho and SrF_2:Ho,Yb phosphors exhibit the red UCL, which corresponding to correlated color temperatures 6711-7474 K and 4162-7333 K, respectively.

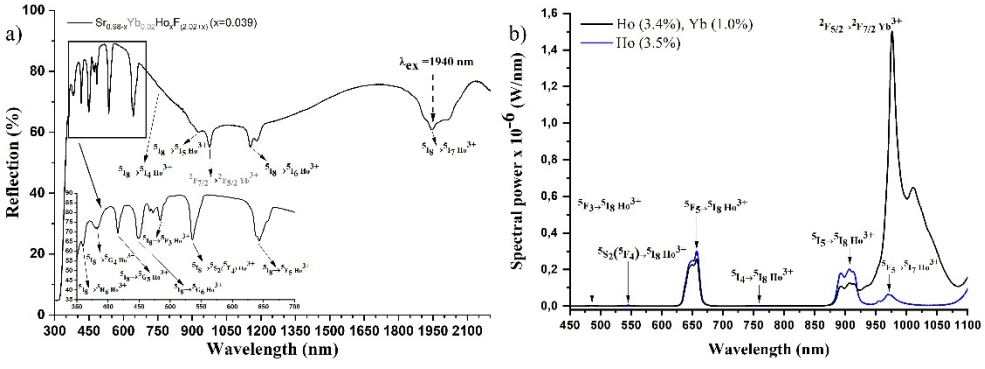

Fig. 1. The diffuse reflection spectra (a) of Ho^{3+} and Yb^{3+} ions. The UCL spectra of the SrF_2:Ho(3.5%) and SrF_2:Ho(3.4%),Yb(1.0%) phosphors (b).

The present results indicate that co-doping of SrF_2:Ho phosphors with Yb^{3+} ions enhances UCL and allows visualization of laser radiation in the 2.0 μm and 1.0 μm regions.

References

1. X. Liu, H. Chen, Y. Wang, Y. Si, H. Zhang, X. Li, Z. Zhang, B. Yan, S. Jiang, F. Wang, S. Weng, W. Xu, D. Zhao, J. Zhang, F. Zhang. Nat. Commun. **12**, 1, pp. 5662 (2021)
2. A. Ghazy, M. Safdar, M. Lastusaari, H. Savin, M. Karppinen. Sol. Energy Mater. Sol. Cells. **230**, pp. 111234 (2021)
3. H. Suo, Q. Zhu, X. Zhang, B. Chen, J. Chen, F. Wang. Mater. Today Phys., **21**, pp. 100520 (2021)
4. M. Wang, M. Li, M. Yang, X. Zhang, A. Yu, Y. Zhu, P. Qiu, C. Mao. Nano Res., **8**, 6, pp. 1800 (2015)
5. F. Auzel. Chem. Rev., **104**, 1, pp. 139 (2004)
6. A.A. Lyapin, S.V. Gushchin, S.V. Kuznetsov, P.A. Ryabochkina, A.S. Ermakov, V.Yu. Proydakova, V.V. Voronov, P.P. Fedorov, S.A. Artemov, A.D. Yapryntsev, V.K. Ivanov. Opt. Mater. Express., **8**, 7, pp. 1863 (2018)
7. A.N. Chabushkin, A.A. Lyapin, P.A. Ryabochkina, S.N. Ushakov, P.P. Fedorov. J. Lumin., **167**, pp. 120 (2015)

Fine structure of spectral lines in $YVO_4:Ho^{3+}$

Tatyana Igolkina[1,2], *Elena* Chukalina[1], *Sergei* Klimin[1,hhh], and *Marco* Bettinelli[3]

[1]Institute of Spectroscopy, Russian Academy of Sciences, 5, Fizicheskaya Str., Troitsk, Moscow, 108840, Russian Federation
[2]Moscow Institute of Physics and Technology (National Research University), Dolgoprudnyi, 141700, Russian Federation
[3]Dipartimento di Biotecnologie, University of Verona and INSTM, Strada Le Grazie 15, Verona 37134, Italy

Abstract. Single crystals of $YVO_4:Ho^{3+}$ were studied by means of high-resolution Fourier spectroscopy. A well-resolved hyperfine structure of the lines, due to the splitting of Γ_5 doublets, was found. The observed deformation splittings and spectral satallites evidence the presence of defects in the studied crystals and can be used for the control of the quality of the crystals.

Holmium doped yttrium vanadate, $YVO_4:Ho^{3+}$, has many possible applications; in particular, it is an active laser medium with a high quantum efficiency near 2 μm [1, 2]. YVO_4:*RE* crystals (*RE* is a rare earth ion) are also of interest for applications in the field of optical storage and data processing [3]. The successful implementation of optical quantum memory using hyperfine (HF) levels of the Nd^{3+} ion in YVO_4:Nd crystals was reported [4]. High-resolution spectroscopy makes it possible to register the fine structure of lines associated with both the hyperfine structure (HFS) and various deformations that occur in crystals during growth, which allows to control the quality of the crystal. Previously, HFS was observed in the optical spectra of $YPO_4:Ho^{3+}$ [5], isostructural to vanadate, for lines related to f-f transitions in the Ho^{3+} ion. In this work, we studied $YVO_4:Ho^{3+}$ (0.1 and 1 at.%) crystals by high-resolution Fourier spectroscopy in order to find the manifestations of HF and deformation splittings, as well as the features of the lineshapes related to *f-f* transitions in the Ho^{3+} ion.

Single crystals of $YVO_4:Ho^{3+}$ (0.1 and 1 at.%) were grown by the solution-melt method using $Pb_2V_2O_7$ flux. The absorption spectra were recorded on a Bruker IFS 125 HR Fourier spectrometer in a wide spectral region from 4000 to 12000 cm^{-1} and a temperature range from 4 to 300 K. A Cryomech ST 403 closed-loop cryostat and a Lake Shore Model 335 thermal controller were used to obtain and control low temperatures.

In the absorption spectra of $YVO_4:Ho^{3+}$, a well-resolved hyperfine structure of lines was found, due to the splitting of Γ_5 doublets, mainly by the magnetic dipole HF interaction, into 8 equidistant components, being twice degenerate in the projection of the nuclear spin. The nonequidistant nature of the HFS, the shape of the line wings, and the doublet structure of some lines are due to the manifestation of random deformations in crystals. Figure 1 shows two close lines with allowed hyperfine and deformation splittings. To explain the observed doublet structure of the lines, we used the model that we applied earlier for the isostructural compound $YPO_4:Pr^{3+}$ [6]. The result of such a modeling is also shown in Figure 1.

In addition, the occurrence of defects in crystals explains the presence of weak satellites situated near some main lines. The analysis of the dependence of the integral intensities of individual satellites and the main line on the holmium impurity concentration testifies in favor of the fact that defect centers are not associated with the process of incorporation of RE

[hhh]Corresponding author: klimin@isan.troitsk.ru

impurities into the crystal during its growth by the solution-melt method using a flux. This fact is confirmed by data from the literature [2, 3].

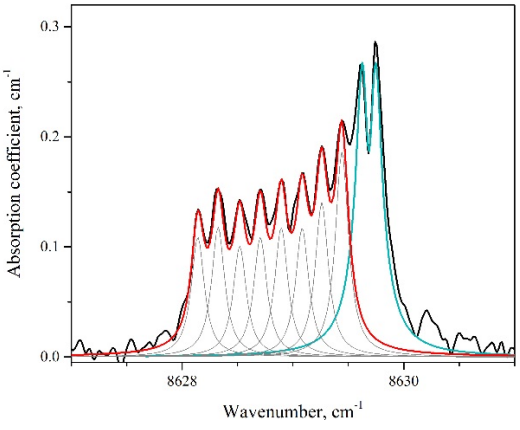

Fig. 1. Two absorption lines with a fine structure in the region of the $^5I_8 \rightarrow {}^5I_6$ transition in the Ho^{3+} ion in the $YVO_4:Ho^{3+}$ (0.1 at.%) crystal. T=20 K. Eight elementary contours describe the shape of the line with HFS. The doublet shape of the high-frequency line is described within the framework of the model proposed in [6].

The results obtained are of practical importance and can be used for laser applications, applications in the field of quantum information science, and quality control of crystal growth.

E. C., T. I., and S. K. are grateful for the financial support of the Ministry of Science and Higher Education of Russia under Grant No. 0039-2019-0004. M. B. thanks E. Viviani (Univ. Verona) for expert technical assistance.

References

1. S. Gołvab, P. Solarz, G. Dominiak-Dzik, T. Lukasiewicz, M. Świrkowicz, W. Ryba-Romanowski, Applied Physics B, **74**, 237 (2002)
2. A. Malinowska, E. Wierzbicka, M. Lefeld-Sosnowska, K. Wieteska, W. Wierzchowski, T. Lukasiewicz, M. Świrkowicz, W. Graeff, Acta Physica Polonica, A, **117**, 328 (2010)
3. S. Polosan, M. Bettinelli, T. Tsuboi, physica status solidi c, **4**, 1352 (2007)
4. R. Moncorgé, M. Velazquez, P. Goldner, O. Guillot-Noël, H.L. Xu, M. Nilsson, S. Kröll, E. Cavalli, M. Bettinelli, Journal of Physics: Condensed Matter, **17**, 6751 (2005)
5. M. Mazzera, R. Capelletti, A. Baraldi, E. Buffagni, N. Magnani, M. Bettinelli, Journal of Physics: Condensed Matter, **24**, 205501 (2012)
6. S.A. Klimin, E.P. Chukalina, K.N. Boldyrev, T.A. Igolkina, M.S. Radionov, M.C. Chou, M.N. Popova, Journal of Luminescence, **235**, 118003 (2021)

Synthesis and optical properties of Co doped γ-AlON

Aleksey V. Ishchenko[1,iii], *Nailya S.* Akhmadullina[2], *Ivan I.* Leonidov[3], *Vladimir P.* Sirotinkin[2], *Anton S.* Lysenkov[2], *Yuri F.* Kargin[2]

[1]Ural Federal University, NANOTECH Center, 620002 Yekaterinburg, Russia
[2]A.A. Baikov Institute of Metallurgy and Material Science, Russian Academy of Sciences, 119334 Moscow, Russia
[3]Institute of Solid State Chemistry, Ural Branch, Russian Academy of Sciences, 620990 Yekaterinburg, Russia

Abstract. The report describes a method for the synthesis of aluminum oxynitride AlON doped with a cobalt impurity. The features of the phase composition of the samples at different concentrations of cobalt have been studied. The optical characteristics are determined and pulsed cathodoluminescence spectra are measured. The emission of intrinsic and impurity defects was found. The optical band gap of AlON:Co was estimated.

Ceramic materials based on nitrides show high thermal, chemical and mechanical stability. This promotes their application in many technological areas, including mechanical engineering, aerospace, chemical and medical industries. Aluminum oxynitrides (AlON) are considered to be one of the most promising phosphor hosts [1]. Rare-earth metal ions are used to dope AlON to tune the physicomechanical and optical properties [2]. The limits of their solubility in AlON and other oxynitrides are known. Meanwhile, such data are not available for most of transition metals. We have systematically studied aluminum oxynitrides doped with 3d metal ions. The presented part of our research is focused on Co^{3+}-activated γ-AlON.

The samples of AlON:Co were synthesized by high-temperature annealing of cobalt-doped Al_2O_3 and AlN mixtures at 1750°C for 2 h under N_2 atmosphere. Co^{3+}-doped Al_2O_3 was obtained via modified sol-gel method from $Al(iPrO)_3$ with the addition of $Co(OAc)_4$ $4H_2O$. The cobalt content was 0.01, 0.05, 0.1, 0.2, 0.5, 1.0, 2.0, and 5.0 at.% (relative to aluminum). The diffraction patterns for all the samples show a set of peaks of the main phase identified as Al_5O_6N or γ-AlON. It is interesting to note that γ-AlON even with 0.01 at.% cobalt dopant does not contain corundum impurities. To overcome the formation of corundum during the synthesis of aluminum oxynitride magnesium is used as a rule in concentrations from 0.5 at.% up to 10 at.%. However, apparently cobalt can also be effective in this capacity. With the cobalt content of 1.0 at. % and more, metallic cobalt is identified in trace amounts. Therefore, the solubility limit of cobalt in aluminum oxynitride lies in the range of 0.5–1.0 at. % relative to aluminum.

To evaluate the optical properties of the Al_2O_3–AlN–CoO ternary system at the fixed Al_2O_3:AlN ratio of 2:1 and cobalt content of 0.01 to 5.0 at. % (relative to aluminum) we measured the absorption and pulsed cathodoluminescence spectra (PCL) of AlON:Co (Fig. 1). The absorption spectra exhibit a typical AlON band with a maximum at 256 nm and an edge of the fundamental absorption in the region below 230 nm. Estimation of the optical gap by the Tauc method from absorption spectra shows that the range of its values lies at 5.64–5.78 eV. A gradual increase in the gap width with the cobalt content is found at concentrations of 0.5–

[iii] Corresponding author: a-v-i@mail.ru

1 at.% (which correspond to the solubility limit of cobalt in AlON) and higher. Three broad luminescence bands with maxima at 485, 595, and 770 nm are observed in the PCL spectra, while the integrated luminescence intensity rapidly decreases with the increasing cobalt content (Fig. 1c). It can be concluded that the corresponding bands in the spectra are associated with intrinsic defects in AlON and with the presence of impurities, presumably Mn^{2+} and Fe^{2+} ions.

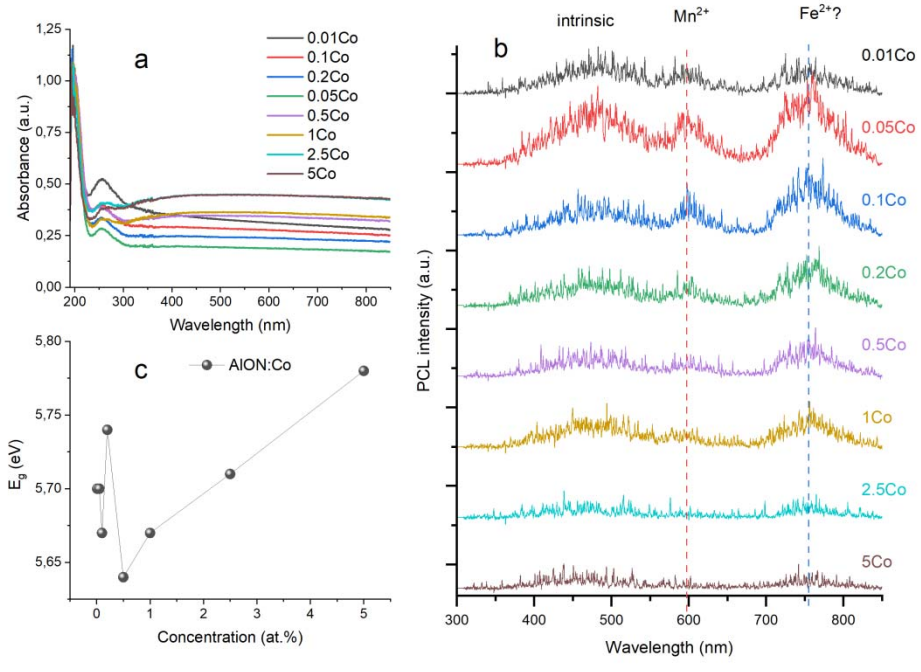

Fig. 1. Absorption (a) and PCL (b) spectra of AlON:Co samples with different Co concentration and variation of energy gap versus Co content (c)

The authors are grateful to the Russian Science Foundation for financial support of this work (project no. 22-23-00958).

References

1. Yu.F. Kargin, N.S. Akhmadullina, K.A. Solntsev, Inorg. Mat. **50** (13), 1325 (2014)
2. N.S. Akhmadullina, O.N. Shishilov, Yu.F. Kargin, Izv. Acad. Sciences. Ser. Chem. **5**, 825 (2020)

Spectroscopic study of the spin-reorientation transition in $ErCrO_3$ crystals

Artjoms Jablunovskis[1] and *Elena* Chukalina[2,jjj]

[1]Moscow Institute of Physics and Technology (National Research University), 141701 Dolgoprudny, Moscow region, Russia
[2]Institute of Spectroscopy, Russian Academy of Sciences, 108840 Troitsk, Moscow, Russia

Abstract. An analysis of the high-resolution absorption spectra in the region of the $^4I_{15/2} \rightarrow {}^4I_{13/2,11/2}$ transitions in Er^{3+} ions at temperatures near the spin-reorientation transition temperature $T_{SR} = 9.5 \pm 0.5$ K allowed detecting the coexistence of low- and high-temperature phases in the $ErCrO_3$ crystal at helium temperatures for the first time.

Orthochromites $RCrO_3$ (R = Y, La – Lu) with a distorted perovskite structure are assigned to the family of multiferroics. Orthochromites can be used to create magnetic cooling devices, as solid fuel cells, negative temperature coefficient thermistors, photovoltaic materials, and catalysts [1]. In connection with possible practical applications, information is needed on changes in the crystal and magnetic structure during phase transitions in $RCrO_3$. Such information can be obtained from the analysis of the temperature dependence of the shape of spectral lines related to *f-f* transitions in rare-earth ions R^{3+} (R = Ce – Yb). According to magnetic studies [2], in the series of $RCrO_3$ (R=Dy, Nd, Tb, Er) compounds, erbium orthochromite has the most pronounced anisotropic properties. At the Neel temperature $T_N = 133$ K, the subsystem of Cr^{3+} ions undergo antiferromagnetic ordering into the Γ_4 spin configuration (in Berto's notation). A further decrease in temperature leads to a spin-reorientation transition to the antiferromagnetic configuration Γ_1 at $T_{SR} = 10$ K [2].

Previously, spectroscopic studies of oriented $ErCrO_3$ crystals were carried out in the near infrared (IR) and visible regions of the spectrum [3]. The data in the literature on the energy structure of the ground $^4I_{15/2}$ multiplet of the Er^{3+} ion is incomplete, and for the $^4I_{13/2,\,11/2}$ multiplets they are completely absent.

In this work, we studied the high-resolution absorption spectra of $ErCrO_3$ crystals in the mid-IR range in order to obtain crystal-field (CF) levels of the ground and IR multiplets of the Er^{3+} ion, as well as for revealing the features of the spin-reorientation phase transition.

The studied crystals were grown in the group of M. M. Lukina in the 1980s at the Faculty of Geology of the Lomonosov Moscow State University. The transmission spectra were registered on a Bruker IFS 125HR Fourier spectrometer in the spectral region 5000 – 11000 cm^{-1} with a resolution up to 0.045 cm^{-1}. The sample was fixed in a Cryomech ST403 closed-cycle cryostat. The measurements were carried out in the temperature range from 5 to 300 K.

From the spectra analysis, precise position of CF levels of the $^4I_{15/2,\,13/2,\,11/2}$ multiplets of the Er^{3+} ion (Kramers doublets) in the paramagnetic $ErCrO_3$ were determined. The study of the temperature dependence of the splittings of Kramers doublets made it possible to determine the temperatures of antiferromagnetic ordering $T_N = 133$ K and of the spin-reorientation transition $T_{SR} = 9.5 \pm 0.5$ K. At the temperature T_{SR}, there is a sharp change in the character of spectral line splitting (Fig. 1a).

[jjj] Corresponding author: echukalina@isan.troitsk.ru

Let us consider in more detail the features of the splitting of the absorption line corresponding to the transition from the ground state to the second CF level of the $^4I_{13/2}$ multiplet of the Er^{3+} ion at three temperatures (Fig. 1a). The spectrum at 7.5 K is a superposition of the spectra at temperatures above (12 K) and below (4.5 K) T_{SR}, which is characteristic of a first-order spin-reorientation transition. The values of the exchange splittings of the ground Kramers doublet $^4I_{15/2}(1)$ of the Er^{3+} ion in two spin configurations Γ_4 and Γ_1 of $ErCrO_3$ are 8.0±0.5 cm^{-1} and 9.5±0.5 cm^{-1}, respectively.

The low-temperature spectrum should reflect the Γ_1 configuration in the $ErCrO_3$ crystal. However, the absorption line $^4I_{15/2}(1)\rightarrow{}^4I_{13/2}(2)$ at T = 4.5 K, shown in Fig. 1b has a complex shape, which is described by at least eight elementary contours. Four of them correspond to the scheme of splitting of the ground and excited states at temperatures above T_{SR} (dashed lines), the second four components are described by the values of exchange splittings at temperatures below T_{SR} (solid line) (Fig. 1b). This fact testifies in favor of the assumption about the coexistence of two magnetic configurations (Γ_4 and Γ_1) at temperatures below T_{SR}, which has not been observed before, as far as we know.

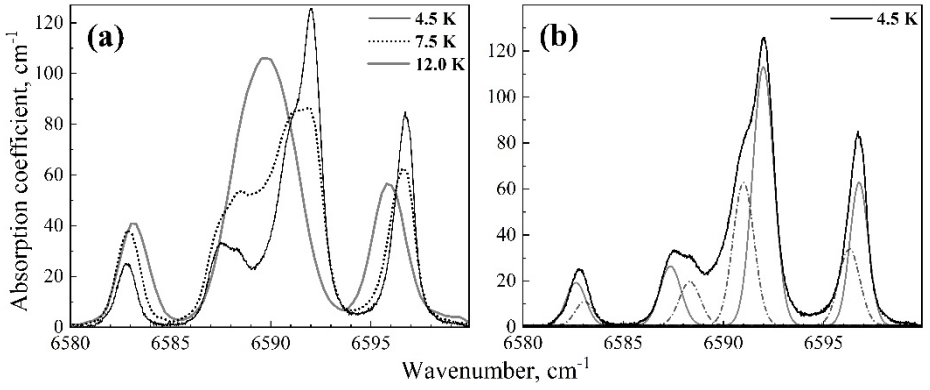

Fig. 1. Absorption line in the region of the $^4I_{15/2}(1)\rightarrow{}^4I_{13/2}(2)$ transition in the Er^{3+} ion in the spectra of $ErCrO_3$ crystal at three temperatures (a), and at T = 4.5 K together with elementary contours simulating the complex shape of the line (b).

References

1. Y. Zhu, J. Xia, S. Wu et. al., iScience, **25**, 104111 (2022)
2. L.H. Yin, J. Yang, P. Tong et. al., J. Mater. Chem. C., **4**, 11198 (2016)
3. A. Hasson, R.M. Hornreich, Y. Komet, B.M. Wanklyn, I. Jaeger, Phys. Rev. B, **12**, 5051 (1975)

Spectroscopic and structural properties of natural turkestanite crystals

Ekaterina Kaneva[1,kkk], *Tatiana* Radomskaya[1], *Olga* Belozerova[1], and *Roman* Shendrik[1]

[1]Vinogradov Institute of Geochemistry SB RAS, Irkutsk, Russia

Abstract. The results of a combined EPMA, SCXRD, and luminescence study of tetragonal crystals of turkestanite from the Dara-i-Pioz alkaline deposit (Tadjikistan) are reported. Major element analysis provided (wt%): K_2O 4.13(6), CaO 8.1(1), Na_2O 2.3(1), ThO_2 25.8(4), UO_2 3.6(4) and SiO_2 55.9(1). For the first time the structure refinement from natural turkestanite single-crystal is presented. The luminescence of the uranyl ion UO_2^+ is observed in turkestanite. In the excitation spectrum the bands corresponding to a charge transfer transition from the 2p states of the ligand to the 5f state of uranium were found.

Turkestanite, $Th(Ca,Na)_2(K,\square)Si_8O_{20}$ (where $\square$ – vacancy), is a single-layer sheet-silicate, named after the discovery locality (the Turkestan Ridge). It belongs to the ekanite group with general formula $AB_2CSi_8O_{20}$, where A = Th (ekanite, turkestanite, steacyite), U (arapovite) or La (iraqite); B = Ca (ekanite, iraqite), Ca/Na (turkestanite, arapovite) or Na/Ca (steacyite), and C = □ (ekanite) or K/□ (turkestanite, steacyite, arapovite, iraqite). Turkestanite was described for the first time by [1]. [2] carried out a Rietveld structure refinement on the powder and confirmed the space group *P*4/*mcc*. Recently [3] reported single-crystal structural data for synthesized under hydrothermal conditions Th and U compounds isostructural to turkestanite.

In this work, a detailed crystal chemical and spectroscopic investigation using a multi-analytical approach was carried out for the first time on a natural turkestanite specimen from the Dara-i-Pioz alkaline massif (Tajikistan). A combination of electron probe microanalysis (EPMA; Superprobe JEOL JXA-8230 instrument, WDS mode), single-crystal X ray diffraction (SCXRD; AXS D8 VENTURE automated diffractometer, MoKα radiation), and luminescence measurements (Perkin Elmer LS-55 spectrofluorimeter) was employed.

From single-crystal structural refinement, turkestanite resulted tetragonal, space group *P*4/*mcc*, a = 7.5708(3), c = 14.730(1), V = 844.27(6) Å^3, Z = 2.

In the turkestanite crystal structure the symmetrically independent crystallographic atomic sites are: the tetrahedrally coordinated Si; 8-coordinated *A* and *B*; and the extra-framework *C* site. The formula shows the *A* site filled mainly by Th, with minor U. The *B* site is occupied by Ca and minor amount of Na. The *C* site contains K, and it is not filled completely. The following crystal-chemical formula can be proposed for the studied turkestanite from the Dara-i-Pioz massif (calculated on the basis of 8 Si apfu): $(K_{0.75}\square_{0.25})(Ca_{1.24}Na_{0.65})(Th_{0.84}U_{0.12})Si_8O_{19.72}(OH)_{0.28}$. The formula is balanced on the basis of $O^{2-} \leftrightarrow OH^-$ substitution mechanism. The O3 site bond valence value (1.89 vu) is compatible with this replacement. It should be noted that the presence of water molecules in the crystal structure of turkestanite was reported only once by [1]. In this work, no clear evidence of the presence of water molecules was found by means of structural refinement and IR spectroscopy. Three types of channels may be distinguished inside the crystal structure of turkestanite.

[kkk] Corresponding author: kev604@mail.ru

Channel I and II is extended along the *a*- and *b*-axis and delimited by both tetrahedra and polyhedra and by four-membered tetrahedral rings, respectively. Channel III is formed by tetrahedral rings and extends parallel to the *c*-axis. Effective channel widths of the Channel I, II and III are 2.12 × 1.48 Å, 1.23 × 0.79 Å, and 1.06 × 1.06 Å, respectively. Despite the channels occurring, turkestanite cannot be considered as microporous; however, the channel I of turkestanite is large enough to theoretically contain guest atoms, for instance, water molecules. Similar feature have been identified also in tubular agrellite from Dara-i-Pioz [4].

Lighter elements in the actinide series often bind with two oxygen anions forming actynil ions. The uranyl ion UO_2^+ luminescence with maximum at 19100 cm^{-1} is observed in turkestanite (Fig. 1). This band has vibrational structure attributed to O–U–O symmetrical stretching mode 740 cm^{-1}. In the excitation spectrum the bands located at 27200, 29200, 34500, 35900 cm^{-1} are found. These bands correspond to charge transfer transition from 2p states of the ligand to 5f state of uranium.

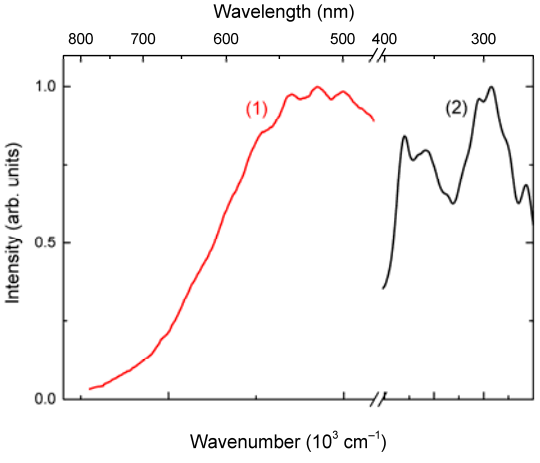

Fig. 1. Luminescence under 380 nm excitation (1) and excitation spectra monitored at 510 nm (2) of turkestanite.

This research was supported by the Russian Science Foundation (project no. 22-27-00183).

References

1. L.A. Pautov, A.A. Agakhanov, E.V. Sokolova, Yu.K. Kabalov. Proc. Russ. Min. Soc. 126, 6, 45 (1997)
2. Yu.K. Kabalov, E.V. Sokolova, L.A. Pautov, J. Schneider. Crystallogr. Rep. 43, 4, 584 (1998)
3. G.B. Jin, L. Soderholm. J. Solid State Chem. 221, 405 (2015)
4. E. Kaneva, A. Bogdanov, R. Shendrik. Sci. Rep. 10, 15569 (2020)

Energy transfer and thermoluminescence in $LiMgPO_4$:Re

Dina Kellerman[1,III], *Michael* Kalinkin[1], *Dmitry* Akulov[1], *Nadezhda* Medvedeva[1], *Rinat* Abashev[1,2], and *Alexander* Surdo[1,2]

[1]Institute of Solid State Chemistry, UB RAS, 620990 Ekaterinburg, Russia
[2]Institute of Metal Physics, UB RAS, 620137 Ekaterinburg, Russia

Abstract. Olivine-type phosphate $LiMgPO_4$ doped with rare-earth elements is currently considered as a new dosimetric material suitable for both OSL and TSL applications and able to compete with top commercial detectors. In this work, we present the results of combined experimental and *ab initio* studies. It has been established that all rare earths can be divided into two groups. Such dopants as Eu, Sm, Gd, Tb, Dy, Tm manifest themselves in TSL spectra by the appearance of a characteristic set of lines reflecting the luminescence of rare-earth elements as a result of *f-f* transitions from an excited state to a lower one, while Pr, Ce, Er, Ho, Nd only greatly enhance the two-humped TSL spectra of the phosphate matrix. The observed effect was attributed to non-radiative energy transfer from some RE^{3+} ions to matrix defects.

1 Introduction

Nowadays, lithium-magnesium phosphate with the olivine structure is of special importance for radiation dosimetry applications. $LiMgPO_4$ turned out to be suitable for both optically (OSL) and thermally (TSL) stimulated luminescence [1-2]. Although pure $LiMgPO_4$ is capable of accumulating energy under ionizing irradiation and retaining it for a long time, the presence of activator ions (especially lanthanides) in its structure is required to significantly enhance the dosimetric response. In most works, terbium was chosen as an activator ion, more often in combination with boron [3-4]. In this work, we have synthesized $LiMgPO_4$: RE (RE – trivalent rare-earth ions from Ce^{3+} to Yb^{3+}), considered the thermoluminescence of doped phosphates and proposed a model explaining the regularities found.

2 Results

Thermoluminescence in pure $LiMgPO_4$ is due to the presence of set of defects whose energy levels are in the forbidden gap. These defects act as traps for electrons and holes, resulting in the TSL glow curve with five overlapping peaks in the temperature range of 300-600 K. The most probable traps are oxygen vacancies located at three crystallographically nonequivalent positions (O1, O2, O3). They can be either neutral or once or twice ionized. In this work, it was established that all rare-earth elements (with the exception of Yb) significantly enhance thermoluminescence of $LiMgPO_4$ and can serve as a source of additional hole or electron traps. We determined the spectral composition of the thermoluminescence and showed the presence of two broad lines at 360 nm and 650 nm in the TSL spectrum of the phosphate matrix. All rare-earths dopants in $LiMgPO_4$ can be divided into two groups. Such rare-earths as Eu, Sm, Gd, Tb, Dy, Tm manifest themselves in TSL spectra by the appearance of a characteristic set

[III] Corresponding author: dina.kellerman@yandex.ru

of lines reflecting the luminescence of rare-earth elements as a result of *f-f* transitions from an excited state to a lower one, while Pr, Ce, Er, Ho, Nd only greatly enhance the two-humped TSL spectra of the $LiMgPO_4$ (Fig.1). The observed effect was attributed to non-radiative energy transfer from RE^{3+} ions to matrix defects. This process can take place if the energy of RE upper emission levels is close to the energy of the defects. Such defects are probably ionized vacancies located at O1 position.

Regardless of the dopant, all irradiated samples exhibit intensified thermoluminescence. The best and almost similar characteristics are demonstrated by $LiMgPO_4$: Er and $LiMgPO_4$: Tb

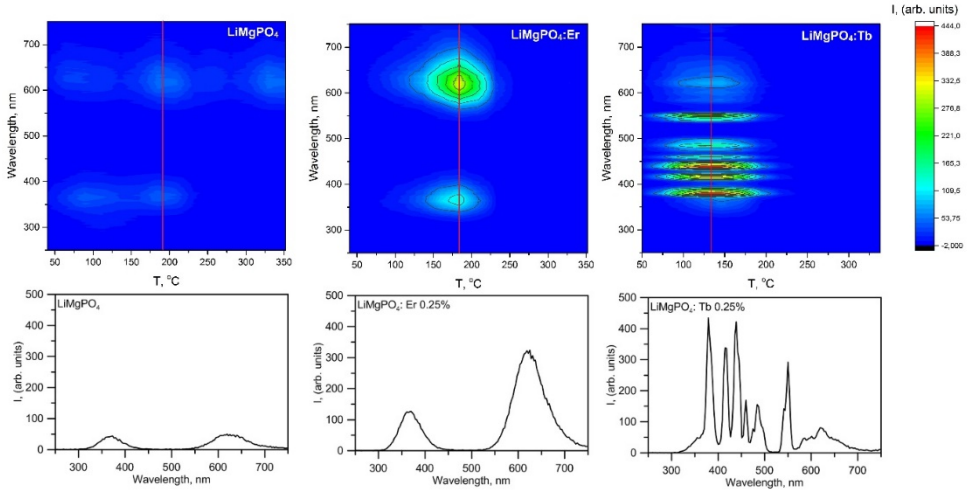

even though terbium acts as a TSL activator and erbium is a sensitizer, enhancing the stimulated luminescence of the matrix.

Fig. 1. Contour plots of TSL spectra recorded for $LiMgPO_4$, $LiMgPO_4$: Er and $LiMgPO_4$: Tb and cross sections at the temperatures of peak intensity (indicated by the lines).

The authors gratefully acknowledge the financial support from the Russian Science Foundation (Grant No. 20-13-00121).

References

1. B. Dhabekar, S.N. Menon, E. A. Raja, A.K. Bakshi, A.K. Singh, M.P. Chougaonkar, Y.S. Mayya, Nucl. Instrum. Methods Phys. B, **269** 1844 (2011)
2. C.B. Palan, N.S. Bajaj, A. Soni, S.K. Omanwar, Bull. Mater. Sci., **39** 1157 (2016)
3. H. Tang, L. Lin, C. Zhang, Q. Tang, Inorg. Chem., **58** 9698 (2019)
4. W. Gieszczyk, P. Bilski, A. Mrozik, M. Kłosowski, B. Marczewska, A. Sas-Bieniarz, M. Perzanowski, T. Zorenko, Y. Zorenko, Materials, **13** 2032 (2020

Modification of borosilicate glasses activated with rare earth ions by electron beam irradiation

Vlad A. Kravets [1,mmm], *Ekaterina* V. Dementeva[1], *Maria* V. Zamoryanskaya[1]

[1] Ioffe Institute, 26 Politekhnicheskaya st., St Petersburg 194021, Russian Federation

Abstract. The work was aimed at studying the phenomena arising in Eu-activated borosilicate glasses upon irradiation with an electron beam. It has been demonstrated that both an increase in the luminescence yield of glasses and a decrease are possible depending on the power density and irradiation time. The heating temperature of the samples was estimated at different electron beam irradiation densities. It is shown that the processes are radiation stimulated. When a sample is irradiated with an electron beam with a high power density, a change in the surface topography and composition is observed. In this work, changes in the efficiency of activator excitation capture before and after modification by an electron beam were determined.

Currently, there is a search for radiation-resistant amorphous scintillators, including those for the encapsulation of radioactive elements, from the surface of which radioactive radiation comes out. When irradiated with an electron beam, dynamic processes occur in the samples, which can lead to both reversible (electron capture by deep levels) and irreversible (formation and annealing of defects) changes in the solid. These processes can lead to a significant change in the luminescence yield depending on the irradiation conditions.

The aim of this work is to study the processes of modification of REI-activated borosilicate glasses by an electron beam and to study the cause of the change in the luminescence yield in borosilicate glasses after modification. Part of the work is aimed at studying the radiation resistance of activated glass. Two systems of borosilicate glass with different compositions were chosen as samples. First, the well-known borosilicate system close to SON 68 [3] was chosen. SON 68 glasses are chemically and thermally resistant and, according to their characteristics, are considered suitable for the immobilization of nuclear waste. As the second system, a new multicomponent borosilicate glass with bismuth was synthesized. Such a system was chosen because heavy bismuth glasses have a high density and refractive index, which makes them a promising matrix for activation by rare earth ions [4]. Trivalent europium, which has intense luminescence in the red optical range, was chosen as the REI activator in glasses. Eu can also be used as a luminescent probe, the spectrum of which is extremely sensitive to structural changes in doped materials. The homogeneity of the composition and luminescent properties of the samples was studied, and the concentration dependences of the luminescence intensity on the content of the activator were obtained. The glasses were modified by an electron beam with different power densities. It has been demonstrated that both an increase in the luminescence yield of glasses and a decrease are possible depending on the power density and irradiation time. The heating temperature of the samples was estimated at different electron beam irradiation densities. It is shown that the processes are radiation-stimulated. When a sample is irradiated with an electron beam with a high power density, a change in the surface topography and composition is observed. In the work, the change in the efficiency of excitation capture by activators before and after irradiation with an electron beam according to the method proposed in [5] was

[mmm] Corresponding author: author@email.org

determined, and the nature of the change in the luminescence yield of the activator after glass modification was explained. The author is grateful to Starukhin A.N. for help in obtaining PL spectra, Popova T.B. for the study of samples by the EPMA method, Nashchekin A.M. for the study of samples by the SEM method.

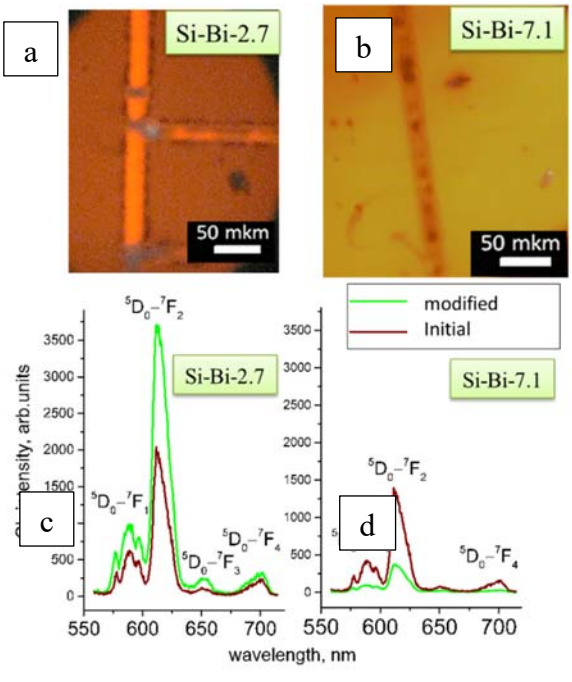

Fig. 1. Cathodoluminescence microscopy images of modified areas of samples Si-Bi-2.7 (a) and Si-Bi-7.1 (b). Cathodoluminescence spectra of samples samples Si-Bi-2.7 (c) and Si-Bi-7.1 (d) obtained from the modified and initial area.

References

1. K.N. Orekhova, R. Tomala, D. Hreniak, et al, Opt. Mater., 74, 170–175 (2016).
2. A. K. Bedyal, et al, Nucl. Instrum. Methods Phys. Res. B: Beam Interactions with Materials and Atoms, 351, 27–34 (2015).
3. M.I. Iojovan, & W.E. Lee, Metall. Mater. Trans., 837–851 (2010).
4. Egorysheva A.V., Volodin V.D., Skorikov V.M., Yurkov G.Yu., Sorokin N.I., Inorganic Materials. T. 46. № 4. C. 434-438 (2010)
5. M.V. Zamoryanskaya, A.N. Trofimov Opt. Spectrosc., 115, 1 79–85 (2013).

Energy transfer processes in $Zn_xCd_{1-x}WO_4$ solid solutions

Nataliya Krutyak[1,nnn], *Dmitry* Spassky[2], and *Boris* Zadneprovski[3]

[1]Physics Department, M.V. Lomonosov Moscow State University, 119991 Leninskie Gory 1, Moscow, Russia
[2]Skobeltsyn Institute of Nuclear Physics, M.V. Lomonosov Moscow State University, 119991 Leninskie Gory 1, Moscow, Russia
[3]All-Russian Research Institute for Synthesis of Materials, Institutskaya str. 1, 601600, Alexandrov, Russia

Abstract. A complete series of $Zn_xCd_{1-x}WO_4$ solid solutions were synthesized by spontaneous crystallization technique. Powder X-ray diffraction study revealed that homogeneous solid solutions with wolframite structure were formed at $0 \le x \le 1$. The luminescence and excitation spectra of $Zn_xCd_{1-x}WO_4$ crystals have been measured under UV excitation in a wide temperature region. The analysis of the energy transfer processes on the basis of presented experimental data is performed.

Solid solutions of intrinsic scintillating materials with excitonic emission show scintillation yield higher than that in their constituents due to the changes in energy transfer processess, induced by structural disorder in mixed crystals [1]. Alkali-earth and transition metal tungstates are of particular interest as scintillating materials due to their attractive luminescent properties [2]. Tungstates-based solid solutions can combine and improve the scintillation and luminescence properties of their constituents. Since the values of the lattice parameters and cations ionic radii are close in $CdWO_4$ and $ZnWO_4$, these compounds can form a complete set of solid solutions [3, 4]. Optical measurements revealed that the $Zn_xCd_{1-x}WO_4$ crystals had a high optical transmittance of about 65% in the range of 350–600 nm [4]. However, the luminescent properties of zinc-cadmium tungstates crystals have been poorly studied so far. Here, we present the results of the study of the effect of cationic substitution on the energy transfer mechanism of $Zn_xCd_{1-x}WO_4$ solid solutions.

A series of $Zn_xCd_{1-x}WO_4$ (x = 0–1) crystals were obtained by spontaneous crystallization from a solution of ZnO, CdO and WO_3 oxides in a NaCl melt. According to XRD analysis, all samples are characterized by a single phase of wolframite. Emission and luminescence excitation spectra, as well as temperature dependences of the luminescence were studied in the temperature range 77–500 K using a laboratory setup based on a LOT-Oriel MS-257 spectrograph.

The X-ray fluorescence technique was used for determining the actual Zn/Cd ratios in the mixed crystals. The results from a single crystals of cross-section of around 0.5 mm are in good agreement with the ratios predetermined in the melt.

It was found that all $Zn_xCd_{1-x}WO_4$ crystals are characterized by intrinsic luminescence associated with the radiative decay of self-trapped excitons (STE) on WO_6 complexes. The broadening of the luminescence spectra is more pronounced for mixed compositions that can be attributed to the partial structural disorder and the presence of an additional band of defect-related luminescence. The fit of luminescence band at 490 nm with two Gaussian functions

[nnn] Corresponding author: krutyakn@yahoo.com

also implies its non-elementary origin and demonstrates the contribution of the component peaking at 564 nm in each spectrum. The redistribution of both components in the luminescence spectrum depends on the *x* value in the $Zn_xCd_{1-x}WO_4$ crystals.

In the luminescence excitation spectra of the crystals, a low-energy shift of the fundamental absorption edge was observed with the increase of zinc content. A similar linear dependence of the threshold shifts in the excitation spectra of STE luminescence on the concentration of the substitutional cation also took place for $Zn_xMg_{1-x}WO_4$ mixed crystals [5]. The threshold of the excitation spectrum is shown to shift to the low-energy region with the temperature increase due to the increase of electron phonon interaction rate. Emission intensity rapidly drops at higher excitation energies thus demonstrating low energy transfer efficiency from the separated electron- hole pairs to the emission centers.

Temperature dependences of intrinsic luminescence intensity (λ_{ex} = 290 nm) have been obtained in temperature region 80-500 K. The decrease of emission intensity at T > 250 K relates to intraband temperature quenching of luminescence. A linear dependence of the activation energy of the thermal quenching process on the concentration of substitutional cations is demonstrated. TSL excitation spectra allow determining the threshold for the formation of separated charge carriers in the studied crystals. An analysis of the TSL excitation spectrum for $CdWO_4$ allowed to estimate the energy E_{e-h} required to creation of separated electrons and holes, which is 4.6 eV.

This work was supported by the Russian Science Foundation under grant 21-12-00219.

References

1. A.V. Gektin, A.N. Belsky, and A.N. Vasil'ev, IEEE TRANSACTIONS ON NUCLEAR SCIENCE, 61, 1 (2014)
2. P. Lecoq, A. Gektin, M. Korzhik, Inorganic Scintillators for Detector Systems, Springer International Publishing Switzerland (2017)
3. M.A. Dahlborg, G.Svensson, Acta Chemica Scandinavica, **53**, 12 (1999)
4. J. Zhang, J. Pan, J. Yin, J. Wang, J. Pan, H. Chen, R. Mao, CrystEngComm., **17**, 18 (2015)
5. N. Krutyak, V. Nagirnyi, D. Spassky, I. Tupitsyna, A. Dubovik, A. Belsky, Radiat. Meas., **90** (2016)

Laser spectroscopy of europium molybdate epitaxial films on $SrTiO_3$ (001) substrates

Alexey Kulinkin[1,ooo], *Artem* Arzhanov[2], *Konstantin* Magaryan[3], *Alexander* Korovin[1], *Danila* Kuzin[1], *Yilin* Wang[4], *Ling* Huan[4,5], *Maria* Yagovkina[1], *Vladimir* Sakharov[1], *Andrey* Naumov[2,3], *Alexander* Smirnov[1], and *Nikolai* Sokolov[1]

[1]Ioffe Institute RAS, St. Petersburg, 194021, Russia
[2]Moscow Pedagogical State University, Moscow, 119435, Russia
[3]Institute of Spectroscopy RAS, Moscow, 108840, Russia
[4]Institute of Advanced Materials, Nanjing Tech University, Nanjing, 211816, China
[5]College of Chemistry, Xinjiang University, Urumqi, 830046, China

Abstract. Submicron europium molybdate layers have been grown on $SrTiO_3$(001) substrates by laser molecular beam epitaxy. Electron and X-ray diffraction measurements of the films grown in optimized growth conditions revealed their epitaxial ordering and tetragonal crystal structure with c-axis normal to the substrate surface. Optical properties of the films have been explored using laser spectroscopy with tunable dye laser. These studies confirmed single phase nature of the best films and well-pronounced difference between Eu^{3+} spectra observed in this work and earlier reported spectra for $Eu_2(MoO_4)_3$.

Europium molybdates are interesting materials system because variability of crystal structures and unique optical properties of Eu ions. Structure and optical properties of monoclinic and orthorhombic phases of $Eu_2(MoO_4)_3$ are relatively well studied, see e.g. [1]. However there is only few studies of europium molybdate tetragonal phase. In early work [2], it was reported on synthesis and characterization of Eu_xMoO_4 crystalline powders (x=0.67-1.0) with tetragonal scheelite-type structure. To our knowledge, europium ion photoluminescence (PL) in these compounds was not studied yet. In this work, we show possibility of growth of epitaxial europium molybdate films on $SrTiO_3$(001) substrates by laser molecular beam epitaxy and study of Eu^{3+} photoluminescence by laser spectroscopy.

Europium molybdate films were grown on $SrTiO_3$(001) substrates by ablation with excimer laser of α-$Eu_2(MoO_4)_3$ ceramic target. The substrate temperature was in the range of 400–800 °C and the thickness of the films was 300–500 nm. Growth process was *in situ* monitored by reflection high-energy electron diffraction (RHEED). It was found that RHEED patterns of the films grown at optimized substrate temperature and oxygen pressure (P_{O2}=0.1 mbar) demonstrate well-pronounced streaky RHEED pattern at grazing E-beam incidence angle, which indicated epitaxial growth of the film with smooth surface, Fig.1a. Further analysis of RHEED patterns and their modelling resulted in conclusion that the crystal lattice of the film has tetragonal symmetry and c-axis of the cell is normal to the substrate surface. High resolution X-ray diffraction measurements showed the dominance of single crystal phase and let us to find the interlayer spacing in the film d=11.508 Å. Medium energy ion scattering measurements showed that the Eu/Mo ratio in the films grown at P_{O2}=0.1 mbar is about 0.85. Interestingly, the microcrystals synthesized in [2] at this Eu/Mo ratio showed tetragonal scheelite-type crystal structure.

ooo Corresponding author: alexey.kulinkin@mail.ioffe.ru

Spectroscopy measurements were carried out using confocal microscope-spectrometer setup [3] based on Coherent Radiation CR-699 tunable dye laser for selective excitation of Eu^{3+} photoluminescence and SOL Instruments grating spectrometer for PL analysis.

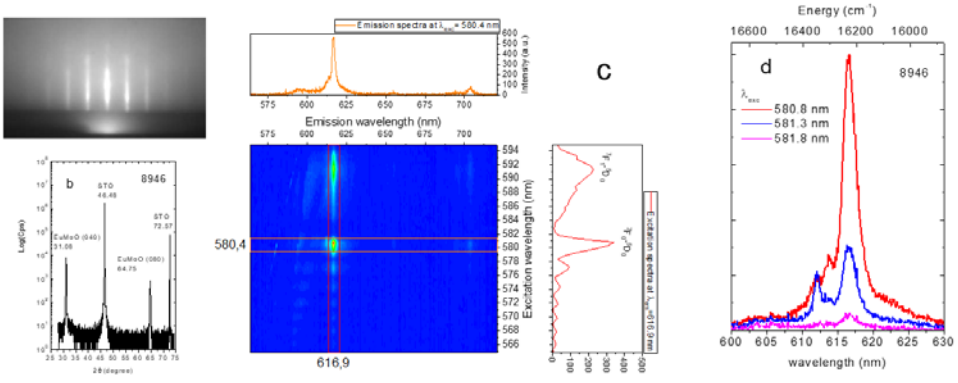

Fig. 1. Structure and Eu^{3+} PL spectra of #8946: a) RHEED pattern; b) XRD - ϑ-2ϑ curve; c) EEM spectrum for excitation in the region of the $^5D_0$-$^7F_0$ and $^5D_0$-$^7F_1$ transitions and PL caused by $^5D_0$-$^7F_2$ transitions; d) PL spectra in the region of $^5D_0$-$^7F_2$ transitions at different excitation wavelength λ_{exc}.

Fig. 1c shows Excitation-Emission Matrix (EEM) spectrum for #8946 sample, structural characteristics of which are presented in Figs. 1a,b. One can see that strong PL line with maximum at 616.9 nm dominates in the emission spectra at dye laser excitation in the range of 566-594 nm. This line originates from allowed electrodipole $^5D_0$-$^7F_2$ transitions in Eu^{3+} ions. Maximum of its intensity was observed at the wavelength of the laser 580.4 nm corresponding to $^5D_0$-$^7F_0$ transition. Relatively broad asymmetric band at 582-594 nm in the excitation spectrum shown at the right panel of Fig. 1c is due to the magnetodipole $^5D_0$-$^7F_1$ transitions. Fig. 1d shows that excitation at λ_{exc}=581.3 nm results in drastic change of PL spectra shape: in addition to the main PL line at 616.9 nm more narrow emission line at 612.0 nm appears. At this λ_{exc} the PL spectrum (blue line in Fig. 1d) is very similar to the PL spectrum of Eu^{3+} ion in the site with local S_4 symmetry observed in $SrWO_4$:Eu with scheelite-type structure [4].

The work was supported by the Russian Foundation for Basic Research (grant GFEN_a 21-52-53029) and partially supported by the National Science Foundation of China for Basic Research (grant 22111530015). A.A., K.M., and A.N. are members of the Leading Scientific School of the Russian Federation (grant of the President of the Russian Federation NSh-776.2022.1.2).

References

1. V.V. Atuchin et al., J. Phys. Chem. C **118**, 15404 (2014)
2. E. Banks, M. Nemiroff, Inorg. Chem. **13**, 2715 (1974)
3. I.Yu. Eremchev, M.Yu. Eremchev, A.V. Naumov, Phys. Usp. 62, 294 (2019)
4. G. Jia, C. Wang, S. Xu, J. Phys. Chem. C 114, 17905 (2010)

Li/Zn ratio effect on manganese spectral properties in germanate glass-ceramics

Ekaterina Kulpina[1,ppp], *Anastasiia* Babkina[1], and *Ksenia* Zyryanova[1]

[1]ITMO University, 199034, 4 Birzhevaya Line, Saint Petersburg, Russia

Abstract. A series of lithium-zinc-germanate glass-ceramics doped with manganese ions was synthesized. The simultaneous presence of Mn^{4+} ions with red luminescence in the region of 670 nm and Mn^{2+} ions with long persistent green luminescence at 540 nm was found, and the ratio between the intensities of different luminescence bands is determined by the ratio of Li_2O and ZnO in the glass composition. The maximum quantum yield for red luminescence was 60%, for green luminescence – 21%.

1 Introduction

Currently, the development of glass-ceramic phosphors based on transition metal ions as an alternative to expensive rare-earth ions is an urgent topic. Mn^{4+} ions are actively used to create phosphors in the red region of the spectrum. However, when developing glass-ceramic materials activated by manganese ions, the problem arises of reducing manganese ions in the matrix to the 2+ or 3+ state, which are more stable. The most promising in terms of stabilization of the tetravalent state of manganese is the germanate matrix, since the ionic radii of Ge^{4+} and Mn^{4+} are quite close, and germanium ions are often located in the center of a structure of the GeO_6 type [1]. When adding zinc to the composition of glass-ceramic germanate materials, it is also possible to obtain an intense green phosphorescence of Mn^{2+} ions, which replace zinc ions in the crystal structure [2]. Thus, by varying the composition of the surrounding matrix, it is possible to change the position of the maximum of the luminescence band of manganese ions over a wide range.

2 Materials and methods

The object of study in the present work was a series of lithium-zinc-germanate glasses of the composition (30-x) Li_2O – x ZnO – 70 GeO_2, doped with 0.1 mol.% MnO_2. Glass was synthesized in a Gero laboratory high-temperature furnace in corundum crucibles at a temperature of 1250°C for 30 minutes. The glass transition and crystallization peak temperatures of some compositions were determined using a Netzsch STA 449F1 Jupiter differential scanning calorimeter. The synthesis of glass-ceramics was carried out via single-stage heat treatment inducing homogeneous crystallization followed by interfacial-controlled growth.

PLE and PL spectra were recorded by LS-55 spectrofluorimeter (Perkin Elmer) in the range of 200–800 nm. The absolute PL quantum yield was measured on an Absolute PL Quantum Yield Measurement System (Hamamatsu). The luminescence lifetime was obtained using an LS-55 spectrofluorimeter by recording luminescence spectra with different time delays after

[ppp] Corresponding author: katrinakulpina@yandex.ru

the excitation pulse and subsequent approximation of the experimental data by a two-exponential function.

3 Results

The results of the DSC study showed the presence of one exothermic region, the maximum of which shifts to the higher temperatures with an increase in the content of zinc oxide in the glass composition. Glass-ceramics synthesized at a temperature of 640°C for 2 hours demonstrate different luminescent properties depending on the Li/Zn ratio in the glass composition (Fig. 1). For compositions containing more lithium oxide, after heat treatment, a narrow band appears in the region of 667 nm, which corresponds to the $^2E_g(G) \rightarrow {}^4A_{2g}(F)$ transition of Mn^{4+} ions in an octahedral environment. The equimolar substitution of lithium with zinc leads to the appearance of a broad band in the region of 540 nm, the contribution of which to the luminescence spectrum increases with an increase in the zinc oxide content in the glass composition. Green luminescence in germanate matrix with zinc can be associated with Mn^{2+} ions in a tetragonal environment [3].

The lifetime of the luminescence in the 670 nm region for all compositions is about 1.1 - 1.3 ms, the maximum quantum yield is 60% for a composition containing lithium and zinc oxides in a ratio of 20/10. For the band in the region of 540 nm, the lifetime varies within 8.5-10 ms. The quantum yield increases with increasing zinc content in the glass composition and reaches a maximum value of 21% for a composition containing 7.5% Li_2O and 22.5% ZnO.

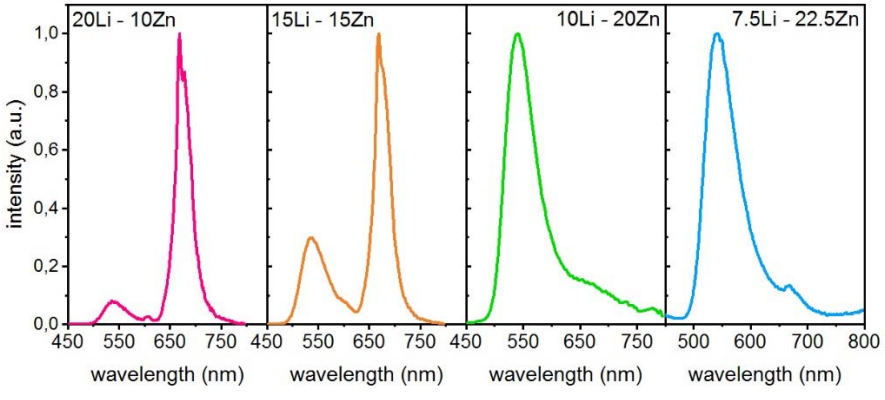

Fig. 1. PL spectra of lithium-zinc-germanate glass-ceramics containing manganese ions, λ_{ex}=335 nm.

References

1. J. Kunitomo, R. Suzuki, Y. Takahashi, et al., J. Ceram. Soc. Japan **122**, 725 (2014)
2. Y. Zhuang, J. Ueda, S. Tanabe, Appl. Phys. Lett. **105**, 3 (2014)
3. Y. Jin, Y. Hu, H. Duan, et al., RSC Adv. **4**, 11360 (2014)

Analysis of the impurity composition of zirconia ceramics by photoluminescence spectroscopy

Nataliya Larina[1,qqq], *Polina* Ryabochkina[1], *Elena* Lomonova[2], and *Efim* Chernov[3]

[1]National Research Mordovia State University, Institute of Physics and Chemistry, 68 Bolshevistskaya str., 430005 Saransk, Republic of Mordovia, Russia
[2]Prokhorov General Physics Institute of the Russian Academy of Sciences, Scientific Center of Laser Materials and Technologies, 38 Vavilov str., 119991 Moscow, Russia
[3]Research and Production Enterprise JSC «ECON», 9 Lesnaya str., 249037 Obninsk, Russia

Abstract. The impurity composition of ceramic samples of $(ZrO_2)_{0,909}(Y_2O_3)_{0,09}(Eu_2O_3)_{0,001}$ solid solutions was analyzed using photoluminescence spectroscopy. The compacts were obtained from crushed fused samples of similar composition using uniaxial compaction and slip casting techniques. Microimpurities of the Cr^{3+} and Al^{3+} ions were identified in the study samples. Their presence is associated with the technological conditions of ceramic synthesis. An uncontrolled impurity of the Cr_2O_3-Al_2O_3 solid solution was also revealed to be contained by individual inclusions in ceramic compacts.

Ceramic materials based on stabilized zirconia combine a number of unique properties. Due to this, they have a wide range of applications in many fields of science and technology [1-3]. For example, the high oxygen-ionic conductivity at elevated temperatures of these materials makes them suitable as oxygen sensors in gaseous media and as electrolytic membranes in solid oxide fuel cells (SOFCs) etc. [3-5].

As is known, the electrical conductivity and thermomechanical properties of ceramic solid electrolytes depend on the technology of their preparation, as well as on the characteristics and methods of synthesis of the initial powders. Differences in the structure of the material and the content of impurities in it may be associated with this.

The presence of uncontrolled impurities in stabilizing zirconia ceramics can be investigated by a wide range of physical-chemical methods. However, the photoluminescent spectroscopic methods, which have higher sensitivity compared to other spectrophotometric methods, are the most promising in the study of ceramic electrolyte plates. It also has a non-destructive effect on the structure of the materials under investigation.

In this work, the impurity composition of $(ZrO_2)_{0,909}(Y_2O_3)_{0,09}(Eu_2O_3)_{0,001}$ ceramic was investigated using photoluminescent spectroscopy. They were obtained from milled fused samples of similar composition by uniaxial pressing and slip casting. In the compacts studied, the presence of uncontrolled impurity as a Cr_2O_3-Al_2O_3 solid solution was revealed. Photoluminescent spectroscopy and confocal microscopy methods have shown that this impurity localizes to the surface of the ceramic as individual inclusions (Fig. 1).

The phase composition of the ceramic was analyzed using X-ray diffraction and Raman spectroscopy. The X-ray diffraction results indicate that the compacts prepared using various methods are single-phase and consist of cubic ZrO_2 with close values of the crystal lattice parameters. Other phases were not found. According to Raman spectroscopy, the study ceramics have a t”-phase structure, which is close to the fluorite structure.

[qqq] Corresponding author: saharova.1996@mail.ru

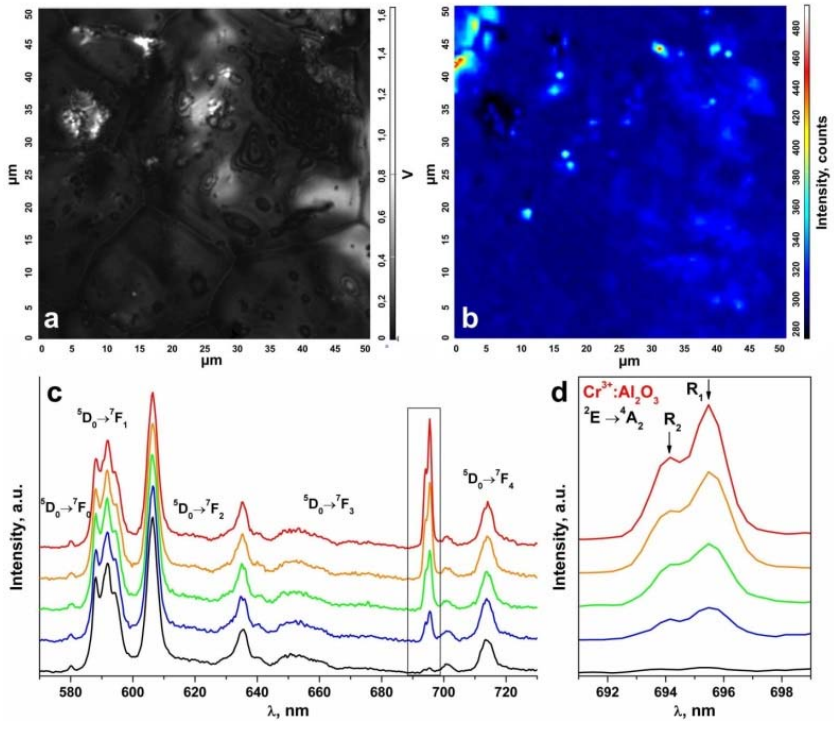

Fig. 1. (a) – Surface image of $(ZrO_2)_{0,909}(Y_2O_3)_{0,09}(Eu_2O_3)_{0,001}$ ceramic samples synthesized using slip casting; (b) – R_1 and R_2 luminescence band intensity distribution map for the Cr^{3+} ions in Al_2O_3 in the surface area shown in Fig. (a); (c) – luminescence spectra of the ceramic samples excited with a λ = 473 nm laser, T = 300 K, corresponding to the intensity scale in Fig. (b); (d) – R_1 and R_2 luminescence bands of the Cr^{3+} ions in Al_2O_3 for the $^2E \rightarrow {}^4A_2$ transition.

The local structure of ceramics was studied by photoluminescent spectroscopy using Eu^{3+} ions as a spectroscopic probe. The local crystalline environment of Eu3+ ions in $(ZrO_2)_{0,909}(Y_2O_3)_{0,09}(Eu_2O_3)_{0,001}$ ceramics, formed with the participation of oxygen vacancies, has been found to be identical to the local environment of Eu^{3+} ions in crystals of the same composition.

References

1. Y.W. Chen, J. Moussi, J.L. Drury, et al., Expert Rev. Med. Devices. V. **13**, 945 (2016)
2. U. Peuchert, Y. Okano, Y. Menke, et al., J. Eur. Ceram. Soc. V. **29**. 283 (2009)
3. N. Mahato, A. Banerjee, A. Gupta, et al., Prog. Mater. Sci. V. **72**. 141 (2015)
4. Y. Mansilla, M. Arce, C. Gonzalez Oliver, et al., Mater. Today: Proc. V. **14**. 92 (2019)
5. J.W. Fergus, J. Power Sources. V. **162**. 30 (2006)

$Na_5Rb_7Sc_2(WO_4)_9$:Yb^{3+}/Ho^{3+} or Yb^{3+}/Tm^{3+}: upconversion luminescence and temperature sensing characteristics

Olga A. Lipina[1,rrr], *Yana V.* Baklanova[1], *Tatyana S.* Spiridonova[2], and *Elena G.* Khaikina[2,3]

[1]Institute of Solid State Chemistry, UB RAS, 620990 Ekaterinburg, Russia
[2]Baikal Institute of Nature Management, SB RAS, 670047 Ulan-Ude, Russia
[3] Buryat State University, 670000 Ulan-Ude, Russia

Abstract. A new series of Yb^{3+}/Ho^{3+} and Yb^{3+}/Tm^{3+} codoped $Na_5Rb_7Sc_2(WO_4)_9$ has been prepared using the conventional solid state reaction method. The crystal structures have been refined with the Rietveld method using the powder X-ray diffraction data for $Na_5Rb_7Sc_2(WO_4)_9$. The compounds crystallize in the trigonal crystal system (sp. gr. *R*32, *Z* = 3). Upconversion luminescence has been detected under 980 nm laser diode excitation. The optimal Ho^{3+}/Yb^{3+} and Tm^{3+}/Yb^{3+} ratios have been determined. The luminescent characteristics of the most representative samples have been studied at 25 – 225°C to evaluate the optical temperature-sensing properties. The calculated values of the absolute and relative sensitivities indicate that $Na_5Rb_7Sc_2(WO_4)_9$:Yb^{3+}/Ho^{3+} and Yb^{3+}/Tm^{3+} are promising phosphors for non-contact thermometry.

Ho^{3+} or Tm^{3+} ions doped inorganic compounds have attracted much attention due to a wide variety of their applications. They can be used as active media of solid-state lasers, generating radiation at 1.3–4.0 μm spectral range [1], and as upconversion materials, converting infrared radiation in the visible region. The latter is widely used in bioimaging, anticounterfeiting, sub-band gap energy harvesting and temperature sensing [2–4].

In the present report the luminescence properties of $Na_5Rb_7Sc_{1.95}Yb_{0.05-x}Ho_x(WO_4)_9$ and $Na_5Rb_7Sc_{1.95}Yb_{0.05-x}Tm_x(WO_4)_9$ (x = 0.0025−0.025) tungstates have been studied. The polycrystalline samples were obtained via the ceramic technology by annealing the stoichiometric mixtures of Na_2WO_4, Rb_2WO_4, $Sc_2(WO_4)_3$ and $Ln_2(WO_4)_3$ (*Ln* = Ho, Tm, Yb) at 773–823 K for 120–150 h. The crystal structures were refined with the Rietveld method using the powder X-ray diffraction data for $Na_5Rb_7Sc_2(WO_4)_9$. The compounds crystallize in the trigonal crystal system (sp. gr. *R*32, *Z* = 3) [5].

Under 980 nm laser diode excitation (P = 50 mW/mm^2), $Na_5Rb_7Sc_{2-x-y}Yb_xHo_y(WO_4)_9$ and $Na_5Rb_7Sc_{2-x-y}Yb_xTm_y(WO_4)_9$ powders yield yellow or violet emission, respectively, which is visible to the naked eye. Typical upconversion luminescence spectra of $Na_5Rb_7Sc_{1.95}Yb_{0.05-x}Ho_x(WO_4)_9$ consist of two main bands in the green (530−570 nm) and red (635−680 nm) spectral ranges, which are caused by the $^5F_4$, $^5S_2 \rightarrow {}^5I_8$ and $^5F_5 \rightarrow {}^5I_8$ transitions in Ho^{3+} ions. The greatest emission intensity has been detected for the $Na_5Rb_7Sc_{1.95}Yb_{0.03}Ho_{0.02}(WO_4)_9$ sample. Thus, the optimal ratio between activator ions (Ho^{3+}) and sensitizer ions (Yb^{3+}) has been found to be 2/3. The luminescent characteristics of this sample have been studied additionally in the range of 25–225°C (298–498 K). The corresponding emission spectra are shown in Fig. 1*a*. An uneven decrease in intensity of the main luminescence lines should be noted. The integrated intensity of the bands at 530–570 nm measured at 225°C is only 15% of

[rrr] Corresponding author: LipinaOlgaA@yandex.ru

the initial value, while for the lines at 635−680 nm range, the drop in intensity is not so significant (~56 %). The calculated I_{red}/I_{green} ratio varies from 1.2 to 3.4 (Fig. 1*b*); an increasing contribution of the red component leads to a change in the emission color from yellow (25 °C) to orange red (225 °C).

The upconversion luminescence spectra of $Na_5Rb_7Sc_{2-x-y}Yb_xTm_y(WO_4)_9$ (λ_{ex} = 980 nm, P = 50 mW/mm^2) contain the intensive bands at 460–500 nm and 760–850 nm, associated with the $^1G_4 \rightarrow {}^3H_6$ and $^3H_4 \rightarrow {}^3H_6$ transitions in Tm^{3+} ions, and several weak peaks centered at 653 nm ($^1G_4 \rightarrow {}^3F_4$) and 692 nm ($^3F_{2,3} \rightarrow {}^3H_6$). Additional temperature studies were carried out for $Na_5Rb_7Sc_{1.95}Yb_{0.045}Tm_{0.005}(WO_4)_9$ sample, the Tm^{3+}/Yb^{3+} ratio is 1/9 (Fig. 1*c*). Heating the powder up to 225 °C leads to a gradual decrease in the intensities of almost all luminescence lines except the broad band in the 675–725 nm region ($^3F_{2,3} \rightarrow {}^3H_6$ transition). The temperature dependence of the fluorescence intensity ratio between this band and the line in infrared range, I_{692nm}/I_{806nm}, has been studied.

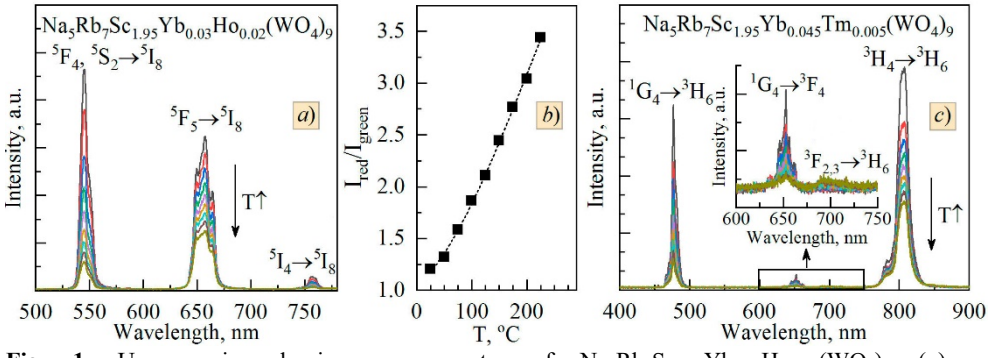

Fig. 1. Upconversion luminescence spectra of $Na_5Rb_7Sc_{1.95}Yb_{0.03}Ho_{0.02}(WO_4)_9$ (*a*) and $Na_5Rb_7Sc_{1.95}Yb_{0.045}Tm_{0.005}(WO_4)_9$ (*c*) phosphors measured at different temperatures. The temperature dependence of I_{red}/I_{green} for $Na_5Rb_7Sc_{1.95}Yb_{0.03}Ho_{0.02}(WO_4)_9$ (*b*).

The found values of the absolute and relative sensitivities suggest that Yb^{3+}/Ho^{3+} and Yb^{3+}/Tm^{3+} codoped $Na_5Rb_7Sc_2(WO_4)_9$ are promising phosphors for non-contact temperature sensing.

This work was supported by the RFBR (grant no. 20-03-00533).

References

1. M. Eichhorn, Appl. Phys. B **93**, 269 (2008)
2. H. Suo, Q. Zhu, X. Zhang, B. Chen, J. Chen, F. Wang, Mater. Today Phys. **21**, 100520 (2021)
3. R. Martín-Rodríguez, S. Fisher, A. Ivaturi, B. Froehlich, K. W. Krämer, J. C. Goldschmidt, B. S. Richards, A. Meijerink, Chem. Mater. **25**, 1912 (2013)
4. M. Dramicánin, *Luminescence Thermometry: Methods, Materials, and Applications* (Woodhead Publishing, ch. 6, pp. 113–157, 2018)
5. T. S. Spiridonova, A. A. Savina, E. V. Kovtunets, E. G. Khaikina, Chimica Techno Acta **8**, 20218412 (2021)

Study of the local field effects in impurity center spectroscopy by fluorescence nanoscopy

A.V. Naumov[1,2,3, sss], *M.G.* Gladush[1,2,3], *T.V.* Plakhotnik[4], *I.Yu.* Eremchev[1,2,3]

[1] Lebedev Physical Institute of the Russian Academy of Sciences, Russia
[2] Institute of Spectroscopy of the Russian Academy of Sciences, Russia
[3] Moscow State Pedagogical University, Russia
[4] Queensland University, Brisbane, Australia

Abstract. We show how the nanoscopy techniques with single fluorescent molecules can be extended to perform advanced characterization of dielectric materials. In our study the single molecules in a dielectric host are used as sensitive multi-parameter local probes which revel a few aspects of the light-matter interactions at the nanoscale. Measuring enough of the probes simultaneously gives us an opportunity for mapping dielectric parameters of the host material. The mapping procedure is based on the model for the excitation lifetime dependence on the local field in the medium. We show the mapping results may be accurate down to nanometers and give reliable averages at micro- and macro-scales.

In recent years, researchers have been interested in the effects that determine the kinetics of luminescence of impurity radiating centres, since the ability to control the kinetics of luminescence reveals fundamentally new opportunities in solving actual problems of quantum optics, materials science, laser technology and biophysics. Starting with the work of E.M. Parcell [1] where the possibility of modifying (controlling) spontaneous radiation in the radio frequency range was discussed, it was understood that the change of the characteristics of the local field should lead to a change in the radiation time T_1 in the optical range as well. With the advent of new technologies for the synthesis of nanomaterials, as well as the tools for precision manipulation of objects on the nanometer scale, it became possible to investigate the Parcell effect in the optical range, including at the level of a single quantum emitter: e.g. [2], studied the amplification and attenuation of luminescence of single molecules as a result of interaction with metal nanoparticle [3], demonstrated the ability to manipulate the luminescence kinetics of single *NV*-centers in diamonds by placing the nanocrystalline on the surface of the hyperbolic metamaterial, in [4] the authors described a sharp decrease in the attenuation time of the luminescence of Eu^{3+} ions in nanospheres due to the emergence of the photon mode of the whispering gallery.

The local field effects also manifest themselves in a wide range of experiments, where the dependence of time T1 of the impurity centers on the value of the index of refraction n of the transparent matrix (e.g., [5,6]) is investigated. $T_1(n)$ dependencies have been found for rare earth color centers in inorganic crystals and glass, as well as colloidal semiconductor quantum points in liquid and solid solutions and have been interpreted under various theoretical models (see [7,8] and references there). For organic impurity environments, however, the question of local field effects and the related dependency of $T_1(n)$ has only recently become the subject of much discussion [9].

[sss] Corresponding author: a_v_naumov@mail.ru

In this work we analyze the results of measurements of single terrylene molecules in different matrices at cryogenic temperatures down to 30 mK [10,11]. This allowed us to find the values of T_1 and to construct the histograms of distributions of these times for different matrices [12]. It makes it possible to cinstruct mapping of the effect in the plane of the sample [13]. The distributions we found were analyzed in the context of local field effects on the dynamics of the excited state of the molecules. An improved theoretical model has been developed to explain the $T_1(n)$ relationship.

Authors acknowledge Ministry of Education of Russia (state task AAAA-20-120061890084-9). A.V.N., M.G.G. and I.Yu.E are members of the Leading Scientific School of the Russian Federation (grant of the President of the Russian Federation NSh-776.2022.1.2).

References

1. E. M. Purcell, Phys Rev **69**, 681 (1946).
2. P. Anger, P. Bharadwaj, L. Novotny, Phys. Rev. Lett. **96**, 113002 (2006).
3. M. Y. Shalaginov, V. V. Vorobyov, J. Liu, M. Ferrera, A. V. Akimov, A. Lagutchev, A. N. Smolyaninov, V. V. Klimov, J. Irudayaraj, A. V. Kildishev, A. Boltasseva, V. M. Shalaev, Laser Photon. Rev. **9**, 120 (2015).
4. S. V. Zaitsev, A. N. Gruzintsev, Y. V. Yermolayeva, N. A. Matveevskaya, I. I. Zverkova, G. A. Emelchenko, A. V. Tolmachev, Jetp Lett. **106**, 145 (2017).
5. R. S. Meltzer, S. P. Feofilov, B. Tissue, H. B. Yuan, Phys. Rev. B **60**, 14012 (1999).
6. T. Senden, F. T. Rabouw, A. Meijerink, ACS Nano **9**, 1801 (2015).
7. K. Dolgaleva, R. W. Boyd, Adv. Opt. Photonics **4**, 1 (2012).
8. D. V. Kuznetsov, V. K. Roerich, M. G. Gladush, J. Exp. Theor. Phys. **113**, 647 (2011).
9. T. A. Anikushina, M. G. Gladush, A. A. Gorshelev, A. V. Naumov, Faraday Discuss. **184**, 263 (2015).
10. E. A. Donley, V. Burzomato, U. P. Wild, T. Plakhotnik, J. Lumines. **83**-4, 255 (1999).
11. E. A. Donley, S. Bonsma, V. Palm, V. Burzomato, U. P. Wild, T. Plakhotnik, J. Lumines. **87**-9, 109 (2000).
12. M. G. Gladush, T. A. AnikushinaA. A. Gorshelev, T. V. Plakhotnik, A. V. Naumov, "J. Exp. Theor. Phys. **128**(5), 655 (2019).
13. A. V. Naumov, A. A. Gorshelev, M. G. GladushT. A. Anikushina, A. V. Golovanova, J. Köhler, L. Kador, Nano Lett. **18**(10), 6129 (2018).

Low temperature study of photoluminescence excitation spectra of CVD diamond films with GeV-centers

Ivan Yu. Eremchev[1,2], *Arthur Yu.* Neliubov[2,3,ttt], *Kirill N.* Boldyrev[1], *Victor G.* Ralchenko[4], *Vadim S.* Sedov[4], *Andrey V.* Naumov[1,2,5], *Lothar* Kador[6]

[1] Institute of Spectroscopy RAS, Troitsk 108840, Russia
[2] Lebedev Physical Institute of the Russian Academy of Sciences, Troitsk Branch, Moscow, Troitsk, 108840, Russia
[3] Skolkovo Institute of Science and Technology, Moscow 121205, Russia
[4] Prokhorov General Physics Institute of the Russian Academy of Sciences, Moscow, 119991, Russia
[5] Moscow State Pedagogical University, Moscow 119991, Russia
[6] Institute of Physics, University of Bayreuth, Bayreuth, 95440, Germany

Abstract. This paper presents the results of studies of low-temperature fluorescence excitation (PLE) spectra of small ensembles (up to single emitters) of Germanium-Vacancy (GeV) color centers in diamond films synthesized by chemical deposition from the gas phase in the microwave plasma CVD reactor ARDIS-100 (2.45 GHz) using Germane gas.

In present work [1] we report the results of low-temperature study of Photo Luminescence Excitation (PLE) spectra study of small ensembles (down to single emitter) of Germanium-Vacancy (GeV) color centers in thin diamond films, synthesized by chemical vapor deposition in an ARDIS-100 microwave plasma CVD reactor (2.45 GHz) using Hermane gas [2]. Two samples with low and ultralow concentrations of embedded color centers were investigated.

PLE spectra were measured on two experimental setups. The first setup [4] was a luminescence cryogenic microscope, allowing the measurement of spectra in a wide temperature range (4.5-70 K) with high spatial (~1μm) and spectral resolution (~ 12 GHz) in the wide spectral range 598-604 nm (region of GeV luminescence excitation). The second experimental setup [3] had a similar scheme, but allowed measuring fluorescence excitation spectra with greater spectral resolution (~2 MHz), which was necessary for the resolution of the GeV-center BFL circuit at cryogenic temperatures.

In the first sample, zero phonon lines (ZPL) of emitters were clustered in the spectral bandwidth of 2nm centered at 601.5nm (Figure1). The spectra could be conditionally divided into two types. The first type at 5 K represented the well-known ZPL quartet structure (Fig1.a). Similar spectra were previously obtained in HPHT microdiamonds with GeV centers [5]. The ratio of intensities between the lines in the quartet varied in different parts of the sample. The second type of spectra looked like a sum of extremely narrow (FWHM < 0.01 nm) spectral lines (Fig.1b) whose number and spectral position varied in different regions of the sample. The reason for the appearance of these lines can be explained by the presence of extreme local stresses in the crystal lattice of CVD-diamond and its influence on the structure of energy levels of the color centers. It should be noted, that annealing of the sample at high temperature (1200 C) in an argon atmosphere led to a decrease in the fraction of spectra of the second type.

[ttt] Corresponding author: nelyubov.a@phystech.edu

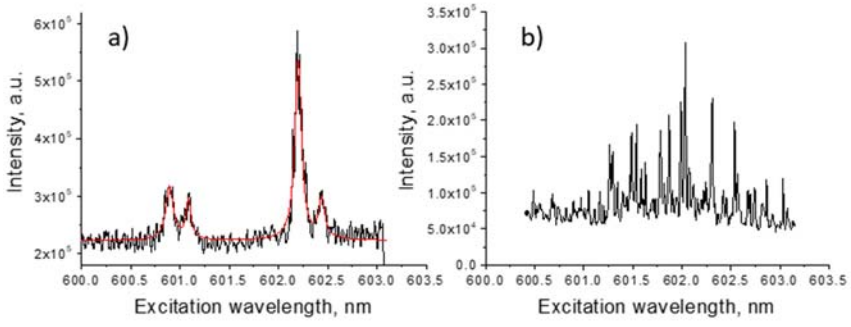

Fig. 1. PLE spectra from two diffraction-limited regions (~1μm^2) of CVD diamond with low concentration of GeV color centers(T=5K). (a) First type of spectra consisting of the ZPL quartet. (b) The second type of spectra, which is a set of extremely narrow and intense lines clustered around the most intense line in ZPL quartet.

Single narrow ZPLs were detected in the fluorescence excitation spectra of GeV centers in the sample with ultra-low concentration (see example in Fig. 2b). Some of these single ZPLs demonstrated blinking, which indirectly confirms that these lines belong to single color centers. Figure 2 shows the distribution of the ZPL widths measured at 7 K. In addition, the temperature dependences of the widths of single BFLs were obtained and the temperature broadening parameters were analyzed, which is of interest for the study of electro-phonon interaction in such systems.

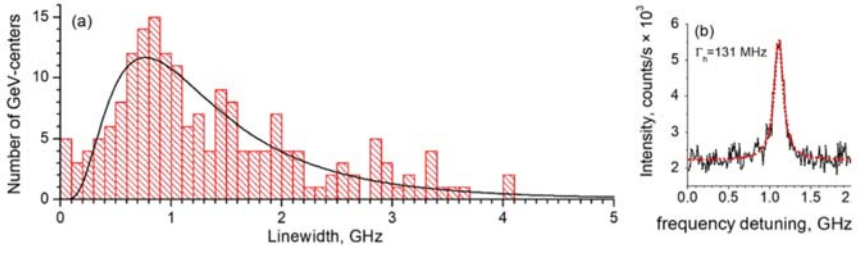

Fig. 2. (a) Linewidth distribution of single GeV centers in a sample with ultra-low concentration at 7K. (b) Example of the PLE spectrum of a single GeV center measured at 7K.

The authors are grateful for the support for RFBR (project No. 18-29-19200). I.Yu.E., A.Yu.N., K.N.B., and A.V.N. are members of the Leading Scientific School of the Russian Federation (grant of the President of the Russian Federation NSh-776.2022.1.2).

References

1. I. Y. Eremchev, A. Y. Neliubov, K. N. Boldyrev, V. G. Ralchenko, V. S. Sedov, L. Kador, A. V. Naumov. *J. Phys. Chem. C*, **125** (32), 17774–17785 (2021).
2. V. Sedov et al. *Diamond and Related Materials*, **90,** 47-53 (2018).
3. A. Naumov, I. Y. Eremchev, and A. A. Gorshelev. *Eur. Phys. J. D*, **68**, no. 11 (2014).
4. I.Yu. Eremchev, M.Yu. Eremchev, A.V. Naumov, *Physics Uspekhi*, **62** (3) (2019).
5. E. A. Ekimov, S. G. Lyapin, K.N. Boldyrev et al. JETP Lett. **102** (11), 811 (2015).

On field dependence of nonreciprocity in optical spectra of CuB_2O_4

Alexey Nurmukhametov[1,uuu] and *Mikhail* Eremin[1]

[1]Institute of Physics, Kazan Federal University, 16a Kremlyovskaya St., Kazan, Russia 420008

Abstract. The energy levels and wave functions of the copper ion in (4b) site, as well as the probabilities of magnetic and electric dipole transitions are calculated. The results of microscopic calculations and symmetry analysis are compared with the experimental data in strong applied magnetic fields [1]. The interaction parameters of copper 3d-electrons with the electrical component of the light wave have been refined.

1 Introduction

Dynamical magnetoelectric effects arise if the optical transition probability contains terms that are linear in both the electric and magnetic components of the light wave. These effects are attracting more and more attention in recent years. Interesting experimental data was obtained for the CuB_2O_4 crystal [1]: the absorption coefficient changes by several times under the reversal of the incident light wave vector or the direction of the applied magnetic field – this phenomenon is called "nonreciprocity". The goal of this work is to analyse available experimental data based on a microscopic theory of copper ion hole ($3d^9$) in this crystal.

2 Energy levels and wave functions

The Hamiltonian of the model contains the operators of the crystal field, spin-orbit, exchange, and Zeeman interactions:

$$\hat{H} = \sum_{k,q} B_q^{(k)} \hat{C}_q^{(k)} + \lambda \hat{\boldsymbol{l}}\hat{\boldsymbol{s}} + J_{gg}\hat{P}_g \sum_{i=1}^{4} \langle \boldsymbol{s}_i \rangle \hat{\boldsymbol{s}} + \mu_B \left(\hat{\boldsymbol{l}} + 2\hat{\boldsymbol{s}}\right)\boldsymbol{B}. \quad (1)$$

Here the parameters of the crystal field are [2] $B_0^{(2)} = -2.20$ eV, $B_0^{(4)} = 1.23$ eV, $B_4^{(4)} = 1.74$ eV, the spin-orbit interaction parameter $\lambda = -12$ meV, exchange integral $J_{gg} = 3.62$ meV, $\hat{P}_g$ is the projection operator onto the ground orbital state. The energy levels scheme and the transition of interest is shown on Fig. 1a.

3 Results and discussion

The operator of magnetic dipole transitions was used in the standard form considering the ratio between the light wave components: $\boldsymbol{B}^{\omega} = \frac{1}{k}\sqrt{\varepsilon\mu}[\boldsymbol{k} \times \boldsymbol{E}^{\omega}]$, $\sqrt{\varepsilon\mu} \approx 1.75$. To calculate the electric dipole transitions, we use an effective operator that considers the "admixing" to the ground $3d^9$ electronic configuration of the copper ion the states of the excited configuration of opposite parity $3d^84p$, as well as the states with electron transfer from the 2p and 2s shells of

[uuu] Corresponding author: srgalex@list.ru

neighbouring oxygen ions to the unfilled 3d shell [4]. In case of materials where both space and time inversion symmetry is broken, which CuB_2O_4 is an example of, the net probability of transition $\sum\left[\langle g|\hat{H}_E + \hat{H}_M|e\rangle\right]^2$ contains additional terms linear by the magnetic and electric components of the light wave $E_\alpha^\omega H_\beta^\omega$. When the direction of the wave vector changes, so does the relative sign of the operators $\hat{H}_E$ and $\hat{H}_M$ (to comply with the Right-Hand Rule **E**, **H**, **k**), which leads to a change in the total absorption intensity. The magnitude of the effect nontrivially depends on the magnitude of the applied magnetic field as illustrated in Fig. 1(b, c). We note that in [1], the fine structure of levels associated with exciton states was not resolved, which makes it possible to use the simplified model (1) without taking into account the Davydov splitting.

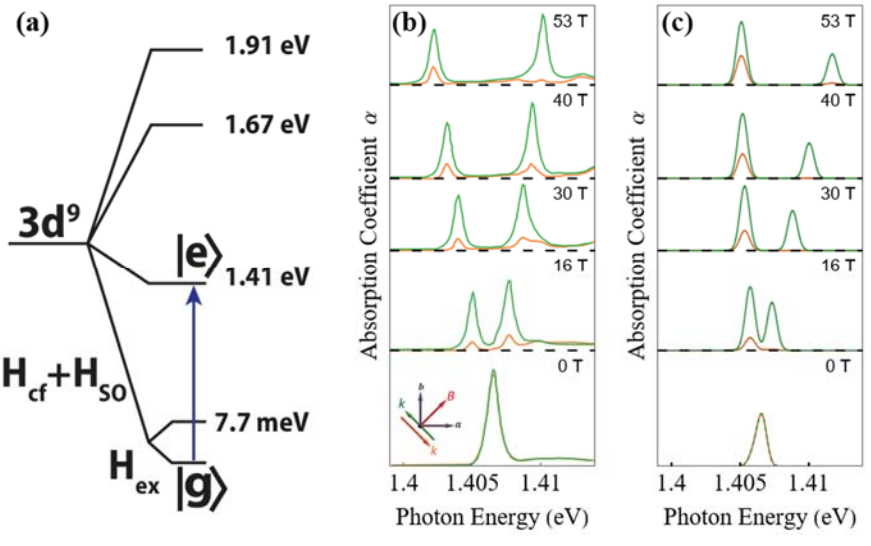

Fig. 1. (a) Scheme of energy splitting of Cu^{2+} (^2D) [1-3]. The blue arrow shows the studied optical transition. **(b, c)**. Change in absorption intensity upon wave vector reversal for various magnitudes of the applied magnetic field. **(b)** – experimental data from [1], **(c)** – results of our calculation.

This work was supported by the Foundation for the Advancement of Theoretical Physics and Mathematics BASIS.

References

1. S. Toyoda, N. Abe, S. Kimura, Y. H. Matsuda, T. Nomura, A. Ikeda, S. Takeyama, and T. Arima, Phys. Rev, Lett., **115**, 267207 (2015).
2. M. V. Eremin, and A. R. Nurmukhametov, JETP Lett., **114**, 35-39 (2021).
3. R. V. Pisarev, A. M. Kalashnikova, O. Schops, and L. N. Bezmaternykh, Phys. Rev. B., **84**, 075160 (2011).
4. M. V. Eremin, J. Exp. Theor. Phys. **129**, 990 (2019).

Transition metal and intrinsic luminescence of scapolite under synchrotron radiation excitation

Tatiana Radomskaya[1,2], *Ekaterina* Kaneva[1,2], *Elizaveta* Pankrushina[3], *Anna* Kozlova[4], *Victoria* Krasivykh[2,5], *Vladimir* Pankratov[6, vvv], and *Roman* Shendrik[1]

[1]Vinogradov Institute of Geochemistry SB RAS, Irkutsk, Russia
[2]Sidorov Mineralogical Museum, Irkutsk National Technical University, Irkutsk, Russia
[3]Zavaritsky Institute of Geology and Geochemistry UB RAS, Ekaterinburg, Russia
[4]National University of Science and Technology MISiS, Moscow, Russia
[5]Siberian School of Geosciences, Irkutsk National Research Technical University, Irkutsk, Russia
[6]Institute of Solid State Physics, University of Latvia, Riga, Latvia

Abstract. Intrinsic as well as Fe^{3+} and Mn^{2+} related luminescence properties in scapolite mineral are studied under VUV synchrotron radiation excitation. The luminescence attributed to self-trapped excitons in Na-Cl cages and exciton-like excitation in $(CO_3)^{2-}$ anion complex are detected and demonstrated. The extrinsic luminescence of Mn^{2+} and Fe^{3+} ions can be excited under energy, which is below the energy of band-to-band transitions.

Scapolite is a well-known mineral family forming a solid solution between meionite and marialite with the ($Ca_4Al_6Si_6O_{24}CO_3$) and ($Na_4Al_3Si_9O_{24}Cl$) formulations. These compounds crystalize in the *I*4/*m* space group and contain the cages in the crystal structure. Such microporous materials could be promising materials for radioactive waste contaminations, photodynamical therapy and luminophores for versatile applications [1, 2].

In this article, we study the scapolite mineral from the Slyudyanka, Irkutsk region, Russia with the following empirical formula: $Ca_{3.13}Na_{0.68}K_{0.02}(Al_{5.4}Si_{6.6}O_{24})(CO_3)_{0.58}(SO_4)_{0.16}Cl_{0.08}$. The samples were studied using ESR, optical absorption, FTIR, and Raman spectroscopy. The luminescence study was performed using FinEstLumi endstation [3] of FinEstBeAMS beamline [4] at MAX IV synchrotron facility (Lund, Sweden).

In the scapolite sample studied, a bright luminescence signal under excitation exceeding the band-to-band energy value is observed. It is assumed that the double band peaked at 350 and 400 nm excited in the region 5.5-6 eV can be attributed to intrinsic luminescence related to $(CO_3)^{2-}$ complexes. On the other hand, it is suggested that the double band at about 250 and 300 nm excited in the region 7-8 eV could be related to the excitation of self-trapped exciton in the Na-Cl cages (Fig. 1). These bands can be detected only at a temperature below 77 K.

In addition, the broad luminescence at about 500 nm is observed under excitation 5.5-6 eV and 7.5 eV. This band most likely corresponds to Mn^{2+} centers in scapolite. Another broad band at 700 nm is attributed to extrinsic Fe^{3+} centers under excitation in the region 5-6 eV.

The studied samples have blue color due to the presence of $(CO_3)^{\bullet-}$ anion-radicals. They were detected by ESR and optical absorption spectroscopy. Similar color centers have been studied in irradiated microporous cancrinites [5]. The wide absorption band with vibrational structure peaked at about 600 nm. The scapolite is bleached at a temperature higher than 400 °C. The blue color of the scapolite is restored after irradiation with UV photons with energy higher than 5.5 eV. The mechanism of $(CO_3)^{\bullet-}$ anion-radical creation is excitonic-like similar to cancrinites [6].

[vvv] Corresponding author: vpank@latnet.lv

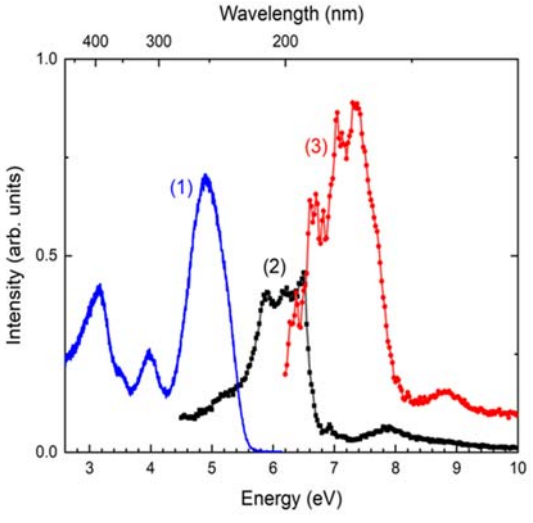

Fig. 1. Luminescence (curve 1) and excitation spectra monitored at 400 nm (curve 2) and 250 nm (curve 3) wavelengths.

References

1. S. Bahrani et al, *Fundamental developments in the zeolite process* (Interface Science and Technology vol. 32, 2021)
2. F. Blumentritt et al. Phys. Chem. Lett., **11** 4591 (2020)
3. V. Pankratov et al. Rad. Meas., **121** 91 (2019)
4. K. Chernenko et al., J. Synchr. Rad. 28 1620 (2021)
5. R. Shendrik et al. Crystals, **11** 280 (2021)
6. E. Kaneva, R. Shendrik J. Lum, **243** 118628 (2022)

Magnetic resonance in alkali atoms under zero time-averaged magnetic fields

Evgeny Popov[1,www], and *Sergey* Voskoboinikov[2]

[1]Laboratory of Quantum Processes and Measurements, ITMO University, 199034, 3b Kadetskaya Line, Saint Petersburg, Russia
[2]Institute of Computer Science and Technology, Peter the Great St.Petersburg Polytechnic University, 195251, 29 Polytechnicheskaya, St.Petersburg, Russia

Abstract. In this work, we discuss the existence of an unusual magnetic resonance in the Zeeman structure. The observation of this resonance does not require an external constant magnetic field, which forms the resonance frequency. That resonance is formed by only AC-magnetic field and resonance frequency is low-depend from invariable external magnetization.

The phenomenon of electron paramagnetic resonance in alkali atoms is based on the Zeeman Effect [1-2]. Fine or hyperfine levels of atoms split into Zeeman sublevels in an external DC magnetic field. By applying a transverse AC magnetic field with a resonance frequency, we act transitions between Zeeman sublevels in an atomic ensemble. Electron paramagnetic resonance is an effective method for observing the collective effects of atomic ensembles in spectroscopy [3-4]. It is also widely used in magnetometry [5-6], due to the width of the magnetic resonance is several orders less than the width of the optical resonance. Therefore, gas cells with alkali atoms are used as a sensitive element in the measurement of the magnetic field [7].

We suggest a new scheme of electronic parametric resonance, in which DC magnetic field is equal to zero. To observe this parametric electron magnetic resonance we put alkali atoms inside a cell with two orthogonal AC magnetic fields:

$$B_x = B_0 \cos 2\omega t, \quad B_y = 0, \quad B_z = B_0 \cos \omega t \tag{1}$$

where B_0 is amplitude of magnetic field and ω is frequency of magnetic field. Note, that frequency of transverse B_x magnetic field is double of frequency of longitudinal B_z magnetic field.

Unexpected that magnetic resonance is observed under absence of external DC magnetic field when alkali atoms are pumped by laser field with circular polarization. We named this effect parametric electron paramagnetic resonance. In the Fig.1 we can see two picks of longitudinal polarization of alkali atoms. The resonance frequencies are proportional to amplitude B_0. We explain these resonances by the appearance of repetitive dynamics of the polarization vector without atomic relaxation. These repetitive trajectories can be observed only for determine frequencies.

[www] Corresponding author: enp-tion@yandex.ru

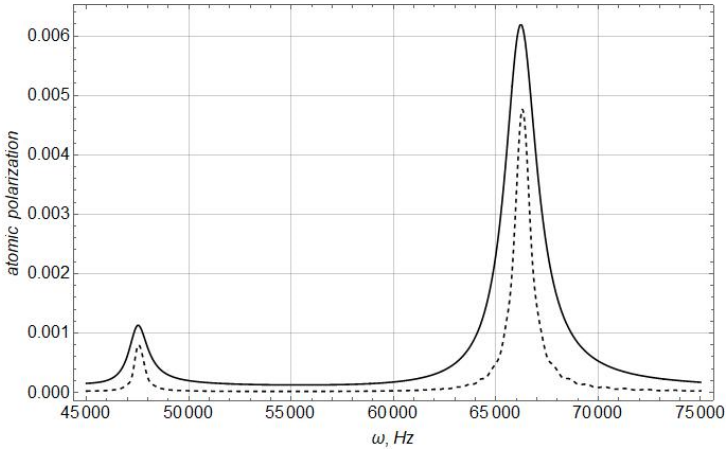

Fig.1 – parametric electron paramagnetic resonance in ^{87}Rb. The solid curve discribes atomic polarization on F = 1 hyperfine sublevel. The dashed curve discribes atomic polarization on F = 2 hyperfine sublevel. Atomic polarization is described by the expectation value of the z-projection of angular momentum.

Full mathematic model of the dynamics is very difiicult and we don't show all calculations in the text. The most interesting feature of the parametric electron magnetic resonance is stability against low-frequency noise.

The acknowledgements: this work was financially supported by Russian Ministry of Education (Grant No. 2019-0903)

References

1. T. Kubo, Applied Optics **11**, 7, p.1515-1520 (1972)
2. E. Zavoisky, Fizicheskiĭ Zhurnal, **9**, p. 211–245 (1945)
3. A. Kastler, Science, **158**, 3798, p. 214-221 (1967)
4. E. Popov, V. Bobrikova, S. Voskoboinikov, K. Barantsev, S. Ustinov, A. Litvinov, A. Vershovskii, S. Dmitriev, V. Kartoshkin, A. Pazgalev, M. Petrenko, JETP Letters, **108**, 8, p. 513-518 (2018)
5. E. Aleksandrov, A. Vershovskii, Physics–Uspekhi, **52**, 6, p. 573-601 (2009)
6. D. Budker and D. Kimball, "Optical magnetometry" // Cambridge University Press (2013), 406 p
7. D. Budker, D. Kimball, S. Rochester, V. Yashchuk, and M. Zolotorev, Phys. Rev. A **62**, 4, p. 043403 (2000)

Luminescence features of the ceramics based on cubic $(Zr_{0.82-x}Hf_xY_{0.17}Eu_{0.01})O_{1.91}$

Azaliia A. Shakirova[1,xxx], *Ekaterina V.* Dementeva[1], *Grigorii A.* Gusev[1], *Tatyana B.* Popova[1], *Boris E.* Burakov[1], *Maria V.* Zamoryanskaya[1]

[1]Ioffe Institute RAS, Saint-Petersburg, 194021 Russia

Abstract. The luminescent properties of cubic ceramics $(Zr_{0.82-x}Hf_xY_{0.17}Eu_{0.1})O_{1.91}$ with different contents of hafnium (x = 0; 0.2; 0.41; 0.62; 0.82) were studied. Cathodoluminescence (CL) and photoluminescence (PL) spectra and excitation spectra were obtained. It was found that the luminescence spectra of the samples depend on the type of excitation. In addition to the main europium luminescence bands, the CL spectra exhibited bands of high-energy transitions, which were absent in the PL spectra. Also, upon photoexcitation at a wavelength of 440 nm, a defective band was present. The excitation spectra of the luminescence emission band of europium showed that the additional pumping of the excitation energy of the $^5D_0$ level from higher energy levels.

Recently, an urgent task is the development of radiation-resistant thermoluminescent dosimeters, which are used to analyze the consequences of radiation accidents and environmental disasters. As a material that will be the basis of such a dosimeter, cubic hafnium dioxide with zirconium can be used. Such a material has mechanical and radiation resistance, and is also capable of absorbing neutrons [1, 2].

A series of samples of cubic ceramics $(Zr_{0.82-x}Hf_xY_{0.17}Eu_{0.1})O_{1.91}$ with different content of hafnium (x = 0; 0.2; 0.41; 0.62; 0.82) was studied in this work. Ceramics was obtained by cold pressing of the initial charge followed by sintering in air at a temperature of 1500°C for three hours. The mixture was synthesized by co-precipitation from a common aqueous solution [3]. The required ratio of elements in the composition was controlled by electron probe microanalysis.

CL and PL (λ_{ex}=270 nm) spectra of samples were obtained (Fig. 1). The CL spectra show the main europium emission bands ($^5D_0$-$^7F_{1,2,3}$), as well as emission bands from high-energy transitions ($^5D_0$-$^7F_0$, $^5D_1$-$^7F_1$ and $^5D_3$-$^7F_3$) (Fig. 1a). The PL spectrum contains both the $^5D_0$-$^7F_{1,2,3}$ emission bands and a defective band with an intensity maximum at 440 nm (Fig. 1b).

It should be noted that when luminescence is excited by a beam, the maximum luminescence intensity is exhibited by the $(Zr_{0.62}Hf_{0.2}Y_{0.17}Eu_{0.1})O_{1.91}$ sample; upon photoexcitation – by the sample $(Hf_{0.82}Y_{0.17}Eu_{0.1})O_{1.91}$.

The luminescence excitation spectrum of the samples (λ_{em}=592 nm, $^5D_0$-$^7F_1$ Eu^{3+} transition) (Fig. 2a) shows the transfer of excitation energy to the $^5D_0$ level from higher energy levels. A study of the luminescence excitation spectrum of the defective band (λ_{em}=440 nm) shows the most efficient excitation at a wavelength of 350 nm (fig. 2b).

As a result of the work, it was shown that the luminescence spectra depend on the type of excitation. The CL band with a maximum at 440 nm is possibly associated with oxygen vacancies, like oxygen vacancies in cubic ZrO_2 [4].

[xxx] Corresponding author: azaliya.s@inbox.ru

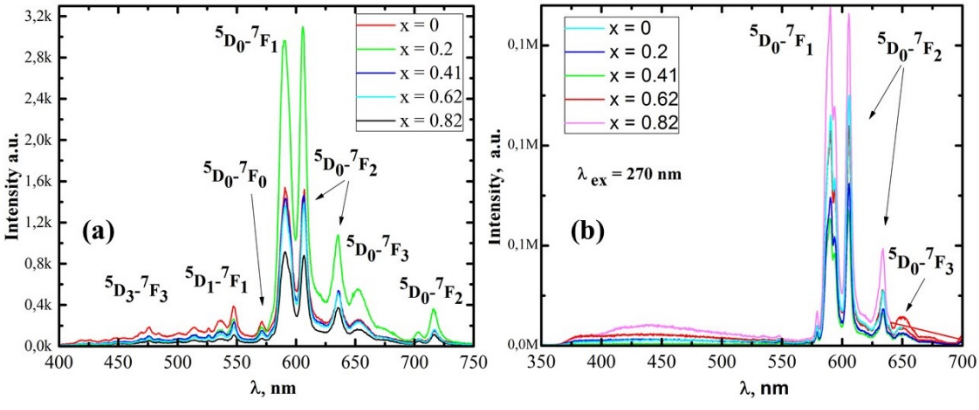

Fig. 1. (a) – CL spectra, (b) – PL spectra.

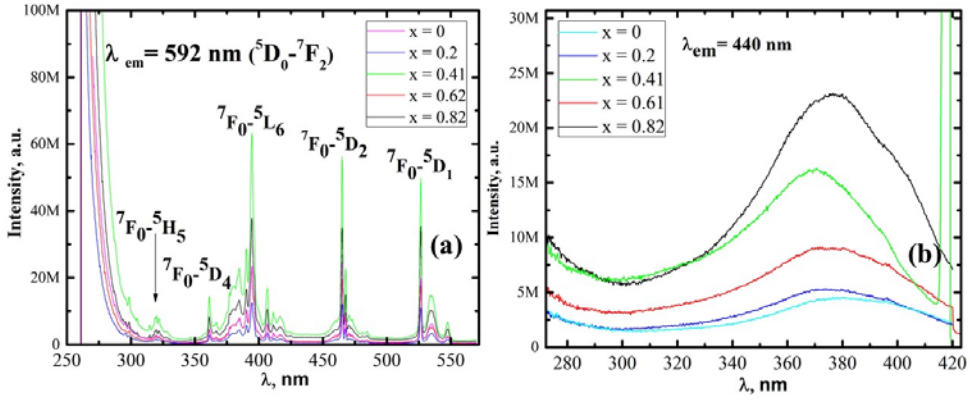

Fig. 2. Excitation spectra (a) – λ_{em} = 592 nm, (b) – λ_{em} = 440 nm of samples.

References

1. V.G. Sevastyanov, E.P. Simonenko et al., Mater. Chem. Phys. 153, 78 (2015)
2. E. Montes, P. Ceron et al., Ceram. Int., 44, 8081 (2018)
3. E.V. Ivanova, V.A. Kravets et al., J. Alloys Compd, 808, 151778 (2019).
4. K. Joy, I.J. Berlin et al., J. Phys. Chem. Solids, 72, 673 (2011)

Absorption and emission spectra of congruent $LiNbO_3:Er^{3+}$ crystals in the 400-1650 nm range

Aleksandr P. Skvortsov[1,yyy], *Aleksandr B.*Pevtsov[1], and *Katalin* Polgar[2]

[1]Ioffe Institute RAS, 26 Politekhnicheskaya, St.Petersburg, Russia
[2]Wigner Research Centre for Physics of HAS, Konkoly-Thege 29-33, Budapest, Hungary

Abstract. Photoluminescence and absorption spectra are investigated in congruent $LiNbO_3:Er^{3+}$(0.25%) crystals in a wide spectral range at room temperature. Under optical pumping by a semiconductor laser diode operating at 808 nm, the samples demonstrated both "conventional" luminescence (centered at around 1540 nm and 980 nm) and rather intense anti-stokes emission (centered at around 526 nm, 550 nm and 660 nm). The effects of multiphoton energy transfer and phonon relaxation processes on anti-stokes luminescence in the congruent lithium niobate crystals are discussed.

It is well known that lithium niobate crystals both pure and doped with rare earth ions and iron group ions are promising material for quantum electronics. In present work we have studied the absorption and luminescence spectra of Er^{3+} ions in congruent $LiNbO_3$ crystals in visible and near IR ranges (400-1650 nm).

The congruent crystals have been grown from the melt by Czochralski method using the apparatus described in [1]. The pulling rate was 1 mm/h, the rotation speed of the seed was 10 /min, the growth axis was being the trigonal <0001>. Monodomainization has been carried out in the furnace by means of passing 5 mA current through the boule after growth but before cooling down to room temperature. The activators were added to the melt in form of oxides. The concentration of Er^{3+} ions was 0.25 % by weight. Oriented (1×5×10) mm^3 samples were cut from bulk crystals. The domain structure was controlled by microscope after chemical etching in a mixture of concentrated hydrofluoric and nitric acids.

The experiments were carried out at room temperature. The photoluminescence (PL) spectra in the 400-1650 nm range were measured using the Horiba Jobin-Yvon T64000 spectrometer equipped with Si and InGaAs charge coupled devices (CCDs). The transmittance spectra were obtained in the 330-1650 nm range (with step 0.8 nm) using the Varian Cary 5000 spectrophotometer.

Figure 1 illustrates the transmission and PL spectra of $LiNbO_3:Er^{3+}$ crystals. Optical transmission studies reveal structured absorption band centered around 370 nm, 410nm, 452 nm, 493 nm, 526 nm, 550 nm,658 nm, 807 nm, 980 nm and 1533 nm, which may be connected with the intraconfigurational f-f transitions from ground $^4I_{15/2}$ manifold to the higher manifolds $^4G_{11/2}$, $^2H_{9/2}$, $^4F_{5/2}$, $^4F_{7/2}$, $^2H_{11/2}$, $^4S_{3/2}$, $^4F_{9/2}$, $^4I_{9/2}$, $^4I_{11/2}$ and $^4I_{13/2}$ correspondently.

The PL was excited by laser diode operating at 808 nm, which coincides with the $^4I_{15/2} \rightarrow {}^4F_{9/2}$ transition in Er^{3+} ions. The PL study reveals two sorts of luminescence. First: the usual PL in long-wave part of spectrum peaked at 980 nm and 1533 nm connected with $^4I_{11/2} \rightarrow {}^4I_{15/2}$ and $^4I_{13/2} \rightarrow {}^4I_{15/2}$ transitions. Second: the anti-Stokes luminescence in short wave part of

yyy Corresponding author: a.skvortsov@mail.ioffe.ru

spectrum peaked at 660 nm, 550 nm and 526 nm. These emission bands are associated with $^4F_{9/2} \rightarrow {}^4I_{15/2}$, $^4S_{3/2} \rightarrow {}^4I_{15/2}$ and $^2H_{11/2} \rightarrow {}^4I_{15/2}$ transitions.

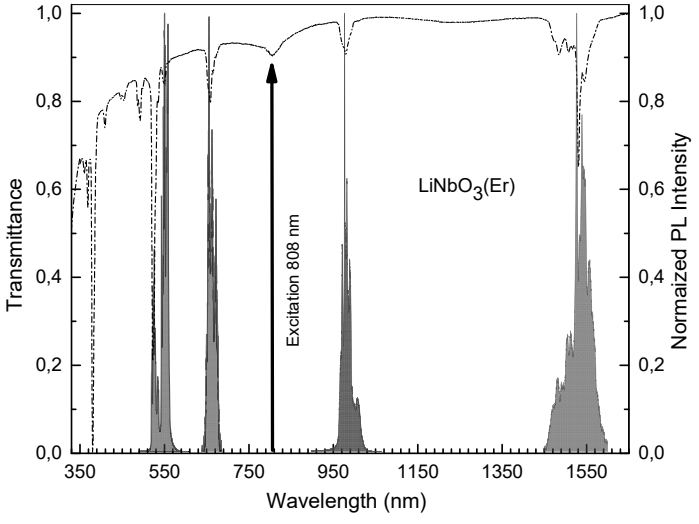

Fig. 1. PL and transmission spectra of $LiNbO_3$: Er^{3+} crystals at room temperature.

The observed lines of short-wavelength luminescence upon long-wavelength excitation are associated with the features of the processes of multiphonon energy transfer and photon relaxation in congruent lithium niobate crystals.

References

1. F. Schmidt, R. Voszka, Crystal Research and Technology, **16**, k127 (1981)

Dipole-dipole interactions in the photoluminescence excitation and emission spectra of two quantum emitters

Ekaterina Smirnova[1, 2, zzz], *Natalia* Lozing[1,3], and *Maxim* Gladush[1,3,4]

[1]Lebedev Physical Institute RAS, Troitsk Branch, Moscow, 108840 Russia
[2]Higher School of Economics National Research University, Moscow, 101000 Russia
[3]Institute for Spectroscopy RAS, Troitsk Branch, Moscow, 108840 Russia
[4]Moscow Pedagogical State University, Moscow, 119435, Russia

Abstract. In this work we investigate two closely spaced two-level emitters driven by a cw-laser. The emitters may differ in their transition frequencies and transition moments. Furthermore, we take in the account different arrangement of excitation and detection geometries. We derive the master equation for this system using the original method based on the reduced density matrices and corresponding correlation operators (Bogolyubov-Born-Green-Kirkwood-Yvon hierarchies). The master equation is shown to describe the dipole-dipole coupling and the cooperative entanglement between the particles naturally, without any phenomenological terms. Excitation and emission spectra are calculated for different geometries using quantum kinetic approaches. One can observe the presence of dipole-dipole interaction in these spectra.

One of the methods for studying materials is fluorescent nanoscopy [1], i.e., the restoration of the structure (dynamics) of a material through the registration of a fluorescent signal from optically active particles embedded in a sample. Single quantum emitters can act as probes, as well as their small ensembles, the light emitted by them contains rich information about the local environment. The simplest ensemble is a paired emitter. In such system, sub- and superradiant cooperative states, first described by Dicke [2], are realized. The nature of the radiation of a paired system is extremely sensitive to the excitation geometry, the location of the emitters in the pair, and the difference in their individual properties.

In this work we consider a system “two emitters + photons”, which is described by density matrix ρ. Each emitter is approximated as a two-level system with a transition frequency ω_i and a transition dipole moment $\mathbf{d}_i$. The density matrix of full systems obeys Neuman equation with the Hamiltonian, that consists of free energies of atoms and phonons plus the interaction between atoms and phonons. It is important to note here that the interaction between the emitters is not written explicitly but is given through the interaction via photons.

Using the reduction property of density matrixes and performing bogolubov hierarchies we obtained the master equation describing two-particle density matrix:

[zzz] Corresponding author: ekatri.smirnova@gmail.com

$$\frac{d}{dt}\rho_{aa'} = -i\sum_i \Delta_i[\hat{\sigma}_i^+\hat{\sigma}_i^-, \rho_{aa'}] + i\sum_i [\Omega_i(\mathbf{r}_i)\hat{\sigma}_i^- + \Omega_i^*(\mathbf{r}_i)\hat{\sigma}_i^+, \rho_{aa'}]$$
$$+ i\sum_{i\neq j}\Omega_{ij}[\hat{\sigma}_i^+\hat{\sigma}_j^-, \rho_{aa'}] - \sum_{i,j}\gamma_{ij}([\hat{\sigma}_i^+, \hat{\sigma}_j^-\rho_{aa'}] + [\rho_{aa'}\hat{\sigma}_i^+, \hat{\sigma}_j^-])$$
$$-\frac{1}{\hbar^2}\sum_{i,j}\left([\hat{\sigma}_i^+, [\hat{\sigma}_i^+, \rho_{aa'}]\int_0^t dt'\mathbf{d}_i\overleftrightarrow{\mathbf{W}}(\mathbf{r}_i, \mathbf{r}_j, t, t')\,\mathbf{d}_j e^{i\omega_j(t-t')} + h.c.\right).$$

The first four terms in the right-hand side are well-known in the literature and represent interaction with laser field mode, dipole-dipole interaction, and individual and collective relaxation. The last term in this equation is new and is called the scattered field correlation tensor. It is responsible for various exchange channels between the populations and coherences induced by multiple scattering of photons.

With the help of the correlation tensor, one can calculate the steady state total excitation intensity. These dependences are in good agreement with the experimental works [3-4]. The emission spectra were calculated by using the quantum mechanical average of the photon creation and annihilation operators. The results are demonstrated on Fig. 1.

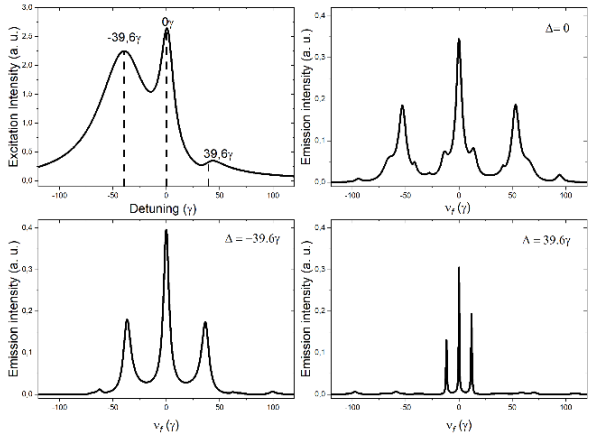

Fig. 1. Excitation spectrum with corresponding to each peak emission spectra. Parameters of the emitters: $\omega_1 - \omega_2 = 10\gamma, d_1 = 1.5d_2, r_{12} = 0.06\,\lambda$. The laser and the detector are in the same plane, and both make angle of 45 degrees to the interatomic axis. The angle between laser and detector direction is 90 degrees.

The authors are members of the Leading Scientific School of the Russian Federation (grant of the President of the Russian Federation NSh-776.2022.1.2).

References

1. A. V. Naumov, Physics-Uspekhi, **56(6)**, 605 (2013)
2. R. H. Dicke, Phys. Rev., **93(1)**, 99 (1954)
3. C. Hettich, C. Schmitt, J. Zitzmann, S. Kuhn, I. Gerhardt, V. Sandoghdar, Science, **298(5592)**, 385 (2002)
4. J. B. Trebbia, Q. Deplano, P. Tamarat, B. Lounis, Nature communications, **13(1)**, 1 (2022)

Spectroscopy of divalent samarium in halide single crystals

Dmitry Sofich[1,aaaa], *Vladimir* Kozlovskiy[1], *Evgeny* Radzhabov[1], and *Roman* Shendrik[1]

[1]Vinogradov Institute of Geochemistry SB RAS, Irkutsk, Russia

Abstract. The results of spectroscopic studies of Sm^{2+} doped alkali-earth fluoride (CaF_2, SrF_2, and BaF_2), BaBrI and CsI single crystals are given. It is found bright 5d-4f luminescence of Sm^{2+} ions in CsI and MF_2 (M=Ca,Sr) crystals, 4f-4f luminescence in BaF_2 and combination of 4f-4f and 5d-4f emission in BaBrI.

Scintillators are important materials for the detection of ionizing radiation. The most popular scintillators are doped with Ce^{3+}, Eu^{2+} impurities. Their luminescence lies in blue spectral region where maximum of sensitivity of traditional photodectors – PMT is located. However, novel photodetector based on avalanche photodiode has a maximum sensitivity in the red spectral range. Therefore, the activators emitting in the red spectral are required.

The promising activator is divalent samarium. It demonstrates surprisingly good NIR scintillation performance [1 - 3]. In present work, optical spectroscopy results of Sm^{2+} doped alkali-earth halide crystals CaF_2, SrF_2, BaF_2 and BaBrI in comparison with alkali halide CsI single crystals are presented.

CaF_2, SrF_2, BaF_2 and BaBrI crystals were grown using Bridgman technique in graphite crucible in vacuum. In CaF_2, SrF_2, and BaF_2 crystals, samarium was in 3+ state and it was reduced to 2+ state after additive coloration of these crystals [4]. In BaBrI crystal all samarium ions is in divalent state.

CsI crystal were grown using Czochralski method in graphite crucible and reduced atmosphere. In growing crystals Sm^{3+} is not found with luminescence methods.

In the MF_2 (M=Ca,Sr) and CsI crystals wide band at about 700 nm attributed to 5d-4f luminescence was observed at room temperature (Fig. 1). In BaF_2-Sm^{2+} sharp lines at about 690-800 nm correspond to 4f-4f transitions in Sm^{2+}. In BaBrI-Sm^{2+} crystals wide band peaked at 700 nm and the sharp lines are together observed at room temperature. During cooling 5d-4f luminescence of Sm^{2+} disappears in MF_2 (M=Ca, Sr) and BaBrI crystals.

It was found large light output under X-ray excitation of Sm^{2+} luminescence in BaBrI and CsI crystals. That makes it possible to apply these materials for NIR scintillators and X-ray phosphors. In the article, the possible energy transfer mechanisms are discussed.

The position of the 5d and 4f($^5D_0$ and $^5D_1$) levels of Sm^{2+} in Dorenbos diagram should be adjusted to match the experimental results for CaF_2, SrF_2, BaF_2, BaBrI and CsI crystals.

[aaaa] Corresponding author: sofich-dmitriy@live.com

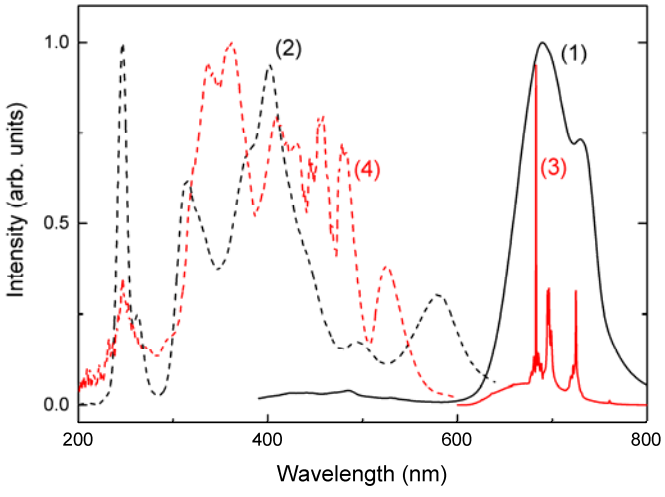

Fig. 1. Luminescence and excitation spectra of Sm^{2+} ions in CsI (1, 2) and BaBrI (3, 4).

References

1. Wolszczak, W., K. W. Krämer, and P. Dorenbos. J.lum. **222** 117101 (2020)
2. Shalaev, A et al NIM B **467** 17 (2020)
3. Sofich, D.; Shendrik, R.; Rusakov, A.; Shalaev, A.; Myasnikova, A. AIP Conf. Proc. **2392** 040004 (2021)
4. Radzhabov, E.A. Opt. Mat., **85** 127 (2018)

Epitaxial growth and photoluminescence of europium molybdate films on $SrTiO_3$ and Al_2O_3

Nikolai Sokolov[1,bbbb], *Alexandr* Korovin[1], *Danila* Kuzin[1], *Alexey* Kulinkin[1], *Alexandr* Smirnov[1], *Vladimir* Sakharov[1], *Maria* Yagovkina[1], *Yilin* Wang[2], *Konstantin* Magaryan[3], *Sergey* Naumov[4], and *Ling* Huan[2,5]

[1]Ioffe Institute, St. Petersburg, 194021, Russia
[2]Institute of Advanced Materials, Nanjing Tech University, Nanjing, 211816, China
[3]Moscow Pedagogical State University, Moscow, 119435, Russia
[4]M.N. Mikheev Institute of Metal Physics UB of RAS, Ekaterinburg, 620108, Russia
[5]College of Chemistry, State Key Laboratory of Chemistry and Utilization of Carbon Based Energy Resources, Xinjiang University, Urumqi, 830046, China

Abstract. Submicron europium molybdate films have been grown on $SrTiO_3$ and Al_2O_3 substrates by laser molecular beam epitaxy. Reflection high-energy electron diffraction (RHEED) patterns clearly indicated epitaxial growth of the films. Photoluminescence (PL) measurements using 532 and 325 nm laser excitation showed strong dependence of PL spectra shape on growth conditions and its correlation with RHEED observations. It was found that the most distinct fine structure in Eu^{3+} PL spectra was observed in the epitaxial films grown on $SrTiO_3$ substrates.

Researchers' attention to the lanthanide molybdates is well-known, see e.g. [1]. The most interesting materials belonging to this big family are europium molybdates, which are attractive for basic studies because of different Eu valency (2+ or 3+) in these compounds as well as display and phosphor applications. The main crystal phases observed in this material are tetragonal $EuMoO_4$ with scheelite-type structure, stable at room temperature monoclinic α-$Eu_2(MoO_4)_3$, metastable orthorhombic β′-$Eu_2(MoO_4)_3$ and tetragonal β-$Eu_2(MoO_4)_3$ phases [2,3]. Recent comprehensive information on structure and physical properties of europium molybdate ceramics is presented in [4]. However as far as we know, practically there is no reports on growth and optical studies of europium molybdate epitaxial films. Fabrication of such films could provide opportunities to use the effect of epitaxial stabilization of metastable phases as well as realization of new heterostructures with attractive for applications properties. In this work, we study laser molecular beam epitaxial growth and photoluminescence (PL) properties of europium molybdate films.

Europium molybdate films were grown on $SrTiO_3$(001) and Al_2O_3(0001) substrates by ablation with excimer laser of α-$Eu_2(MoO_4)_3$ ceramic target. The substrate temperature T_{sub} was in range of 400–800 °C and the thickness of the films was 300–500 nm. The growth was *in situ* monitored by reflection high-energy electron diffraction (RHEED). It was found that observed RHEED patterns strongly depended on T_{sub} and oxygen buffer gas pressure.

Growth of films on $SrTiO_3$(001) at P_{O2}=0.1 mbar resulted in appearance of well-pronounced RHEED patterns showing epitaxial film growth. In case of #8946, grown at T_{sub}=600°C streaky pattern indicating smooth surface of the film was observed (not shown). During growth at T_{sub}=800°C bright spots dominated in the pattern, Fig. 1. This enabled

[bbbb] Corresponding author: nsokolov@fl.ioffe.ru

modelling of the pattern; the results for tetragonal lattice showed in this figure by red circules. Good coincidence of the experimental and simulated patterns can be seen. High resolution X-ray diffraction measurements showed growth of single phase crystalline film with interlayer spacing along the surface normal d=11.508 Å and with the width of ω-curve below 0.5 deg.

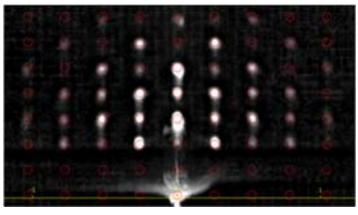

Fig. 1. RHEED of #8950, T_{sub}=800°C.

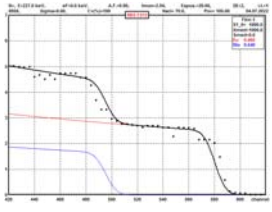

Fig. 2. MEIS of 500 nm sample.

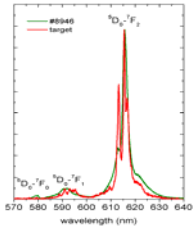

Fig. 3. PL of target&#8946

Eu/Mo ratio in the layers was determined using medium energy ion scattering (MEIS) technique. It was found that this ratio for used in this work growth conditions is 0.85, which is between 0.67 expected for $Eu_2(MoO_4)_3$ and 1.0 for $EuMoO_4$, Fig. 2. Obtained for the epitaxial films data for crystal structure and chemical composition well correlate with the data reported in [3] for microcrystalline Eu_xMoO_4 powders and gave enough convincing evidence that Eu deficient scheelite tetragonal structure is realized in our epitaxial films.

Photoluminescence (PL) was measured at 300 K and 80 K using 532 nm and 325 nm lasers. Fig. 3 shows RT PL spectra of ceramic target consisting of α-$Eu_2(MoO_4)_3$ microcrystals and epitaxial #8946 sample. One can see that the spectra are quite different, which agrees with the difference in crystal structure of these two objects. In the spectrum measured from #8946 sample well-pronounced fine structure with relatively narrow strongest line at 616 nm is observed. At the shorter wavelengths (581–602 nm) weaker structure related to magnetodipole $^5D_0$–$^7F_1$ transitions is seen. It is noteworthy that the ratio of integral intensities of red emission caused by $^5D_0$–$^7F_2$ transitions to that of $^5D_0$–$^7F_1$ transitions reflects the symmetry variation of Eu^{3+} ions in different samples. In [5] was shown that this ratio is related with the number of surfaces Eu^{3+}, which has lower crystal field symmetry than those embedded inside the thin film. It was also found that PL spectra of the epitaxial layers measured under excitation at 325 nm and 532 nm are noticeably different, which makes attractive laser spectroscopy technique.

The work was supported by the RFBR (grant GFEN_a 21-52-53029) and partially supported by the National Science Foundation of China for Basic Research (grant 22111530015). K.M. is a member of the Leading Scientific School of the Russian Federation (grant of the President of the Russian Federation NSh-776.2022.1.2).

References

1. V.A. Efremov, Russ. Chem. Rev. **59**, 627 (1990)
2. L.H. Brixner, P.E. Bierstedt, A.W. Sleight, M.S. Licis, Mater. Res. Bull. **6**, 545 (1971)
3. D. Machon, V.P. Dmitriev, V.V. Sinitsyn, G. Lucazeau, Phys.Rev. B **70**, 094117 (2004)
4. V.V. Popov, A.P. Menushenkov et al, Solid State Sci. **112**, 106518 (2021)
5. J. Zhou, Y. Wei, Y. Pan, Y. Wang, Z. Yuan, et al, Nat. Commun., **12,** 2948 (2021).

$MgAl_2O_4$ ceramics doped with high level of Eu^{3+} ions concentrations

Damir Valiev[1,cccc], *Oleg* Khasanov[1], *Edgar* Dvilis[1], *Vladimir* Paygin[1], *Lin* Chaolu[1] and *Sergey* Stepanov[1]

National Research Tomsk Polytechnic University, 634050, Tomsk, Russia

Abstract. $MgAl_2O_4$ ceramics doped with high level of Eu^{3+}ions were prepared by the SPS method. The crystal structure and luminescent properties have been studied in detail. The X-ray diffraction spectrum showed that the two-phase structure of $MgAl_2O_4$ and $AlEuO_3$ appeared after the doped Eu^{3+} concentration exceeded 3 wt.%. There are several emission bands in the luminescence spectrum of the $MgAl_2O_4$:Eu^{3+} ceramics are recorded. The nature of luminescent centers and decay time parameters discussed in detail.

1 Introduction

To date, the current research on $MgAl_2O_4$:Eu^{3+} is mainly devoted to the preparation and study of spinel powders [1]. There are no systematic studies in the literature on the synthesis of $MgAl_2O_4$:Eu^{3+} ceramics with the optimal doping concentrations and luminescence characteristics. In this work, $MgAl_2O_4$doped with Eu^{3+} luminescent ceramics were synthesized by the Spark Plasma Sintering method. A to study the effect of the high level europium ions concentration on the structural and luminescent properties of $MgAl_2O_4$:Eu^{3+}ceramics.

2 Results and discussion

Commercially available $MgAl_2O_4$ spinel nanopowder (Baikowski Malakoff Inc., USA, purity above 99.999%, average particle size 200 nm) served as the starting material for luminescent $MgAl_2O_4$ ceramics. Powders of rare earth elements Eu_2O_3 (purity 99.999%, average particle size 50 nm, Nevatorg, Russia) were used to manufacture ceramics. The powder was consolidated on an SPS 515S Spark Plasma Sintering unit (Syntex Inc., Japan) to obtain dense ceramics. The desired amount of powder (2.8 g) was placed in a graphite die with an inner diameter of 20 mm. SPS conditions were as follows: sintering temperature T=1400°C, vacuum P=10-3 Pa, pressure 72 MPa, heating rate 5°C/min. The heating time was 10 min. The prepared ceramic samples were cylindrical plates 2.5 mm thick and 20 mm in diameter. Before characterization, the samples were polished on a polishing machine (300 Pro Buehler, Germany) with a MetaDi diamond suspension (Buehler, Germany). X-ray diffraction analysis (XRD) of the resulting ceramic sample was carried out using an XRD-7000S Shimadzu diffractometer (Japan). Pulsed cathodoluminescence (PCL) was excited using a GIN-600 high-current electron accelerator ($t_{1/2}$–10 ns, average electron energy 250 keV, excitation energy density ~23 mJ/cm^2).

The reflection positions correspond to standard data according to PDF no. 21-1152 and PDF no. 30-0012. Samples have a cubic syngony. When the Eu_2O_3 doping concentration is less

[cccc]Corresponding author: rubinfc@tpu.ru

than 3 wt. %, the spinel phase is observed in the samples. With an increase in the activator concentration above 3 wt. %, the second phase of europium aluminate $AlEuO_3$ appears, which indicates that Eu^{3+} ions predominantly occupy the Mg sites of the spinel lattice.

In the cathodoluminescence spectrum of $MgAl_2O_4$ ceramics, the emission band near 440 nm in the blue spectral region is usually attributed to the Mg^{2+} vacancy (Fig. 1a) [2]. The emission band in the spectral region 500 – 550 nm is debatable and can be attributed to the radiative transitions $4f^7 – 4f^6 5d^1$ of the Eu^{2+} ion [1]. The emission band near 614 nm corresponds to the $^5D_0 \rightarrow {}^7F_2$ electric dipole transition due to the fact that Eu^{3+} occupies the Mg^{2+} position. The intensity ratio of the emission bands is shown in Fig. 1b.

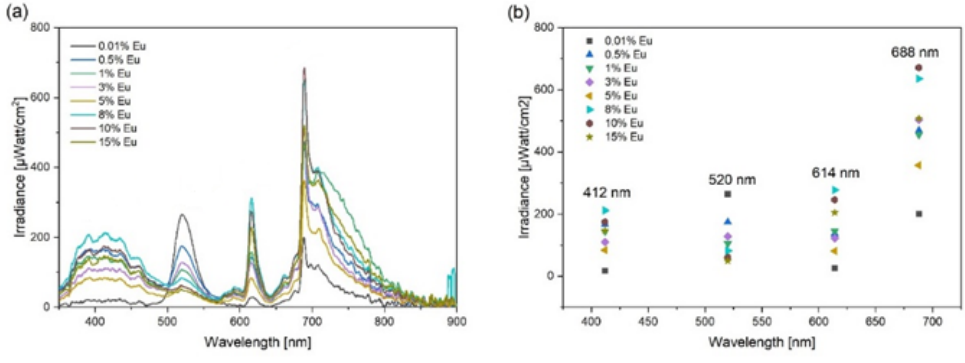

Fig. 1. (a) Pulsed cathodoluminescence spectrum of $MgAl_2O_4$ ceramics doped with variable concentration Eu^{3+} ions; (b) maximum intensity values for different emission bands.

A series of emission bands in the red region of the spectrum at 688 nm corresponds to radiative transitions in the chromium ion [2]. As shown in Fig. 1(b), the sensitivity of each emission peak to the concentration of europium ions is different. The optimal concentrations corresponding to the emission peaks at 412, 520, 614, and 688 nm are 8 wt. %, 0.01 wt. %, 8 wt. % and 10 wt. %, respectively.

As a result of the research, ceramic samples based on $MgAl_2O_4$ were obtained. The effect of concentration on the structural and luminescent properties of spinel doped with europium ions was found.

This work was funded by Russian Science Foundation No. 21-73-10100.The research was carried out using the equipment of the CSU NMNT TPU, supported by the RF MES project #075-15-2021-710.

References

1. C.R. García, L.A. Diaz-Torres, J. Oliva, G.A. Hirata, Opt. Mater. 37, (2014)
2. D. Valiev, O. Khasanov, E. Dvilis, S. Stepanov, E. Polisadova, V. Paygin, Ceram. Int. 44 (2018)

The improving effect of structural and luminescent properties of YAG:Ce^{3+} ceramics fabricated by powerful ultrasonic assistance

Damir Valiev[dddd], *Oleg* Khasanov, *Edgar* Dvilis, *Vladimir* Paygin and *Sergey* Stepanov

National Research Tomsk Polytechnic University, 634050 Tomsk, Russia

Abstract. Yttrium aluminum garnet (YAG) ceramics doped with Ce^{3+} were prepared by dry compaction the common uniaxial pressing and under powerful ultrasound assistance (PUA) to sintering. Initial ceramic powders of $Y_3Al_5O_{12}$ doped with Ce^{3+} (YAG: Ce) were synthesized by the solid-state reaction method. The structure and luminescent properties of sintered ceramics were investigated. It was demonstrated that the powerful ultrasonic assistant during the dry pressing stage has a positive effect on the structural and luminescent characteristics of YAG: Ce ceramics. The consolidation of the sintered material is very intensive accompanied by a decrease in the number of pores and grain growth at a sintering temperature of 1650 ºC. The luminous efficiency of YAG:Ce^{3+} ceramics vary from 120 to 219 lm/W (no PUA) and from 120 to 250 lm/W (prepared in PUA conditions) closely related with the phase purity and implicitly with sintering temperature. It was demonstrated the positive effect of treatment by PUA on the thermal properties of ceramics. Up to 250 °C, the PL intensity practically does not change. PUA during dry pressing shows an effective approach for ceramics processing.

1 Introduction

One of the latest directions in the field of solid-state lighting technology is luminescent ceramics applications [1-3]. The advantages of ceramics as solid-state light converters in w-LEDs are based on the possibility of varying thermal, optical, and mechanical properties. This is important for harsh operating conditions: high pump fluxes, high temperatures with a long service life. The thermal conductivity of dense ceramics is almost 100% of the theoretical, that is significantly higher than that of converters made of phosphor powders in such matrices as epoxy resin or silicone. This allows for faster, more efficient conversion of incident light with minimal energy dissipation in the material.

In the present work, we have used technology for phosphor powder ultrasonic compaction. This approach is applied to the pressed powder material in the axial and transverse directions. Powerful ultrasonic (PU) pressing technology produces ceramics with optimum performance and improved luminous efficiency. The usage of PU conditions during the compaction of the powder made it possible to reduce friction between the powder particles and the wall of the mold. To reduce the residual stress gradient and achieve the absence of warpage and uniform shrinkage during the sintering process. It is enhanced the relative density and luminous efficiency of YAG:Ce ceramics.

[dddd] Corresponding author: rubinfc@tpu.ru

2 Results and discussion

A homogeneous mechanical mixture of chemically pure reagents Al_2O_3 (99.99%), Y_2O_3 (99.99%), CeO_2 (99.99%) was used as the starting powders. The synthesis procedure is described in more detail in Ref. [24]. The phosphor powder was molded using cold static uniaxial pressing in a steel press die under the simultaneous influence of ultrasonic vibrations at pressures of 400 MPa on an IP-500 AVTO automatic press (ZIPO, Russia) [20]. The power of the ultrasound waves of the master generator was 800W. YAG:Ce ceramics sintering was performed in a high-temperature LHT 02/18 furnace (Nabertherm, Germany) in an air atmosphere at temperatures of 1550 – 1700 °C with a controlled heating and cooling rate of 200 ºC/min. Holding time at a given sintering temperature was 8 hours. The cylindrical YAG: Ce ceramics were obtained with about 1.5 mm at high with a diameter of about 8.5 mm.

X-ray phase analysis confirmed that ceramic samples have a stoichiometric yttrium-aluminum garnet with a cubic structure. The main wide luminescence band appears in the spectral range of 400 – 750 nm. The 5d – 4f radiative transitions in the cerium ion are responsible for this emission band. These weak luminescence bands of YAG: Ce^{3+} ceramics in the spectral range of 400 – 470 nm are possibly due to YAl antisite defects and charged oxygen vacancies (F+ and F centers). The position of the main luminescence band is in the range from 515 nm to 560 nm in all YAG:Ce ceramics are observed. The half-widths of the luminescence bands of all the investigated ceramics are close and differ slightly with the sintering temperature. The luminous efficiency of YAG: Ce ceramics with and without PUA conditions was measured using an integrating sphere. A LED with a wavelength λ_{max} = 447 nm served as a source of luminescence exciting radiation. The maximum value of luminous efficiency at a temperature of 1650 °C for the investigated ceramics prepared in PU conditions is about 240 lm/W, which is higher compared with ceramics prepared in no PU conditions.

The positive effect of ultrasonic treatment on the luminescent performances of ceramics was revealed. In the structure of sintered YAG: Ce ceramics with and without treatment by PU did not observe some changes after XRD data analysis. Thermal treatment from 1650 °C to 1700 °C leads to a decrease in the ceramics pore and fusion agents are formed. It was demonstrated the positive effect of treatment by PUA on the thermal properties of ceramics. Up to 250 °C, the PL intensity practically does not change. It was shown that the reflection in the main excitation band and the luminous efficiency of YAG: Ce ceramics directly depend on the residual porosity of the ceramics.

The application of powerful ultrasonic assistance during the dry pressing and then sintering luminescent ceramics can be useful for the improvement of ceramics emission properties for lighting engineering development.

This work was funded by Russian Science Foundation No. 21-73-10100. The research was carried out using the equipment of the CSU NMNT TPU, supported by the RF MES project #075-15-2021-710.

References

1. L. Zhang, B. Sun, L. Gu, W. Bu, X. Fu, R. Sun, T. Zhou, F.A. Selim, C. Wong, H. Chen, Appl. Surf. Sci. **455,** (2018)
2. L.G.D. Silveira, L.F. Cótica, I.A. Santos, M.P. Belançon, J.H. Rohling, M.L. Baesso, Mater. Lett. **89** (2012)
3. X. Liu, H. Zhou, Z. Hu, X. Chen, Y. Shi, J. Zou, J. Li, Opt. Mater. **88** (2019)

Optical properties of $La_3Ga_5SiO_{14}$, $La_3Ga_{5.5}Ta_{0.5}O_{14}$ and $Ca_3TaGa_3Si_2O_{14}$ single crystals

Evgeniia Zabelina[1,eeee], *Nina* Kozlova[1], and *Oleg* Buzanov[2]

[1]NUST "MISiS", Laboratory "Single crystals and Stock on their base", 119049 Leninskii pr., 4, b. 2, Moscow, Russia
[2] "Fomos-MATERIALS", 107023, Buzheninova str., 16, b. 1, Moscow, Russia

Abstract. The optical properties of $La_3Ga_5SiO_{14}$, $La_3Ga_{5,5}Ta_{0,5}O_{14}$ and $Ca_3TaGa_3Si_2O_{14}$ single crystals were studied in the wavelength range (200-800) nm. The spectral dependences of the moments of the dipole transition deviation angles $\theta(\lambda)$ were used to characterize the absorption processes in these crystals. The coefficients of the specific angle of the polarization plane rotation ρ were obtained by direct measurement and spectrophotometric methods. Discreet ρ values were approximated by Vyšín equation and the Drude formula. In the investigated region of wavelengths, the linear dependence of Drude formula is fulfilled for CTGS, the highest deviations from the linearity were observed for LGS. The discrete values of the refractive coefficients *No* and *Ne* were measured by the prism method, the obtained values were approximated by the Sellmeier equation.

Langasite (LGS, $La_3Ga_5SiO_{14}$), langatate (LGT, $La_3Ga_{5,5}Ta_{0,5}O_{14}$) and catangasite (CTGS, $Ca_3TaGa_3Si_2O_{14}$) are crystal group of the calcium gallium germanate structural type, which was discovered in the early 80s of the XX century in the USSR while searching for new laser media [1]. These crystals belong to the point symmetry group 32 and, hence, are optically anisotropic, i.e. they are birefringent, possess dichroism and gyrotropy. Due to the occupancy of the positions in the structure with certain elements, CTGS are classified as ordered crystals, and LGS and LGT - as disordered. The nature of defect centers in these crystals and the nature of gyrotropy is not clear now.

The aim of this work was to study the optical properties of LGS, LGT, and CTGS considering their optical anisotropy.

The crystals were grown at "Fomos-MATERIALS" by the Czochralski method in Ir crucibles in an argon atmosphere with the addition of oxygen. The optical properties of the crystals were studied in the accredited laboratory "Single crystals and Stock on their base". The spectral dependences of transmission were measured on the "Agilent Technologies" Cary-5000 spectrophotometer. The specific rotation of the polarization plane ρ was measured with the propagation of light along the 3rd order axis by the direct method at a wavelength of λ=630 nm and by the spectrophotometric interferometric method presented in [2] using the spectral dependences of transmission in crossed and parallel polarizers.

For all crystals, on the spectral dependences of transmission we observed pronounced absorption bands at ~290 nm, in the regions of ~(360–370) nm and ~(460–480) nm. Based on the measured in polarized light transmission coefficients of the ordinary *To* and extraordinary *Te* waves, for the first time for these crystals, the spectral dependences of the moments of the dipole transition deviation $\theta(\lambda)$ were calculated using the method presented in [3]. $\theta(\lambda)$ spectral

[eeee] Corresponding author: zabelina.ev@misis.ru

dependences allow to take into account the absorption of ordinary and extraordinary waves, to reveal absorption bands that are weakly visible on the spectral dependences of transmission and to estimate the degree of the ordering of the crystal by the $\theta(\lambda)$ deviation from θ=45°, corresponding to an ideal ordered crystal. Analysis of the $\theta(\lambda)$ spectral dependences showed that the least deviation from θ=45° is observed for CTGS, and the highest deviation is observed for LGS.

The discrete quantities ρ obtained by two methods are best approximated by the Vyšín equation [2, 4]:

$$\rho = \frac{K_{V1}\lambda^2}{(\lambda^2 - \lambda_{V1}^2)^2} + \frac{K_{V2}}{(\lambda^2 - \lambda_{V2}^2)} \tag{1}$$

where K_{V1}, K_{V2} – constants; λ_{V1}, λ_{V2} – characteristic wavelengths.

The presence of impurity atoms and structural imperfections of the crystal lattice cause deviations from the linear dependence of the Drude formula [5, 6]:

$$1/\rho = A\lambda^2 + \lambda_0 \tag{2}$$

where A – constant, that depends on matrix elements of interband transitions; λ_0 – characteristic wavelength.

The linear dependence of Drude formula is fulfilled for CTGS, the highest deviations from the linearity were observed for LGS. These results are in good agreement with the results, obtained by the $\theta(\lambda)$ spectral dependences analyzes.

The discrete values of the refractive indices *No* and *Ne* were measured by the prism method. LGT crystals have the highest refractive indices, and LGS crystals have the lowest. The obtained values were approximated by the Sellmeier equation.

References

1. B. Mill, A. Butashin, G. Khodzhabagyan, E. Belokoneva, N. Belov, Dokl.AN USSR **264** (1982) [in Russian].
2. K. Kaldybaev, A. Konstantinova, Z. Perekalina *Gyrotropy of uniaxial absorbing crystals*. (Publishing House of the Institute of Socio-Economic and Industrial-Environmental Problems of Investment, Moscow, 2000) [in Russian].
3. F. Litvin *Molecular Spectroscopy: Fundamentals of Theory and Practice* (Infra-M, Moscow, 2018).
4. V. Vyšín, V. Jankù Opt. Com. **3** (1971).
5. V. Kizel, V. Burkov *Gyrotropy of the crystals* (Nauka, Moscow, 1980) [in Russian].
6. T. Dimov, Zh. Bunzarov, I. Iliev, P. Petkova, Y. Tzoukrovski J. of Phys: Conf. Ser. V. **253** (2010).

AUTHORS INDEX

Научное издание

XVIII International Feofilov Symposium on Spectroscopy of Crystals Doped with Rare Earth and Transition Metal Ions (IFS-2022)

Book of abstracts

August 22-27, 2022
Moscow, Russia

Авторская редакция

Рецензент: д.ф.-м.н., зав. кафедрой «Математика»
Московского политехнического университета Андреев С.Н.

Издательство «Тровант»
ЛР № 071961 от 01.09.99.
108841, г. Москва, г. Троицк, м-н «В», д.52.
Тел. (495) 775-43-35, (495) 851-09-67, 850-21-81
web: www.trovant.ru e-mail: tan@trovant.ru

ISBN 978-5-89513-513-6